# Diffraction and Scattering of High Frequency Waves

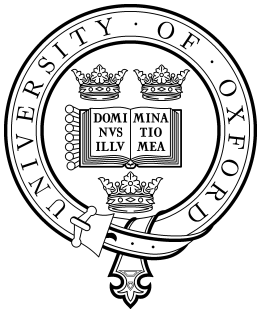


John Andrew Fozard

Jesus College

University of Oxford

A thesis submitted for the degree of

*Doctor of Philosophy*

September 2005

# Acknowledgements

I would like to thank my supervisor, Jon Chapman for his encouragement and advice. This work would not have been possible without the very generous funding of BAE SYSTEMS, whose industrial problems have motivated most of the work within this thesis. I am also grateful for the advice, comments and stimulating discussion I received from Colin Sillence and Andy Thain (now at EADS)

With regards the work on scattering, I thank Uzy Smilansky and Bryce McLeod for a number of interesting discussions about this topic.

# Abstract

This thesis examines certain aspects of diffraction and scattering of high frequency waves, utilising and extending upon the Geometrical Theory of Diffraction (GTD).

The first problem considered is that of scattering of electromagnetic plane waves by a perfectly conducting thin body, of aspect ratio $\mathcal{O}(k^{-\frac{1}{2}})$, where $k$ is the dimensionless wavenumber. The edges of such a body have a radius of curvature which is comparable to the wavelength of the incident field, which lies inbetween the sharp and blunt cases traditionally treated by the GTD. The local problem of scattering by such an edge is that of a parabolic cylinder with the appropriate radius of curvature at the edge. The far field of the integral solution to this problem is examined using the method of steepest descents, extending the recent work of Tew [44]; in particular the behaviour of the field in the vicinity of the shadow boundaries is determined. These are fatter than those in the sharp or blunt cases, with a novel transition function.

The second problem considered is that of scattering by thin shells of dielectric material. Under the assumption that the refractive index of the dielectric is large, approximate transition conditions for a layer of half a wavelength in thickness are formulated which account for the effects of curvature of the layer. Using these transition conditions the directivity of the fields scattered by a tightly curved tip region is determined, provided certain conditions are met by the tip curvature. In addition, creeping ray and whispering gallery modes outside such a curved layer are examined in the context of the GTD, and their initiation at a point of tangential incidence upon the layer is studied.

The final problem considered concerns the scattering matrix of a closed convex body. A straightforward and explicit discussion of scattering theory is presented. Then the approximations of the GTD are used to find the first two terms in the asymptotic behaviour of the scattering phase, and the connection between the external scattering problem and the internal eigenvalue problem is discussed.

# Contents


**1 Introduction** **1**

1.1 Thesis plan . . . 3

1.1.1 Statement of originality . . . 4

**2 Electromagnetism** **6**

2.1 Maxwell's equations . . . 6

2.2 Time-harmonic fields . . . 7

2.3 Non-dimensionalization . . . 8

2.4 Two-dimensional problems . . . 9

2.5 Interfaces between media . . . 9

2.5.1 Perfectly conducting medium . . . 10

2.5.2 Impedance boundary conditions . . . 11

2.6 Radiation conditions . . . 13

**3 Diffraction** **15**

3.1 Geometrical Theory of Diffraction . . . 16

3.1.1 Generalized Fermat's principle . . . 17

3.1.2 Rays and the WKBJ approximation . . . 19

3.1.3 Geometrical optics . . . 24

3.1.4 Tangential incidence . . . 25

3.1.5 Wedges and edges . . . 31

**4 Diffraction by Thin Bodies** **33**

4.1 Formulation of the problem . . . 34

4.1.1 Geometrical optics field . . . 35

4.1.2 Inner problem near "edges" . . . 35

4.1.3 Decomposition of inner problem into polarisations . . . 36

4.1.4 Solution of the scalar problems . . . 38

4.2 Asymptotic expansion of the fields . . . 41
4.2.1 Asymptotic expansion in the Sommerfeld case . . . 42
4.2.2 Expansion in the upper physical half plane $0 < \phi < \pi$ . . . 44
4.2.3 Expansion in the lower physical half plane $\pi < \phi < 2\pi$ . . . 46
4.2.4 Asymptotic expansion in the $O(k)$ edge-curvature case . . . 55
4.3 Creeping ray fields . . . 72
4.3.1 Creeping ray fields on almost flat bodies . . . 73
4.4 Body with curved mid-line . . . 73
4.5 Matching with the $\mathcal{O}(1)$ curvature solution . . . 75
4.5.1 Large curvature limit of the GTD approximation . . . 76
4.5.2 Large-$\beta$ limit of the tightly-curved edge solution . . . 77
4.6 Comparison of exact and asymptotic results . . . 79
4.6.1 Evaluation of Parabolic Cylinder Functions . . . 79
4.6.2 Calculation of the exact fields . . . 80
4.6.3 Calculation of the asymptotic approximations . . . 81
4.6.4 Discussion of results . . . 83
4.7 Summary and conclusions . . . 86

**5 Dielectric Structures** **90**
5.1 Formulation of problem (and numerical solution methods) . . . 91
5.2 GTD for dielectric structures . . . 92
5.3 Approximate methods for thin layers . . . 97
5.4 Approximate boundary conditions . . . 99
5.4.1 Derivation of approximate boundary or transition conditions . . . 101
5.4.2 Transition conditions for a high contrast dielectric layer . . . 102
5.4.3 Integral form of the scattered field . . . 107
5.5 Plane wave incidence on a thin dielectric layer . . . 108
5.6 Plane wave scattering from a tightly curved tip . . . 110
5.7 Tangential incidence upon thin layers . . . 113
5.7.1 Propagating and leaky modes in thin layers . . . 114
5.7.2 Propagating and surface modes for cylindrical layers . . . 115
5.7.3 Comparison between approximate and exact reflection and transmission coefficients . . . 118
5.7.4 Approximate boundary conditions near tangency . . . 120
5.7.5 Airy layer fields . . . 122
5.7.6 Location of solutions of the propagation relation . . . 125

5.7.7 Fock region . . . 127
5.7.8 Matching with scattered fields . . . 129
5.8 Summary and conclusions . . . 139

**6 Obstacle Scattering** **141**
6.1 The exterior Helmholtz problem . . . 141
6.2 The scattering matrix . . . 142
6.2.1 Physically-motivated definition . . . 142
6.2.2 Lax and Phillips's definition . . . 145
6.2.3 High frequency approximation of the scattering matrix . . . 148
6.3 Large-wavenumber asymptotics of the scattering phase . . . 149
6.3.1 The scattering phase . . . 150
6.3.2 Exact calculation for a circular scatterer . . . 150
6.3.3 An integral formula for the scattering phase . . . 152
6.3.4 Approximating the surface integral . . . 154
6.3.5 Three dimensional case . . . 159
6.4 Counting function for the interior eigenvalues . . . 161
6.5 Internal-external duality . . . 163
6.5.1 Eigenvalues of the internal problem and the scattering phase . . . 163
6.6 Physical significance of the scattering phase . . . 166
6.7 Summary . . . 166

**7 Discussion and Further Work** **168**
7.1 Thesis summary . . . 168
7.2 Further work . . . 169
7.2.1 Chapter 3 . . . 169
7.2.2 Chapter 4 . . . 169
7.2.3 Chapter 5 . . . 170
7.2.4 Chapter 6 . . . 171
7.3 Other questions arising . . . 171

**A Parabolic Cylinder Functions** **173**
A.1 Definition . . . 173
A.2 Integral form . . . 173
A.3 Recurrence relations, reflection and connection formulae . . . 174
A.3.1 Recurrence relations . . . 174
A.3.2 Reflection formula . . . 175

A.3.3 Connection formulae . . . . . 175
A.4 Asymptotic expansion of the functions . . . . . 175
A.4.1 Expansion for large $\nu$, with $z = \mathcal{O}(1)$ . . . . . 175
A.4.2 Expansion for large $z$, with $\nu = \mathcal{O}(1)$ . . . . . 176
A.4.3 Expansion for large $\nu$ and $z$, with $z = \sqrt{2}e^{-\frac{\pi i}{4}}x$, $x > 0$ and $\nu$ not near $-ix^2/2$ . . . . . 176
A.4.4 Expansion for small $|z|$ . . . . . 180

**B Discussion of Behaviour of the Integrands in the Thin Edge Problem 183**
B.1 Phase-amplitude expansions . . . . . 183
B.2 Saddle points . . . . . 186
B.3 Far-fields of the integrands (for large $|\nu|$) . . . . . 188

**C Asymptotic Expansion of Ratio of $\beta$-dependent PCFs 190**

**D Perturbed Saddle Point Contributions 192**

# List of Figures


2.1 Interface between two media, labelled 1 and 2 respectively, illustrating the sign of the unit normal $\boldsymbol{n}$ in (2.25). . . . . 10

3.1 Some of the different types of ray paths predicted by the generalization of Fermat's principle. . . . . 19
3.2 Asymptotic regions for tangential incidence of plane wave. . . . . 27
3.3 Curvilinear locally tangential and normal coordinates $s$ and $n$ for the Fock-Leontovich region. . . . . 27
3.4 Coordinate system for shed creeping ray field. . . . . 30
3.5 Shadow boundaries for plane wave and line source illumination. . . . . 31

4.1 Incidence of a plane wave upon a thin body. . . . . 34
4.2 Coordinate system for the inner problem. . . . . 36
4.3 The various different regions in the physical $(\xi, \eta)$ or $(r, \phi)$ plane for the expansions of (4.30), (4.31). . . . . 45
4.4 Schematic of the method of approximation of $I_s$ in the upper half plane $0 < \phi < \pi$. . . . . 46
4.5 The real part of the phase, in the complex $\nu$ plane, for the dominant term in the phase-amplitude expansion of the integrand of $I_s$. . . . . 46
4.6 Contours for the integrals $I_s$, $I_s^1$ and $I_s^2$. . . . . 48
4.7 Contours used for the approximation of $I_s^1$ and $I_s^2$, when the reflected field is present. . . . . 49
4.8 Plots of the real part of the phase for the integrands of $I_s^1$, $I_s^2$ and $I_s$. . . 52
4.9 Contours used for the approximation of $I_s^1 + I_s^2$, when the reflected field is not present. . . . . 53
4.10 Contours used in the approximation of $I_d^1 + I_d^2$ and $I_n^1 + I_n^2$, when the reflected field is present and $\beta$ is non-zero. . . . . 63
4.11 Asymptotic regions for a thin scatterer with curved midline. . . . . 76

4.12 Asymptotic regions for the GTD analysis of diffraction by a parabola, showing the dependence of the size of these regions upon the curvature $\kappa_0$ at the tip. . . . . 77
4.13 Contours of integration for the numerical evaluation of the diffracted field for the diffraction coefficient when $\pi < \phi < 2\pi - \phi_0$. . . . . 82
4.14 Plots of the real and imaginary parts versus observation angle for the exact expression for $I_d$ and the asymptotic approximation when $r = 20$, $\phi_0 = 1$ and $\beta = 1$. . . . . 86
4.15 As for Figure 4.14 but with $r = 50$. . . . . 86
4.16 As for Figure 4.14 but with $\beta = \frac{1}{10}$. . . . . 87
4.17 As for Figure 4.14 but with $\beta = \frac{3}{2}$. . . . . 87
4.18 Plots of the real and imaginary parts of the exact value of $I_d$, and its asymptotic approximations . . . . . 88
4.19 As for Figure 4.18, but showing the absolute values of the exact value of $I_d$ and its approximations. . . . . 88
4.20 Plots of the real and imaginary parts of the exact value of $I_d$ near the reflected boundary, the transition region approximations, and the diffracted field in $\pi < \phi_0 < 2\pi - \phi_0$ from the integral representation (4.113). . . . . 89
4.21 As for Figure 4.20, but with $\beta = \frac{1}{5}$. . . . . 89

5.1 Reflection and refraction at the interface between two materials. . . . . 93
5.2 Conversion between evanescent and real rays. . . . . 94
5.3 Critical incidence upon a convex object with lower refractive index than the surrounding medium. . . . . 94
5.4 Tangential incidence upon a dielectric cylinder. . . . . 95
5.5 Path of a ray through a thin layer. . . . . 97
5.6 Transmission of rays through a dielectric structure. . . . . 100
5.7 Reflection and transmission at a curved shell. . . . . 109
5.8 Coordinate system for tip diffracted field. . . . . 113
5.9 Propagating and surface modes for a cylindrical layer in the TE polarization case. . . . . 117
5.10 Propagating and surface modes for a cylindrical layer in the TM polarization case. . . . . 118
5.11 Comparison between exact and approximate reflection and transmission coefficients for TE polarization. . . . . 121
5.12 As for Figure 5.11 except for TM polarization. . . . . 122

5.13 Locations of solutions of the propagation relation for Airy layer modes. . 127
5.14 Comparison between the exact and approximate solutions for the propagation constants for near tangential modes. . . . . 127
5.15 Regions for matching between the Fock solution and the GO field. . . . . 130
5.16 Contours of integration in region I. . . . . 134
5.17 Contours of integration for remainder integrals in region II. . . . . 134
5.18 Multiply-reflected fields near tangential incidence. . . . . 135

6.1 Far-field of a compact obstacle, showing the merging of the shadow boundary and transition regions far from the obstacle. . . . . 149
6.2 Coordinate system for the Fock-Leontovich solution used to estimate the contributions from near-tangential incidence. . . . . 157
6.3 Relationship between interior and exterior ray-paths. . . . . 164

A.1 Contour of integration for the integral representations (A.3) and (A.4). Here the wavy line denotes the branch cut of the logarithm. . . . . 174
A.2 Stokes lines, anti-Stokes lines and branch cuts for the asymptotic expansions of $D_\nu(\bar{p}\xi)$. . . . . 177
A.3 Saddle points and paths of steepest descent in the complex $\hat{t}$ plane for the integral representations of the PCFs. . . . . 181
A.4 Steepest descent paths on the boundaries between the regions in Figure (A.2). . . . . 182

B.1 Regions of differing asymptotic behaviour in the $\hat{\nu}$ plane for the integrands of $I_s$ and $I_s^1$. . . . . 184
B.2 Regions of differing asymptotic behaviour in the $\hat{\nu}$ plane for the integrand of $I_s^2$. . . . . 186
B.3 Hills and valleys for the integrands of $I_s$, $I_s^1$ and $I_s^2$ in the complex $\nu$ plane. 189

# Chapter 1

# Introduction

Wave propagation underlies a huge number of physical and biological phenomena. However in everyday life waves are most commonly encountered in the form of light and sound, and the behaviours of both these phenomena are governed by linear wave equations. The study of such equations has been one of the more prominent areas of applied mathematics over the past century. This is partly because of the wide range of very important applications, and partly because of the many interesting mathematical problems encountered in their study. These mathematical problems have encouraged the development of many new theoretical, numerical and approximation techniques.

One situation where the behaviour of waves is of particular practical importance, and which provides the primary motivation to the work of this thesis, is that of microwave propagation. Radio waves were first used to detect objects in the early $20^{\text{th}}$ century, and aided by the development of the cavity magnetron during the Second World War, microwaves became a powerful tool in the detection of aeroplanes and ships. Microwave radar has subsequently been employed in a wide range of uses, both military and peaceful, including meteorology, navigation and the Global Positioning System. Microwaves are not only used for detection and measurement, but are also utilised for communication because of the high bandwidth which may be attained.

There are often a large number of antennas on a modern aeroplane, both for communication and for radar systems. Although every effort is made to separate antennas in frequency, space and time of use, because of the large number of antennas interference is still an issue. To correct the signals for interference it is necessary to predict the fields received by one due to another on the same object. Another important property which it is important to be able to predict (and control) is the distribution of the scattered radiation when a distant source of waves is incident upon the aircraft (known as the

bi-static radar cross section).

These electromagnetic properties can either be determined by complicated and expensive experiments, or by computational solutions. The aerodynamical properties of an aeroplane are usually the primary concern, and so the effect upon the antenna system and the radar cross section are just some of the different factors in the design process. In order to optimise their properties it is necessary to be able to be able to rapidly and robustly evaluate the effect of modifications in the structure or its properties. The wavelength of the microwave radiation is usually in the range 1cm to 1m, and so the objects under consideration are electrically large, by which we mean that the object is large compared with the wavelength. The scattered fields can be found by various different direct numerical methods; however the size of the numerical problem obtained depends upon the square of the ratio of the size of the body to the wavelength of the fields (for a surface integral formulation). Despite advances in the numerical analysis of the linear algebra problems arising, and the steady but rapid increases in computing technology, the amount of memory and time required to calculate the behaviour of the three-dimensional electromagnetic problem (for wavelengths at the shorter end of the range) is still on the boundaries of viability. Moreover, numerical methods become significantly more complicated when the structure is not perfectly conducting, but has varying surface or material properties.

Alternatively, it is possible to exploit the fact that the object is large compared with the wavelength to make asymptotic approximations of the scattered fields. This approximation is known as the Geometrical Theory of Diffraction (GTD), and essentially describes the fields in terms of rays, along which the waves propagate. At discontinuities in the geometry or properties of the structure, or at points of tangency of the rays upon the structure, diffraction may occur. The ray solutions are not valid near these points, and it is necessary to consider local problems near these points in order to find smooth solutions, and to determine the diffracted fields. Because of the local nature of these solutions the problem will, in general, reduce to a canonical problem in a simpler geometry. Despite having been originally developed in the 1950s, the theory is not complete. In this thesis we will consider a number of these canonical problems. These include the problem of scattering by the edge of a thin body, which has radius of curvature which is comparable with the incident wavelength (such as the leading edge of a wing for example), and problems related to the propagation of waves through a thin layer of dielectric material with high refractive index (such as a radome, which is a thin structure used to protect an antenna and maintain an aerodynamic flow).

We will also examine one of the more theoretical aspects of scattering theory, namely the scattering matrix for the (scalar) problem in the exterior of an obstacle. Using the same GTD approximations as in the rest of the thesis we will examine the asymptotic behaviour of a property of this scattering matrix, namely the scattering phase, and discuss its relationship to the corresponding problem in the interior of the obstacle.

In the majority of this thesis we will only consider solutions where the locations and nature of all sources and scatterers are constant, and the fields have $e^{-i\omega t}$ time-dependence, where $\omega$ is the frequency of the sources which excite the fields. This is referred to as the frequency-domain problem (in contrast to the time-domain problem, where the sources and scatterers may vary with time, and the fields may have more general time dependence).

## 1.1 Thesis plan

In Chapter 2 we introduce Maxwell's equations, which are the governing equations for macroscopic electromagnetic phenomena. We discuss their nondimensionalization, and also examine the associated boundary and radiation conditions for the time-harmonic wave equation in the exterior of an object.

In Chapter 3 we discuss the high frequency approximation of solutions of Maxwell's equations, known as the Geometrical Theory of Diffraction. We will summarise in particular the results of Saward [121] and Coats [30] which are relevant to the work of this thesis.

The remainder of the thesis then divides naturally into three distinct sections, connected by the application of the methods of Chapter 3.

In Chapter 4 we will consider the problem of electromagnetic scattering by thin bodies, of aspect ratio $\mathcal{O}(k^{-\frac{1}{2}})$. One of the radii of curvature near the edge of such a body will be found to be of the same order of magnitude as the incident wavelength, so that the problem of scattering near the edge lies between that for a blunt body and that for a sharp edge. The local canonical problem is scattering of a plane wave by a parabolic cylinder. Although the problem of diffraction by a parabola whose radius of curvature is large compared to the wavelength has been studied by a number of authors [66] [113], that with the radius of curvature of the same order as the wavelength was analysed only recently by Engineer, King and Tew [44]. Here we will generalise, correct and extend this work. We will examine the corresponding problem for a flat body with curved mid-line, and in particular the initiation of creeping waves upon such a body. In addition, we will

numerically evaluate our asymptotic expressions for the fields diffracted by the tip region, and compare them with the exact results for a parabolic cylinder.

In Chapter 5 we will study the problem of wave propagation through a radome. It is desirable that such a structure does not interfere with the operational performance of the antennas, and also that it does not adversely affect the radar cross section properties of the body. We will consider the simple case of a half-wavelength thick dielectric shell, and formulate transition conditions which may be used to approximate the effects of such a layer. These transition conditions will include corrections to account for the curvature of the layer, and we will use them to study the problem of scattering by a tightly curved tip region (this tip region will be required to have small radius of curvature when compared with the wavelength outside the obstacle, but large radius of curvature when compared with the wavelength within the radome material). We will also extend the analysis of Chapter 3 to examine whispering gallery and creeping waves propagating almost tangentially to such a thin layer, and examine their initiation by tangential incidence of a plane wave.

In Chapter 6 we will discuss the problem of scattering in the exterior of an obstacle in the framework of scattering theory (in the scalar case). We will provide a physically-motivated definition of the various concepts involved, and explain the relationship between this and more abstract definitions of the scattering matrix. We will then define a function known as the scattering phase, which is related to the eigenvalues of the scattering matrix. The asymptotic methods of Chapter 3 will then be used to find the behaviour of this function for large wavenumber. This will be seen to have similar asymptotic behaviour to the counting function for the eigenvalues of the interior problem, and we will discuss the relationship between the problems in the interior and exterior of an obstacle.

### 1.1.1 Statement of originality

Chapter 2 introduces Maxwell's equations, which govern electromagnetic wave phenomena, and also the various radiation and boundary conditions. Chapter 3 discusses the Geometrical Theory of Diffraction. This has recently been placed in a modern asymptotic framework in the theses [134], [121] and [30], and this chapter is essentially a summary of these results.

Chapter 4 will extend the work of [44] to the three-dimensional electromagnetic case. The integral solutions found in Section 4.1 are known [17]. Sections 4.2 onwards are novel in so far as they differ from [44]. Along with a number of corrections to the actual results listed there, and the extension to the case of Dirichlet boundary conditions, the

detailed consideration of the fields in the shadow boundary and transition regions is entirely original. Sections 4.4 and 4.6 are entirely novel.

Chapter 5 is novel except where stated in the text, although similar boundary conditions (ignoring curvature effects which we include) have been used previously to model thin layers of material. The results in Sections 5.5 and 5.7 are novel.

Chapter 6 is mainly a discussion of known results about scattering theory, although we present the various definitions in a simple and explicit form. The analysis of Section 6.3, extending the work of [89] to find the first-order correction to the asymptotic behaviour, is new.

# Chapter 2

# Electromagnetism

In this chapter we will briefly outline the standard physical model for microwave propagation, including the various boundary and radiation conditions.

## 2.1 Maxwell's equations

Microwave radiation is an electromagnetic phenomenon, and so involves the behaviour of two vector fields: the electric field $\mathcal{E}$, and the magnetic induction $\mathcal{B}$. The geometry of our diffraction and scattering problems will be on a macroscopic scale, and so to avoid considering the complicated interactions between the fields and sub-atomic particles we will use a simplified model in which all quantities have been averaged over an intermediate length scale (for details see [65], section 6.6). Electric charge then has volume density $\rho_e$, and electric current has current density vector $\mathcal{J}$. To allow for the interactions between the fields and matter we introduce two additional fields, the electric displacement[1] $\mathcal{D}$, and the magnetic field $\mathcal{H}$. The evolution of these fields is governed by the system of equations

$$\nabla \wedge \mathcal{E} + \frac{\partial \mathcal{B}}{\partial t} = 0 \tag{2.1}$$

$$\nabla \wedge \mathcal{H} - \frac{\partial \mathcal{D}}{\partial t} = \mathcal{J}, \tag{2.2}$$

$$\nabla . \mathcal{D} = \rho_e, \tag{2.3}$$

$$\nabla . \mathcal{B} = 0, \tag{2.4}$$

which was first posed by James Clark Maxwell. Further discussion as to the physical significance of each of these equations may be found in [65, 137].

[1] We note that $\mathcal{D}$ and $\mathcal{B}$ are sometimes called the electric and magnetic flux densities.

This system is closed by the constitutive relations, which describe the interaction between the fields and the medium of propagation. For a linear, isotropic medium these are of the form

$$\mathcal{D} = \epsilon\mathcal{E}, \quad \mathcal{B} = \mu\mathcal{H}. \tag{2.5}$$

where $\epsilon$ is the (electric) permittivity, and $\mu$ is the (magnetic) permeability. In free-space the permittivity has the constant value $\epsilon_0 = 8.8542 \times 10^{-12} Fm^{-1}$ (in S.I. units), and the permeability has the constant value $\mu_0 = 4\pi \times 10^{-7} Hm^{-1}$. In the presence of matter the electric field redistributes the charge distribution within atoms, or causes molecules with permanent dipoles to align with the field. This charge distribution modifies the applied field, and almost all materials have a permittivity $\epsilon$ greater than $\epsilon_0$. The ratio $\hat{\epsilon} = \epsilon/\epsilon_0$ is known as the dielectric constant of the material. The magnetic field may also interact with matter, but, other than in the special case of ferro-magnetic materials, $\mu$ differs from $\mu_0$ by few tenths of a percent or less.

In conducting materials charged particles are able to flow through the material under the influence of an applied electric field. The size and direction of these currents is given by Ohm's law

$$\mathcal{J} = \sigma\mathcal{E}, \tag{2.6}$$

where $\sigma$ is the conductivity of the material, and we also allow there to be an externally generated source current density $\mathcal{J}_c$.

In general these constitutive relationships may have a much more complicated form, but this simple linear model is adequate for most materials at microwave frequencies and moderate amplitudes.

## 2.2 Time-harmonic fields

In the remainder of this thesis we will only consider fields and sources which have sinusoidal dependence on time, with period $\frac{2\pi}{\omega}$, and where all sources and boundaries are static. We write

$$\mathcal{E} = \Re\left(e^{-i\omega t}\mathbf{E}\right) \quad \mathcal{H} = \Re\left(e^{-i\omega t}\mathbf{H}\right) \quad \mathcal{J}_c = \Re\left(e^{-i\omega t}\mathbf{J}_c\right) \quad \rho_e = \Re\left(e^{-i\omega t}\rho\right) \tag{2.7}$$

and Maxwell's equations for a linear, isotropic medium become,

$$\nabla \wedge \mathbf{E} - i\omega\mu\mathbf{H} = 0, \tag{2.8}$$

$$\nabla \wedge \mathbf{H} + i\omega\epsilon\mathbf{E} = \mathbf{J}_c + \sigma\mathbf{E}, \tag{2.9}$$

$$\nabla.(\epsilon\mathbf{E}) = \rho, \tag{2.10}$$

$$\nabla.(\mu\mathbf{H}) = 0. \tag{2.11}$$

These equations may also be obtained by taking a Fourier transformation in the time variable of the fields and source terms in (2.1)-(2.4).

## 2.3 Non-dimensionalization

We now proceed to non-dimensionalize our equations. This allows us to work with dimensionless quantities, and establish the relevant parameters governing the solution. It also enables us to make comparisons of the sizes of various terms in later equations, and so make simplifications by ignoring those terms which are insignificant. In order to do this we scale the electric field with its typical magnitude $E^0$, and the spatial coordinates by the length scale $L$ of the geometry of the problem. For plane wave incidence upon a body with curvature, $L$ is often taken to be an average radius of curvature of the body. However for some special geometries, such as incidence of a plane wave upon a semi-infinite plane, there may be no natural length scale.

Denoting the dimensionless quantities by hats, we write

$$\mathbf{E} = E^0\hat{\mathbf{E}}, \quad \mathbf{x} = L\hat{\mathbf{x}}. \tag{2.12}$$

We then choose our scalings for the other variables to be

$$\mathbf{H} = \sqrt{\frac{\epsilon_0}{\mu_0}}E^0\hat{\mathbf{H}}, \quad \mathbf{J}_c = \sqrt{\frac{\epsilon_0}{\mu_0}}\frac{E^0\hat{\mathbf{J}}_c}{L}, \quad \sigma = \sqrt{\frac{\epsilon_0}{\mu_0}}\frac{\hat{\sigma}}{L}, \quad \rho = \frac{\epsilon_0 E^0\hat{\rho}}{L}, \quad \epsilon = \epsilon_0\hat{\epsilon}, \quad \mu = \mu_0\hat{\mu}, \tag{2.13}$$

which minimises the number of parameters in the problem, and also agrees with Coats [30]. The equations become

$$\hat{\nabla} \wedge \hat{\mathbf{E}} - ik\hat{\mu}\hat{\mathbf{H}} = \mathbf{0}, \tag{2.14}$$

$$\hat{\nabla} \wedge \hat{\mathbf{H}} + ik\hat{\epsilon}\hat{\mathbf{E}} = \sigma\hat{\mathbf{E}} + \hat{\mathbf{J}}_c, \tag{2.15}$$

$$\hat{\nabla}.(\hat{\epsilon}\hat{\mathbf{E}}) = \hat{\rho}, \tag{2.16}$$

$$\hat{\nabla}.(\hat{\mu}\hat{\mathbf{H}}) = 0. \tag{2.17}$$

where $k = \frac{\omega L}{c}$ is the non-dimensional wavenumber, and $c = 1/\sqrt{\epsilon_0\mu_0}$ is the speed of light. From this point we will work solely with dimensionless quantities, and so will omit the hats in later formulae.

In most of this thesis $\hat{\epsilon}$ and $\hat{\mu}$ are considered to be piecewise constant, and this simplifies the equations. In this case (2.16) and (2.17) become

$$\nabla.\mathbf{E} = \frac{\rho}{\epsilon}, \qquad \nabla.\mathbf{H} = 0, \tag{2.18}$$

and when we take the curl of (2.14) or (2.15) we do not obtain terms containg $\boldsymbol{\nabla}\hat{\epsilon}$ or $\boldsymbol{\nabla}\hat{\mu}$.

## 2.4 Two-dimensional problems

In some of the later work we will consider problems where the geometry of the problem and the incident fields are two dimensional, and so independent of $z$, say. It is then found that Maxwell's equations reduce to two scalar problems for $E_z$ and $H_z$, which are the components of the electric and magnetic field in the $z$-direction. These two problems may be solved independently, provided that they are not coupled by the boundary conditions. For transverse electrical (TE) polarization

$$\mathbf{E} = \phi(x, y)\mathbf{e}_z, \tag{2.19}$$

where $\mathbf{e}_z$ is a unit vector in the direction of increasing $z$. In free space, and in the absence of current and charge density, Maxwell's equations become

$$(\nabla^2 + k^2)\phi = 0, \tag{2.20}$$

$$\mathbf{H} = \frac{1}{ik}\nabla \wedge (\phi \mathbf{e}_z). \tag{2.21}$$

Similarly for transverse magnetic (TM) polarization

$$\mathbf{H} = \phi(x, y)\mathbf{e}_z, \tag{2.22}$$

and Maxwell's equations are that

$$(\nabla^2 + k^2)\phi = 0, \tag{2.23}$$

$$\mathbf{E} = -\frac{1}{ik}\nabla \wedge (\phi \mathbf{e}_z). \tag{2.24}$$

Similar equations may be found within a medium with constant $\epsilon$ and $\mu$.

## 2.5 Interfaces between media

There are often a number of surfaces within the domain under consideration across which the material properties change abruptly. The field vectors may not be continuous at these surfaces, and so Maxwell's equations fail to hold in the classical sense. Instead, either by consideration of the equations in conservation form [30], or in integral form [66],[14], we find that the fields satisfy

$$\boldsymbol{n}\wedge(\mathbf{E}_2-\mathbf{E}_1) = \mathbf{0}, \quad \boldsymbol{n}\wedge(\mathbf{H}_2-\mathbf{H}_1) = \mathbf{J}_s, \quad (\mathbf{D}_2-\mathbf{D}_1).\boldsymbol{n} = \rho_s, \quad (\mathbf{B}_2-\mathbf{B}_1).\boldsymbol{n} = 0, \tag{2.25}$$

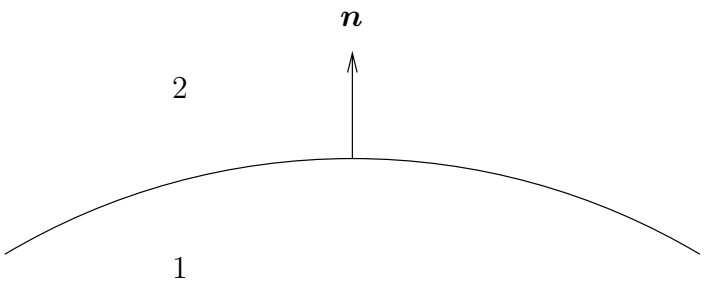


**Figure 2.1:** Interface between two media, labelled 1 and 2 respectively, illustrating the sign of the unit normal $\boldsymbol{n}$ in (2.25).

across a boundary[2], which we will refer to as continuity conditions. Here the subscript 1 denotes the limit of the field as we approach the boundary from medium 1, and similarly for medium 2. The vector $\boldsymbol{n}$ is the unit normal to the interface, pointing into medium 2. There are source terms in some of these conditions, as it is possible for charges within a material to concentrate in a very thin layer near such an interface, giving rise to a surface charge density $\rho_s$. However, a time-harmonic surface charge density is only possible when one of the materials has non-zero conductivity. If one of the media has infinite conductivity there may also be a surface current $\mathbf{J}_s$ which flows in such a layer.

In general, Maxwell's equations must be solved in the whole region under consideration, along with the boundary conditions at every interface. However, in certain circumstances it is possible to ignore the fields within some of the media, and instead impose boundary conditions on the fields at their surfaces.

### 2.5.1 Perfectly conducting medium

Within a perfect electrical conductor the conductivity is infinitely large, and so in order for there not to be an infinite current flowing we require that the electric field vanishes inside the conductor. Using (2.1) we then see that the magnetic field inside the conductor must be constant, and as we are only interested in time-harmonic fields, the magnetic field must also be zero within the conductor.

If we consider the interface between a perfect conductor and an imperfectly conducting or dielectric medium, then from (2.25) we have that

$$\boldsymbol{n} \wedge \mathbf{E} = \mathbf{0}, \qquad \mathbf{H}.\boldsymbol{n} = 0, \tag{2.26}$$

upon the interface, where here $\mathbf{E}$ and $\mathbf{H}$ are the limits of the fields as we approach the

[2]Strictly, a static boundary, although if the velocity of the boundary is small compared to the speed of light then these conditions will be good approximations.

boundary within the medium which is not a perfect conductor. For time-harmonic fields the second condition is redundant, as it is a consequence of the first condition and (2.14).

The surface charges and currents give rise to a non-zero normal component of the electric field, and a non-zero tangential magnetic field

$$\mathbf{E}.\boldsymbol{n} = \frac{\rho_s}{\epsilon}, \qquad \boldsymbol{n} \wedge \mathbf{H} = \mathbf{J}_s \tag{2.27}$$

where $\boldsymbol{n}$ is the outwards-pointing unit normal to the perfect conductor. These surface charge and current distributions are almost always initially unknown, but (2.26) alone is sufficient to uniquely determine the fields.

### 2.5.2 Impedance boundary conditions

Although most metals have very high conductivity at microwave frequencies, the perfectly-conducting boundary conditions are only approximate. For materials with large but finite conductivity there are non-zero electric and magnetic fields within the conductor, which cause volume currents to flow. However, these are only present in a thin layer[3] near the surface, the thickness of which is known as the skin-depth. We find that the fields approximately satisfy an impedance boundary condition at the surface. This relates the components of the field and their normal derivatives, or alternatively the tangential components of the two fields.

We will briefly consider the impedance boundary conditions on the interface $z = 0$ between free space, and a highly conducting material in the half space $z < 0$. From examining (2.15) we see that, in the frequency domain, the effect of finite conductivity is equivalent to the material having a complex permittivity

$$\epsilon' = \epsilon + \frac{i\sigma}{k}. \tag{2.28}$$

Such a complex permittivity may be also be used to model a lossy dielectric. The surface charge density in (2.25) may be found from the continuity of the tangential components of $\mathbf{H}$ and (2.15), and we deduce that

$$\epsilon_1' \mathbf{E}.\boldsymbol{n} = \epsilon_2' \mathbf{E}.\boldsymbol{n} \tag{2.29}$$

at the boundary.

The refractive index $N$ of the conducting medium is defined as the root of $N^2 = \mu\epsilon'$ which has positive real part, and as the conductivity is large $|N| \gg 1$. In order to simplify

[3] This is a different (and thicker) layer to that for the surface charges and currents.

the analysis slightly we rescale the spatial coordinates with $k^{-1}$. The field components then satisfy

$$(\nabla^2 + N^2)\mathbf{H} = (\nabla^2 + N^2)\mathbf{E} = 0, \tag{2.30}$$

within the conducting medium ($z < 0$), and

$$(\nabla^2 + 1)\mathbf{H} = (\nabla^2 + 1)\mathbf{E} = 0, \tag{2.31}$$

in free space ($z > 0$). The equation (2.30) is exact for uniform media, and a good approximation for media whose properties vary only slowly on a wavelength scale. We assume that the fields only vary on an $\mathcal{O}(1)$ length scale along the interface in $z > 0$, and so in order for there to be a balance of terms in (2.30) we see that the fields in $z < 0$ must be rapidly varying in the $z$ direction. We scale $z = \mid N \mid^{-1} z'$ and set $N' = N/ \mid N \mid$. In the conducting medium we find (to leading order) that

$$\frac{\partial^2 \mathbf{E}}{\partial z'^2} + N'^2 \mathbf{E} \;\; = \;\; 0, \tag{2.32}$$

and the same equation holds for the magnetic field. Therefore we find that

$$\mathbf{E} \sim \mathbf{E}_0(x, y) \exp(-iN'z'), \qquad \mathbf{H} \sim \mathbf{H}_0(x, y) \exp(-iN'z') \tag{2.33}$$

within the conducting medium, when we choose the solutions which propagate away from the surface. Using the continuity conditions (2.25) we have that

$$\epsilon' E_z(x, y, 0-) = E_z(x, y, 0+), \qquad \mu H_z(x, y, 0-) = H_z(x, y, 0+). \tag{2.34}$$

From the continuity of the tangential components of $\mathbf{E}$ and $\mathbf{H}$, and applying the divergence free condition on each side of the interface in turn, we find that the normal derivatives of $E_z$ and $H_z$ are continuous across the interface. Calculating the normal derivatives of the fields on the conducting side of the interface from (2.33), and using the continuity conditions at the boundary, we find that

$$\frac{\partial E_z}{\partial z} = -ik\eta E_z, \quad \frac{\partial H_z}{\partial z} = -\frac{ik}{\eta} H_z \tag{2.35}$$

for the free space field on the boundary in our original coordinate system, where here $\eta = \sqrt{\frac{\mu}{\epsilon'}}$ is known as the impedance of the surface. For two dimensional problems similar boundary conditions may be found for the two scalar problems introduced in Section 2.4. For TE polarization we have that

$$\frac{\partial \phi}{\partial n} = -\frac{ik}{\eta}\phi, \tag{2.36}$$

and for TM polarization we have

$$\frac{\partial \phi}{\partial n} = -ik\eta\phi. \tag{2.37}$$

By using Maxwell's equations within the conducting medium, and continuity of the tangential field components at the interface, we can find that

$$\boldsymbol{n} \wedge \mathbf{E} = \eta\, \boldsymbol{n} \wedge (\boldsymbol{n} \wedge \mathbf{H}), \tag{2.38}$$

or equivalently

$$E_x = -\eta H_y, \qquad E_y = \eta H_x, \tag{2.39}$$

and it is possible to show that (2.35) and (2.38) are equivalent [123]. These conditions may be applied at a curved interface provided the curvature is small compared to the external wavelength. Similar conditions may also be used to model a number of different materials and situations; we will discuss this further in Chapter 5.

One aspect of note is that, in the case of TM polarization, surface waves may propagate along the surface of a conductor [66, §7.7]. For a good conductor this mode decays very rapidly in the direction of propagation (but this is not the case for a coated surface).

## 2.6 Radiation conditions

As is the case for Helmholtz' equations, Maxwell's equations and the boundary conditions are not sufficient to ensure uniqueness for the solution in a domain that extends to infinity. One situation where this can be seen is for scattering by a perfectly conducting disc. We can add to any solution a plane wave which propagates in a direction in the same plane as the disc, and which is polarized such that the electric field of the plane wave is normal to the disc (and so the magnetic field of the plane wave is tangential to the disc). This new solution can be seen to satisfy Maxwell's equations and the perfectly conducting boundary conditions (2.26). In order to eliminate this non-uniqueness we must impose additional conditions upon the behaviour of the fields at infinity.

In the case where all obstacles, and all current and charge sources (if any) are contained within a bounded region, the appropriate conditions are the Silver-Müller radiation conditions [31, 66]. We require that the field decays sufficiently rapidly at infinity, so that

$$\mathbf{E} = \mathcal{O}\left(\frac{1}{r}\right), \qquad \mathbf{H} = \mathcal{O}\left(\frac{1}{r}\right), \tag{2.40}$$

in the three dimensional case (in two dimensions the condition is that the fields must decay like $\mathcal{O}(r^{-\frac{1}{2}})$). In addition we require that there is no inward-propagating field at

infinity, which is ensured by the conditions

$$\hat{\boldsymbol{r}} \wedge \mathbf{H} + \mathbf{E} = o(1), \tag{2.41}$$

$$\hat{\boldsymbol{r}} \wedge \mathbf{E} - \mathbf{H} = o(1). \tag{2.42}$$

Note that there is again redundancy in these conditions for the time-harmonic problem, and either of the last two conditions along with Maxwell's equations in free space imply all the others [31].

In the case where the incident field is due to a distant source, and so taken to be a plane wave, we may still apply the radiation conditions considered above, but only to the scattered portion of the field (the total field less the incident field).

For structures which extend to infinity, such as an infinite plane or semi-infinite half plane, then these radiation conditions are not applicable. Instead alternative methods have to be employed, such as demanding that the scattered field is propagating away from the boundary [30].

# Chapter 3

# Diffraction

When a wave encounters an impenetrable obstacle it is found that, instead of forming a sharp shadow, as would be expected if wave energy travelled in straight lines, there are waves which propagate into the "unlit" region. This process is known as diffraction[1], and one situation in which this is easy to see is for water waves entering a harbour, which spread out as they pass through the opening in the harbour wall. Similar effects may be readily observed for sound waves travelling through an open door or window.

However for visible light diffraction is not commonly observed, and the shadows of obstacles appear to be completely dark, with abrupt edges[2]. The diffraction of light was not observed until the experiments of Grimaldi and Gregory in the $17^{\text{th}}$ century. Even after these observations the nature of light was a subject of much controversy until Young's experiments at the end of the $18^{\text{th}}$ century, and not fully understood until the much later formulation of Maxwell's equations and the discovery of quantum theory. Before these recent developments the assumption that light consists of transverse waves allowed many problems to be studied. In particular Fresnel developed a mathematical theory of diffraction, which was used by Poisson to predict a bright spot in the shadow of a circular disc (due to constructive interference between the waves diffracted at the edge).

The fundamental difference between light and other wave phenomena is that the wavelength of light is far smaller than the the typical length scale of the scatterer. Under the assumption that the wavelength of the waves is small a ray approximation can be developed, for which light in a homogeneous medium does indeed travel in straight lines.

[1] This word was coined by Grimaldi from the Latin word *diffringere*, which means to break into pieces, or to shatter.

[2] For a point or plane wave source; for an extended source such as the Sun it is well known that the edge of the shadow has a penumbra region within which there is a gradual transition from light to dark.

This approximation breaks down where the ray solution is not smooth, such as at sharp edges of an obstacle or near tangency, and diffraction may occur at these points. The amplitudes of these diffracted fields (relative to the incident field) will diminish as the wavelength of the incident field decreases.

Such a theory is naturally also valid for other types of electromagnetic radiation. For microwaves the wavelength is still small compared to the geometry of the problem, but it is much longer than for visible light. Therefore the short-wavelength approximation is still valid, but the diffracted rays are found to have much greater (relative) amplitude.

## 3.1 Geometrical Theory of Diffraction

The geometrical theory of diffraction (GTD) is a high frequency approximation to the solution to Helmholtz' equation (or Maxwell's equations). As for geometrical optics the fields will propagate along rays, which in a homogeneous medium are straight lines. In addition to the direct and reflected rays of geometrical optics we will also include diffracted rays. All these rays will be seen to satisfy a generalized form of Fermat's principle. By introducing the WKBJ approximation, which decomposes the rapidly (spatially) varying fields into phase and amplitude terms, differential equations will be found which give the phase and amplitude associated with a family of rays. Using these solutions, and by imposing suitable boundary conditions upon the scattered ray fields, we will find the fields reflected by an obstacle. However, for diffracted rays we will in general not be able to find the initial amplitude and phase of the diffracted rays at the point of diffraction using ray theory alone. The amplitudes of these diffracted ray fields become infinite near such points, and so the ray approximation breaks down. From the high frequency assumption we expect that the behaviour of the fields near the point of diffraction, and so the initial data for the diffracted rays, will depend only upon the local geometry of the obstacle. To leading order these local problems will reduce to canonical problems in simpler geometries, the solutions to many of which can be found by analytical means. The initial data for the diffracted rays are then found by asymptotic matching between the diffracted rays and the solutions to these inner problems.

The ray solutions will also break down at caustics or foci of the ray fields, and in the vicinity of discontinuities in the ray fields such as that which occurs at the boundary between the lit and shadowed regions. Suitable local solutions must be found to regularise the singular behaviour of the solutions near these points, and these will be found to match with the ray solutions. In this manner we will be able to construct asymptotic solutions

to the diffraction problem which give approximations to the fields at all points.

### 3.1.1 Generalized Fermat's principle

Fermat's principle states that a light ray between two points $A$ and $B$ has optical path length

$$\int_A^B N(\boldsymbol{x})\ ds \tag{3.1}$$

which is stationary[3] with respect to (admissible) perturbations of the path. Here $s$ denotes arc length along the curve, and $N(\boldsymbol{x})$ is the refractive index. For an isotropic medium with continuously differentiable refractive index let $\mathbf{r}(s)$ be a continuously differentiable ray. Then for any (continuously differentiable) variation $\boldsymbol{\eta}(s)$, with $\boldsymbol{\eta} = \mathbf{0}$ at the endpoints $A$ and $B$, stationarity of the optical path length requires that

$$\begin{aligned} 0 &= \left.\frac{\partial}{\partial\epsilon}\right|_{\epsilon=0} \int_A^B N(\boldsymbol{r}+\epsilon\boldsymbol{\eta}) \left\{\boldsymbol{r}_s^2 + 2\epsilon \boldsymbol{r}_s.\boldsymbol{\eta}_s + \epsilon^2\boldsymbol{\eta}_s^2\right\}^{\frac{1}{2}}\ ds, &(3.2)\\ &= \int_A^B \left\{\boldsymbol{\nabla} N.\boldsymbol{\eta} + N\boldsymbol{r}_s.\boldsymbol{\eta}_s\right\}\ ds, &(3.3)\\ &= \left[N\boldsymbol{r}_s.\boldsymbol{\eta}\right]_A^B + \int_A^B \left\{\boldsymbol{\nabla} N - (N\boldsymbol{r}_s)_s\right\}.\boldsymbol{\eta}\ ds. &(3.4)\end{aligned}$$

From this we see that along such a ray

$$(N\boldsymbol{r}_s)_s = \boldsymbol{\nabla} N, \tag{3.5}$$

(agreeing with the equation (2.6) from [75]), and in the special case of a homogeneous medium

$$\boldsymbol{r}_{ss} = 0, \tag{3.6}$$

so in this situation rays are straight lines.

This predicts those rays which are directly transmitted between source and observation points. However rays which are reflected from the obstacle are in general not stationary points of optical path length for all perturbations, as usually there are nearby paths which have smaller optical path length and which do not meet the obstacle. The obstacle acts as a secondary source of waves (in order to satisfy the boundary conditions), and so there should be a system of rays which approximates this reflected field. The solution proposed in [73] is to separately consider each of the classes of continuous

[3]This path is usually a local minimum, but it is possible for this path length to be a saddle point, for instance in the case of reflection by a concave mirror (by concave we mean a mirror which is curved away from the observer, as is the case for a shaving mirror).

paths $D_{rst}$ which meet the obstacle(s) in $r$ smooth arcs on the surface, $s$ points on edges or discontinuities of the boundary, and $t$ points at vertices.

To illustrate this we will consider reflection from an obstacle in a homogeneous medium. Fermat's principle then requires that rays away from the surface consist of straight lines, and a minimal path for a reflected ray will meet the surface at a single point $P$ (where $s = s_P$). The ray is not differentiable at $P$, and so we are unable to integrate by parts over the whole path. Instead we obtain an end point contribution from $s_p$, namely

$$- \left[\boldsymbol{r}_s.\boldsymbol{\eta}(s_P)\right]_-^+ \tag{3.7}$$

and this must also vanish for all permissible choices of $\boldsymbol{\eta}(s_P)$. If we require that the perturbed path also meets the surface at some point near $s = s_P$ then $\boldsymbol{\eta}(s_P)$ must lie in the tangent plane to the surface. Choosing the orthogonal vectors $\boldsymbol{t}_1$ and $\boldsymbol{t}_2$ to span the tangent plane at $P$, where $\boldsymbol{t}_1$ is parallel to the projection of $\boldsymbol{r}_s(P-)$ on to the tangent plane, then this condition becomes

$$\left(\boldsymbol{r}_s(P+) - \boldsymbol{r}_s(P-)\right).\boldsymbol{t}_1 = 0 \qquad \boldsymbol{r}_s(P+).\boldsymbol{t}_2 = 0. \tag{3.8}$$

From this we recover the usual laws of reflection; that the incident and reflected rays lie in a plane containing the normal to the surface, and that the angles made by the incident and reflected rays with the normal to the surface are equal.

Similar analysis may be performed for other types of rays. For rays diffracted by an edge (or wedge), as illustrated in Figure 3.1(b), the angles made by the incident and diffracted ray with the wedge must be equal, whereas for diffraction by a vertex (Figure 3.1(a)) the diffracted ray may be in any direction, although the incident and diffracted rays must both meet the obstacle at the vertex. Of particular interest are those rays which share an arc with the surface of the body, such as those found in the shadow of a convex obstacle. Then the ray must be tangent to the surface at the points where the ray meets and leaves the surface, assuming the surface is smooth at both those points (Figure 3.1(c)). The portion of the ray which is in contact with the surface is also found to be a geodesic of the surface.

There are a large number of different types of diffracted ray path, some of which are illustrated in Figure 3.1. We expect that diffraction will occur at all points or lines at which the surface or the boundary conditions are not smooth. If we consider the reflected fields to be generated by sources upon the boundary then contributions from near such discontinuities will not completely cancel in the short-wavelength limit. However discontinuities in the derivatives of higher order, such as that illustrated in Figure 3.1(f), will yield diffracted fields with asymptotically smaller amplitudes.

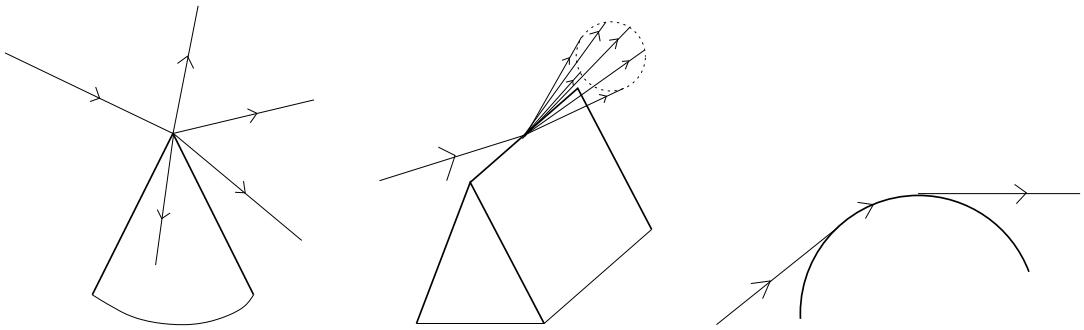

(a) Cone tip or vertex

(b) Edge or wedge

(c) Surface diffracted or creeping rays

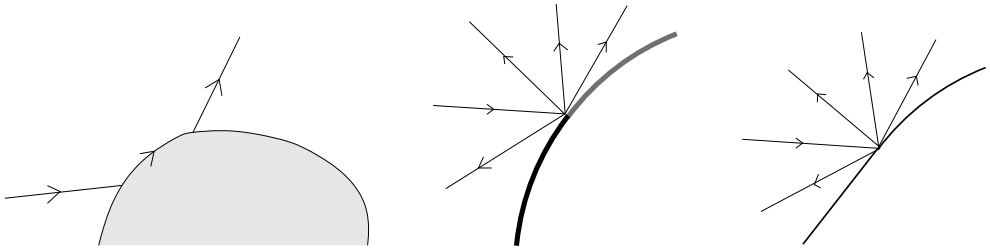

(d) Lateral waves (for penetrable structures) or surface waves (impedance boundary)

(e) Impedance jump

(f) Curvature discontinuity

**Figure 3.1:** Some of the different types of ray paths predicted by the generalization of Fermat's principle.

### 3.1.2 Rays and the WKBJ approximation

We will now consider the high-frequency approximation of solutions to Helmholtz' equation (or Maxwell's equations in the electromagnetic case). In a homogeneous medium each of the Cartesian components of the fields satisfies Helmholtz' equation, and so for simplicity we will initially examine this equation. We will subsequently discuss the differences in the vector case.

We wish to consider the asymptotic behaviour for large $k$ of solutions of

$$(\nabla^2 + N^2 k^2)\phi = 0. \tag{3.9}$$

The fundamental assumption we will make is that, in the high frequency limit, wave propagation is a local phenomenon, and in particular that the field locally resembles a plane wave (or a sum of plane waves when multiple ray fields are present). Therefore we

introduce the WKBJ ansatz

$$\phi(\boldsymbol{x}) = A(\boldsymbol{x})e^{iku(\boldsymbol{x})} \tag{3.10}$$

where the amplitude $A(\boldsymbol{x})$ and phase $u(\boldsymbol{x})$ vary on an $\mathcal{O}(1)$ length scale. We seek an asymptotic approximation to $A$ of the form

$$A(\boldsymbol{x}) \quad \sim \quad A_0(\boldsymbol{x}) + \frac{1}{ik}A_1(\boldsymbol{x}) + \frac{1}{(ik)^2}A_2(\boldsymbol{x}) + \ldots \tag{3.11}$$

(where the the asymptotic sequence is in inverse powers of $ik$ rather than $k$ to simplify some of the subsequent formulae). If this ansatz is substituted into Helmholtz' equation, and the coefficients of each power of $k$ are set equal to zero, then we obtain the sequence of equations

$$\left\{(\boldsymbol{\nabla}u)^2 - N^2\right\}A_0 = 0, \tag{3.12}$$

$$2\boldsymbol{\nabla}A_0.\boldsymbol{\nabla}u + A_0\nabla^2 u = 0, \tag{3.13}$$

$$2\boldsymbol{\nabla}A_m.\boldsymbol{\nabla}u + A_m\nabla^2 u = -\nabla^2 A_{m-1} \qquad m = 1, 2, \ldots. \tag{3.14}$$

Provided $A_0$ is non-zero the first equation (3.12) becomes

$$(\boldsymbol{\nabla}u)^2 = N^2(\boldsymbol{x}), \tag{3.15}$$

which is known as the eikonal equation. This equation is a first order PDE, and so may be solved by Charpit's method [99]. In two dimensions, if we set $p = \frac{\partial u}{\partial x}$, $q = \frac{\partial u}{\partial y}$, and write $F = \frac{1}{2}\left\{p^2 + q^2 - N^2\right\}$ then the equations of a characteristic are that

$$p_\tau = -F_x = NN_x \quad q_\tau = -F_y = NN_y \quad x_\tau = F_p = p \quad y_\tau = F_q = q \quad u_\tau = pF_p + qF_q = N^2 \tag{3.16}$$

and so these characteristics, which are the rays of the solution, satisfy

$$\mathbf{r}_{\tau\tau} = \frac{1}{2}\boldsymbol{\nabla}N^2 \qquad u_\tau = N^2, \tag{3.17}$$

or in terms of arc length $\sigma$

$$(N\boldsymbol{r}_\sigma)_\sigma = \boldsymbol{\nabla}N \qquad u_\sigma = N. \tag{3.18}$$

In the remainder of this section we will consider the case of a medium with constant refractive index, in which rays are straight lines, and without loss of generality we will set $N = 1$. If initial data $u_0(s)$ is given on the curve $(x_0(s), y_0(s))$, then $p_0(s)$ and $q_0(s)$ are found from the solution of

$$p_0(s)^2 + q_0(s)^2 = 1 \tag{3.19}$$

$$u_0'(s) = p_0(s)x_0'(s) + q_0(s)y_0'(s). \tag{3.20}$$

In general there will be two solutions for $p_0(s)$ and $q_0(s)$, but often only one of these will give a physically sensible solution. If the data is given upon an obstacle then the rays must propagate away from the obstacle at the boundary, and in any case the rays must be outgoing at infinity. From Charpit's equations (3.16) we find that $p$ and $q$ are constant on a ray, and that

$$x = p_0(s)\tau + x_0(s), \qquad y = q_0(s)\tau + y_0(s), \qquad u = \tau + u_0(s). \tag{3.21}$$

In the three-dimensional case the eikonal equation may be solved in a similar fashion, and again the rays are found to be straight lines for a homogeneous medium. The phase $u(x)$ of the solution may then be found (in principle) in the region of space spanned by the characteristics which pass through the initial data.

The amplitude of the ray solution may then be found from the amplitude (or transport) equations (3.13) and (3.14). As $\boldsymbol{\nabla} A_m . \boldsymbol{\nabla} u = \frac{\partial A_m}{\partial \tau}$ we see that each of these equations is a first-order linear ordinary differential equation for $A_m$ along the rays. Therefore, once $A_{m-1}$ and $\nabla^2 u$ are known, $A_m$ may be found by integration. If we let $J(s,\tau)$ be the Jacobian of the mapping from ray coordinates $(s,\tau)$ to Cartesian components $(x,y)$ then

$$\nabla^2 u = \frac{\partial p}{\partial x} + \frac{\partial q}{\partial y} = \frac{\partial p}{\partial s}\frac{\partial s}{\partial x} + \frac{\partial q}{\partial s}\frac{\partial s}{\partial y} = \frac{J_\tau}{J}, \tag{3.22}$$

(where the last equality is obtained by considering the inverse of (3.21)). The solutions of the amplitude equations are then seen to be

$$A_0(s,\tau)J(s,\tau)^{\frac{1}{2}} = A_0(s,0)J(s,0)^{\frac{1}{2}}, \tag{3.23}$$

$$A_m(s,\tau)J(s,\tau)^{\frac{1}{2}} = A_m(s,0)J(s,0)^{\frac{1}{2}} - \frac{1}{2}\int_0^\tau J(s,\tau')^{\frac{1}{2}}\nabla^2 A_{m-1}(s,\tau')\, d\tau'. \tag{3.24}$$

If the initial data is given on a wavefront, which is a surface on which $u$ is constant, then we may find a simple expression for $J$. In two dimensions we find that

$$J(s,\tau) = J(s,0)\frac{\rho+\tau}{\rho} \tag{3.25}$$

where $\rho$ is the initial curvature of the wavefront, with sign chosen such that $\rho > 0$ for an outgoing cylindrical wave. In three dimensions if the principal radii of curvature of the wavefront surface are $\rho_1$ and $\rho_2$ then the Jacobian is

$$J(s,\tau) = J(s,0)\frac{(\rho_1+\tau)(\rho_2+\tau)}{\rho_1\rho_2}. \tag{3.26}$$

Using these expressions in (3.23) we see that the leading order amplitude becomes infinite when $\tau + \rho_{1,2} = 0$, which corresponds to caustics of the ray-field. At such singularities the

WKBJ ansatz becomes invalid, and a local analysis must be performed to find smooth solutions valid near such points.

If we consider a narrow tube of rays then (3.23) tells us that $A_0^2 d\sigma$ is constant along the rays, where $d\sigma$ is the cross sectional area of the tube. This corresponds to conservation of energy[4] to leading order along the ray tube. (Alternatively we may rewrite equation (3.13) as $\boldsymbol{\nabla}.(A_0^2 \boldsymbol{\nabla} u)$, and identify $A_0^2 \boldsymbol{\nabla} u$ with the leading order flux of energy).

Equation (3.24) for the higher order amplitude terms is more difficult to solve, as it requires the calculation of $\nabla^2 A_{m-1}$ along a ray. In a number of special cases, such as when the ray system coincides with a simple coordinate system, or reflection from simple geometries, these terms may be calculated explicitly (some examples of which are listed in [76], including the case of plane wave incidence along the axis of symmetry upon a parabolic cylinder). For axial incidence upon a body of revolution a rather complicated expression for first order correction to the reflected field may be found in [17]. In the case of a general two-dimensional wave-field expressions for $\nabla^2$ in ray coordinates, along with recurrence relations from which $A_m$ for all $m$ be may be found, are given in [27]. These formulae are very unwieldy, and so terms beyond leading order are generally not calculated explicitly except when further approximations may be made (for instance in the case of paraxial rays). However they may be used for numerical purposes, or manipulated by means of a symbolic algebra package. Care must be taken when the rays are initiated at a caustic or focus, as is the case for edge diffracted rays, as quantities in equations (3.23) and (3.24) become infinite as we approach the singularity.

This system of equations yields an approximation to the fields, sometimes known as the Luneberg-Kline expansion, which is in the form of an asymptotic expansion [57] for large $k$. The series for $A$ is in general not convergent, but if the series is truncated after a fixed number of terms then the error in the approximation (at a fixed point) tends to zero more rapidly than the last term retained in the series as $k$ tends to infinity.

#### 3.1.2.1 Electromagnetic case

Although each of the Cartesian components of the electric and magnetic fields in a homogeneous medium separately satisfies Helmholtz' equation, additional conditions need to be satisfied for the fields to be valid solutions of Maxwell's equations. If the components of the electric field satisfy Helmholtz' equation then we require that $\nabla.\mathbf{E} = 0$, and that the magnetic field satisfies (2.14).

[4] As $A$ is possibly complex valued in actual fact the energy flow is proportional to $\mid A_0 \mid^2$, but the argument of $A_0$ can be seen to be constant along a ray from (3.23).

The behaviour of the vector solutions is made more clear if we introduce the WKBJ ansatz in vector form, namely

$$\mathbf{E} = \mathbf{E}_a e^{iku_0(x)}, \qquad \mathbf{H} = \mathbf{H}_a e^{iku_0(x)}, \tag{3.27}$$

where $\mathbf{E}_a$ has asymptotic expansion for large $k$

$$\mathbf{E}_a \quad \sim \mathbf{E}_0 + \tfrac{1}{ik}\mathbf{E}_1 + \tfrac{1}{(ik)^2}\mathbf{E}_2 + \ldots \tag{3.28}$$

and where $\mathbf{H}_a$ has a corresponding expansion. Substituting these expansions into Maxwell's equations (2.14) and (2.15) and equating terms which contain equal powers of $k$ yields the equations

$$\boldsymbol{\nabla} u \wedge \mathbf{E}_0 - \hat{\mu}\mathbf{H}_0 = 0, \tag{3.29}$$

$$\boldsymbol{\nabla} u \wedge \mathbf{H}_0 + \hat{\epsilon}\mathbf{E}_0 = 0, \tag{3.30}$$

and

$$\boldsymbol{\nabla} u \wedge \mathbf{E}_m - \hat{\mu}\mathbf{H}_m = -\boldsymbol{\nabla} \wedge \mathbf{E}_{m-1}, \tag{3.31}$$

$$\boldsymbol{\nabla} u \wedge \mathbf{H}_m + \hat{\epsilon}\mathbf{E}_m = -\boldsymbol{\nabla} \wedge \mathbf{H}_{m-1}, \tag{3.32}$$

for $m \geq 1$. From the leading order equations (3.29) and (3.30) we find (by taking the vector product of $\boldsymbol{\nabla} u$ with (3.29)) that

$$(\boldsymbol{\nabla} u)^2 = \hat{\epsilon}\hat{\mu} = N^2(x), \tag{3.33}$$

as in the scalar case, and also that

$$\mathbf{E}_0.\boldsymbol{\nabla} u = \mathbf{H}_0.\boldsymbol{\nabla} u = \mathbf{E}_0.\mathbf{H}_0 = 0. \tag{3.34}$$

Equation (3.34) gives the additional requirement that $\mathbf{E}_0$, $\mathbf{H}_0$ and $\boldsymbol{\nabla} u$ must be orthogonal, as is the case for an electromagnetic plane wave.

The vector form of the transport equations is more difficult to derive, and in a homogeneous medium it is easier to proceed from the fact that each of the Cartesian components satisfies equation (3.9) and so to leading order is given by (3.23). Therefore the directions of $\mathbf{E}_0$ and $\mathbf{H}_0$ do not change along a ray, and their amplitudes are also given by (3.23). The fields are divergence free to leading order if $\mathbf{E}_0.\boldsymbol{\nabla} u = 0$ and $\mathbf{H}_0.\boldsymbol{\nabla} u = 0$ and so we see that, provided (3.29) and (3.30) are satisfied on the initial data, we may calculate the leading order fields using the results of the scalar case.

For inhomogeneous media the full equations must be considered. By some involved manipulation of equations (3.29) - (3.32) it is possible to obtain the transport equation [68]

$$2(\boldsymbol{\nabla} u.\boldsymbol{\nabla})\mathbf{E}_m + \hat{\mu}\mathbf{E}_m\boldsymbol{\nabla}.\left(\frac{1}{\hat{\mu}}\boldsymbol{\nabla} u\right) + \frac{1}{N^2}\left(\mathbf{E}_m.\boldsymbol{\nabla} N^2\right)\boldsymbol{\nabla} u = \\ -\boldsymbol{\nabla}\left(\frac{1}{\hat{\epsilon}}\boldsymbol{\nabla}.(\hat{\epsilon}\mathbf{E}_{m-1})\right) + \hat{\mu}\boldsymbol{\nabla}\wedge\left(\frac{1}{\hat{\mu}}\boldsymbol{\nabla}\wedge\mathbf{E}_{m-1}\right), \tag{3.35}$$

and the magnetic field is found to satisfy the same equation but with $\mathbf{E}$, $\hat{\mu}$ and $\hat{\epsilon}$ replaced by $\mathbf{H}$, $-\hat{\epsilon}$ and $-\hat{\mu}$. For the leading order amplitude it may be shown that these amplitude equations reduce to

$$\boldsymbol{\nabla}.\left(\frac{1}{\hat{\mu}}\mathbf{E}_0^2\boldsymbol{\nabla} u\right) = 0, \qquad \boldsymbol{\nabla}.\left(\frac{1}{\hat{\epsilon}}\mathbf{H}_0^2\boldsymbol{\nabla} u\right) = 0, \tag{3.36}$$

which again correspond to conservation of energy along the rays.

### 3.1.3 Geometrical optics

We now consider the problem of incidence of a ray field upon an obstacle, and find an approximation to the scattered fields using the WKBJ method.

For simplicity we consider a two-dimensional convex obstacle in free space ($N = 1$), illuminated by an incident plane wave $\phi_i = e^{ikx}$. We impose the Dirichlet condition $\phi = 0$ upon the smooth boundary $(x_0(s), y_0(s))$, which is parametrized by arc length $s$ (measured in a clockwise direction), and set $\phi = \phi_i + \phi_s$. As in the previous section we introduce the WKBJ ansatz

$$\phi_s \sim \sum_{n=0}^{\infty}\frac{A_n}{(ik)^n}e^{iku} \tag{3.37}$$

for the scattered field. The boundary condition upon the scatterer is that

$$0 \sim e^{ikx} + \sum_{n=0}^{\infty}\frac{A_n}{(ik)^n}e^{iku} \tag{3.38}$$

and so the initial data for the ray solution are that $u = x_0(s)$, $A_0 = -1$ and $A_n = 0$. Now from the eikonal equation $p_0(s)^2 + q_0(s)^2 = 1$, so $p_0 = \cos\alpha(s)$, $q_0 = \sin\alpha(s)$ for some continuous $\alpha(s)$. Similarly, as the boundary is parametrized by arc length there is a function $\psi(s)$ such that $x_0'(s) = \cos\psi(s)$ and $y_0'(s) = \sin\psi(s)$. The curvature of the surface is then given by $\kappa(s) = -\psi'(s)$ (where we have chosen $\kappa$ to be positive for a convex obstacle). The launch angle $\alpha(s)$ of the scattered rays may be found from (3.20),

which becomes $\cos\psi = \cos(\psi - \alpha)$. The scattered field must propagate away from the boundary, and so $\alpha = 2\psi$ in the lit region $0 < \psi \pmod{2\pi} < \pi$, whereas in the shadow region $\alpha = 0$. To find the amplitude of the ray solution we need to evaluate the Jacobian of the ray mapping, which is

$$J = \left| \begin{array}{cc} x_s & x_\tau \\ y_s & y_\tau \end{array} \right| = \left| \begin{array}{cc} -\tau\alpha' \sin\alpha + \cos\psi & \cos\alpha \\ \tau\alpha' \cos\alpha + \sin\psi & \sin\alpha \end{array} \right| = \sin(\alpha(s) - \psi(s)) - \alpha'(s)\tau. \qquad (3.39)$$

In the lit region $\alpha'(s) = 2\psi'(s) = -2\kappa(s)$, whereas in the shadow region $\alpha'(s) = 0$. From (3.23) we find that the leading order solution for the scattered field in the lit region is

$$\phi_s \sim -\left(\frac{\sin\psi(s)}{\sin\psi(s) + 2\kappa(s)\tau}\right)^{\frac{1}{2}} e^{ikx_0(s)+ik\tau} \qquad (3.40)$$

where

$$x = x_0(s) + \tau\cos\psi(s), \qquad y = y_0(s) + \tau\sin\psi(s). \qquad (3.41)$$

The solution in the shadow region is found to be

$$\phi_s \sim -e^{ikx} \qquad (3.42)$$

to all orders in $k$, and so when we add this to the incident field we see that the total field in the unlit region is exponentially small.

We see from (3.40) that this approximate solution breaks down at a number of points. If the curvature $\kappa(s)$ is negative (which corresponds to a concave boundary) at a point in the lit region then the ray field has a caustic when $\tau = -\frac{1}{2\kappa}\sin\psi$. The solution is also not smooth near points of tangency, as $\tau$ and $\sin\psi$ both vanish there. There is additionally a discontinuity in the ray solution across the shadow boundary (the line dividing the lit and unlit regions) as the incident field switches off abruptly across this line.

Caustics of the ray field are studied in [121]. Apart from in a boundary layer near the caustic, the effect on the ray solution is to simply cause the rays to undergo a phase shift of $\frac{\pi}{2}$ as they pass through the caustic (for rays which pass through a focus this phase shift is $\pi$). However, to find the diffracted field in the shadow of the obstacle we need to match between the diffracted rays and inner solutions for regions near the point of tangency, and near the surface of the scatterer in the shadow of the obstacle.

### 3.1.4 Tangential incidence

Using Fermat's principle we expect that the diffracted fields in the shadow of an obstacle will consist of rays which are launched tangentially to the boundary. These can be

considered to be shed by a creeping or surface wave (in actual fact, a sum of a number of such modes) which travels along the boundary from the point of tangency into the unlit region. We expect that the amplitude of the launched rays will depend linearly upon the amplitude of the surface wave, and so this surface wave will be a sum of terms decaying exponentially along the boundary.

The initial data for the diffracted rays cannot simply be found by using the boundary conditions. Originally [81] the launch coefficients were found by making the assumption that the launch coefficients and decay rate depend only upon the local properties of the boundary (to leading order, the boundary conditions and the curvature of the boundary). The unknown coefficients were then found by examining the asymptotic expansion of the exact solutions in some special geometries (in particular for a circular cylinder and a sphere).

An alternative method is to consider the local solution in a boundary layer (which we will refer to as an Airy layer) near the surface of the obstacle [152], [82]. This gives the decay rates of the creeping wave modes. The initial amplitudes of the creeping wave modes are then found by matching with the local solution in the Fock-Leontovich region (F-L in Figure 3.2) [46] [140] near the point of tangency, and matching between the boundary layer and the system of shed tangential rays (for which the boundary is a caustic) yields the launch coefficients for the diffracted rays.

This ray solution is still not smooth, as the solution is discontinuous near the shadow boundary (S-B in Figure 3.2). We will see that there are a number of transition regions (T-R in Figure 3.2) near this boundary, within which solutions may be found which provide a smooth transition between the reflected and diffracted fields.

All of this analysis is studied in more detail in [134], [121] and [140], and so here we just state the results and scalings for each of the asymptotic regions in the specific case of plane wave incidence upon an obstacle with Dirichlet boundary conditions.

#### 3.1.4.1 Fock-Leontovich region

We first introduce curvilinear locally tangential and normal coordinates[5] $s$ and $n$ as shown in Figure 3.3, where where $s$ is arc length along the surface from the point of tangency, and $n$ is distance in a normal direction from the boundary. The incident and scattered fields are almost tangential to the boundary in this region, and so we seek a solution of

[5]It is possible to instead find the solution in the F-L region using cartesian coordinates [140], but this coordinate system is needed in the Airy layer.

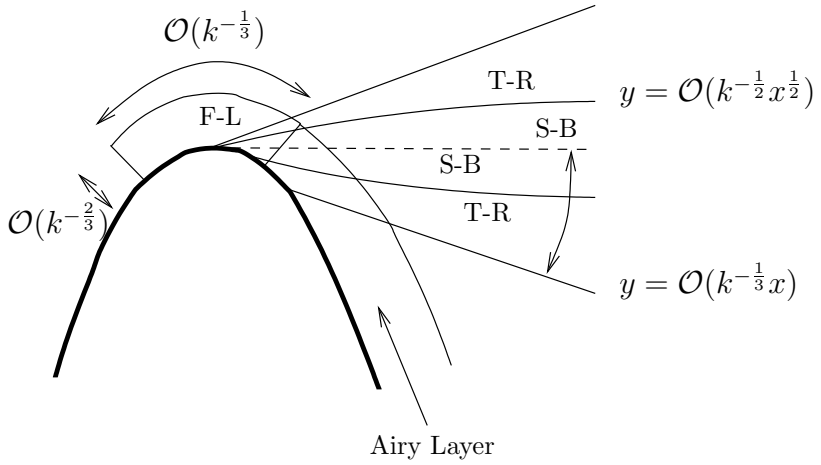


**Figure 3.2:** Asymptotic regions for tangential incidence of plane wave.

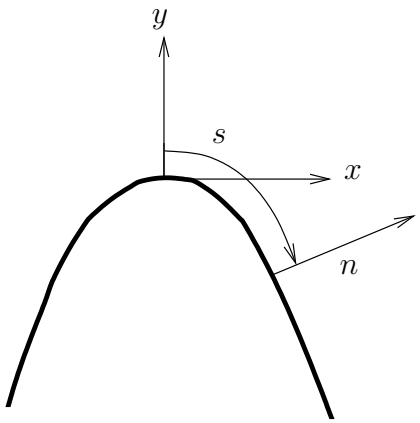


**Figure 3.3:** Curvilinear locally tangential and normal coordinates $s$ and $n$ for the Fock-Leontovich region.

the form

$$\phi = A(s,n)e^{iks}. \tag{3.43}$$

Fock initially found the fields in this region by examining the solution of scattering by a paraboloid, but later realised that a parabolic equation for $A$ could be found by making the assumption that the derivatives of the amplitude in the normal direction are much greater than those in a tangential direction. We therefore introduce the scalings $s = k^{-\frac{1}{3}}\kappa_0^{-\frac{2}{3}}\tilde{s}$ and $n = k^{-\frac{2}{3}}\kappa_0^{-\frac{1}{3}}\tilde{n}$, where $\kappa_0$ is the curvature of the obstacle at the point of tangency.

We wish to find a solution to Helmholtz' equation which satisfies the boundary condition

$$\phi = 0 \tag{3.44}$$

on the surface ($n = 0$), and which matches with the incident field. We seek an asymptotic expansion for large $k$ of $A$ of the form

$$A \sim A_0(\tilde{s}, \tilde{n}) + k^{-\frac{1}{3}} A_1(\tilde{s}, \tilde{n}) + k^{-\frac{2}{3}} A_2(\tilde{s}, \tilde{n}) + \dots . \tag{3.45}$$

When these scalings and this expansion are substituted into Helmholtz' equation then, to leading order, it becomes

$$\frac{\partial^2 A_0}{\partial \tilde{n}^2} + 2i \frac{\partial A_0}{\partial \tilde{s}} + 2\tilde{n} A_0 = 0. \tag{3.46}$$

The appropriate solution to this inner problem is then found to be

$$\phi = 2^{\frac{1}{3}} e^{iks} \int_{-\infty}^{\infty} \left( \mathrm{Ai}(-2^{\frac{1}{3}}(p + \tilde{n})) - \frac{\mathrm{Ai}(-2^{\frac{1}{3}} p)}{\mathrm{Ai}(-2^{\frac{1}{3}} e^{\frac{2\pi i}{3}} p)} \mathrm{Ai}(-2^{\frac{1}{3}} e^{\frac{2\pi i}{3}} (p + \tilde{n})) \right) e^{-i\tilde{s}p} dp, \tag{3.47}$$

This solution matches with the inner limit of the incident and reflected fields. We also expect that it will match with a wave which travels along the surface of the obstacle, shedding rays into the unlit region, and we will consider this creeping wave in the next section.

#### 3.1.4.2 Airy layer and shed creeping field

We now examine the solution in the boundary layer near the obstacle in the unlit region, which we will refer to as the Airy layer. The solution in this layer will consist of a series of creeping ray modes, which propagate almost tangentially to the boundary, shedding diffracted rays tangentially to the boundary. The analysis in the Airy layer will give the decay rate for these modes, and by matching both with the Fock region solution and the shed rays the launch coefficients for the diffracted rays may be found.

In this boundary layer we introduce the scaling $n = k^{-\frac{2}{3}} \hat{n}$ ($s$ is now distance on the original outer length scale), and seek a solution of the form

$$\phi = A(s, \hat{n}) e^{iks + ik^{\frac{1}{3}} v(s)}. \tag{3.48}$$

We again pose an asymptotic expansion of $A$ in inverse powers of $k^{-\frac{1}{3}}$. When this ansatz for the solution is substituted into Helmholtz' equation and terms of equal order in $k$ are equated then the first two non-trivial equations are

$$\frac{\partial^2 A_0}{\partial \hat{n}^2} - 2v'(s) A_0 + 2\hat{n}\kappa(s) A_0 = 0, \tag{3.49}$$

$$\frac{\partial^2 A_1}{\partial \hat{n}^2} - 2v'(s) A_1 + 2\hat{n}\kappa(s) A_1 = -2i \frac{\partial A_0}{\partial s}. \tag{3.50}$$

By means of the substitution $\eta = \kappa^{-\frac{2}{3}}(s)(\kappa(s)\hat{n} - v'(s))$ we find that

$$A_0 = \alpha(s)\mathrm{Ai}(-2^{\frac{1}{3}}e^{\frac{2\pi i}{3}}\eta), \tag{3.51}$$

and the boundary condition is satisfied if

$$\mathrm{Ai}(2^{\frac{1}{3}}\kappa(s)^{-\frac{2}{3}}v'(s)) = 0 \tag{3.52}$$

so we find that

$$v'(s) = 2^{-\frac{1}{3}}\kappa^{\frac{2}{3}}(s)e^{-\frac{2\pi i}{3}}a_m, \tag{3.53}$$

where $a_m$ is the $m^{\text{th}}$ root of $\mathrm{Ai}(a_m) = 0$ (all of which lie on the negative real axis). However the dependence of the amplitude of a mode on $s$ is not determined by the leading order equation, and instead must be found from the solvability condition for the equation for $A_1$. This solvability condition becomes

$$\frac{d}{ds}\int_0^\infty A_0^2 \, d\hat{n} = 0 \tag{3.54}$$

and from this it can be found that the variation in $A_0$ along a creeping ray is proportional to $\kappa(s)^{\frac{1}{6}}$. From (3.53) we find that $v'(s)$ has positive imaginary part, and so from (3.48) it can be seen that the amplitude of the creeping ray mode decreases as it propagates along the surface. The launch coefficient for each of the modes may be found by matching with the solution in the Fock-Leontovich region, where each of the creeping modes corresponds to a pole contribution from (3.47), and the total solution in the Airy layer is found to be

$$\begin{aligned}\phi \sim &- \frac{2\pi e^{-\frac{\pi i}{6}}\kappa(s)^{\frac{1}{6}}}{\kappa_0^{\frac{1}{6}}}\times \\ &\times \sum_{m=0}^{\infty}\frac{\mathrm{Ai}(e^{-\frac{2\pi i}{3}}a_m)}{\mathrm{Ai}'(a_m)}\mathrm{Ai}(-2^{\frac{1}{3}}e^{\frac{2\pi i}{3}}\kappa(s)^{\frac{1}{3}}\hat{n} + a_m)\exp\left(iks + \frac{ik^{\frac{1}{3}}a_m e^{-\frac{2\pi i}{3}}}{2^{\frac{1}{3}}}\int_0^s \kappa(s')^{\frac{2}{3}}ds'\right).\end{aligned} \tag{3.55}$$

This solution then can be seen to match with the shed creeping ray field, which is a system of diffracted rays which are launched tangentially from the boundary. To do this we introduce ray coordinates $(\rho, \tau)$ as shown in Figure 3.4, where $\rho$ is the distance along the surface from the point of tangency to where the ray is launched, and $\tau$ denotes distance along the ray. By matching with the Airy layer the shed field is found to be

$$\phi \sim -\sum_0^\infty \frac{\sqrt{\pi}e^{-\frac{\pi i}{12}}2^{\frac{1}{6}}\mathrm{Ai}(e^{-\frac{2\pi i}{3}}a_m)}{k^{\frac{1}{6}}\kappa_0^{\frac{1}{6}}\kappa(\rho)^{\frac{1}{6}}\mathrm{Ai}'(a_m)\sqrt{\tau}}\exp\left(ik(\rho+\tau) + ik^{\frac{1}{3}}a_m e^{-\frac{2\pi i}{3}}2^{-\frac{1}{3}}\int_0^\rho \kappa(\rho')^{\frac{2}{3}}d\rho'\right). \tag{3.56}$$

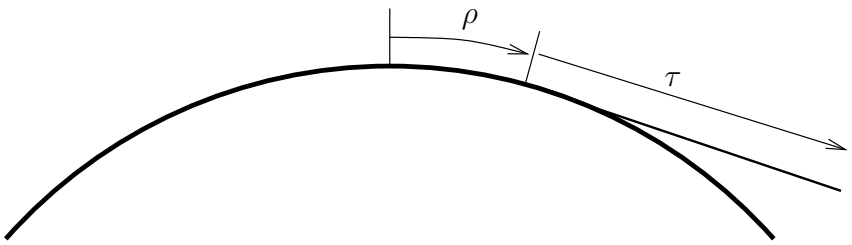


**Figure 3.4:** Coordinate system for shed creeping ray field.

The terms for $m \geq 1$ are all exponentially small when $s = \mathcal{O}(1)$ compared with the leading order mode, and so it is possible that the coefficients of the higher order modes might change abruptly (due to the Stokes phenomena) as they propagate along the boundary in the shadow region.

#### 3.1.4.3 Shadow boundary

Across the shadow boundary the incident field switches off, and so the geometrical optics fields are discontinuous across this line. The actual fields are analytic at points away from the boundary, and so there must be a region near this line within which the incident field switches off smoothly.

For plane wave incidence let $x$ be distance along the shadow boundary, and $y$ distance normal to the shadow boundary. If we introduce the scaling $y = k^{-\frac{1}{2}}\hat{y}$, and write $\phi = A(x, \hat{y})e^{ikx}$, then to leading order Helmholtz' equation becomes

$$\frac{\partial^2 A}{\partial \hat{y}^2} + 2i\frac{\partial A}{\partial x} = 0. \tag{3.57}$$

A suitable solution can be found by similarity methods, in terms of the variable $\xi = \hat{y}/\sqrt{x}$, namely

$$\phi \sim \frac{1}{2}\ \mathrm{erfc}\left(-\frac{\hat{y}e^{-\frac{\pi i}{4}}}{\sqrt{2x}}\right) e^{ikx}, \tag{3.58}$$

and this can be seen to match with the $\mathcal{O}(1)$ terms in the ray solutions for the incident field and the shadow region.

In the case when the incident field is due to a point source at an $\mathcal{O}(1)$ distance, rather than a plane wave, then the shadow boundary is a hyperbolic region rather than a parabolic region, as illustrated in Figure 3.5. For plane wave incidence it can be seen from the above solution that the shadow boundary is essentially parabolic in profile, subtending an infinitely small angle in the far field. However, in two dimensions, an incident cylindrical wave gives hyperbolic shadow boundary regions (as can be seen in



**Figure 3.5:** Shadow boundaries for plane wave and line source illumination. The shadow boundary is parabolic for plane wave incidence (left-hand diagram), and hyperbolic for line source incidence (right-hand diagram).

[30]), and so these affect a small but finite portion of the far field directivity of the scattered fields.

#### 3.1.4.4 Transition Region

The above solution for the shadow boundary region does not match with the limit of the reflected field as we approach the shadow boundary, or with the limit of the shed creeping ray solution for rays launched near the point of tangency. It seems quite likely that rays reflected or shed from points within the Fock-Leontovich region will not have the same form as those which are reflected or shed from points outside the Fock region. This indeed proves to be the case, and there are transition regions above and below the shadow boundary region within which the scattered field has different behaviour.

If we return to the coordinate system used in the shadow boundary region, and introduce the scaling $y = k^{-\frac{1}{3}}\tilde{y}$ then the solution in both of these transition regions becomes

$$\phi \sim -\frac{e^{\frac{\pi i}{12}} \exp\left(ikx + ik^{\frac{1}{3}}\frac{\tilde{y}^2}{2x} - i\frac{\tilde{y}^3}{6x^3\kappa_0}\right)}{k^{\frac{1}{6}}\kappa_0^{\frac{1}{3}}\sqrt{2\pi x}} \int_{-\infty}^{\infty} \frac{\mathrm{Ai}(-2^{\frac{1}{3}}p)}{\mathrm{Ai}(-2^{\frac{1}{3}}e^{\frac{2\pi i}{3}}p)} \exp\left(\frac{ip\tilde{y}}{x\kappa_0^{\frac{1}{3}}}\right) dp, \tag{3.59}$$

which is found through matching with the solution in the Fock-Leontovich region.

### 3.1.5 Wedges and edges

Not all scatterers are smooth, and in particular many possess sharp edges or wedges. From the discussion of the generalized Fermat's principle we expect that the scattered fields will consist of fields reflected from one or both faces of the edge or wedge, along with a diffracted field (which consists of cones of rays which make the same angle with the edge as the incident ray at each point along the discontinuity). The launch coefficients

for the diffracted rays may be found by matching the ray solution with the solutions of inner problems, and in general this inner region is of size $\mathcal{O}(k^{-1})$ about each point on the edge. The inner problem usually reduces to the canonical problem of plane wave diffraction by an infinite half-plane or wedge, and in many circumstances the analytic solution to this problem can be found.

As in the case of a smooth body the ray solutions for the incident and reflected fields switch off abruptly across a number of lines in the plane (in general these are different lines for the reflected and incident field, which contrasts with the case of a smooth body where these fields switch on/off across the same line), and it may be seen that the amplitude of the diffracted fields also becomes large near the shadow boundaries. The same shadow boundary solutions may be found in this region as for scattering by a smooth body, and in this case the local error function solutions do not only smooth the discontinuity in the reflected field, but also cancel with the singularity in the diffractivity for the leading order diffracted fields, giving a solution which remains finite everywhere except near the edge (where the inner solution must be used), and near caustics of the reflected and diffracted fields.

# Chapter 4

# Diffraction by Thin Bodies

In Chapter 3 we reviewed the problem of diffraction of a high-frequency plane wave by a smooth convex obstacle. Using the Geometrical Theory of Diffraction, which combined ray methods with local analysis near points at which diffraction occurred, we saw that it was possible to find an asymptotic description of the fields at all points external to the scatterer.

On a thin body, with an $\mathcal{O}(k^{-\frac{1}{2}})$ aspect ratio, there are tightly curved "edges" where one of the radii of curvature is of the same order of magnitude as the wavelength[1]. Such a situation lies between the cases of a blunt body and a sharp edge, and neither of these (formally invalid) results gives an acceptable scattered field. Instead we will generalise and extend the two-dimensional scalar analysis of Engineer et al. [44] to the three-dimensional electro-magnetic problem. This will only prove possible analytically for a perfectly conducting body, when the inner problem of diffraction by a parabolic cylinder decomposes into two uncoupled scalar problems, corresponding to different polarisations of the electro-magnetic fields. The two resulting problems are essentially two dimensional, and will reduce to the problem of scattering by a thin parabola considered (for one of the two boundary conditions) in [44]. The solutions to these scalar problems may be written as integrals of special functions.

In a similar manner to [44] we will find the far field of the inner problem, which we then match into a system of diffracted rays. Our most significant extension to this work is the detailed analysis of the shadow boundary within which the reflected field is switched on/off. This proves to be much larger in extent than the corresponding transition regions

[1]It is possible to see that an aspect ratio of $\mathcal{O}(k^{-\frac{1}{2}})$ corresponds to a tip radius of curvature of the same order as the wavelength by considering the ellipse $\frac{x^2}{a^2} + \frac{y^2}{b^2} = 1$, for which the radii of curvature at the ends of the major axis are both $b^2/a$. If we non-dimensionalize with the length $a$, the radius of curvature at the tip is $b^2/a^2$, which is the square of the aspect ratio $b/a$.

found for blunt bodies or sharp edges.

## 4.1 Formulation of the problem

We will consider an E-M plane wave incident upon a thin body with flat mid-surface and aspect ratio $\mathcal{O}(k^{-\frac{1}{2}})$. This is representative of the leading edge of an aircraft wing. Choosing a coordinate system with $y$ axis normal to the mid-plane of the body, the upper and lower surfaces will be described by

$$y = k^{-\frac{1}{2}} f^{\pm}(x, z), \tag{4.1}$$

for some functions $f^{\pm}$, and we will assume that the surface is everywhere smooth.

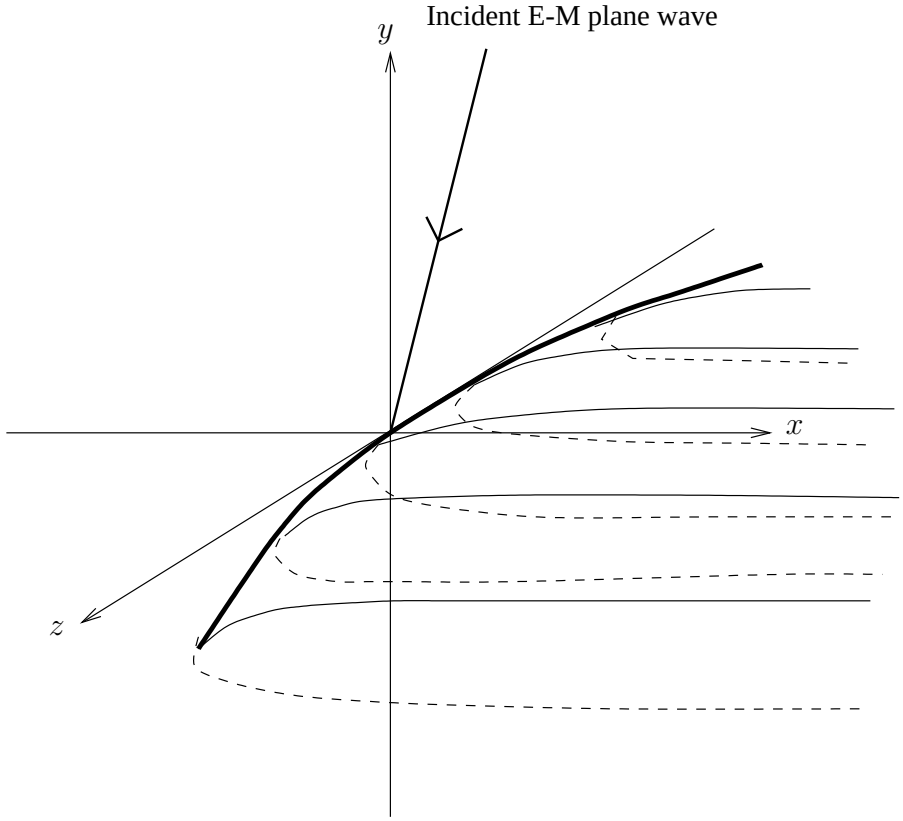


**Figure 4.1:** Incidence of a plane wave upon a thin body.

Outside the body the fields will satisfy the free-space Maxwell equations in the form (2.14) - (2.17), and we will impose perfectly conducting boundary conditions upon the surface. As the domain under consideration is infinite we will also require that the scattered fields satisfy the radiation conditions (2.40) - (2.42) to ensure uniqueness.

### 4.1.1 Geometrical optics field

The field reflected by the body may be found by the usual geometrical optics methods, as discussed in Section 3.1.3. However this approximation is not valid for those rays which reflect from points on the scatterer where the curvature of the body is very large; more precisely, it is invalid for those points at a distance $\mathcal{O}(k^{-1})$ from the edges of the body, where the radius of curvature is of the same order of magnitude as the wavelength. As the geometrical optics approximation breaks down there we expect diffraction to occur at the edges of the scatterer.

For all practical purposes the outer reflected field may be found by the standard ray tracing method. However from (4.1) we see that away from its edges the scatterer is approximately flat, with $\mathcal{O}(k^{-\frac{1}{2}})$ curvature and thickness. This allows us to pose an ansatz of the form

$$\psi = A(x, y, z)e^{iku(x,y,z)+ik^{\frac{1}{2}}U(x,y,z)} \tag{4.2}$$

(as in [44], where the 2-D scalar case was discussed) for each of the Cartesian components of the electric and magnetic fields. This may be substituted into Maxwell's equations, and the equations and boundary conditions (including the location of the boundary) expanded in powers of $k$. By this method it is possible to find the approximate reflected field, which exists where the reflected field would be present if the scatterer was flat and infinitely thin. In fact, for a known shape (such as the parabolic cylinder we will consider later) it is easier to calculate the reflected fields from the geometrical optics formula of Section 3.1.3, and then asymptotically expand the fields in the form (4.2).

### 4.1.2 Inner problem near "edges"

In addition to the geometrical optics contribution we expect there to be a diffracted field from the tightly curved edges. By considering Fermat's principle, as discussed in [74], this will consist of a cone of outgoing rays, which each make the same angle with the edge as the incident wave (as in the case of diffraction by a sharp edge or wedge). In order to find the phase and amplitude of these diffracted rays we need to consider an inner region near the edge. We will solve this inner problem, and then match its far field with the diffracted rays in the outer problem.

If we consider a point on the leading edge of the body, we may assume without loss of generality that this point is at the origin, with the leading edge along the $z$-axis. As the surface is smooth we may invert the maps $f^+$ and $f^-$ locally to give the surface in the form $x = g(k^{1/2}y, z)$. To obtain a leading-order balance in Maxwell's equations

(2.14) - (2.17), we rescale the spatial coordinates with the non-dimensional wavelength $k^{-1}$. Maxwell's equations are as before except with $k = 1$, and the surface becomes

$$k^{-1}x = g(k^{-\frac{1}{2}}y, k^{-1}z). \tag{4.3}$$

Expanding $g$ in its power series about the origin, and assuming all of its derivatives to be $\mathcal{O}(1)$, we find that

$$x = \frac{y^2}{2}g_{yy}(0,0) + \mathcal{O}(k^{-\frac{1}{2}}). \tag{4.4}$$

Thus the inner problem is that of scattering of an obliquely incident E-M wave (with wavenumber $k = 1$) by a parabolic cylinder.

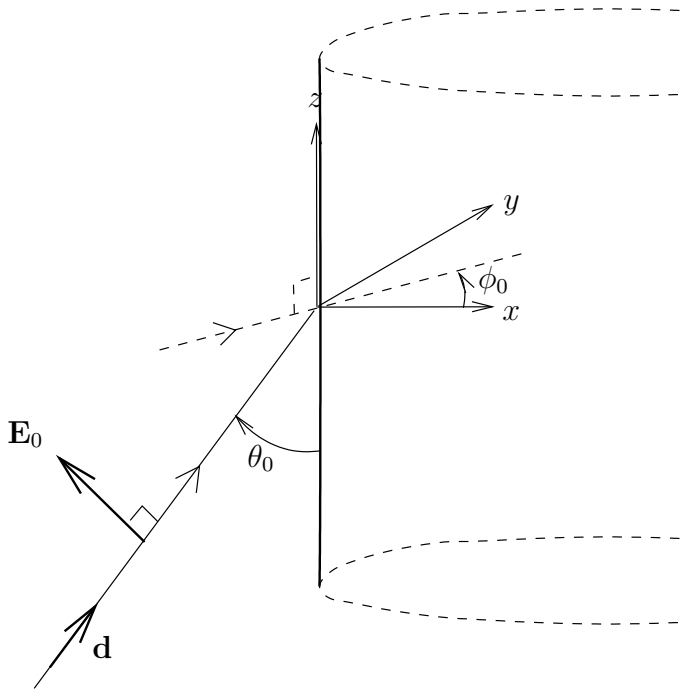


**Figure 4.2:** Coordinate system for the inner problem. Here **d** is the direction of propagation of the incident plane wave.

### 4.1.3 Decomposition of inner problem into polarisations

In this inner coordinate system, the incident plane wave may be expressed in the form

$$\mathbf{E} = \mathbf{E_0}\exp(i\boldsymbol{x}.\mathbf{d}), \tag{4.5}$$

where

$$\mathbf{E_0} = (l_0, m_0, n_0) \quad \text{and} \quad \mathbf{d} = (\cos\phi_0 \sin\theta_0, \sin\phi_0 \sin\theta_0, \cos\theta_0), \tag{4.6}$$

and $\mathbf{H}$ can be found from this by one of Maxwell's equations (2.14).

As noted by Jones [66] and Wait [145], this field may be decomposed into two modes for which $H_z$ and $E_z$ are zero respectively, namely

$$\mathbf{E} = \mathbf{E}_1 \exp(i\boldsymbol{x}.\mathbf{d}), \qquad \mathbf{E}_1 = l_1(-\cos\phi_0, -\sin\phi_0, \tan\theta_0), \tag{4.7}$$

and

$$\mathbf{E} = \mathbf{E}_2 \exp(i\boldsymbol{x}.\mathbf{d}), \qquad \mathbf{E}_2 = l_2(\sin\phi_0, -\cos\phi_0, 0), \tag{4.8}$$

where $l_1 = n_0 \cot\theta_0$, and $l_2 = l_0 \sin\phi_0 - m_0 \cos\phi_0$. The whole problem is linear, so we may consider these two modes incident upon the edge separately, and then combine the two solutions to find the total fields. As the incident fields only depend on $z$ through a multiplicative factor $\exp(iz\cos\theta)$ we may assume that the $z$- dependence of the scattered fields is also of this form. When we do this the problems become essentially two dimensional. For the polarization where $E_z$ is zero everywhere, Maxwell's equations become

$$(\nabla^2_{x,y} + \sin^2\theta_0)H_z = 0, \tag{4.9}$$

and

$$E_x \sin^2\theta_0 = i\frac{\partial}{\partial y}H_z, \qquad E_y \sin^2\theta_0 = -i\frac{\partial}{\partial x}H_z, \tag{4.10}$$

$$H_x = -\cos\theta_0 E_y, \qquad H_y = \cos\theta_0 E_x, \tag{4.11}$$

and the perfectly conducting boundary condition (2.26) is that $\frac{\partial H_z}{\partial n} = 0$ on the boundary of the cylinder. For the other polarization, where $H_z$ is everywhere zero, we similarly find that $E_z$ must satisfy the 2-D Helmholtz equation (with wavenumber $\sin\theta_0$) and the boundary condition is now that $E_z = 0$ on the boundary. The other field components may again be found from $E_z$ and Maxwell's equations. If $\psi_n$, $\psi_d$ have a wavenumber $\cos\theta$ in the $z$-direction, and satisfy $(\nabla^2_{x,y} + \sin^2\theta_0)\psi = 0$ outside the parabolic cylinder, along with Neumann and Dirichlet boundary conditions respectively on the boundary, then (as in [66] p. 482),

$$\mathbf{E} = \frac{l_1}{\sin\theta_0\cos\theta_0}(\mathbf{e}_z + i\cos\theta_0\nabla)\psi_d + \frac{il_2}{\sin\theta_0}\mathbf{e}_z \wedge \nabla\psi_n, \tag{4.12}$$

and

$$\mathbf{H} = \frac{il_1}{\sin\theta_0\cos\theta_0}\mathbf{e}_z \wedge \nabla\psi_d - \frac{l_2}{\sin\theta_0}(\mathbf{e}_z + i\cos\theta_0\nabla)\psi_n, \tag{4.13}$$

satisfy Maxwell's equations (in our inner coordinates). Furthermore, if $\psi_n$ and $\psi_d$ satisfy the scalar radiation conditions with an incident plane wave

$$\psi_i = \exp(i(x\sin\theta_0\cos\phi_0 + y\sin\theta_0\sin\phi_0)), \tag{4.14}$$

then the E-M fields may be seen to satisfy appropriate radiation conditions for incidence of the plane wave (4.5), namely that the far field of the scattered part of this inner solution propagates away from the edge.

### 4.1.4 Solution of the scalar problems

On scaling both $x$ and $y$ with $(\sin\theta_0)^{-1}$ the two scalar problems become

$$\left(\frac{\partial^2}{\partial x^2}+\frac{\partial^2}{\partial y^2}+1\right)\psi=0 \tag{4.15}$$

with

$$\psi_d=0, \quad \frac{\partial\psi_n}{\partial n}=0, \quad \text{on} \quad y=\pm\beta(2x)^{\frac{1}{2}}, \tag{4.16}$$

where, in the notation used earlier,

$$\beta=(g_{yy})^{-\frac{1}{2}}(\sin\theta_0)^{\frac{1}{2}}. \tag{4.17}$$

We also require that the solutions satisfy the scalar radiation conditions for this incident plane wave, namely

$$\psi-\psi_i=\mathcal{O}(1/r), \quad \left(\frac{\partial}{\partial r}+i\right)(\psi-\psi_i)=o(1/r), \qquad \text{as } r\to\infty. \tag{4.18}$$

#### 4.1.4.1 Parabolic coordinates

As the boundary is a parabola it is natural to work in a parabolic cylinder coordinate system $(\xi,\eta)$, which is related to Cartesian coordinates by

$$x=\frac{\xi^2}{2}-\frac{\eta^2}{2}+\frac{\beta^2}{2}, \qquad y=\xi\eta. \tag{4.19}$$

We have chosen the origin of our parabolic coordinate system to be at $x=\frac{\beta^2}{2}$, $y=0$, as the boundary is then given by $\eta=\beta$. Helmholtz' equation becomes

$$\frac{\partial^2\psi}{\partial\xi^2}+\frac{\partial^2\psi}{\partial\eta^2}+(\xi^2+\eta^2)\psi=0, \tag{4.20}$$

and the incident plane wave is now

$$\psi_i=\exp\left\{i\left(\left(\frac{\xi^2-\eta^2+\beta^2}{2}\right)\cos\phi_0+\xi\eta\sin\phi_0\right)\right\}. \tag{4.21}$$

In order to simplify the following work slightly we will write

$$\psi=\exp\left(\frac{i\beta^2\cos\phi_0}{2}\right)\Psi \tag{4.22}$$

to remove a common pre-factor from the expressions for the fields. We shall find it convenient to also use polar coordinates $(r, \phi)$ centred at the focus of the parabola, and these are related to the parabolic coordinates by

$$\xi = \sqrt{2r}\cos\frac{\phi}{2}, \qquad \eta = \sqrt{2r}\sin\frac{\phi}{2}. \tag{4.23}$$

Parabolic coordinates are one of the small number of coordinate systems for which Helmholtz' equation is separable (see [95] and [66] for discussion of others). The separable solutions are of the form $\Xi(\xi)H(\eta)$, where $\Xi(\xi)$ is one of

$$D_\nu(\bar{p}\xi), D_\nu(-\bar{p}\xi), D_{-1-\nu}(p\xi), D_{-1-\nu}(-p\xi), \tag{4.24}$$

and $H(\eta)$ is one of

$$D_\nu(p\eta), D_\nu(-p\eta), D_{-1-\nu}(\bar{p}\eta), D_{-1-\nu}(-\bar{p}\eta). \tag{4.25}$$

Here $\nu$ is a possibly complex-valued constant, $p = \sqrt{2}e^{\frac{\pi i}{4}}$, and an overline represents complex conjugation. The functions $D_\nu(z)$ are parabolic cylinder functions (PCFs), and their properties are summarized in Appendix A.

#### 4.1.4.2 Representation of incident field

In order to solve our problem we require a representation of the incident plane wave in terms of these separable solutions. We will then find the scattered field as a linear combination of those separable solutions which are outgoing at infinity.

It is, however, not necessary to find an exact representation of the incident plane wave; all that we require is a representation with the same incoming behaviour in the far field. Thus, as noted in [66, p 469] we may use the result of Cherry [29] that

$$I_i \;=\; \frac{1}{2}\Psi_i \mathrm{erfc}(\bar{p}\sqrt{r}\sin\frac{1}{2}(\phi_0-\phi)) \;\equiv\; \frac{i}{2\sqrt{2\pi}}\int_{-\frac{1}{2}-i\infty}^{-\frac{1}{2}+i\infty}\frac{(\tan\frac{\phi_0}{2})^\nu}{\cos\frac{\phi_0}{2}}(D_{-1-\nu}(-\bar{p}\eta)D_\nu(\bar{p}\xi))\frac{d\nu}{\sin(\nu\pi)}, \tag{4.26}$$

where $\Psi_i = \exp\left\{i\left(\left(\frac{\xi^2-\eta^2}{2}\right)\cos\phi_0 + \xi\eta\sin\phi_0\right)\right\}$. From the asymptotic expansion of the complementary error function [3] we find that

$$I_i = \Psi_i + \frac{e^{ir+\frac{\pi i}{4}}}{2\sqrt{2\pi r}\sin\frac{1}{2}(\phi_0-\phi)} + \mathcal{O}(r^{-1}) \tag{4.27}$$

as $r$ tends to infinity in $\phi_0 < \phi < 2\pi$ (the illuminated region), and

$$I_i = \frac{e^{ir+\frac{\pi i}{4}}}{2\sqrt{2\pi r}\sin\frac{1}{2}(\phi_0-\phi)} + \mathcal{O}(r^{-1}) \tag{4.28}$$

as $r$ tends to infinity elsewhere (the shadow region). Thus the far field of $I_i$ consists of the incoming plane wave along with an outgoing field. Now all we need to do is to add on a further outgoing field to satisfy the boundary conditions on the parabola.

Motivated by the form of $I_i$, we will consider the set of separable solutions with $\nu = -\frac{1}{2} + i\mu$ for real $\mu$. By using the expansions (A.15) - (A.17) for the large $z$ behaviour of $D_\nu(z)$ we see that $D_{-1-\nu}(\bar{p}\eta)D_\nu(\bar{p}\xi)$ is the only one of our separable solutions which is outgoing for large (positive) $\xi$ and $\eta$. Thus we attempt to write the total field as

$$\Psi = I_i + \int_{-\frac{1}{2}-i\infty}^{-\frac{1}{2}+i\infty} F(\nu) D_\nu(\bar{p}\xi) D_{-1-\nu}(\bar{p}\eta) d\nu \tag{4.29}$$

where $F(\nu)$ is a suitable weight function. Choosing $F(\nu)$ to satisfy the boundary conditions on $\eta = \beta$, we find that the solutions $\Psi_n$ and $\Psi_d$ are

$$\Psi_n = \frac{i}{2\sqrt{2\pi}} \int_{-\frac{1}{2}-i\infty}^{-\frac{1}{2}+i\infty} \frac{(\tan\frac{\phi_0}{2})^\nu}{\cos\frac{\phi_0}{2}} (D_{-1-\nu}(-\bar{p}\eta) + \frac{D'_{-1-\nu}(-\bar{p}\beta)}{D'_{-1-\nu}(\bar{p}\beta)} D_{-1-\nu}(\bar{p}\eta)) D_\nu(\bar{p}\xi) \frac{d\nu}{\sin(\nu\pi)}, \tag{4.30}$$

$$\Psi_d = \frac{i}{2\sqrt{2\pi}} \int_{-\frac{1}{2}-i\infty}^{-\frac{1}{2}+i\infty} \frac{(\tan\frac{\phi_0}{2})^\nu}{\cos\frac{\phi_0}{2}} (D_{-1-\nu}(-\bar{p}\eta) - \frac{D_{-1-\nu}(-\bar{p}\beta)}{D_{-1-\nu}(\bar{p}\beta)} D_{-1-\nu}(\bar{p}\eta)) D_\nu(\bar{p}\xi) \frac{d\nu}{\sin(\nu\pi)}; \tag{4.31}$$

these expressions agree with the various integral representations in [66], [113], [44]. We note that that it is impossible to satisfy impedance boundary conditions (with constant impedance) on the parabola by this method, as

$$\frac{\partial}{\partial n} = \frac{1}{\sqrt{\xi^2 + \eta^2}} \frac{\partial}{\partial \eta}, \tag{4.32}$$

so the problem is not separable. For a blunt parabola with $\beta \gg 1$, then $\beta^2 + \xi^2$ is approximately constant in the region near the point of tangency, but in the current work $\beta$ will be $\mathcal{O}(1)$.

It is possible to find solutions to the (two-dimensional) problem of normal incidence upon a dielectric parabola [150] (and also for a coated perfectly conducting parabola [96]). The starting point for these solutions is the expression

$$\Psi_i = \begin{cases} \sec\frac{\phi_0}{2} \sum_{n=0}^\infty \frac{(i\tan\frac{\phi_0}{2})^n}{n!} D_n(\bar{p}\xi) D_n(p\eta) & 0 < \phi_0 < \frac{\pi}{2} \\ \operatorname{cosec}\frac{\phi_0}{2} \sum_{n=0}^\infty \frac{(i\cot\frac{\phi_0}{2})^n}{n!} D_n(p\xi) D_n(\bar{p}\eta) & \frac{\pi}{2} < \phi_0 < \pi \end{cases} \tag{4.33}$$

for the incident plane wave. In the case $0 < \phi_0 < \frac{\pi}{2}$ a solution was sought in the form

$$\Psi = \begin{cases} \Psi_i + \sum_{n=0}^\infty a_n D_n(\bar{p}\xi) D_{-n-1}(\bar{p}\eta) & \eta > \beta \\ \sum_{n=0}^\infty b_n D_n(\bar{p}N^{\frac{1}{2}}\xi) D_n(pN^{\frac{1}{2}}\eta) & 0 < \eta < \beta. \end{cases} \tag{4.34}$$

The constants $a_n$ and $b_n$ are determined by continuity of $\Psi$ and $\frac{1}{\hat{\mu}}\frac{\partial \Psi}{\partial \eta}$ at $\eta = \beta$ (in the case of TE polarization). However, unlike the case of a penetrable circular cylinder, the functions describing the tangential variation of the fields are not the same inside and outside the parabolic cylinder. The continuity conditions therefore yield an infinite matrix equation, and the solutions are difficult to study numerically. Some simplification was possible [150] in the case when both $\beta N^{\frac{1}{2}}$ and $\beta$ are small, as the PCFs may be approximated by their power series expansions for small argument. The expressions for the coefficients of the series are still in a very complicated form, and are not amenable to further analysis.

Solutions have also been found for the two-dimensional problem of a line source parallel to a parabolic cylinder [84], [17, Ch. 7] (we note here that the integrals of the two results have different integrands). The integral of [84] has been studied by stationary phase methods in the case when the line source is on the surface of the cylinder, and the curvature at the tip is large [19]. This integral for line source incidence is of a similar form to those considered below, but the integrand contains more distinct PCFs (nine in the general case, and six when the source is on the surface), and so the analysis of the integrals is correspondingly more complicated.

We note here that, by the principle of reciprocity, the directivity of the far field generated by a line source within the $\mathcal{O}(k^{-1})$ tip region can be found from the above solutions for plane wave incidence. At a point within the inner region $\xi$, $\eta$, $\beta$ are all $\mathcal{O}(1)$, and so we cannot approximate this expression for the fields any further.

For a line source at a distance much greater than a wavelength away from the tip, the incident field within the inner region will be approximately a plane wave, and so we expect that the results of this chapter will be valid (to leading order), except in the vicinity of the shadow boundaries.

## 4.2 Asymptotic expansion of the fields

We now consider the asymptotic expansions of $\Psi_d$ and $\Psi_n$ for large $r$, as we wish to match the far field of our inner solution into an outgoing cone of diffracted rays and the reflected geometrical optics field in the outer problem. Our method will, in essence, follow the analysis of [44]. Despite a number of technical mistakes (a number of the integrals used in their analysis are not convergent), this method gives broadly correct expressions for the far-fields. We will carefully apply the method of steepest descents, deforming the contours of integration in the complex plane. As a preliminary step we first consider the

case when $\beta = 0$, in which our parabola becomes the half-plane $y = 0$, $x > 0$.

### 4.2.1 Asymptotic expansion in the Sommerfeld case

The diffraction of a plane wave by a half-plane (or knife-edge) was first studied by Sommerfeld [136], and it is well known that its solution may be written in terms of complementary error functions (or Fresnel integrals) [121]. Since the first part of integrals (4.30) and (4.31) is just (4.26), even for non-zero $\beta$, we will only consider the expansion of the remaining part

$$I_s = \frac{i}{2\sqrt{2\pi}} \int_{-\frac{1}{2}-i\infty}^{-\frac{1}{2}+i\infty} \frac{(\tan\frac{\phi_0}{2})^\nu}{\cos\frac{\phi_0}{2}} D_{-1-\nu}(\bar{p}\eta) D_\nu(\bar{p}\xi) \frac{d\nu}{\sin(\nu\pi)}. \tag{4.35}$$

(The total fields are then $\Psi_d = I_i - I_s$ and $\Psi_n = I_i + I_s$). Like $I_i$, this integral has an exact representation in terms of a complementary error function. However, when we find the far-field approximation of the integral $I_s$ directly, the method of expansion differs only slightly from the corresponding method for non-zero $\beta$. Thus it proves profitable to consider this expansion when $\beta$ is zero first, since we may compare this with the known answer. There are a number of regions in the physical plane for which the treatment of integral $I_s$ differs, due to the varying behaviour of the integrand, and corresponding to the presence or absence of each of the ray fields; these may be seen in Figure 4.3.

#### 4.2.1.1 Exact behaviour of the integral

As noted above, the integral $I_s$ may be expressed exactly as

$$I_s = \frac{1}{2} \exp\left(ir\cos\left(\phi_0 + \phi\right)\right) \mathrm{erfc}(\sqrt{r}\bar{p}\sin\frac{1}{2}(\phi_0 + \phi)), \tag{4.36}$$

and from the asymptotic expansion of the complementary error function we have that, in the limit of large $r$,

$$I_s = \exp\left(ir\cos(\phi_0 + \phi)\right) + \frac{e^{ir+\frac{\pi i}{4}}}{2\sqrt{2\pi r}\sin\frac{1}{2}(\phi_0 + \phi)} + \mathcal{O}(r^{-1}) \tag{4.37}$$

in the region where the reflected field is switched on ($2\pi - \phi_0 < \phi < 2\pi$), and

$$I_s = \frac{e^{ir+\frac{\pi i}{4}}}{2\sqrt{2\pi r}\sin\frac{1}{2}(\phi_0 + \phi)} + \mathcal{O}(r^{-1}) \tag{4.38}$$

elsewhere.

#### 4.2.1.2 Series Expansions

The behaviour of the integrand of $I_s$ for large $|\nu|$ is discussed in Appendix B.3, and from this we see that when $0 < \phi_0 < \frac{\pi}{2}$ we may complete the contour of integration by an arc at infinity in the right-hand half of the complex plane, and when $\frac{\pi}{2} < \phi_0 < \pi$ by an arc in the left-hand half. The integrand has poles at the integers, and by summation of the residue contributions from these poles we find that

$$I_s = \frac{1}{\sqrt{2\pi}} \sum_{n=0}^{\infty} \frac{(-\tan\frac{\phi_0}{2})^n}{\cos\frac{\phi_0}{2}} D_{-1-n}(\bar{p}\eta) D_n(\bar{p}\xi) \quad \text{for} \quad 0 < \phi_0 < \frac{\pi}{2} \tag{4.39}$$

or

$$I_s = -\frac{1}{\sqrt{2\pi}} \sum_{n=0}^{\infty} \frac{(-\tan\frac{\phi_0}{2})^{-1-n}}{\cos\frac{\phi_0}{2}} D_n(\bar{p}\eta) D_{-1-n}(\bar{p}\xi) \quad \text{for} \quad \frac{\pi}{2} < \phi < \pi. \tag{4.40}$$

For $\phi_0 = \frac{\pi}{2}$ the first of these series converges when $|\xi| < \eta$, and the second when $|\xi| > \eta$. A naïve attempt to find the far field of $I_s$ would be to replace the PCFs in these sums by their asymptotic expansions (A.15) - (A.17) for large argument. However, although $\xi$ and $\eta$ are large (for $\phi$ not near $\pi$), the index of summation $n$ ranges from zero to infinity, and the expansions (A.15) - (A.17) are only valid for sufficiently small order. We shall see later that for certain angles of observation (when the terms in the series decay exponentially in $n$) this approximation is in fact valid. However, in general we must approximate the PCFs by the expansions valid for both large order and argument, and it proves simpler to instead manipulate the original integral representations.

#### 4.2.1.3 Phase-Amplitude Expansions

In order to find the asymptotic expansion of $I_s$, and other integrals, we will need to assess the behaviour of their integrands in the $\nu$ plane. To do this we consider the expansions of Appendix A.4.3 for the $\xi$- and $\eta$-dependent PCFs within the integrands. These asymptotic forms are valid for large order and/or argument[2], but have a fairly complicated nature, as they have numerous Stokes lines and branch cuts in the $\nu$-plane. A complete description of these, along with their explicit forms, is given in Appendix A.

When we introduce the scalings

$$\nu = r\hat{\nu}, \quad \xi = \sqrt{r}\hat{\xi}, \quad \eta = \sqrt{r}\hat{\eta}, \tag{4.41}$$

these approximations of the integrands are of the form

$$\sum_j A_j(\hat{\xi}, \hat{\eta}, \hat{\nu}) \exp\left(r u_j(\hat{\xi}, \hat{\eta}, \hat{\nu})\right), \tag{4.42}$$

[2]Provided that the order and argument are not such that they are near the turning points of the differential equation (A.1), where the PCFs must be expanded in terms of Airy functions [113], [44].

and different expansions are found in different regions of the $\hat{\nu}$ plane, whose boundaries are the Stokes lines of the approximations. We will refer to $A_j$ as the amplitude of each of the terms, and $u_j$ as its phase. These expansions consist of a series of terms, as we expand the reciprocals of trigonometric functions as series of exponentials, and the expansions of the PCFs in most regions consist of a number of terms with distinct phases. In general there will be only one term whose phase has largest real part; this term will be exponentially larger that the others. We will refer to this term as dominant, and the others as being subdominant. Provided we are not near an anti-Stokes line of this expansion (where the real part of the phase of two or more terms is the same) we may ignore all but the dominant term, as the other terms will be exponentially small. However care must be taken such that the integrals of these subdominant terms are still exponentially small. In the later work this will be ensured by checking that the integrand is exponentially small whenever the contour of integration crosses an anti-Stokes line, or if that is not that case by considering the contribution to the integral from near this point (this will invariably be a contribution from near the origin, and we will be able to approximate the PCFs by simpler functions in this region).

### 4.2.2 Expansion in the upper physical half plane $0 < \phi < \pi$

In the upper physical half plane (see Figure 4.3) $\xi$ is positive, and by carefully considering the phase-amplitude approximations of Appendix B.1 it is possible to show that the integrand of $I_s$ decays exponentially away from the real axis along the contour of integration (as can be observed in Figure 4.5). Thus, as noted in [113] and [44], the dominant contribution to the integrand is from a section of the integration contour where $\nu$ is near $-\frac{1}{2}$.

As the integrand decays exponentially along the contour of integration away from $\nu = -\frac{1}{2}$ we may truncate the region of integration to the segment $[-\frac{1}{2} - iKr^\alpha, -\frac{1}{2} + iKr^\alpha]$, introducing only an exponentially small error when $K$ is an $\mathcal{O}(1)$ constant and $\alpha > 0$. If $\alpha < \frac{1}{2}$ the expansions (A.15) for the PCFs (for $\mathcal{O}(1)$ order and large argument) will be valid, and we may approximate the PCFs on this restricted contour by these expansions. The approximate integrand still decays exponentially away from the origin, and so we may extend the region of integration back to the original contour, again introducing only an exponentially small error. The approximate integral is then

$$I_s = \frac{ie^{ir+\frac{\pi i}{4}}}{4\sqrt{2\pi r}\sin\frac{\phi}{2}\cos\frac{\phi_0}{2}} \int_{-\frac{1}{2}-i\infty}^{-\frac{1}{2}+i\infty} \left(\frac{\tan\frac{\phi_0}{2}}{\tan\frac{\phi}{2}}\right)^\nu \frac{d\nu}{\sin(\nu\pi)} + \mathcal{O}(r^{-1}) \tag{4.43}$$

and we find that we may complete the contour of integration with an arc at infinity in

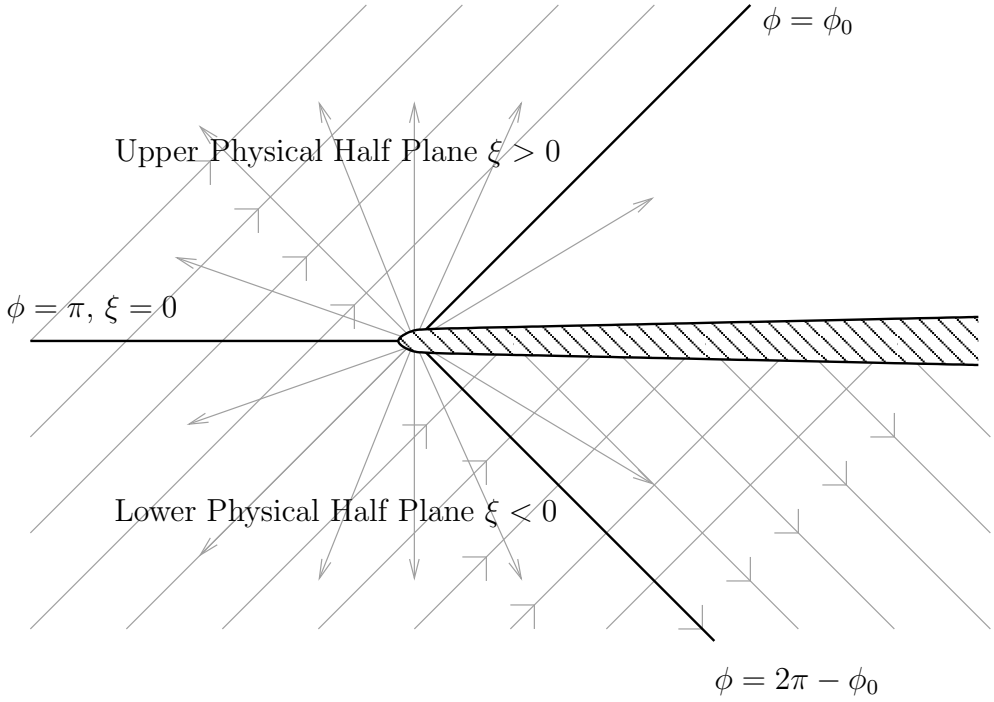


**Figure 4.3:** The various different regions in the physical $(\xi, \eta)$ or $(r, \phi)$ plane for the expansions of (4.30), (4.31). Here the incident field makes an angle $\phi_0$ with the mid-line of the thin edge, and so the incident and reflected fields are present in $\phi_0 < \phi < 2\pi$ and $2\pi - \phi_0 < \phi < 2\pi$ respectively. The black lines denote the boundaries across which our treatment of integral $I_s$ differs.

the left hand half-plane if $0 < \phi < \phi_0$, and in the right hand half plane when $\phi_0 < \phi < \pi$. As with the original integrand there are poles at the integers, and we obtain the residue series

$$\begin{aligned} I_s &\sim -\frac{e^{ir+\frac{\pi i}{4}}}{2\sqrt{2\pi r}\sin\frac{\phi}{2}\cos\frac{\phi_0}{2}} \sum_{n=0}^{\infty} \left(-\frac{\tan\frac{\phi_0}{2}}{\tan\frac{\phi}{2}}\right)^{-1-n} \qquad \text{for} \quad 0 < \phi < \phi_0, \\ I_s &\sim \frac{e^{ir+\frac{\pi i}{4}}}{2\sqrt{2\pi r}\sin\frac{\phi}{2}\cos\frac{\phi_0}{2}} \sum_{n=0}^{\infty} \left(-\frac{\tan\frac{\phi_0}{2}}{\tan\frac{\phi}{2}}\right)^{n} \qquad \text{for} \quad \phi_0 < \phi < \pi. \end{aligned} \tag{4.44}$$

In either case the series sum to give

$$I_s \sim \frac{e^{ir+\frac{\pi i}{4}}}{2\sqrt{2\pi r}\sin\frac{1}{2}(\phi_0 + \phi)} \tag{4.45}$$

which is part of the diffracted field in the Sommerfeld case (the remainder being supplied by the far field of $I_i$).

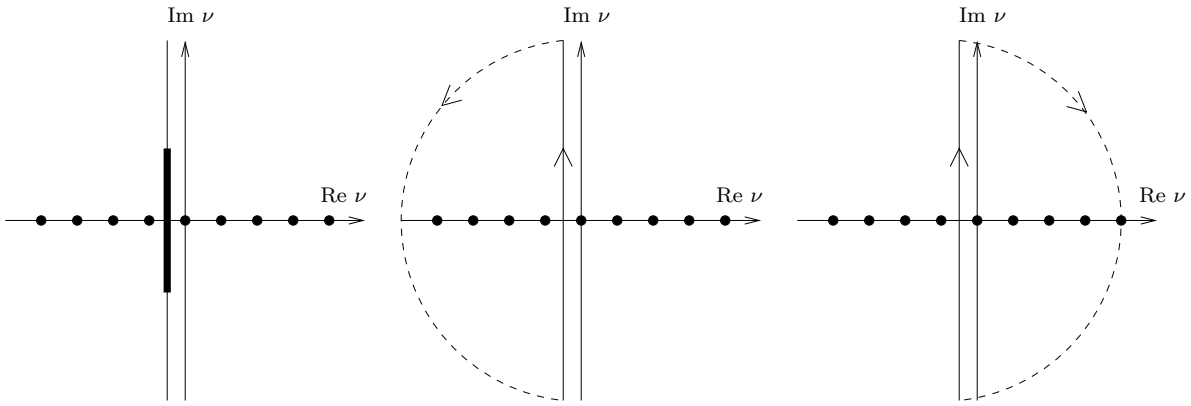


**Figure 4.4:** Schematic of the method of approximation of $I_s$ in the upper half plane $0 < \phi < \pi$. We restrict the contour of integration to a region of size $\mathcal{O}(r^\alpha)$, $0 < \alpha < \frac{1}{2}$ near $\nu = -\frac{1}{2}$ (in bold). We may then replace the PCFs in the integrand by their expansions (A.15) on this smaller region, and then extend the integral back to its original contour, which may be completed by an arc at infinity to the left or right for $0 < \phi < \phi_0$ or $\phi_0 < \phi < \pi$ respectively. The diffracted field is given by the poles of the approximate integrand at the integers.

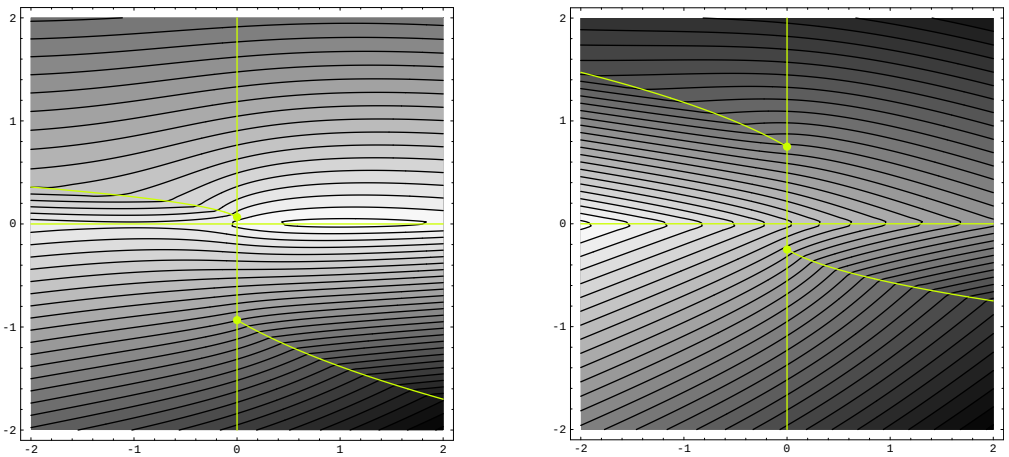

**Figure 4.5:** The real part of the phase, in the complex $\nu$ plane, for the dominant term in the phase-amplitude expansion of the integrand of $I_s$. Here lighter shading indicates a more positive real part. The first plot is for $0 < \phi < \phi_0$, $0 < \phi_0 < \frac{\pi}{2}$, and the second for $0 < \phi < \phi_0$, $\frac{\pi}{2} < \phi_0 < \pi$. We note that the integrands decay exponentially away from the real axis. The yellow lines are the anti-Stokes lines for the asymptotic expansion of the integrand, as discussed in Appendix B.1.

### 4.2.3 Expansion in the lower physical half plane $\pi < \phi < 2\pi$

In this region $\xi$ is negative, and the phase-amplitude expansions of section (A.4.3) for $D_\nu(\bar{p}\xi)$ are not valid for negative $\xi$. It is possible to extend the steepest descents analysis

of Appendix (A.4.3) to this case, but the expansion for $D_\nu(\bar{p}\xi)$ is slightly more complicated. Also, we wish to minimise the number of different phase-amplitude terms present in the approximation of the integrand at each point in the $\nu$ plane. Therefore we will instead follow [44] and apply the connection formula (A.11) to write $I_s$ as

$$I_s = \frac{i}{2\sqrt{2\pi}} \int_{-\frac{1}{2}-i\infty}^{-\frac{1}{2}+i\infty} \frac{(\tan\frac{\phi_0}{2})^\nu}{\cos\frac{\phi_0}{2}} D_{-1-\nu}(\bar{p}\eta) \left\{ \frac{e^{\nu\pi i} D_\nu(-\bar{p}\xi)}{\sin(\nu\pi)} - i\sqrt{\frac{2}{\pi}} e^{\frac{\nu\pi i}{2}} \Gamma(1+\nu) D_{-1-\nu}(-p\xi) \right\} d\nu. \tag{4.46}$$

We note that the two integrals found by splitting the integrand of this expression in the manner

$$I_s \;=\; I_s^1 + I_s^2, \tag{4.47}$$

with

$$I_s^1 \;=\; \frac{i}{2\sqrt{2\pi}} \int \frac{(\tan\frac{\phi_0}{2})^\nu}{\cos\frac{\phi_0}{2}} e^{\nu\pi i} D_{-1-\nu}(\bar{p}\eta) D_\nu(-\bar{p}\xi) \frac{d\nu}{\sin(\nu\pi)}, \tag{4.48}$$

$$I_s^2 \;=\; \frac{1}{2\pi} \int \frac{(\tan\frac{\phi_0}{2})^\nu}{\cos\frac{\phi_0}{2}} e^{\frac{\nu\pi i}{2}} \Gamma(1+\nu) D_{-1-\nu}(\bar{p}\eta) D_{-1-\nu}(-p\xi) d\nu, \tag{4.49}$$

do not converge separately on the original contour of integration; we can see from Appendix B.3 that the valleys of the new integrands at infinity differ from those of the original integrand. There are two ways to circumvent this difficulty. One method is to deform the original contour $C_i$ to either $C_l$ (for $\frac{\pi}{2} < \phi < \pi$) or $C_r$ (for $0 < \phi_0 < \frac{\pi}{2}$), as shown in Figure 4.6, before splitting the integral into two. We are then free to deform the two integrals independently, provided that the contours start and finish in the same valleys as before. The alternative method, which we will use almost all of the time, is to ensure that when we deform the contours for the two separate integrals they lie together when $\nu$ has large imaginary part, so that the dominant part of the integrands cancel (leaving terms which decay exponentially as we go towards $-i\infty$). This constraint leads to a "forked" contour of integration in the lower $\nu$ plane (as in Figure 4.7, for example).

Again, we may make the scalings (4.41), and expand our new integrands in phase-amplitude form. The saddle points of these expansions are those points where the derivative of the phase vanishes, and from Appendix B.2 we find that one of $I_s^1$ and $I_s^2$ has a saddle point when $2\pi - \phi_0 < \phi < 2\pi$, but otherwise neither integrand has a saddle point.

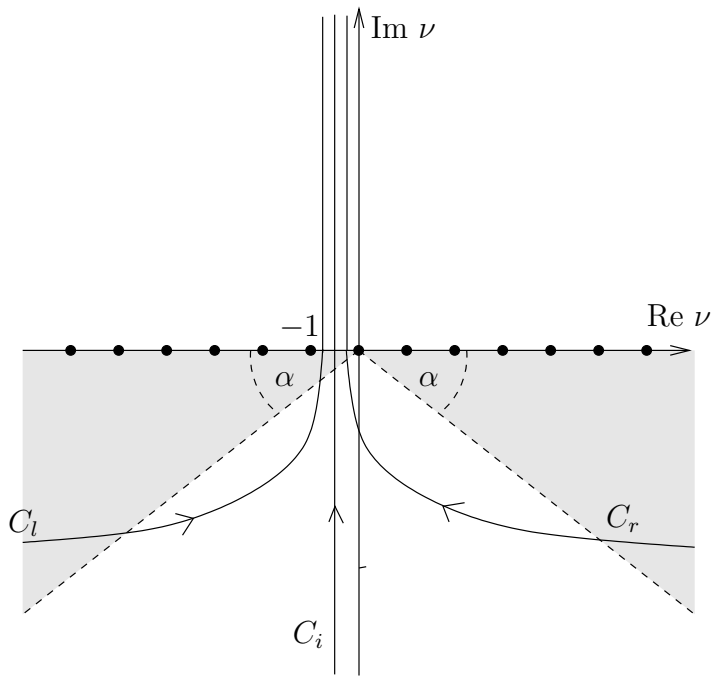


**Figure 4.6:** Contours for the integrals $I_s$, $I_s^1$ and $I_s^2$. The original contour for $I_s$ is $C_i$. If we apply the connection formula (A.11) to write $I_s = I_s^1 + I_s^2$, and wish to consider the new integrals separately then we need to deform the contours to $C_l$ or $C_r$ when $\frac{\pi}{2} < \phi_0 < \pi$ or $0 < \phi_0 < \frac{\pi}{2}$ respectively. The valleys (for very large $|\nu|$) for the integrands in each case are shaded, and $\alpha = \tan^{-1}\left(\frac{\pi}{2|\log\tan\frac{\phi_0}{2}|}\right)$ as discussed in Appendix B.3.

#### 4.2.3.1 Reflected field present: $2\pi - \phi_0 < \phi < 2\pi$

From the discussion in Appendix B.2 we find that the integrand of $I_s^1$ has a saddle point when $2\pi - \phi_0 < \phi < 3\pi - 2\phi_0$, and the integrand of $I_s^2$ has a saddle point when[3] $3\pi - 2\phi_0 < \phi < 2\pi$.

The latter condition cannot hold unless $\phi_0 > \frac{\pi}{2}$, but in either case the saddle point is at

$$\hat{\nu} = -i\sin(\phi_0 + \phi)\sin\phi_0. \tag{4.50}$$

Our strategy is as follows. We first use the phase-amplitude approximations to find suitable contours on which we may approximate the integrals by the method of steepest descents. We will then deform the contours of the exact integrals to these paths, before approximating their integrands. Finally we approximate these new integrals by the method of steepest descents. There are two reasons to proceed in this way. Firstly, as can be seen in Appendix B.1, the approximations of the integrands have a large number

[3]This differs from [44], in which it was claimed that the integrand of $I_s^2$ has a saddle point for $2\pi - \phi_0 < \phi < 2\pi$, and that the integrand of $I_s^1$ has no saddle point.

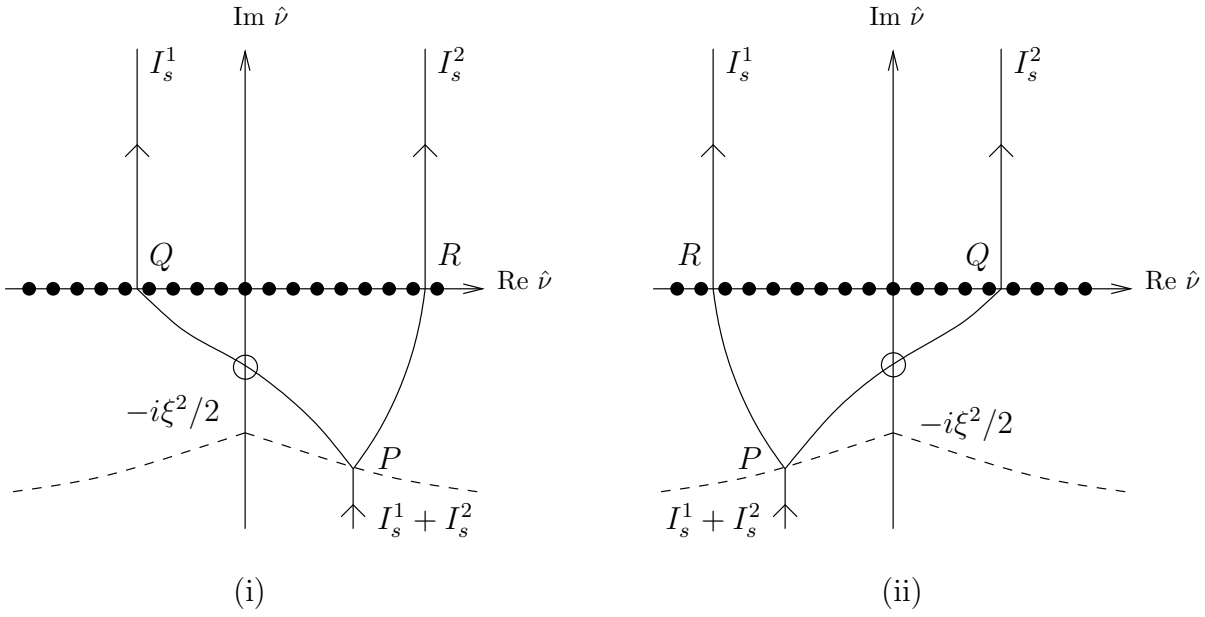


**Figure 4.7:** Contours used for the approximation of $I_s^1$ and $I_s^2$, when the reflected field is present. The contours of integration are deformed to those of case (i) when $2\pi - \phi_0 < \phi < 3\pi - 2\phi_0$, and case (ii) when $3\pi - 2\phi_0 < \phi < 2\pi$. The integrands of $I_s^1$ and $I_s^2$ respectively have a saddle point (denoted by the empty circle) at $\nu = -i\sin(\phi_0 + \phi)\sin\phi_0$. The filled circles along the real axis indicate the poles of $I_s^1$ at the integers (and the poles of $I_s^2$ at the strictly negative integers), and the dotted lines indicate the anti-Stokes lines of $D_\nu(\bar{p}\xi)$ in the lower half plane.

of branch cuts, and so if we were to first approximate the integrand and then deform it to its steepest descent path we would have to deal with a number of extra contributions because of these branch cuts. Secondly, we will make errors (generally of $\mathcal{O}(\frac{1}{r})$) in approximating our integrands by their asymptotic expansions. If the dominant contribution to the integral is not from a small section of the contour of integration the errors made in this approximation may be significant compared to those terms obtained from expansion of the (now) approximate integral.

We will deform the contour of integration for the integral containing the saddle point to a path of steepest descent through the saddle, and which connects the valleys at $\pm i\infty$. This is complicated by the fact that the phase of the (dominant term in the approximation of the) integrand proves not to be differentiable at the anti-Stokes lines of the expansions. Ordinarily, unless our steepest descent path were to encounter another saddle point, the real part of the phase would necessarily decrease along the steepest descent path away from the saddle. Thus this path would have to connect two valleys of the integrand. However, the lack of smoothness across an anti-Stokes line allows the behaviour of the

phase to change without the presence of another saddle.

When we consider the steepest descent path through the saddle point we see that such complications occur at the point $P$, as shown in Figure 4.7, on one of the anti-Stokes lines of the $\xi$- dependent PCF in the lower half of the complex $\nu$ plane. Across this line we find that the integrand now grows exponentially toward $-i\infty$, as a term which was formerly subdominant to that containing the saddle becomes the dominant term in the expansion of the integrand. It is this term which resulted in the exact integrals $I_s^1$ and $I_s^2$ failing to converge along the original contour $C_i$, and so as mentioned before we will let the contours of both integrals be concurrent[4] from $-i\infty$ to $P$. If this path is taken to be parallel to the imaginary $\nu$ axis we find from our phase-amplitude expansions that the integrand for the sum of the two integrals decays exponentially away from $P$. Our steepest descent path also encounters an anti-Stokes line at the point $Q$ on the real axis. In Im $\nu > 0$ we find that the integrands both of $I_s^1$ and $I_s^2$ decay exponentially with Im $\nu$, and so in this region we may simply deform the contour of the integral containing the saddle to be a line parallel to the imaginary axis from $Q$ to $i\infty$. Thus we deform the integral containing the saddle to this path from $-i\infty$ to $i\infty$, passing through $P$ and $Q$. For the integral which does not have a saddle we deform its contour to the path which runs parallel to the imaginary axis from $-i\infty$ to $P$, and then follows the path of steepest descent. Again this path may intersect the real axis at some point $R$, and from this point to $i\infty$ we will simply let the contour be parallel to the imaginary axis.

We have now deformed the original contours of integration to one of the two forked contours illustrated in Figure (4.7). We may now apply the phase-amplitude approximations to the integrands, and find that the saddle point contribution is

$$\exp\left(ir\cos\left(\phi_0+\phi\right)\right)\{1+\mathcal{O}(r^{-1})\} \tag{4.51}$$

to leading order, which corresponds to the reflected field. There will also be end-point contributions from near $P$, $Q$, and $R$. However, since the real part of the phase along the contour decreases away from the saddle point these end-point contributions must be exponentially subdominant when compared to the reflected field (unless the saddle lies very close to $P$ or $Q$).

In deforming our contours of integration to the forked contour we find that the contour of $I_s^1$ crosses poles at the negative integers. (We obtain no residue contribution from

[4]In the case when $0 < \phi < \frac{\pi}{2}$ it is in fact possible to let the integration contour of $I_s^1$ be concurrent with the anti-Stokes line from $P$ to $+\infty$. In addition, $I_s^2$ only has poles at the negative integers and may be completed by an arc at infinity in the right hand half plane, so in this case $I_s^2 = 0$. Such contours are seen in [113], but we do not use them in our work.

integral $I_s^2$, as its integrand only has poles at the negative integers, whereas its contour crosses the real axis at a point to the right of $-\frac{1}{2}$). There are $\mathcal{O}(r)$ such poles crossed, and the magnitude of their residue contributions decays exponentially in $|\,\nu\,|$. Provided that $\phi - (2\pi - \phi_0) \gg r^{-\frac{1}{2}}$ this decay is sufficiently rapid that we may truncate the summation after $\mathcal{O}(r^\alpha)$ terms, where $0 < \alpha < \frac{1}{2}$, and approximate the residues using the expansions (A.4.2) for PCFs of large argument and $\mathcal{O}(1)$ order. The terms in the series still decay exponentially, and so we may extend the upper limit of summation to infinity, introducing another exponentially small error. This pole contribution is

$$-\frac{e^{ir+\frac{\pi i}{4}}}{2\sqrt{2\pi r}\sin\frac{\phi}{2}\cos\frac{\phi_0}{2}}\sum_{n=0}^{\infty}\left(\frac{\tan\frac{\phi_0}{2}}{|\tan\frac{\phi}{2}|}\right)^{-1-n} = \frac{e^{ir+\frac{\pi i}{4}}}{2\sqrt{2\pi r}\sin\frac{1}{2}(\phi_0+\phi)}, \qquad (4.52)$$

and corresponds to (part of) the diffracted field.

#### 4.2.3.2 Reflected field not present: $\pi < \phi < 2\pi - \phi_0$

In this region neither of the integrals $I_s^1$ and $I_s^2$ contains a saddle point. As in Section 4.2.2, we will find that the dominant contribution is that from $\nu$ close to $-\frac{1}{2}$ for integral $I_s^1$. However a little care must be taken in deforming the contours to isolate this dominant contribution.

We first deform the contour of integration of $I_s^1$ to one upon which the integrand decays exponentially away from $\nu = -\frac{1}{2}$. In the upper half of the complex $\nu$ plane a line parallel to the imaginary axis is sufficient for this to be the case. In the lower half of the $\nu$ plane we deform the contour to the path of steepest descent (for the phase-amplitude approximations) away from $\nu = -\frac{1}{2}$. This path may intersect an anti-Stokes line of the $\xi$- dependent PCF at a point $P$, as shown in Figure 4.9(ii). If this occurs then we deform the two integration contours to "forked" contours, as for the previous section. Again, we let $I_s^1$ and $I_s^2$ run together from $P$ to $-i\infty$, and deform $I_s^2$ to its path of steepest descent away from $P$ (which intersects the real axis at a point $R$). The combination $I_s^1 + I_s^2$ then decays exponentially from $P$ to $-i\infty$, whereas $I_s^2$ decays exponentially from $P$ to $R$ to $i\infty$. There are no pole contributions from $I_s^2$, and so we find that the dominant contribution is that from $I_s^1$ near $\nu = -\frac{1}{2}$.

If the contour does not intersect this anti-Stokes line then it will run, beneath the real axis, to the valley of the integrand, as shown in Figure 4.9(i). In this case the integral $I_s^2$ is also convergent on this contour. As $I_s^2$ may be completed by an arc in the right hand half plane we find that $I_s^2 = 0$. Thus in this case the dominant contribution to $I_s^1 + I_s^2$ is again that from $I_s^1$ near $\nu = -\frac{1}{2}$.

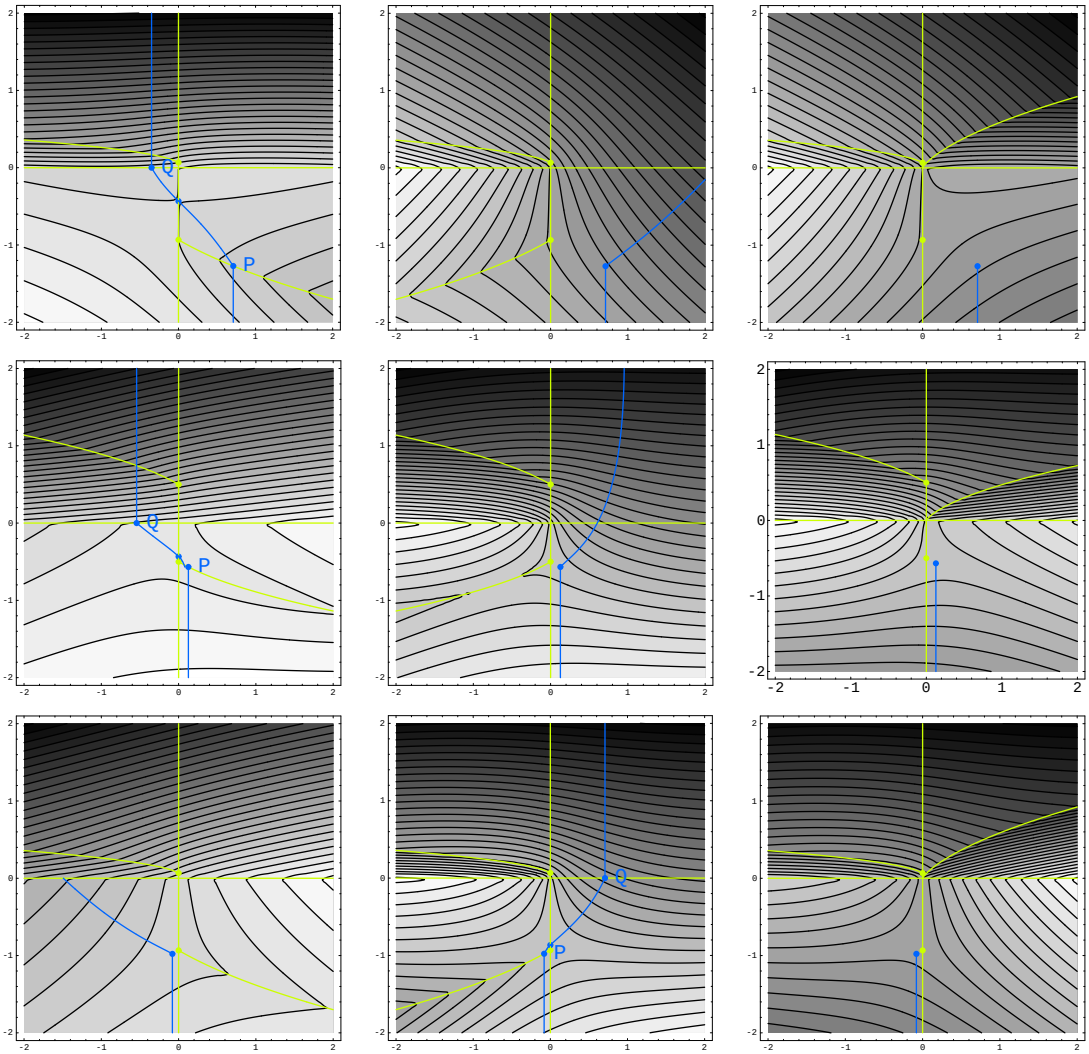


**Figure 4.8:** Plots of the real part of the phase for the integrands of $I_s^1$, $I_s^2$ and $I_s$ (across each row), where again lighter shading indicates a greater real part. The angles of incidence and observation are such that $0 < \phi_0 < \frac{\pi}{2}$ and $2\pi - \phi_0 < \phi < 2\pi$ (first row), $\frac{\pi}{2} < \phi_0 < \pi$ and $2\pi - \phi_0 < \phi < 3\pi - 2\phi_0$ (second row), and $\frac{\pi}{2} < \phi_0 < \pi$ and $3\pi - 2\phi_0 < \phi < 2\pi$ (third row). In each case the contours of integration which we use in our approximation are shown, along with the points $P$ and $Q$.

Provided that $2\pi - \phi_0 - \phi \gg r^{-\frac{1}{2}}$ we may approximate the PCFs by their large argument expansions as before, which gives

$$I_s = \frac{ie^{ir+\frac{\pi i}{4}}}{4\sqrt{2\pi r}\sin\frac{\phi}{2}\cos\frac{\phi_0}{2}} \int_{C_r'} \left(\frac{\tan\frac{\phi_0}{2}}{|\tan\frac{\phi}{2}|}\right)^{\nu} \frac{e^{\nu\pi i}d\nu}{\sin(\nu\pi)} + \mathcal{O}(r^{-1}), \tag{4.53}$$

where the contour $C_r'$ begins and ends in the valley of the integrand, and encircles each of the poles at the integers in the same sense as the original contour. Explicitly, a suitable contour runs below the real axis from $\infty$ to $-\frac{1}{2}$, and then is parallel to the imaginary

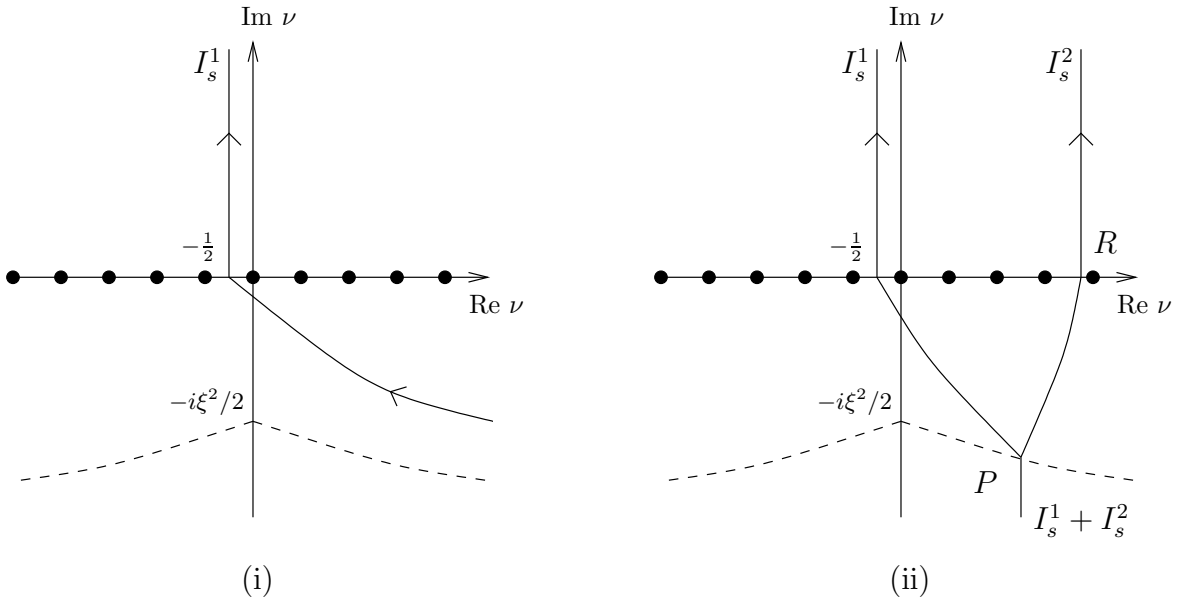


**Figure 4.9:** Contours used for the approximation of $I_s^1 + I_s^2$, when the reflected field is not present. The situation in (i) occurs when the steepest descent path for $I_s^1$ through $\nu = -\frac{1}{2}$ does not intersect the (dashed) anti-Stokes line. The contour of $I_s^2$ may be completed by an arc at infinity in the right hand half of the plane, and (in either case) the integrand of $I_s^2$ only has poles at the negative integers. The situation in (ii) occurs when the steepest descent path intersects the anti-Stokes line at at a point $P$, and then we deform the contours to the forked paths shown.

axis from $-\frac{1}{2}$ to $i\infty$. The contour of this approximate integral may now be completed by an arc in the right hand half plane, and when we do this we obtain the residue series (4.44).

#### 4.2.3.3 Reflected shadow boundary: $\phi = 2\pi - \phi_0 + \mathcal{O}(r^{-\frac{1}{2}})$

From the previous sections we see that the expansion of integral $I_s$ is discontinuous across $\phi = 2\pi - \phi_0$, as the reflected field is only present in $\phi > 2\pi - \phi_0$. This reflected field is supplied by a saddle point of integral $I_s^1$, whose location is given by (4.50), and in terms of our scaled variable $\hat{\nu}$ the dominant contribution to the integral is supplied by a region of integration of size $\mathcal{O}(r^{-\frac{1}{2}})$ about this point. The phase-amplitude expansions for the integrands are discontinuous across the real $\hat{\nu}$ axis, and when $|\phi - (2\pi - \phi_0)| = \mathcal{O}(r^{-\frac{1}{2}})$ this discontinuity is within the saddle-point region. Furthermore, our approximation for the diffracted field in $\phi < 2\pi - \phi_0$ ceases to be valid in this region. Therefore for observation points near the reflected boundary the field must be expressed differently. We expect that the integral should be expressible in terms of complementary error functions, as these are

the canonical form of such endpoint-saddlepoint interaction.

The dominant contribution to $I_s$ again turns out to be from a region of integration for $I_s^1$ near $\nu = -\frac{1}{2}$. We will deform the contours of integration of $I_s^1$ and $I_s^2$ as in the previous section (illustrated in Figure 4.9). This is complicated slightly by the behaviour of $I_s^1$ near the origin, as there may be a saddle point present. However, from (4.55) it is possible to see that the integrand begins to decay exponentially, after at most an $\mathcal{O}(r^{\frac{1}{2}})$ distance, as we go away from $\nu = -\frac{1}{2}$ in the $e^{-\frac{\pi i}{4}}$ direction. After this we may then follow the path of steepest descent.

Motivated by the size and position of the saddle point region we introduce the scalings

$$\tilde{\nu} = r^{-\frac{1}{2}}\nu = r^{\frac{1}{2}}\hat{\nu} \qquad \phi = (2\pi - \phi_0) + r^{-\frac{1}{2}}\tilde{\phi}. \tag{4.54}$$

Our PCFs have slightly simpler asymptotic expansions for $\nu$ in this range, and we find that the dominant contribution to $I_s$ is

$$I_s = \frac{ie^{ir+\frac{\pi i}{4}}}{4\sqrt{2\pi}\sin\frac{\phi_0}{2}\cos\frac{\phi_0}{2}}\int_{C_b}\frac{1}{\sin\left(r^{\frac{1}{2}}\tilde{\nu}\pi\right)}\exp\left(\frac{\tilde{\phi}\tilde{\nu}}{\sin\phi_0} - \frac{i\tilde{\nu}^2}{2\sin^2\phi_0} + r^{\frac{1}{2}}\tilde{\nu}\pi i\right)d\tilde{\nu}\left\{1+\mathcal{O}(r^{-\frac{1}{2}})\right\}, \tag{4.55}$$

where the contour $C_b$ runs from $\infty e^{-\frac{\pi i}{4}}$ to $-\frac{1}{2}r^{-\frac{1}{2}}$, and then to $i\infty$. When we make the exact expansion

$$\frac{1}{\sin\left(r^{\frac{1}{2}}\pi\tilde{\nu}\right)} = \frac{2i}{e^{r^{\frac{1}{2}}\tilde{\nu}\pi i} - e^{-r^{\frac{1}{2}}\tilde{\nu}\pi i}} = \begin{cases} -2ie^{r^{\frac{1}{2}}\tilde{\nu}\pi i}\sum_{n=0}^{\infty}e^{2nr^{\frac{1}{2}}\tilde{\nu}\pi i} & \text{Im }\tilde{\nu} > 0 \\ 2ie^{-r^{\frac{1}{2}}\tilde{\nu}\pi i}\sum_{n=0}^{\infty}e^{-2nr^{\frac{1}{2}}\tilde{\nu}\pi i} & \text{Im }\tilde{\nu} < 0 \end{cases}, \tag{4.56}$$

this becomes

$$\begin{aligned} I_s \sim\ & \frac{e^{ir+\frac{\pi i}{4}}}{2\sqrt{2\pi}\sin\frac{\phi_0}{2}\cos\frac{\phi_0}{2}}\left\{\int_{-\frac{1}{2}r^{-\frac{1}{2}}}^{i\infty}\sum_{n=0}^{\infty}\exp\left(2\tilde{\nu}r^{\frac{1}{2}}(n+1)\pi i + \frac{\tilde{\phi}\tilde{\nu}}{\sin\phi_0} - \frac{i\tilde{\nu}^2}{2\sin^2\phi_0}\right)d\tilde{\nu}\right. \\ & \left. - \int_{\infty e^{-\frac{\pi i}{4}}}^{-\frac{1}{2}r^{-\frac{1}{2}}}\sum_{n=0}^{\infty}\exp\left(-2\tilde{\nu}r^{\frac{1}{2}}n\pi i + \frac{\tilde{\phi}\tilde{\nu}}{\sin\phi_0} - \frac{i\tilde{\nu}^2}{2\sin^2\phi_0}\right)d\tilde{\nu}\right\}. \end{aligned} \tag{4.57}$$

Interchanging the order of summation and integration, it can be found that the major contribution to the integral is from the $n = 0$ term on $e^{-\frac{\pi i}{4}}\infty$ to $-\frac{1}{2}r^{-\frac{1}{2}}$, namely

$$-\frac{e^{ir+\frac{\pi i}{4}}}{2\sqrt{2\pi}\sin\frac{\phi_0}{2}\cos\frac{\phi_0}{2}}\int_{\infty e^{-\frac{\pi i}{4}}}^{-\frac{1}{2}r^{-\frac{1}{2}}}\exp\left(\frac{\tilde{\phi}\tilde{\nu}}{\sin\phi_0} - \frac{i\tilde{\nu}^2}{2\sin^2\phi_0}\right)d\tilde{\nu} \tag{4.58}$$

and when we substitute $s = \frac{e^{\frac{\pi i}{4}}}{\sqrt{2}}\left(\frac{\tilde{\nu}}{\sin\phi_0} + i\tilde{\phi}\right)$ this becomes

$$\frac{e^{ir-\frac{i\tilde{\phi}^2}{2}}}{\sqrt{\pi}}\int_{\frac{e^{\frac{\pi i}{4}}}{\sqrt{2}}\left(i\tilde{\phi}-\frac{r^{-\frac{1}{2}}}{2\sin\phi_0}\right)}^{\infty}e^{-s^2}ds = \ \frac{1}{2}\exp\left(ir - \frac{i\tilde{\phi}}{2}\right)\text{erfc}\left(-\frac{e^{-\frac{\pi i}{4}}\tilde{\phi}}{\sqrt{2}}\right)(1+\mathcal{O}(r^{-\frac{1}{2}})). \tag{4.59}$$

The other terms in (4.57) may each be approximated by their end-point contribution from near $\tilde{\nu} = -\frac{1}{2}r^{-\frac{1}{2}}$, and we find that the leading-order contribution from the $n^{\text{th}}$ term in the series of integrals on the contour from $-\frac{1}{2}r^{-\frac{1}{2}}$ to $i\infty$ cancels with the $(n+1)^{\text{th}}$ term in the series of integrals on $e^{-\frac{\pi i}{4}}\infty$ to $-\frac{1}{2}r^{-\frac{1}{2}}$. The correction from each pair of terms is thus seen to be $\mathcal{O}(r^{-1})$, and so (4.59) is the leading-order expansion of the field in this region. This agrees with the approximation found by introducing the scalings (4.54) in the exact representation (4.36), and expanding this for $r$ large.

Thus we have been able to reproduce the far field expansion (4.37) and (4.38) by directly expanding the integral $I_s$. Having successfully approximated (4.30) and (4.31) in the far field for $\beta = 0$ we now consider the corresponding approximation for non-zero $\beta$.

### 4.2.4 Asymptotic expansion in the $O(k)$ edge-curvature case

We now proceed to examine the asymptotic expansion of integrals (4.30) and (4.31) when $\beta = \mathcal{O}(1)$. For most angles of observation the calculations will be similar to those of Section 4.2.1. However, the region near the reflected boundary will be found to have a significantly different asymptotic structure. Although still subtending a vanishingly small angular extent as $r$ becomes large, this transition region will be found to be asymptotically wider than the shadow boundary for the sharp-edge case.

In this section we will consider the two integrals

$$I_d = -\frac{i}{2\sqrt{2\pi}} \int_{-\frac{1}{2}-i\infty}^{-\frac{1}{2}+i\infty} \frac{(\tan\frac{\phi_0}{2})^\nu}{\cos\frac{\phi_0}{2}} \frac{D_{-1-\nu}(-\bar{p}\beta)}{D_{-1-\nu}(\bar{p}\beta)} D_{-1-\nu}(\bar{p}\eta) D_\nu(\bar{p}\xi) \frac{d\nu}{\sin(\nu\pi)}, \quad (4.60)$$

$$I_n = \frac{i}{2\sqrt{2\pi}} \int_{-\frac{1}{2}-i\infty}^{-\frac{1}{2}+i\infty} \frac{(\tan\frac{\phi_0}{2})^\nu}{\cos\frac{\phi_0}{2}} \frac{D'_{-1-\nu}(-\bar{p}\beta)}{D'_{-1-\nu}(\bar{p}\beta)} D_{-1-\nu}(\bar{p}\eta) D_\nu(\bar{p}\xi) \frac{d\nu}{\sin(\nu\pi)}, \quad (4.61)$$

so that the total fields $\Psi_d$, $\Psi_n$ consist of $I_d$, or $I_n$, along with $I_i$. The integrands are similar to $I_s$, but are now multiplied by an additional factor

$$-\frac{D_{-1-\nu}(-\bar{p}\beta)}{D_{-1-\nu}(\bar{p}\beta)} \quad \text{or} \quad \frac{D'_{-1-\nu}(-\bar{p}\beta)}{D'_{-1-\nu}(\bar{p}\beta)} \quad (4.62)$$

for Dirichlet or Neumann boundary conditions respectively. As $\beta$ is an $\mathcal{O}(1)$ quantity, the only approximation we may make of these terms is that of large $|\nu|$, which is discussed in more detail in Appendix C. When we introduce the scalings (4.41), and use our phase-amplitude approximations, we see from (C.1) - (C.4) that the effect of these new terms is merely to perturb the phases of the approximations by an $\mathcal{O}(r^{-\frac{1}{2}})$ amount and to modify their amplitudes. Therefore, provided that $r$ is sufficiently large, and $\beta$ is not too large,

the general behaviour of the magnitude of the integrand is the same as the previous case. The additional terms simply change the contributions from the saddle points and the poles of the integrands. However, when $\hat{\nu} = r\nu$ is small (in fact, $\mathcal{O}(\beta^{\frac{2}{3}} r^{-\frac{1}{3}})$) the $\beta$-dependent terms in the phase may become comparable in size to the leading-order phase, and so play a significant role in determining the behaviour of the integrand. We will see that such effects are important in a region near to the reflected shadow boundary.

#### 4.2.4.1 Poles of integrands

Another significant effect of these $\beta$-dependent terms is the introduction of additional poles to the integrands from the zeros of $D_{-1-\nu}(\bar{p}\beta)$ and $D'_{-1-\nu}(\bar{p}\beta)$. Each of these functions has countably many zeros in the region $\mathrm{Im}\ \nu > 0,\ \mathrm{Re}\ \nu < -1$, and we label these $\nu_0, \nu_1, \nu_2, \ldots$, and $\nu'_0, \nu'_1, \nu'_2, \ldots$, in order of decreasing real part. For large $\nu$ these roots lie along the anti-Stokes line of $D_{-1-\nu}(\bar{p}\beta)$ in the second quadrant of the complex $\nu$ plane, and by considering (A.12) and (A.13) we find that they have asymptotic expansions

$$\nu_n \sim -2n - 2 - \frac{2\bar{p}\beta}{\pi}(2n+1)^{\frac{1}{2}} + \frac{4i\beta^2}{\pi^2} + \mathcal{O}(n^{-\frac{1}{2}}), \tag{4.63}$$

$$\nu'_n \sim -2n - 1 - \frac{2\bar{p}\beta}{\pi}(2n)^{\frac{1}{2}} + \frac{4i\beta^2}{\pi^2} + \mathcal{O}(n^{-\frac{1}{2}}), \tag{4.64}$$

for large $n$.

#### 4.2.4.2 Expansion in the upper physical half plane $0 < \phi < \pi$

In this region we find that, as long as the radius of curvature at the tip is not too large (where this condition will be made more precise later), we may proceed in exactly the same manner as in the Sommerfeld case. For $\beta = \mathcal{O}(1)$ the integrands of $I_d$ and $I_n$ decay sufficiently rapidly away from $\nu = -\frac{1}{2}$ that we may again approximate the integral by a region near there. We replace the $\xi$- and $\eta$- dependent PCFs by their large argument expansions, and then re-extend the contour of integration to give

$$I_d \sim -\frac{ie^{ir+\frac{\pi i}{4}}}{4\sqrt{2\pi r}\sin\frac{\phi}{2}\cos\frac{\phi_0}{2}} \int_{-\frac{1}{2}-i\infty}^{-\frac{1}{2}+i\infty} \left(\frac{\tan\frac{\phi_0}{2}}{\tan\frac{\phi}{2}}\right)^{\nu} \frac{D_{-1-\nu}(-\bar{p}\beta)}{D_{-1-\nu}(\bar{p}\beta)} \frac{d\nu}{\sin(\nu\pi)}, \tag{4.65}$$

$$I_n \sim \frac{ie^{ir+\frac{\pi i}{4}}}{4\sqrt{2\pi r}\sin\frac{\phi}{2}\cos\frac{\phi_0}{2}} \int_{-\frac{1}{2}-i\infty}^{-\frac{1}{2}+i\infty} \left(\frac{\tan\frac{\phi_0}{2}}{\tan\frac{\phi}{2}}\right)^{\nu} \frac{D'_{-1-\nu}(-\bar{p}\beta)}{D'_{-1-\nu}(\bar{p}\beta)} \frac{d\nu}{\sin(\nu\pi)}, \tag{4.66}$$

as found in [44] for the Neumann case. Again, these contour integrals may be completed by an arc at infinity in the left or right hand half plane when $0 < \phi < \phi_0$ or $\phi_0 < \phi < \pi$

respectively. When $0 < \phi < \phi_0$, the series so obtained are

$$\begin{aligned} I_d &\sim \frac{e^{ir+\frac{\pi i}{4}}\sqrt{\pi}}{2\sqrt{2r}\sin\frac{\phi}{2}\cos\frac{\phi_0}{2}}\left(\sum_{n=0}^{\infty}\left(\frac{\tan\frac{\phi_0}{2}}{\tan\frac{\phi}{2}}\right)^{-1-n}\frac{D_n(-\bar{p}\beta)}{D_n(\bar{p}\beta)}\frac{(-1)^n}{\pi}\right. \\ &\quad \left.+\sum_{m=0}^{\infty}\left(\frac{\tan\frac{\phi_0}{2}}{\tan\frac{\phi}{2}}\right)^{\nu_m}\frac{D_{-1-\nu_m}(-\bar{p}\beta)}{\frac{\partial}{\partial\nu}D_{-1-\nu}(\bar{p}\beta)|_{\nu=\nu_m}}\frac{1}{\sin(\nu_m\pi)}\right), \end{aligned} \tag{4.67}$$

$$\begin{aligned} I_n &\sim -\frac{e^{ir+\frac{\pi i}{4}}\sqrt{\pi}}{2\sqrt{2r}\sin\frac{\phi}{2}\cos\frac{\phi_0}{2}}\left(\sum_{n=0}^{\infty}\left(\frac{\tan\frac{\phi_0}{2}}{\tan\frac{\phi}{2}}\right)^{-1-n}\frac{D'_n(-\bar{p}\beta)}{D'_n(\bar{p}\beta)}\frac{(-1)^n}{\pi}\right. \\ &\quad \left.+\sum_{m=0}^{\infty}\left(\frac{\tan\frac{\phi_0}{2}}{\tan\frac{\phi}{2}}\right)^{\nu'_m}\frac{D'_{-1-\nu'_m}(-\bar{p}\beta)}{\frac{\partial}{\partial\nu}D'_{-1-\nu}(\bar{p}\beta)\big|_{\nu=\nu'_m}}\frac{1}{\sin(\nu'_m\pi)}\right). \end{aligned} \tag{4.68}$$

Using the fact that $D_n(z)$ is an odd (even) function for odd (even) non-negative $n$, we find that the first series of the two expansions is equal to

$$-\frac{e^{ir+\frac{\pi i}{4}}}{2\sqrt{2\pi r}\sin\frac{\phi}{2}\cos\frac{\phi_0}{2}}\sum_{n=0}^{\infty}\left(\frac{\tan\frac{\phi_0}{2}}{\tan\frac{\phi}{2}}\right)^{-1-n} = -\frac{e^{ir+\frac{\pi i}{4}}}{2\sqrt{2\pi r}\sin\frac{1}{2}(\phi_0-\phi)} \tag{4.69}$$

in both cases. When we consider the integrals (4.30) and (4.31) for the total field, we see that this cancels with the diffracted term in the expansion (4.28) of $I_i$.

When $\phi_0 < \phi < \pi$, we may complete the contours of integration for the approximate integrals (4.65), (4.66) in the right hand half plane, and obtain the series

$$I_d \sim -\frac{e^{ir+\frac{\pi i}{4}}}{2\sqrt{2\pi r}\sin\frac{\phi}{2}\cos\frac{\phi_0}{2}}\sum_{n=0}^{\infty}\left(-\frac{\tan\frac{\phi_0}{2}}{\tan\frac{\phi}{2}}\right)^{n}\frac{D_{-1-n}(-\bar{p}\beta)}{D_{-1-n}(\bar{p}\beta)}, \tag{4.70}$$

$$I_n \sim \frac{e^{ir+\frac{\pi i}{4}}}{2\sqrt{2\pi r}\sin\frac{\phi}{2}\cos\frac{\phi_0}{2}}\sum_{n=0}^{\infty}\left(-\frac{\tan\frac{\phi_0}{2}}{\tan\frac{\phi}{2}}\right)^{n}\frac{D'_{-1-n}(-\bar{p}\beta)}{D'_{-1-n}(\bar{p}\beta)}. \tag{4.71}$$

By applying the connection formula (A.11) to the ratio of PCFs, we may rewrite our series[5] as

$$\begin{aligned} I_d &\sim -\frac{e^{ir+\frac{\pi i}{4}}}{2\sqrt{r}\sin\frac{\phi}{2}\cos\frac{\phi_0}{2}}\sum_{n=0}^{\infty}\left(\frac{i\tan\frac{\phi_0}{2}}{\tan\frac{\phi}{2}}\right)^{n}\frac{D_n(p\beta)}{n!D_{-1-n}(\bar{p}\beta)} \\ &\quad +\frac{e^{ir+\frac{\pi i}{4}}}{2\sqrt{2\pi r}\sin\frac{\phi}{2}\cos\frac{\phi_0}{2}}\sum_{n=0}^{\infty}\left(\frac{\tan\frac{\phi_0}{2}}{\tan\frac{\phi}{2}}\right)^{n}, \end{aligned} \tag{4.72}$$

$$\begin{aligned} I_n &\sim -\frac{ie^{ir+\frac{\pi i}{4}}}{2\sqrt{r}\sin\frac{\phi}{2}\cos\frac{\phi_0}{2}}\sum_{n=0}^{\infty}\left(\frac{i\tan\frac{\phi_0}{2}}{\tan\frac{\phi}{2}}\right)^{n}\frac{D'_n(p\beta)}{n!D'_{-1-n}(\bar{p}\beta)} \\ &\quad +\frac{e^{ir+\frac{\pi i}{4}}}{2\sqrt{2\pi r}\sin\frac{\phi}{2}\cos\frac{\phi_0}{2}}\sum_{n=0}^{\infty}\left(\frac{\tan\frac{\phi_0}{2}}{\tan\frac{\phi}{2}}\right)^{n}. \end{aligned} \tag{4.73}$$

[5]These differ from the expansions found in [44] for the Neumann case.

The second of these series in each case is equal to (4.69), and so cancels with the diffracted part of the expansion (4.27) for $I_i$.

We now wish to examine more closely the condition on $r$ and $\beta$ required for this expansion to be valid. We used the approximation

$$D_{-1-\nu}(\bar{p}\eta)D_{\nu}(\bar{p}\xi) \sim \frac{(\cot\frac{\phi}{2})^{\nu}}{2\sqrt{r}\sin\frac{\phi}{2}}e^{ir+\frac{\pi i}{4}}\left(1-\frac{i\nu^2}{2r\sin^2\phi_0}+\cdots\right) \tag{4.74}$$

to write $I_d$ and $I_n$ as

$$I_d \sim -\frac{ie^{ir+\frac{\pi i}{4}}}{4\sqrt{2\pi r}\sin\frac{\phi}{2}\cos\frac{\phi_0}{2}}\int_{-\frac{1}{2}-i\infty}^{-\frac{1}{2}+i\infty}\left(\frac{\tan\frac{\phi_0}{2}}{\tan\frac{\phi}{2}}\right)^{\nu}\frac{D_{-1-\nu}(-\bar{p}\beta)}{D_{-1-\nu}(\bar{p}\beta)}\left(1-\frac{i\nu^2}{2r\sin^2\phi_0}+\cdots\right)\frac{d\nu}{\sin(\nu\pi)}, \tag{4.75}$$

$$I_n \sim \frac{ie^{ir+\frac{\pi i}{4}}}{4\sqrt{2\pi r}\sin\frac{\phi}{2}\cos\frac{\phi_0}{2}}\int_{-\frac{1}{2}-i\infty}^{-\frac{1}{2}+i\infty}\left(\frac{\tan\frac{\phi_0}{2}}{\tan\frac{\phi}{2}}\right)^{\nu}\frac{D'_{-1-\nu}(-\bar{p}\beta)}{D'_{-1-\nu}(\bar{p}\beta)}\left(1-\frac{i\nu^2}{2r\sin^2\phi_0}+\cdots\right)\frac{d\nu}{\sin(\nu\pi)}, \tag{4.76}$$

where we have included the first-order correction terms to (4.65) and (4.66). For our approximation to be valid we need the contribution from this correction term to be small compared to the leading-order term. This is certainly the case if the integrands are exponentially small when $\nu = \mathcal{O}(r^{\frac{1}{2}})$, as the dominant contribution to the integrand is then that from $|\nu| \ll r^{\frac{1}{2}}$. The ratio of $\beta$- dependent PCFs within the integrand may be approximated for large $|\nu|$ using (C.1) and (C.3), and we find that the leading-order part of the integrand in the Dirichlet case is approximately

$$-\frac{ie^{ir+\frac{\pi i}{4}}}{4\sqrt{2\pi r}\sin\frac{\phi}{2}\cos\frac{\phi_0}{2}}\left(\frac{\tan\frac{\phi_0}{2}}{\tan\frac{\phi}{2}}\right)^{\nu}\frac{\exp(2\bar{p}\beta\sqrt{\nu})}{\sin(\nu\pi)}. \tag{4.77}$$

For $\nu = -\frac{1}{2} + i\mu$, with $\mu$ real and $\mu \gg 1$, the modulus of this is approximately

$$\frac{1}{2\sqrt{2\pi r}\sin\frac{\phi}{2}\cos\frac{\phi_0}{2}}\exp\left(\mathrm{Re}\,(2\bar{p}\beta\sqrt{i\mu} - |\mu|\,\pi)\right) \tag{4.78}$$

and so we obtain the (sufficient) condition that $r \gg \beta^4$. When $\beta$ is large the expansion used for the $\beta$- dependent PCFs is only valid for $|\nu| \gg \beta^2$. We will find in Section 4.5.2 that the dominant contribution to the integral is from a point at an $\mathcal{O}(\beta^2)$ distance from the origin in the $\nu$ plane, and so again we see that for the approximation (4.74) to be valid near that point $r \gg \beta^4$. We obtain the same condition, by a similar analysis, in the Neumann case.

#### 4.2.4.3 Expansion near $\phi = \pi$

Unfortunately the analysis for $0 < \phi < \pi$ is not valid near $\phi = \pi$, as $\xi = \sqrt{2r}\cos\frac{\phi}{2}$ is zero there and so we may not use the large argument expansion (A.15) for the $\xi$ dependent PCFs. However we will find that the diffraction coefficient is continuous across this line.

For an incident plane wave with $\phi_0 = 0$ the exact solutions to our scalar diffraction problems are given by

$$\Psi_d = D_0(\bar{p}\xi)\left\{D_0(p\eta) - \frac{D_0(p\beta)}{D_{-1}(\bar{p}\beta)}D_{-1}(\bar{p}\eta)\right\}, \tag{4.79}$$

$$\Psi_n = D_0(\bar{p}\xi)\left\{D_0(p\eta) - \frac{iD_0'(p\beta)}{D_{-1}'(\bar{p}\beta)}D_{-1}(\bar{p}\eta)\right\}. \tag{4.80}$$

The PCFs in these solutions have the simple (exact) forms

$$D_0(z) = e^{-\frac{1}{4}z^2} \qquad D_{-1}(z) = \sqrt{\frac{\pi}{2}}e^{\frac{1}{4}z^2}\mathrm{erfc}\left(\frac{z}{\sqrt{2}}\right), \tag{4.81}$$

and so we find that these solutions have far fields

$$\Psi_d \sim e^{ix} - \frac{e^{ir+\frac{\pi i}{4}}}{\sqrt{2\pi r}\sin\frac{\phi}{2}\mathrm{erfc}\left(\frac{\bar{p}\beta}{\sqrt{2}}\right)}, \tag{4.82}$$

$$\Psi_n \sim e^{ix} - \frac{e^{ir+\frac{\pi i}{4}}}{\sqrt{2\pi r}\sin\frac{\phi}{2}\left(\mathrm{erfc}\left(\frac{\bar{p}\beta}{\sqrt{2}}\right) - \frac{2}{\bar{p}\beta}\sqrt{\frac{2}{\pi}}e^{i\beta^2}\right)}. \tag{4.83}$$

Using these expressions, along with the principle of reciprocity, we find that the diffraction coefficient is continuous at $\phi = \pi$.

#### 4.2.4.4 Expansion in the lower physical half plane $\pi < \phi < 2\pi$

As for the Sommerfeld problem, we use the connection formula (A.11) to rewrite the $\xi$-dependent PCFs. We also find it helpful to apply relations (C.6) and (C.7) to the ratio of $\beta$- dependent PCFs in one of the two integrals obtained (that which is the counterpart of $I_s^1$). When we do this we have that

$$I_d = I_d^1 + I_d^2 + I_d^3, \qquad I_n = I_n^1 + I_n^2 + I_n^3, \tag{4.84}$$

where

$$I_d^1 = -\frac{i}{2}\int_C \frac{(\tan\frac{\phi_0}{2})^\nu}{\cos\frac{\phi_0}{2}}\frac{e^{\frac{\nu\pi i}{2}}}{\Gamma(1+\nu)}\frac{D_\nu(p\beta)}{D_{-1-\nu}(\bar{p}\beta)}D_{-1-\nu}(\bar{p}\eta)D_\nu(-\bar{p}\xi)\frac{d\nu}{\sin(\nu\pi)}, \tag{4.85}$$

$$I_d^2 = -\frac{1}{2\pi}\int_C \frac{(\tan\frac{\phi_0}{2})^\nu}{\cos\frac{\phi_0}{2}}e^{\frac{\nu\pi i}{2}}\Gamma(1+\nu)\frac{D_{-1-\nu}(-\bar{p}\beta)}{D_{-1-\nu}(\bar{p}\beta)}D_{-1-\nu}(\bar{p}\eta)D_{-1-\nu}(-p\xi)d\nu, \tag{4.86}$$

$$I_n^1 = \frac{1}{2}\int_C \frac{(\tan\frac{\phi_0}{2})^\nu}{\cos\frac{\phi_0}{2}}\frac{e^{\frac{\nu\pi i}{2}}}{\Gamma(1+\nu)}\frac{D_\nu'(p\beta)}{D_{-1-\nu}'(\bar{p}\beta)}D_{-1-\nu}(\bar{p}\eta)D_\nu(-\bar{p}\xi)\frac{d\nu}{\sin(\nu\pi)}, \tag{4.87}$$

$$I_n^2 = \frac{1}{2\pi}\int_C \frac{(\tan\frac{\phi_0}{2})^\nu}{\cos\frac{\phi_0}{2}}e^{\frac{\nu\pi i}{2}}\Gamma(1+\nu)\frac{D_{-1-\nu}'(-\bar{p}\beta)}{D_{-1-\nu}'(\bar{p}\beta)}D_{-1-\nu}(\bar{p}\eta)D_{-1-\nu}(-p\xi)d\nu, \tag{4.88}$$

$$I_d^3 = I_n^3 = \frac{i}{2\sqrt{2\pi}}\int_{-\frac{1}{2}-i\infty}^{-\frac{1}{2}+i\infty}\frac{(\tan\frac{\phi_0}{2})^\nu}{\cos\frac{\phi_0}{2}}D_{-1-\nu}(\bar{p}\eta)D_\nu(-\bar{p}\xi)\frac{d\nu}{\sin(\nu\pi)}. \tag{4.89}$$

As before, if we wish to consider the first two integrals in each case independently we must take the contour $C$ to be either $C_l$ (when $\frac{\pi}{2} < \phi_0 < \pi$) or $C_r$ (when $0 < \phi_0 < \frac{\pi}{2}$). The third of the integrals, which is the same in both cases, is convergent on the initial contour $C_i$, and so may be considered separately from the others. It is, in fact, equal to $I_s$ when we replace $\xi$ by $-\xi$. From the discussion of the expansion of this integral we find that it has asymptotic expansion

$$I_3^d = I_3^n \sim -\frac{e^{ir+\frac{\pi i}{4}}}{2\sqrt{2\pi r}\sin\frac{1}{2}(\phi_0-\phi)} \tag{4.90}$$

for large $r$. This cancels with the diffracted component in the expansion of $I_i$ when we consider the total fields.

#### 4.2.4.5 Reflected field not present: $2\pi - \phi_0 - \phi > 0$

In this region the integrands have no saddle-point (in $|\,\nu\,| \gg 1$), and so just as in the Sommerfeld case we may approximate $I_d^1 + I_d^2$ by

$$-\frac{ie^{ir+\frac{\pi i}{4}}}{4\sqrt{r}\sin\frac{\phi}{2}\cos\frac{\phi_0}{2}}\int_{C_r'}\left(\frac{\tan\frac{\phi_0}{2}}{|\tan\frac{\phi}{2}|}\right)^{\nu}\frac{e^{\frac{\nu\pi i}{2}}}{\Gamma(1+\nu)}\frac{D_\nu(p\beta)}{D_{-1-\nu}(\bar{p}\beta)}\frac{d\nu}{\sin(\nu\pi)} \tag{4.91}$$

and $I_n^1 + I_n^2$ by

$$\frac{e^{ir+\frac{\pi i}{4}}}{4\sqrt{r}\sin\frac{\phi}{2}\cos\frac{\phi_0}{2}}\int_{C_r'}\left(\frac{\tan\frac{\phi_0}{2}}{|\tan\frac{\phi}{2}|}\right)^{\nu}\frac{e^{\frac{\nu\pi i}{2}}}{\Gamma(1+\nu)}\frac{D_\nu'(p\beta)}{D_{-1-\nu}'(\bar{p}\beta)}\frac{d\nu}{\sin(\nu\pi)}, \tag{4.92}$$

where the contour $C_r'$ again runs from $+\infty$ to $-\frac{1}{2}$ below the real axis, and then is parallel to the imaginary axis from there to $i\infty$. As in our discussion for $0 < \phi < \pi$, for our expansions to be valid we require the integrands to be exponentially small at an $\mathcal{O}(r^{\frac{1}{2}})$ distance away from $\nu = -\frac{1}{2}$. On further approximating the integrands for large $|\,\nu\,|$ we find we need

$$\exp\left\{\nu\log\left(\frac{\tan\frac{\phi_0}{2}}{|\tan\frac{\phi}{2}|}\right) + 2\bar{p}\beta\sqrt{\nu}\right\} \tag{4.93}$$

to be exponentially small when $|\,\nu\,| = \mathcal{O}(r^{\frac{1}{2}})$ on $C_r'$ in the lower half of the $\nu$ plane. On expanding the logarithmic term for $\phi$ near $2\pi - \phi_0$ we find that this becomes the condition $2\pi - \phi_0 - \phi \gg \beta r^{-\frac{1}{4}}$. We also need the integrands to decay sufficiently rapidly on the half of the contour in the upper half plane, and by a very similar analysis to that in $0 < \phi < \pi$ we find that this condition is again that $r \gg \beta^4$.

Integrals (4.92) and (4.91) may be completed by an arc in the right hand half plane, and we obtain the same diffracted fields as for $\phi_0 < \phi < \pi$ (when we account for the contributions from $I_d^3$ and $I_n^3$).

#### 4.2.4.6 Fully reflected region: $2\pi - \phi_0 < \phi < 2\pi$

Yet again we may proceed in the same manner as for the Sommerfeld case. Compared to integral $I_s^1$, the integrands of $I_d^1$ and $I_n^1$ are multiplied by

$$-\frac{\sqrt{2\pi}e^{-\frac{\nu\pi i}{2}}}{\Gamma(1+\nu)}\frac{D_\nu(p\beta)}{D_{-1-\nu}(\bar{p}\beta)} \quad \text{and} \quad -\frac{i\sqrt{2\pi}e^{-\frac{\nu\pi i}{2}}}{\Gamma(1+\nu)}\frac{D'_\nu(p\beta)}{D'_{-1-\nu}(\bar{p}\beta)} \tag{4.94}$$

respectively. The asymptotic expansions of these functions are discussed in more detail in Appendix C, but we note here that in Im $\nu < 0$ they have leading-order behaviour

$$\mp \exp\left(2\bar{p}\beta\sqrt{\nu}\right), \tag{4.95}$$

for large $|\,\nu\,|$, where the negative or positive sign is taken for the Dirichlet or Neumann problems respectively. The integrands of $I_d^2$ and $I_n^2$ differ from $I_s^2$ by factors of

$$-\frac{D_{-1-\nu}(-\bar{p}\beta)}{D_{-1-\nu}(\bar{p}\beta)} \quad \text{and} \quad \frac{D'_{-1-\nu}(-\bar{p}\beta)}{D'_{-1-\nu}(\bar{p}\beta)}, \tag{4.96}$$

which again have asymptotic approximation (4.95) in the lower half of the $\nu$ plane. Thus we find that when we introduce the scalings (4.41) there is no change to the leading-order phase, and so the saddle points and steepest descent contours are as before in the lower half of the complex $\nu$ plane. There are slight differences in the upper half-plane, as the phase-amplitude expansions of the integrands of $I_d^1$ and $I_n^1$ are now continuous across the negative real axis. Instead they have a discontinuity at the anti-Stokes line of $D_{-1-\nu}(\bar{p}\beta)$, which is also the line on which the poles of the integrand (in the left half of the $\nu$ plane) reside. We will allow our contour of integration for the integral which contains the saddle to follow the steepest descent path until it intersects either this anti-Stokes line, or the positive real axis (which is also an anti-Stokes line), at some point $Q$, and then let the contour run parallel to the imaginary axis from $Q$ to $i\infty$, as shown in Figure 4.10.

The details of the contribution from such a perturbed saddle point are discussed in Appendix D. From this we find that the pairs of integrals $I_d^1$ and $I_d^2$, and $I_n^1$ and $I_n^2$, have saddle point contributions $-R$ and $R$, where

$$\begin{aligned} R \;=\; & \exp\Big\{i(x\cos\phi_0 - y\sin\phi_0) - 2^{\frac{3}{2}}\beta i(\sin\phi_0)^{\frac{1}{2}}(x\sin\phi_0 + y\cos\phi_0)^{\frac{1}{2}} \\ & -i\beta^2\sin\phi_0\left(\frac{x\cos\phi_0 - y\sin\phi_0}{x\sin\phi_0 + y\cos\phi_0}\right) - i\beta^2\cos\phi_0\Big\}\left(1 + \mathcal{O}(r^{-\frac{1}{2}})\right). \end{aligned} \tag{4.97}$$

As before we will also obtain residue contributions from the poles crossed in deforming the contours of integration. In this case only the poles of $I_d^1$ at $\nu_n$ and $I_n^1$ at $\nu'_n$ contribute, as the integrands of $I_d^1$ and $I_n^1$ have no other poles in the half plane Re $\nu < -\frac{1}{2}$, whereas

$I_n^2$ and $I_d^2$ have no poles in the half plane Re $\nu > -\frac{1}{2}$. The residues from these poles may be approximated as for the Sommerfeld problem, and give the contributions

$$\frac{e^{ir+\frac{\pi i}{4}}\sqrt{\pi}}{2\sqrt{2r}\sin\frac{\phi}{2}\cos\frac{\phi_0}{2}}\sum_{m=0}^{\infty}\left(\frac{\tan\frac{\phi_0}{2}}{|\tan\frac{\phi}{2}|}\right)^{\nu_m}\frac{D_{-1-\nu_m}(-\bar{p}\beta)}{\frac{\partial}{\partial\nu}D_{-1-\nu}(\bar{p}\beta)|_{\nu=\nu_m}}\frac{e^{\nu_m\pi i}}{\sin(\nu_m\pi)}, \tag{4.98}$$

in the Dirichlet case, and

$$-\frac{e^{ir+\frac{\pi i}{4}}\sqrt{\pi}}{2\sqrt{2r}\sin\frac{\phi}{2}\cos\frac{\phi_0}{2}}\sum_{m=0}^{\infty}\left(\frac{\tan\frac{\phi_0}{2}}{|\tan\frac{\phi}{2}|}\right)^{\nu'_m}\frac{D'_{-1-\nu'_m}(-\bar{p}\beta)}{\frac{\partial}{\partial\nu}D'_{-1-\nu}(\bar{p}\beta)\big|_{\nu=\nu'_m}}\frac{e^{\nu'_m\pi i}}{\sin(\nu'_m\pi)}, \tag{4.99}$$

in the Neumann case. (Here we have used (C.6), (C.7) to write these in a similar form to those found in the upper half plane). The fields found in this region agree with the analysis of [44]. These series may also be expressed as

$$\frac{e^{ir+\frac{\pi i}{4}}}{2\sqrt{2\pi r}\sin\frac{1}{2}(\phi_0-\phi)}-\frac{ie^{ir+\frac{\pi i}{4}}}{4\sqrt{2\pi r}\sin\frac{\phi}{2}\cos\frac{\phi_0}{2}}\int_{C'_l}\left(\frac{\tan\frac{\phi_0}{2}}{|\tan\frac{\phi}{2}|}\right)^{\nu}e^{\nu\pi i}\frac{D_{-1-\nu}(-\bar{p}\beta)}{D_{-1-\nu}(\bar{p}\beta)}\frac{d\nu}{\sin(\nu\pi)}, \tag{4.100}$$

in the Dirichlet case, and

$$\frac{e^{ir+\frac{\pi i}{4}}}{2\sqrt{2\pi r}\sin\frac{1}{2}(\phi_0-\phi)}+\frac{ie^{ir+\frac{\pi i}{4}}}{4\sqrt{2\pi r}\sin\frac{\phi}{2}\cos\frac{\phi_0}{2}}\int_{C'_l}\left(\frac{\tan\frac{\phi_0}{2}}{|\tan\frac{\phi}{2}|}\right)^{\nu}e^{\nu\pi i}\frac{D'_{-1-\nu}(-\bar{p}\beta)}{D'_{-1-\nu}(\bar{p}\beta)}\frac{d\nu}{\sin(\nu\pi)}, \tag{4.101}$$

in the Neumann case, where the contour $C'_l$ runs from $-\infty$ to $-\frac{1}{2}$ below the poles of the integrand, and then is a straight line from $-\frac{1}{2}$ to $-\frac{1}{2}+i\infty$. ($C'_l$ is therefore very similar to $C_l$ of Figure 4.6, but lies below the poles of the integrand).

#### 4.2.4.7 Convergence of series forms for the diffracted fields

Here we examine the large-$m$ behaviour of the residue series solutions for the diffracted fields, as it is essential that these series converge. In $0 < \phi < \phi_0$ we find that the diffracted field has form

$$\frac{e^{ir+\frac{\pi i}{4}}\sqrt{\pi}}{2\sqrt{2r}\sin\frac{\phi}{2}\cos\frac{\phi_0}{2}}\sum_{m=0}^{\infty}\left(\frac{\tan\frac{\phi_0}{2}}{\tan\frac{\phi}{2}}\right)^{\nu_m}\frac{D_{-1-\nu_m}(-\bar{p}\beta)}{\frac{\partial}{\partial\nu}D_{-1-\nu}(\bar{p}\beta)|_{\nu=\nu_m}}\frac{1}{\sin(\nu_m\pi)}, \tag{4.102}$$

in the Dirichlet case and

$$-\frac{e^{ir+\frac{\pi i}{4}}\sqrt{\pi}}{2\sqrt{2r}\sin\frac{\phi}{2}\cos\frac{\phi_0}{2}}\sum_{m=0}^{\infty}\left(\frac{\tan\frac{\phi_0}{2}}{\tan\frac{\phi}{2}}\right)^{\nu'_m}\frac{D'_{-1-\nu'_m}(-\bar{p}\beta)}{\frac{\partial}{\partial\nu}D'_{-1-\nu}(\bar{p}\beta)\big|_{\nu=\nu'_m}}\frac{1}{\sin(\nu'_m\pi)}, \tag{4.103}$$

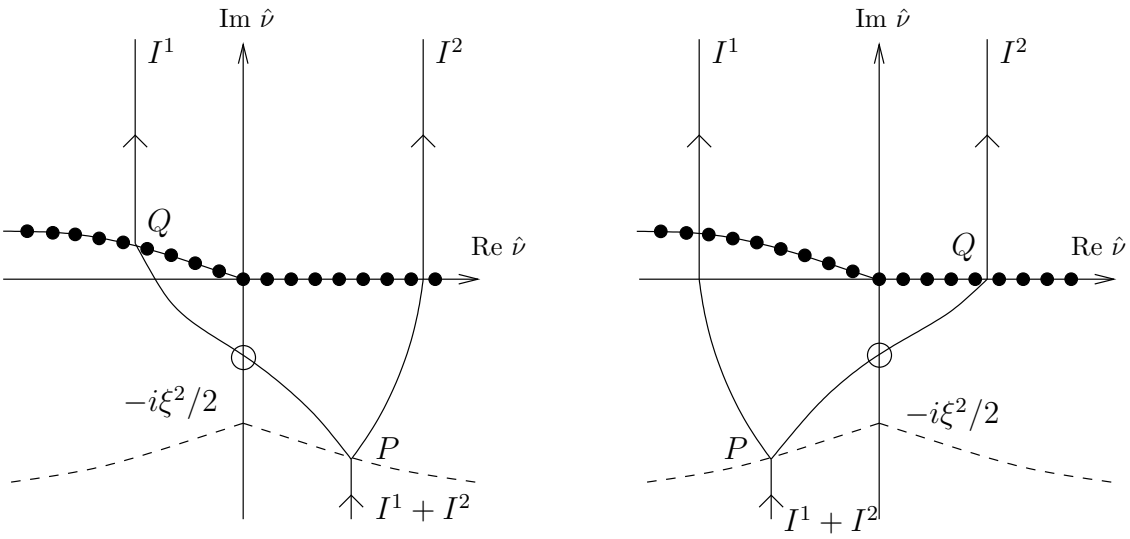


**Figure 4.10:** Contours used in the approximation of $I_d^1 + I_d^2$ and $I_n^1 + I_n^2$, when the reflected field is present and $\beta$ is non-zero. These are essentially the same as for the Sommerfeld problem, except that the integrands of $I_d^1$ and $I_n^1$ are now continuous across the negative real axis, and have a new set of poles ($\nu_m$ or $\nu'_m$), along the anti-Stokes line shown. (The integrands of $I_d^2$ and $I_n^2$ have poles at the negative integers, but these play no part in the approximation).

in the Neumann case. On using the large $\nu$ expansions (Appendix A.4.1) for the PCFs we find that

$$\frac{D_{-1-\nu_m}(-\bar{p}\beta)}{\frac{\partial}{\partial\nu}\, D_{-1-\nu}(\bar{p}\beta)\big|_{\nu=\nu_m}} \frac{1}{\sin(\nu_m\pi)} \quad \sim \quad \frac{2}{\pi}, \tag{4.104}$$

$$\frac{D'_{-1-\nu'_m}(-\bar{p}\beta)}{\frac{\partial}{\partial\nu}\, D'_{-1-\nu}(\bar{p}\beta)\big|_{\nu=\nu'_m}} \frac{1}{\sin(\nu'_m\pi)} \quad \sim \quad -\frac{2}{\pi}, \tag{4.105}$$

and so the late terms in the series (large $m$) are approximately

$$\frac{e^{ir+\frac{\pi i}{4}}}{\sqrt{2\pi r}\sin\frac{\phi}{2}\cos\frac{\phi_0}{2}} \left(\frac{\tan\frac{\phi_0}{2}}{\tan\frac{\phi}{2}}\right)^{p_m}, \tag{4.106}$$

where $p_m$ denotes $\nu_m$ or $\nu'_m$ as appropriate. Using the approximations (4.63) and (4.64) for the poles of the PCFs we find that these series are convergent when $0 < \phi < \phi_0$.

In the region $\phi_0 < \phi < 2\pi - \phi_0$ we find, in the same manner as above, that the late terms in the series have behaviour

$$\mp\frac{e^{ir+\frac{\pi i}{4}}}{2\sqrt{2\pi r}\sin\frac{\phi}{2}\cos\frac{\phi_0}{2}} \left(-\frac{\tan\frac{\phi_0}{2}}{\tan\frac{\phi}{2}}\right)^{m} \exp\left(2\bar{p}\beta\sqrt{m}\right), \tag{4.107}$$

where the minus sign corresponds to the Dirichlet case, and the plus sign the Neumann case. Again, this series is convergent when $\phi_0 < \phi < 2\pi - \phi_0$.

For the diffracted field in $2\pi - \phi_0 < \phi < 2\pi$ we find that the late terms in the series are asymptotically

$$\frac{e^{ir+\frac{\pi i}{4}}}{\sqrt{2\pi r}\sin\frac{\phi}{2}\cos\frac{\phi_0}{2}}\left(\frac{\tan\frac{\phi_0}{2}}{|\tan\frac{\phi}{2}|}\right)^{p_m} e^{p_m\pi i}. \tag{4.108}$$

This series again converges when $2\pi - \phi_0 < \phi < 2\pi$.

#### 4.2.4.8 Summary

Here we list, for convenience, the various asymptotic approximations for the far fields. For Dirichlet boundary conditions the far fields (except for $\phi = \phi_0$ or $\phi = 2\pi - \phi_0$) are of the form

$$\Psi_d \sim \chi(\phi-\phi_0)\Psi_i - \chi(\phi-(2\pi-\phi_0))R + \frac{e^{ir}}{\sqrt{r}}F_d(\phi), \tag{4.109}$$

where $\chi$ is the Heaviside function, $0 < \phi < 2\pi$, and the diffraction coefficient $F_d(\phi)$ is given by

$$F_d = \begin{cases} \dfrac{e^{\frac{\pi i}{4}}\sqrt{\pi}}{2\sqrt{2}\sin\frac{\phi}{2}\cos\frac{\phi_0}{2}}\displaystyle\sum_{m=0}^{\infty}\left(\frac{\tan\frac{\phi_0}{2}}{\tan\frac{\phi}{2}}\right)^{\nu_m}\frac{D_{-1-\nu_m}(-\bar{p}\beta)}{\frac{\partial}{\partial\nu}D_{-1-\nu}(\bar{p}\beta)|_{\nu=\nu_m}}\frac{1}{\sin(\nu_m\pi)} & 0<\phi<\phi_0, \\ -\dfrac{e^{\frac{\pi i}{4}}}{2\sin\frac{\phi}{2}\cos\frac{\phi_0}{2}}\displaystyle\sum_{m=0}^{\infty}\left(\frac{i\tan\frac{\phi_0}{2}}{\tan\frac{\phi}{2}}\right)^{m}\frac{D_m(p\beta)}{m!D_{-1-m}(\bar{p}\beta)} & \phi_0<\phi<2\pi-\phi_0, \\ \dfrac{e^{\frac{\pi i}{4}}\sqrt{\pi}}{2\sqrt{2}\sin\frac{\phi}{2}\cos\frac{\phi_0}{2}}\displaystyle\sum_{m=0}^{\infty}\left(\frac{\tan\frac{\phi_0}{2}}{|\tan\frac{\phi}{2}|}\right)^{\nu_m}\frac{D_{-1-\nu_m}(-\bar{p}\beta)}{\frac{\partial}{\partial\nu}D_{-1-\nu}(\bar{p}\beta)|_{\nu=\nu_m}}\frac{e^{\nu_m\pi i}}{\sin(\nu_m\pi)} & 2\pi-\phi_0<\phi<2\pi. \end{cases} \tag{4.110}$$

Here

$$\Psi_i = \exp\left\{i\left(\left(\frac{\xi^2-\eta^2}{2}\right)\cos\phi_0 + \xi\eta\sin\phi_0\right)\right\} \tag{4.111}$$

is the incident plane wave, and

$$\begin{aligned} R \sim\ & \exp\Big\{i(x\cos\phi_0 - y\sin\phi_0) - 2^{\frac{3}{2}}\beta i(\sin\phi_0)^{\frac{1}{2}}(x\sin\phi_0+y\cos\phi_0)^{\frac{1}{2}} \\ & -i\beta^2\sin\phi_0\left(\frac{x\cos\phi_0 - y\sin\phi_0}{x\sin\phi_0+y\cos\phi_0}\right) - i\beta^2\cos\phi_0\Big\}(1+\mathcal{O}(r^{-\frac{1}{2}})) \end{aligned} \tag{4.112}$$

is the reflected field (supplied by the saddle point). Away from $\phi = 2\pi - \phi_0$ the diffraction coefficient may be written in integral form as

$$F_d = \begin{cases} F_i - \dfrac{ie^{\frac{\pi i}{4}}}{4\sqrt{2\pi}\sin\frac{\phi}{2}\cos\frac{\phi_0}{2}} \displaystyle\int_{-\frac{1}{2}-i\infty}^{-\frac{1}{2}+i\infty} \left(\frac{\tan\frac{\phi_0}{2}}{\tan\frac{\phi}{2}}\right)^{\nu} \frac{D_{-1-\nu}(-\bar{p}\beta)}{D_{-1-\nu}(\bar{p}\beta)} \frac{d\nu}{\sin(\nu\pi)} & 0 < \phi < \pi, \\ -\dfrac{ie^{\frac{\pi i}{4}}}{4\sin\frac{\phi}{2}\cos\frac{\phi_0}{2}} \displaystyle\int_{C_r'} \left(\frac{\tan\frac{\phi_0}{2}}{|\tan\frac{\phi}{2}|}\right)^{\nu} \frac{e^{\frac{\nu\pi i}{2}}}{\Gamma(1+\nu)} \frac{D_{\nu}(p\beta)}{D_{-1-\nu}(\bar{p}\beta)} \frac{d\nu}{\sin(\nu\pi)} & \pi < \phi < 2\pi - \phi_0, \\ F_i - \dfrac{ie^{\frac{\pi i}{4}}}{4\sqrt{2\pi}\sin\frac{\phi}{2}\cos\frac{\phi_0}{2}} \displaystyle\int_{C_l'} \left(\frac{\tan\frac{\phi_0}{2}}{|\tan\frac{\phi}{2}|}\right)^{\nu} \frac{D_{-1-\nu}(-\bar{p}\beta)}{D_{-1-\nu}(\bar{p}\beta)} \frac{e^{\nu\pi i} d\nu}{\sin(\nu\pi)} & 2\pi - \phi_0 < \phi < 2\pi, \end{cases} \tag{4.113}$$

where

$$F_i = \frac{e^{\frac{\pi i}{4}}}{2\sqrt{2\pi}\sin\frac{1}{2}(\phi_0 - \phi)}. \tag{4.114}$$

In the Neumann case we have

$$\Psi_n \sim \chi(\phi - \phi_0)\Psi_i + \chi(\phi - (2\pi - \phi_0))R + \frac{e^{ir}}{\sqrt{r}} F_n(\phi) \tag{4.115}$$

where

$$F_n = \begin{cases} -\dfrac{e^{\frac{\pi i}{4}}\sqrt{\pi}}{2\sqrt{2}\sin\frac{\phi}{2}\cos\frac{\phi_0}{2}} \displaystyle\sum_{m=0}^{\infty} \left(\frac{\tan\frac{\phi_0}{2}}{\tan\frac{\phi}{2}}\right)^{\nu_m'} \frac{D'_{-1-\nu_m'}(-\bar{p}\beta)}{\frac{\partial}{\partial\nu} D'_{-1-\nu}(\bar{p}\beta)\big|_{\nu=\nu_m'}} \frac{1}{\sin(\nu_m'\pi)} & 0 < \phi < \phi_0, \\ -\dfrac{ie^{\frac{\pi i}{4}}}{2\sin\frac{\phi}{2}\cos\frac{\phi_0}{2}} \displaystyle\sum_{m=0}^{\infty} \left(\frac{i\tan\frac{\phi_0}{2}}{\tan\frac{\phi}{2}}\right)^{m} \frac{D'_m(p\beta)}{m! D'_{-1-m}(\bar{p}\beta)} & \phi_0 < \phi < 2\pi - \phi_0, \\ -\dfrac{e^{\frac{\pi i}{4}}\sqrt{\pi}}{2\sqrt{2}\sin\frac{\phi}{2}\cos\frac{\phi_0}{2}} \displaystyle\sum_{m=0}^{\infty} \left(\frac{\tan\frac{\phi_0}{2}}{|\tan\frac{\phi}{2}|}\right)^{\nu_m'} \frac{D'_{-1-\nu_m'}(-\bar{p}\beta)}{\frac{\partial}{\partial\nu} D'_{-1-\nu}(\bar{p}\beta)\big|_{\nu=\nu_m'}} \frac{e^{\nu_m'\pi i}}{\sin(\nu_m'\pi)} & 2\pi - \phi_0 < \phi < 2\pi, \end{cases} \tag{4.116}$$

and the integral form for the diffraction coefficient is

$$F_n = \begin{cases} F_i + \dfrac{ie^{\frac{\pi i}{4}}}{4\sqrt{2\pi}\sin\frac{\phi}{2}\cos\frac{\phi_0}{2}} \displaystyle\int_{-\frac{1}{2}-i\infty}^{-\frac{1}{2}+i\infty} \left(\frac{\tan\frac{\phi_0}{2}}{\tan\frac{\phi}{2}}\right)^{\nu} \frac{D'_{-1-\nu}(-\bar{p}\beta)}{D'_{-1-\nu}(\bar{p}\beta)} \frac{d\nu}{\sin(\nu\pi)} & 0 < \phi < \pi, \\ \dfrac{e^{\frac{\pi i}{4}}}{4\sin\frac{\phi}{2}\cos\frac{\phi_0}{2}} \displaystyle\int_{C_r'} \left(\frac{\tan\frac{\phi_0}{2}}{|\tan\frac{\phi}{2}|}\right)^{\nu} \frac{e^{\frac{\nu\pi i}{2}}}{\Gamma(1+\nu)} \frac{D'_{\nu}(p\beta)}{D'_{-1-\nu}(\bar{p}\beta)} \frac{d\nu}{\sin(\nu\pi)} & \pi < \phi < 2\pi - \phi_0, \\ F_i + \dfrac{ie^{\frac{\pi i}{4}}}{4\sqrt{2\pi}\sin\frac{\phi}{2}\cos\frac{\phi_0}{2}} \displaystyle\int_{C_l'} \left(\frac{\tan\frac{\phi_0}{2}}{|\tan\frac{\phi}{2}|}\right)^{\nu} \frac{D'_{-1-\nu}(-\bar{p}\beta)}{D'_{-1-\nu}(\bar{p}\beta)} \frac{e^{\nu\pi i} d\nu}{\sin(\nu\pi)} & 2\pi - \phi_0 < \phi < 2\pi. \end{cases} \tag{4.117}$$

To find the fields $\psi_d$ and $\psi_n$ from these results we must restore the $e^{i\beta^2(\cos\phi_0)/2}$ prefactor. The listed results are also written in terms of a coordinate system with centre at the

focus of the parabola used in the inner problem. To convert the diffraction coefficients to a polar coordinate system $(r, \phi')$ centred at the tip of the parabola $\phi$ must be replaced by $\phi'$ and the diffraction coefficients multiplied by $e^{-i\beta^2(\cos\phi')/2}$.

We see that these far fields are discontinuous across the line $\phi = \phi_0$, where the incident field switches on, and across the line $\phi = 2\pi - \phi_0$, where the reflected field switches on. However the exact solutions are continuous across these lines, and so we expect to find transition regions within which these fields smoothly switch on or off.

#### 4.2.4.9 Behaviour of these fields for small $\beta$

As noted previously, the exact integrals yield the Sommerfeld solution when $\beta = 0$. The above analysis is valid even for small $\beta$, and so we may find the scattered fields by replacing the $\beta$- dependent PCFs by their power series expansions (A.32) and (A.33) for small $\beta$, as listed in Appendix A.4.4. Using these we find that

$$\frac{D_{-1-\nu}(-\bar{p}\beta)}{D_{-1-\nu}(\bar{p}\beta)} \sim 1 + 2^{\frac{3}{2}}\bar{p}\beta\frac{\Gamma(1+\frac{\nu}{2})}{\Gamma(\frac{1}{2}+\frac{\nu}{2})} \tag{4.118}$$

$$\frac{D'_{-1-\nu}(-\bar{p}\beta)}{D'_{-1-\nu}(\bar{p}\beta)} \sim 1 + 2^{\frac{1}{2}}\bar{p}\beta\left(\nu+\frac{1}{2}\right)\frac{\Gamma(\frac{1}{2}+\frac{\nu}{2})}{\Gamma(1+\frac{\nu}{2})} \tag{4.119}$$

(we note that (4.119) differs in sign from (4.50) of [44]). The second term in these approximations is small compared to the first provided that $\sqrt{\nu}\beta \ll 1$. Approximating the PCFs in the integral representations of the previous section we see that the directivity differs by an $\mathcal{O}(\beta)$ amount from the Sommerfeld case.

Although the expression (4.112) for the reflected field does reduce to the result of the Sommerfeld case as $\beta$ becomes small, this convergence is non-uniform and the reflected fields only agree where $r \ll \beta^{-2}$. This can be seen by considering the validity of this expansion for the $\beta$- dependent PCFs in the vicinity of the saddle point.

#### 4.2.4.10 Incident shadow boundary

Across the line $\phi = \phi_0$ the incident field switches on. This incident field is supplied by $I_i$, which has an exact representation (4.26) in terms of a complementary error function. Thus we see that the incident field switches on in exactly the same manner as for the Sommerfeld case. For $\phi - \phi_0 = \mathcal{O}(r^{-\frac{1}{2}})$ we find that

$$I_i \sim \frac{1}{2}e^{ir\left(1-\frac{1}{2}(\phi-\phi_0)^2\right)}\mathrm{erfc}\left(\frac{1}{2}\bar{p}\sqrt{r}(\phi_0-\phi)\right), \tag{4.120}$$

and so recover the standard shadow boundary smoothing (as for a sharp edge). There is also a diffracted contribution in this region, supplied by $I_d$ or $I_n$, but this can be seen from

the integral forms of the previous section to be continuous across the incident shadow boundary.

#### 4.2.4.11 Reflected transition region

Our approximations are also discontinuous at the line $\phi = 2\pi - \phi_0$, because the reflected field switches on there. We find that the asymptotic approximations (4.109) and (4.115) become invalid as we approach this boundary from either side. Our analysis in $2\pi - \phi_0 < \phi < 2\pi$ becomes invalid when $\phi - (2\pi - \phi_0) = \mathcal{O}(\beta^{\frac{2}{3}} r^{-\frac{1}{3}})$, as the $\mathcal{O}(\beta r^{\frac{1}{2}} \hat{\nu}^{\frac{1}{2}} = \beta \nu^{\frac{1}{2}})$ contribution to the phase from the ratio of $\beta$- dependent PCFs is of the same order of magnitude as the leading-order phase term. As discussed before, on the other side of the boundary ($\phi < 2\pi - \phi_0$) the approximation of the diffracted field breaks down when $(2\pi - \phi_0) - \phi = \mathcal{O}(\beta r^{-\frac{1}{4}})$, as the correction term becomes comparable in size to the leading-order term.

We deform our integration contours to the forked contour $C_b'$ as for the Sommerfeld case, and as on either side of the transition region we find that the dominant contribution to $I_d^1 + I_d^2$ and $I_n^1 + I_n^2$ is that from near $\nu = -\frac{1}{2}$ for $I_d^1$ and $I_n^1$. We introduce the scalings

$$\phi = (2\pi - \phi_0) + r^{-\frac{1}{3}} \tilde{\phi}, \qquad \nu = r^{\frac{2}{3}} \tilde{\nu}, \tag{4.121}$$

and when $\tilde{\nu} = \mathcal{O}(1)$ we may use the expansion (A.20) for the $\xi$- and $\eta$- dependent PCFs, which is considerably simpler than the phase-amplitude expansions (used in the fully reflected region). Using these approximations we find that $I_d^1$ has leading-order behaviour

$$I_d^1 \sim \frac{-ie^{ir+\frac{\pi i}{4}} r^{\frac{1}{6}}}{4 \sin\frac{\phi_0}{2} \cos\frac{\phi_0}{2}} \int_{C_b'} \frac{e^{\frac{r^{\frac{2}{3}} \tilde{\nu} \pi i}{2}}}{\Gamma(1 + r^{\frac{2}{3}} \tilde{\nu})} \frac{D_{r^{\frac{2}{3}} \tilde{\nu}}(p\beta)}{D_{-1-r^{\frac{2}{3}} \tilde{\nu}}(\bar{p}\beta)} \times \exp\left\{ r^{\frac{1}{3}} \left( \frac{\tilde{\nu}\tilde{\phi}}{\sin\phi_0} - \frac{i\tilde{\nu}^2}{2\sin^2\phi_0} \right) - \frac{i\tilde{\nu}^2 \tilde{\phi} \cos\phi_0}{\sin^3\phi_0} + \frac{\tilde{\nu}\tilde{\phi}^2 \cos\phi_0}{2\sin^2\phi_0} - \frac{\tilde{\nu}^3 \cos\phi_0}{2\sin^4\phi_0} \right\} \frac{d\tilde{\nu}}{\sin(r^{\frac{2}{3}} \tilde{\nu} \pi)}, \tag{4.122}$$

and $I_n^1$ is approximately

$$I_n^1 \sim \frac{e^{ir+\frac{\pi i}{4}} r^{\frac{1}{6}}}{4 \sin\frac{\phi_0}{2} \cos\frac{\phi_0}{2}} \int_{C_b'} \frac{e^{\frac{r^{\frac{2}{3}} \tilde{\nu} \pi i}{2}}}{\Gamma(1 + r^{\frac{2}{3}} \tilde{\nu})} \frac{D'_{r^{\frac{2}{3}} \tilde{\nu}}(p\beta)}{D'_{-1-r^{\frac{2}{3}} \tilde{\nu}}(\bar{p}\beta)} \times \exp\left\{ r^{\frac{1}{3}} \left( \frac{\tilde{\nu}\tilde{\phi}}{\sin\phi_0} - \frac{i\tilde{\nu}^2}{2\sin^2\phi_0} \right) - \frac{i\tilde{\nu}^2 \tilde{\phi} \cos\phi_0}{\sin^3\phi_0} + \frac{\tilde{\nu}\tilde{\phi}^2 \cos\phi_0}{2\sin^2\phi_0} - \frac{\tilde{\nu}^3 \cos\phi_0}{2\sin^4\phi_0} \right\} \frac{d\tilde{\nu}}{\sin(r^{\frac{2}{3}} \tilde{\nu} \pi)}. \tag{4.123}$$

These integrals (along with the incident plane wave) will be seen to provide a solution in the transition region which matches smoothly with the approximate solutions for a blunt body (when $\beta$ becomes large) and the Sommerfeld problem (when $\beta$ becomes small). However when $\beta = \mathcal{O}(1)$ we find that we may approximate these integral solutions still further.

Using the expansions of Appendix C the integrands of (4.122) and (4.123) have leading-order approximations

$$\pm \frac{e^{ir+\frac{\pi i}{4}} r^{\frac{1}{6}}}{2\sqrt{2\pi}\sin\frac{\phi_0}{2}\cos\frac{\phi_0}{2}} \times \exp\left\{ r^{\frac{1}{3}} \left( \frac{\tilde{\nu}\tilde{\phi}}{\sin\phi_0} - \frac{i\tilde{\nu}^2}{2\sin^2\phi_0} + 2\bar{p}\beta\sqrt{\tilde{\nu}} \right) - \frac{i\tilde{\nu}^2\tilde{\phi}\cos\phi_0}{\sin^3\phi_0} + \frac{\tilde{\nu}\tilde{\phi}^2\cos\phi_0}{2\sin^2\phi_0} - \frac{\tilde{\nu}^3\cos\phi_0}{2\sin^4\phi_0} \right\} \tag{4.124}$$

in the lower half of the complex $\nu$ plane, with the positive sign in the Dirichlet case, and the negative sign in the Neumann case. The phase of the integrand is

$$u = \frac{\tilde{\nu}\tilde{\phi}}{\sin\phi_0} - \frac{i\tilde{\nu}^2}{2\sin^2\phi_0} + 2\bar{p}\beta\sqrt{\tilde{\nu}}, \tag{4.125}$$

which has saddle points when

$$\frac{du}{d\nu} = \frac{\tilde{\phi}}{\sin\phi_0} - \frac{i\tilde{\nu}}{\sin^2\phi_0} + \frac{\bar{p}\beta}{\sqrt{\tilde{\nu}}} = 0. \tag{4.126}$$

If we write $\tilde{\nu} = -i\tilde{\mu}^2$ this condition becomes the cubic

$$\tilde{\mu}^3 - \tilde{\mu}\tilde{\phi}\sin\phi_0 - \sqrt{2}\beta\sin^2\phi_0 = 0, \tag{4.127}$$

which can be shown to have one positive root $\mu_s$ for $\beta > 0$ and all real $\tilde{\phi}$. We will deform the contours of integration $I_d^1$ and $I_n^1$ to the path of steepest descent through this saddle point, and then use the approximation (4.124) for the integrands. Using this we find that the saddle point contribution is

$$\mp \frac{e^{ir}}{2\sin\frac{\phi_0}{2}\cos\frac{\phi_0}{2}} \left\{ \frac{1}{\sin^2\phi_0} + \frac{\beta}{\sqrt{2}\tilde{\mu}_s^3} \right\}^{-\frac{1}{2}} \times \exp\left\{ r^{\frac{1}{3}} \left( -\frac{i\tilde{\mu}_s^2\tilde{\phi}}{\sin\phi_0} + \frac{i\tilde{\mu}_s^4}{2\sin^2\phi_0} - 2i\beta\sqrt{2}\tilde{\mu}_s \right) + \frac{i\tilde{\mu}_s^4\tilde{\phi}\cos\phi_0}{\sin^3\phi_0} - \frac{i\tilde{\mu}_s^2\tilde{\phi}^2\cos\phi_0}{2\sin^2\phi_0} - \frac{i\tilde{\mu}_s^6\cos\phi_0}{2\sin^4\phi_0} \right\}, \tag{4.128}$$

where the upper (lower) sign corresponds to the Dirichlet (Neumann) case. We will also obtain residue contributions from the string of poles of the integrands of (4.122)

and (4.123) (at the $\nu_n$ or $\nu_n'$) when we deform the contour of integration to the path of steepest descent; the contour crosses $O(r^{\frac{2}{3}})$ such poles, and these give the same residue series for the diffracted fields as in the fully reflected region (except with the $\sin\frac{\phi}{2}$ term in the prefactor approximated by $\sin\frac{\phi_0}{2}$), namely

$$\frac{e^{ir+\frac{\pi i}{4}}\sqrt{\pi}}{2\sqrt{2r}\sin\frac{\phi_0}{2}\cos\frac{\phi_0}{2}}\sum_{m=0}^{\mathcal{O}(r^{\frac{2}{3}})}\left(\frac{\tan\frac{\phi_0}{2}}{|\tan\frac{\phi}{2}|}\right)^{\nu_m}\frac{D_{-1-\nu_m}(-\bar{p}\beta)}{\frac{\partial}{\partial\nu}D_{-1-\nu}(\bar{p}\beta)|_{\nu=\nu_m}}\frac{e^{\nu_m\pi i}}{\sin(\nu_m\pi)} \tag{4.129}$$

in the Dirichlet case, and

$$-\frac{e^{ir+\frac{\pi i}{4}}\sqrt{\pi}}{2\sqrt{2r}\sin\frac{\phi_0}{2}\cos\frac{\phi_0}{2}}\sum_{m=0}^{\mathcal{O}(r^{\frac{2}{3}})}\left(\frac{\tan\frac{\phi_0}{2}}{|\tan\frac{\phi}{2}|}\right)^{\nu_m'}\frac{D'_{-1-\nu_m'}(-\bar{p}\beta)}{\frac{\partial}{\partial\nu}D'_{-1-\nu}(\bar{p}\beta)\big|_{\nu=\nu_m'}}\frac{e^{\nu_m'\pi i}}{\sin(\nu_m'\pi)} \tag{4.130}$$

in the Neumann case. However, when $\tilde{\phi}<0$ we cannot extend the limit of summation to infinity, as these series do not converge. From our discussion in Section 4.2.4.7 we have that the late terms in these residue series have expansion

$$\frac{e^{ir+\frac{\pi i}{4}}}{\sqrt{2\pi r}\sin\frac{\phi_0}{2}\cos\frac{\phi_0}{2}}\left(\frac{\tan\frac{\phi_0}{2}}{|\tan\frac{\phi}{2}|}\right)^{p_m}e^{p_m\pi i} \tag{4.131}$$

for large $m$, where the $p_m$ denote the poles $\nu_m$ or $\nu_m'$ as appropriate. The series diverge when $\tilde{\phi}<0$ because $\frac{\tan\frac{\phi_0}{2}}{|\tan\frac{\phi}{2}|}<1$ and $p_m\to-\infty$ as $m\to\infty$. Using expansions (4.63) and (4.64) for the large $m$ behaviour of these poles we find that the late terms in the series are approximately

$$\frac{e^{ir+\frac{\pi i}{4}}}{\sqrt{2\pi r}\sin\frac{\phi_0}{2}\cos\frac{\phi_0}{2}}\exp\left\{\left(\pi i+\log\left(\frac{\tan\frac{\phi_0}{2}}{|\tan\frac{\phi}{2}|}\right)\right)\left(-2m-\frac{2\bar{p}\beta}{\pi}\sqrt{2m+1}-2+\frac{4i\beta^2}{\pi^2}\right)\right\} \tag{4.132}$$

in the Dirichlet case. When $\tilde{\phi}<0$ the late terms of the series decay exponentially for

$$1\ll m<\mathcal{O}\left(2\beta^2\left(\log\left(\frac{\tan\frac{\phi_0}{2}}{|\tan\frac{\phi}{2}|}\right)\right)^{-2}\right). \tag{4.133}$$

Therefore, provided that $0<(2\pi-\phi_0)-\phi\ll 1$, the terms in series (4.129) initially decay exponentially (before eventually growing), and a similar result may be found for (4.130). Thus we obtain the same series for the diffracted field as in the fully reflected region, terminated at a position where the terms are exponentially small (in $r$); just before the smallest term will suffice.

In summary, for $\beta = \mathcal{O}(1)$ the fields in this transition region are approximately

$$\Psi_d = \Psi_i - R_b + \frac{e^{ir+\frac{\pi i}{4}}\sqrt{\pi}}{2\sqrt{2r}\sin\frac{\phi_0}{2}\cos\frac{\phi_0}{2}} \sum_{m=0}^{\mathcal{O}(r^{\frac{2}{3}})} \left(\frac{\tan\frac{\phi_0}{2}}{|\tan\frac{\phi}{2}|}\right)^{\nu_m} \frac{D_{-1-\nu_m}(-\bar{p}\beta)}{\frac{\partial}{\partial\nu}\, D_{-1-\nu}(\bar{p}\beta)\big|_{\nu=\nu_m}} \frac{e^{\nu_m\pi i}}{\sin(\nu_m\pi)} \tag{4.134}$$

$$\Psi_n = \Psi_i + R_b - \frac{e^{ir+\frac{\pi i}{4}}\sqrt{\pi}}{2\sqrt{2r}\sin\frac{\phi_0}{2}\cos\frac{\phi_0}{2}} \sum_{m=0}^{\mathcal{O}(r^{\frac{2}{3}})} \left(\frac{\tan\frac{\phi_0}{2}}{|\tan\frac{\phi}{2}|}\right)^{\nu'_m} \frac{D'_{-1-\nu'_m}(-\bar{p}\beta)}{\frac{\partial}{\partial\nu}\, D'_{-1-\nu}(\bar{p}\beta)\big|_{\nu=\nu'_m}} \frac{e^{\nu'_m\pi i}}{\sin(\nu'_m\pi)} \tag{4.135}$$

where

$$R_b = \frac{e^{ir}}{2\sin\frac{\phi_0}{2}\cos\frac{\phi_0}{2}} \left\{\frac{1}{\sin^2\phi_0} + \frac{\beta}{\sqrt{2}\tilde{\mu}_s^3}\right\}^{-\frac{1}{2}} \times \tag{4.136}$$
$$\exp\left\{r^{\frac{1}{3}}\left(-\frac{i\tilde{\mu}_s^2\tilde{\phi}}{\sin\phi_0} + \frac{i\tilde{\mu}_s^4}{2\sin^2\phi_0} - 2i\beta\sqrt{2}\tilde{\mu}_s\right) + \frac{i\tilde{\mu}_s^4\tilde{\phi}\cos\phi_0}{\sin^3\phi_0} - \frac{i\tilde{\mu}_s^2\tilde{\phi}^2\cos\phi_0}{2\sin^2\phi_0} - \frac{i\tilde{\mu}_s^6\cos\phi_0}{2\sin^4\phi_0}\right\}.$$

We will now proceed to check that this approximation matches with the solutions in $\pi < \phi < 2\pi - \phi_0$ and $2\pi - \phi_0 < \phi < 2\pi$.

For large positive $\tilde{\phi}$ we find that the positive root of (4.127) has expansion

$$\tilde{\mu}_s \sim (\tilde{\phi}\sin\phi_0)^{\frac{1}{2}} + \frac{\beta\sin\phi_0}{\sqrt{2}\tilde{\phi}} - \frac{3\beta^2\sin\phi_0}{4\tilde{\phi}^3}, \tag{4.137}$$

and using this we may, with some labour, see that our approximation in the transition region matches with the fully reflected field as we move out of the shadow boundary. The approximate integrands (4.124) used in the transition region are just the limit for $\nu = \mathcal{O}(r^{\frac{2}{3}})$ of the phase-amplitude approximations used to calculate the saddle point contribution in the fully reflected region. We made the approximation

$$\exp\left(\nu\log\left(\frac{\tan\frac{\phi_0}{2}}{|\tan\frac{\phi}{2}|}\right)\right) = \exp\left(r^{\frac{1}{3}}\frac{\tilde{\nu}\tilde{\phi}}{\sin\phi_0} + \frac{\tilde{\nu}\tilde{\phi}^2\cos\phi_0}{2\sin^2\phi_0} + \mathcal{O}(r^{-\frac{1}{3}}\tilde{\nu}\tilde{\phi}^3)\right) \tag{4.138}$$

but provided that $0 < \tilde{\phi} \ll r^{\frac{1}{12}}$ the former approximation will not affect the leading-order contribution from the saddle point. (We have also approximated $\sin\frac{\phi}{2} \sim \sin\frac{\phi_0}{2}$, but this is fine provided that $|2\pi - \phi_0 - \phi| \ll 1$).

For large negative $\tilde{\phi}$ the saddle point has position

$$\tilde{\nu} \sim -\frac{2i\beta^2\sin^2\phi_0}{\tilde{\phi}^2} \tag{4.139}$$

to leading-order. Near the saddle point the factor multiplying the dominant terms in the phase is $\mathcal{O}(r^{\frac{1}{3}}\beta^2\,|\tilde{\phi}|^{-1})$, and so the saddle point region is $\mathcal{O}(\sqrt{|\tilde{\phi}|r^{-\frac{1}{6}}\beta^{-1}})$ in width.

In contrast to the Sommerfeld problem we see that the saddle point does not "pass through" the real axis, but instead the approximation breaks down (for $\beta = \mathcal{O}(1)$) when $\tilde{\phi}$ is $O(r^{\frac{1}{3}})$, which corresponds to $(2\pi - \phi_0) - \phi$ being $\mathcal{O}(1)$. The approximation becomes invalid because the factor multiplying the phase (near the saddle point) is no longer large, and because the saddle point is then at a point for which $\nu = \mathcal{O}(1)$, where as the approximation for the ratio of the $\beta$-dependent PCFs is only valid for large $\nu$.

From our previous discussion for the region $\pi < \phi < 2\pi - \phi_0$ we recall that the diffracted fields may be written in the form (4.91) and (4.92). These are just approximations of $I_d^1$ and $I_n^1$ when the dominant contribution is from a region about $\nu = -\frac{1}{2}$. When $(2\pi - \phi_0) - \phi \ll 1$ we find that this integral form for the diffraction coefficient has a saddle point at

$$\nu \;=\; -\frac{2i\beta^2}{\left\{\log\left(\frac{\tan\frac{\phi_0}{2}}{|\tan\frac{\phi}{2}|}\right)\right\}^2} \;\sim\; -\frac{2i\beta^2\sin^2\phi_0}{(2\pi-\phi_0-\phi)^2} \tag{4.140}$$

and the leading-order saddle point contribution is

$$\mp\frac{\beta e^{ir}}{\sqrt{r}\sin\frac{\phi}{2}\cos\frac{\phi_0}{2}}\frac{e^{2i\beta^2/\log\left(\frac{\tan\frac{\phi_0}{2}}{|\tan\frac{\phi}{2}|}\right)}}{\left\{-\log\left(\frac{\tan\frac{\phi_0}{2}}{|\tan\frac{\phi}{2}|}\right)\right\}^{\frac{3}{2}}}. \tag{4.141}$$

In the overlap region[6] $r^{\frac{1}{3}}, r^{\frac{1}{3}}\beta^2 \gg|\,\tilde{\phi}\,|\gg \beta r^{\frac{1}{12}}$ we find that two saddle point approximations agree to leading order. Hence the two approximations match in this region. The approximations of the $\xi$- and $\eta$- dependent PCFs used in the transition region agree to leading order with to those used to find the diffracted field for $\pi < \phi < 2\pi - \phi_0$, so it is not unsurprising that the saddle point contributions agree,

This saddle point analysis of integrals (4.122) and (4.123) was performed under the assumption that $\beta = \mathcal{O}(1)$. We expect that the transition region solution will become an error function smoothing as $\beta$ tends to zero, but this is not the case for the approximate solutions listed above.

When $\beta = \mathcal{O}(r^{-\frac{1}{4}})$, the transition region becomes $\phi - (2\pi - \phi_0) = \mathcal{O}(r^{-\frac{1}{2}})$ in width (which is the same scaling as the reflected shadow boundary in the Sommerfeld case). We now find that the appropriate scalings which give a balance between terms in the

[6]Here the condition $|\tilde{\phi}|\gg \beta r^{\frac{1}{12}}$ ensures that the $-ir^{\frac{1}{3}}\tilde{\nu}^2/(2\sin^2\phi_0)$ term in the phase of (4.124) does not affect the leading-order saddle point contribution, and the $r^{\frac{1}{3}}\beta^2 \gg|\,\tilde{\phi}\,|$ condition ensures that the approximation (4.138) has not broken down near the saddle point. We also require that $|\,\tilde{\phi}\,|\ll r^{\frac{1}{3}}$ so that the large $\beta$- expansions for the ratio of the PCFs are valid near the saddle point.

phase are $\nu = r^{\frac{1}{2}}\check{\nu}$ (so $\tilde{\nu} = r^{-\frac{1}{6}}\check{\nu}$) and $\phi - (2\pi - \phi_0) = r^{-\frac{1}{2}}\check{\phi}$ (so $\tilde{\check{\phi}} = r^{-\frac{1}{6}}\check{\phi}$), and when we introduce these scalings we find that the coefficient multiplying the phase in the exponent is no longer large. Therefore the saddle point analysis breaks down when $\beta$ is of this order. However, the range of $\nu$ is smaller than before ($\nu = \mathcal{O}(r^{\frac{1}{2}})$), and so we may approximate the integrands further (using (A.19) for the $\xi$- and $\eta$- dependent PCFs). We find that the fields in the transition region are now approximately

$$I_d^1 \sim -\frac{ie^{ir+\frac{\pi i}{4}}}{4\sin\frac{\phi_0}{2}\cos\frac{\phi_0}{2}}\int_{C_b'}\frac{e^{\frac{r^{\frac{1}{2}}\check{\nu}\pi i}{2}}}{\Gamma(1+r^{\frac{1}{2}}\check{\nu})}\frac{D_{r^{\frac{1}{2}}\check{\nu}}(p\beta)}{D_{-1-r^{\frac{1}{2}}\check{\nu}}(\bar{p}\beta)}\exp\left\{\frac{\check{\nu}\check{\phi}}{\sin\phi_0}-\frac{i\check{\nu}^2}{2\sin^2\phi_0}\right\}\frac{d\check{\nu}}{\sin(r^{\frac{1}{2}}\check{\nu}\pi)}, \tag{4.142}$$

$$I_n^1 \sim \frac{e^{ir+\frac{\pi i}{4}}}{4\sin\frac{\phi_0}{2}\cos\frac{\phi_0}{2}}\int_{C_b'}\frac{e^{\frac{r^{\frac{1}{2}}\check{\nu}\pi i}{2}}}{\Gamma(1+r^{\frac{1}{2}}\check{\nu})}\frac{D'_{r^{\frac{1}{2}}\check{\nu}}(p\beta)}{D'_{-1-r^{\frac{1}{2}}\check{\nu}}(\bar{p}\beta)}\exp\left\{\frac{\check{\nu}\check{\phi}}{\sin\phi_0}-\frac{i\check{\nu}^2}{2\sin^2\phi_0}\right\}\frac{d\check{\nu}}{\sin(r^{\frac{1}{2}}\check{\nu}\pi)}. \tag{4.143}$$

Along with this there is also a (diffracted) contribution from integrals $I_d^3$ and $I_n^3$, which is supplied by a region of integration of size $\mathcal{O}(r^\alpha)$, $0 < \alpha < \frac{1}{2}$, about $\nu = -\frac{1}{2}$. If we recombine these two integrals we have that

$$\Psi_d \sim I_i - \frac{ie^{ir+\frac{\pi i}{4}}}{4\sqrt{2\pi}\sin\frac{\phi_0}{2}\cos\frac{\phi_0}{2}}\int_{C_b'}\frac{D_{-1-r^{\frac{1}{2}}\check{\nu}}(-\bar{p}\beta)}{D_{-1-r^{\frac{1}{2}}\check{\nu}}(\bar{p}\beta)}\exp\left\{\frac{\check{\nu}\check{\phi}}{\sin\phi_0}-\frac{i\check{\nu}^2}{2\sin^2\phi_0}\right\}\frac{e^{\frac{r^{\frac{1}{2}}\check{\nu}\pi i}{2}}d\check{\nu}}{\sin(r^{\frac{1}{2}}\check{\nu}\pi)}, \tag{4.144}$$

$$\Psi_n \sim I_i + \frac{ie^{ir+\frac{\pi i}{4}}}{4\sqrt{2\pi}\sin\frac{\phi_0}{2}\cos\frac{\phi_0}{2}}\int_{C_b'}\frac{D'_{-1-r^{\frac{1}{2}}\check{\nu}}(-\bar{p}\beta)}{D'_{-1-r^{\frac{1}{2}}\check{\nu}}(\bar{p}\beta)}\exp\left\{\frac{\check{\nu}\check{\phi}}{\sin\phi_0}-\frac{i\check{\nu}^2}{2\sin^2\phi_0}\right\}\frac{e^{\frac{r^{\frac{1}{2}}\check{\nu}\pi i}{2}}d\check{\nu}}{\sin(r^{\frac{1}{2}}\check{\nu}\pi)}. \tag{4.145}$$

In both cases the ratio of $\beta$- dependent PCFs tends to 1 as $\beta$ tends to 0, and as in the discussion of Section 4.2.3.3 we find that the approximations in the transition region reduce to those of the Sommerfeld shadow boundary as $\beta$ becomes small.

## 4.3 Creeping ray fields

We now consider the creeping ray fields on the surface of our thin body, which we expect to be initiated by diffraction at its edges. Unfortunately, both curvatures of the surface are $\mathcal{O}(k^{-\frac{1}{2}})$ at an $\mathcal{O}(1)$ distance away from the edge (in the outer coordinate system), and so our body is asymptotically "flat" there. As discussed in [44] the usual creeping ray analysis for a body with $\mathcal{O}(1)$ curvature is not valid.

### 4.3.1 Creeping ray fields on almost flat bodies

In Figure 4.12 we illustrate the various different asymptotic regions in the problem of tangential incidence upon a body as the curvature at the point of tangency varies. We see from this that for a body with $\mathcal{O}(k^{-\frac{1}{2}})$ curvature the Fock-Leontovich region has $\mathcal{O}(1)$ length along the boundary, and height $\mathcal{O}(k^{-\frac{1}{2}})$ normal to the boundary. Therefore, on such a body the F-L region has significant extent along the boundary, and the curvature may no longer be approximated as being constant within this region.

Explicitly, in the two-dimensional scalar case, we introduce the scalings $n = k^{-\frac{1}{2}}\hat{n}$ and $\kappa(s) = k^{-\frac{1}{2}}\hat{\kappa}(s)$, and seek a solution of the form $\phi = A(s,\hat{n})e^{iks}$. Then, as in [121], Helmholtz' equation becomes

$$\frac{\partial^2 A}{\partial \hat{n}^2} + 2i\frac{\partial A}{\partial s} + 2\hat{\kappa}(s)\hat{n}A = 0, \tag{4.146}$$

to leading order, with Dirichlet or Neumann boundary conditions as appropriate on $\hat{n} = 0$. Were the curvature $\kappa(s)$ to be constant then, as in [121] or [30], we could find the appropriate solution to this PDE by means of a Fourier Transform in $s$. However, when the curvature is a function of position, this problem is much more difficult to solve. There are a family of problems of this type, most notably that relating to a point of inflection on a surface.[7]

In addition to the F-L problem being more complicated, we are unable to utilise the ansatz for the $s$- dependence of the solution which allowed us to find a simpler solution in the Airy region for the $\mathcal{O}(1)$ curvature case. (The term of the form $\exp\left(\frac{ik^{\frac{1}{3}}a_m e^{-\frac{2\pi i}{3}}}{2^{\frac{1}{3}}}\int \kappa^{\frac{2}{3}} ds\right)$ is no longer rapidly varying with $s$ when $\kappa = O(k^{-\frac{1}{2}})$). Instead we must solve the same intractable equation as in the F-L region along the whole surface. This difficulty also occurs for creeping fields initiated by diffraction at a tightly curved or sharp edge on an almost flat body.

## 4.4 Body with curved mid-line

In the previous section we found that creeping ray fields of the usual type are not present upon thin scatterers, as away from the tip region the curvature of the body is small. In order to resolve this difficulty, and to allow us to consider slightly more general scatterers, we will now consider the problem (in the two-dimensional scalar case) of a thin body whose mid-line has $\mathcal{O}(1)$ curvature. The body is now described by

$$y = k^{-\frac{1}{2}} f^{\pm}(x) + h(x), \tag{4.147}$$

[7] It is believed that a solution may have been found to this problem by Tew and Ockendon.

with $\pm$ denoting the upper and lower surfaces of the scatterer, where as before

$$k^{-\frac{1}{2}} f^{\pm}(x) \sim \pm k^{-\frac{1}{2}} \beta (2x)^{\frac{1}{2}} \tag{4.148}$$

for small $x$. Without loss of generality we will assume that $h(0) = h'(0) = 0$, but that $h''(0)$ is $\mathcal{O}(1)$. The curvature of the surface is then given by

$$\kappa(x) \quad = \quad \frac{\pm(-h''(x) - k^{-\frac{1}{2}} f^{\pm\prime\prime}(x))}{(1 + (k^{-\frac{1}{2}} f^{\pm\prime}(x) + h'(x))^2)^{\frac{3}{2}}} \tag{4.149}$$

and for small $x$

$$\kappa(x) \quad \sim \quad \frac{\mp h''(0) + k^{-\frac{1}{2}} \beta (2x)^{-\frac{3}{2}}}{(1 + (\pm k^{-\frac{1}{2}} \beta (2x)^{-\frac{1}{2}} + x h''(0))^2)^{\frac{3}{2}}}. \tag{4.150}$$

There are three asymptotic regions to be considered: $s = \mathcal{O}(k^{-1})$, $n = \mathcal{O}(k^{-1})$, which is the same inner problem considered earlier in this chapter; $s = \mathcal{O}(k^{-\frac{1}{3}})$, $n = \mathcal{O}(k^{-\frac{2}{3}})$, which is a Fock-Leontovič type region within which the curvature of the surface is $\mathcal{O}(1)$; and $s = \mathcal{O}(1)$, $n = \mathcal{O}(k^{-\frac{2}{3}})$, which is a standard creeping ray region (or Airy layer). For simplicity we will only consider the fields on the upper side of the body.

When we introduce the F-L scalings ($s = k^{-\frac{1}{3}} \hat{s}$, $n = k^{-\frac{2}{3}} \hat{n}$) we find that

$$\kappa(\hat{s}) \sim -h''(0) + \beta (2\hat{s})^{-\frac{3}{2}} \tag{4.151}$$

and so, as for our discussion of the F-L region upon almost flat bodies, the curvature is not constant within this region. The Fock-Leontovich equation becomes

$$\frac{\partial^2 A}{\partial \hat{n}^2} + 2i \frac{\partial A}{\partial \hat{s}} + 2\hat{n}(-h''(0) + \beta (2\hat{s})^{-\frac{3}{2}}) A = 0 \tag{4.152}$$

and we wish to find a solution which matches with the outer limit of the inner problem as $\hat{s} \to 0$, and with creeping ray or whispering gallery modes as $\hat{s} \to \infty$. As in [44] we find that for when $\xi \gg 1$, $\eta = \mathcal{O}(1)$ our inner solution has an expansion of the form

$$\Psi_d \sim \sqrt{\frac{\pi}{2}} e^{\frac{i\xi^2}{2}} \sum_m \frac{(\bar{p}\xi \tan\frac{\phi_0}{2})^{\nu_m}}{\cos\frac{\phi_0}{2}} \frac{D_{-1-\nu_m}(\bar{p}\eta)}{\sin(\nu_m \pi)} \frac{D_{-1-\nu_m}(-\bar{p}\beta)}{\frac{\partial}{\partial \nu} D_{-1-\nu}(\bar{p}\beta)\big|_{\nu=\nu_m}}, \tag{4.153}$$

$$\Psi_n \sim -\sqrt{\frac{\pi}{2}} e^{\frac{i\xi^2}{2}} \sum_m \frac{(\bar{p}\xi \tan\frac{\phi_0}{2})^{\nu'_m}}{\cos\frac{\phi_0}{2}} \frac{D_{-1-\nu'_m}(\bar{p}\eta)}{\sin(\nu'_m \pi)} \frac{D'_{-1-\nu'_m}(-\bar{p}\beta)}{\frac{\partial}{\partial \nu} D'_{-1-\nu}(\bar{p}\beta)\big|_{\nu=\nu'_m}}. \tag{4.154}$$

The F-L type region corresponds to the scalings $\xi = k^{\frac{1}{3}} \hat{\xi}$, $\eta = \mathcal{O}(1)$, and the coordinate systems are related by

$$\hat{n} \sim \hat{\xi}(\hat{\eta} - \beta) \qquad \hat{s} \sim \frac{\hat{\xi}^2}{2} + k^{-\frac{2}{3}} \left\{ \frac{\beta^2}{2} \log \hat{\xi} + \frac{\beta^2}{4} + \frac{\beta^2}{2} \log\left(\frac{2k^{\frac{1}{3}}}{\beta}\right) - \frac{(\hat{\eta} - \beta)^2}{2} \right\} \tag{4.155}$$

for $k^{-\frac{2}{3}} \ll \hat{s} \ll 1$ (the increased accuracy in the approximation of $\hat{s}$ is required to match the phases of the solutions correctly). If we write $\Psi = e^{\frac{i\hat{\xi}^2}{2}} B$ then we find that Helmholtz' equation in the F-L region becomes

$$B_{\eta\eta} + 2i\hat{\xi} B_{\hat{\xi}} + (i + \eta^2)B = 0 \tag{4.156}$$

to leading order. When we set $B = e^{-\frac{i}{2}(\hat{\eta}-\beta)^2} \hat{\xi}^{\frac{i\beta^2}{2}} A$, and make the coordinate transformation (4.155) (using only the leading-order terms), then this equation becomes

$$\frac{\partial^2 A}{\partial \hat{n}^2} + 2i\frac{\partial A}{\partial \hat{s}} + 2\hat{n}(\beta(2\hat{s})^{-\frac{3}{2}})A = 0, \tag{4.157}$$

which is the limit for small $\hat{s}$ of (4.152).

We also require that the solution matches with a sum of whispering gallery or creeping ray modes as $\hat{s} \to \infty$. These are of the form

$$\Psi \sim \beta_m (\kappa(s))^{\frac{1}{6}} \mathrm{Ai}(-2^{\frac{1}{3}} e^{\frac{2\pi i}{3}} (\kappa(s))^{\frac{1}{3}} \hat{n} + b_m) \exp\left( iks + \frac{ik^{\frac{1}{3}} b_m e^{-\frac{2\pi i}{3}}}{2^{\frac{1}{3}}} \int^s \kappa(\rho)^{\frac{2}{3}} d\rho \right) \tag{4.158}$$

for creeping rays on a convex boundary ($\kappa > 0$), and

$$\Psi \sim \alpha_m \, |\kappa(s)|^{\frac{1}{6}} \, \mathrm{Ai}(2^{\frac{1}{3}} \, |\kappa(s)|^{\frac{1}{3}} \, \hat{n} + b_m) \exp\left( iks + \frac{ik^{\frac{1}{3}} b_m}{2^{\frac{1}{3}}} \int^s |\kappa(\rho)|^{\frac{2}{3}} \, d\rho \right) \tag{4.159}$$

for whispering gallery modes on a concave boundary ($\kappa < 0$). Here $b_m$ are the roots of $\mathrm{Ai}(z)$ or $\mathrm{Ai}'(z)$, for Dirichlet or Neumann boundary conditions respectively. For $k^{-\frac{1}{3}} \ll s \ll 1$ we see from (4.150) that $\kappa(s) \sim -h''(0)$, and so we find that in this region (4.158) and (4.159) approximately satisfy

$$\frac{\partial^2 A}{\partial \hat{n}^2} + 2i\frac{\partial A}{\partial \hat{s}} + 2\hat{n}(-h''(0))A = 0 \tag{4.160}$$

which is the limit for large $\hat{s}$ of (4.152).

## 4.5 Matching with the $\mathcal{O}(1)$ curvature solution

For an obstacle with $\mathcal{O}(1)$ curvature everywhere an asymptotic approximation for the scattered fields, in the short wavelength limit, may be found using the GTD framework outlined in Chapter 3. We may treat the curvature at the edge of the body as a parameter of the problem, and expect that the high curvature limit of this GTD approximation will match with the small curvature (large $\beta$) limit of the thin body approximation. This will indeed be found to be the case, but only for the distant far fields of the scatterer.

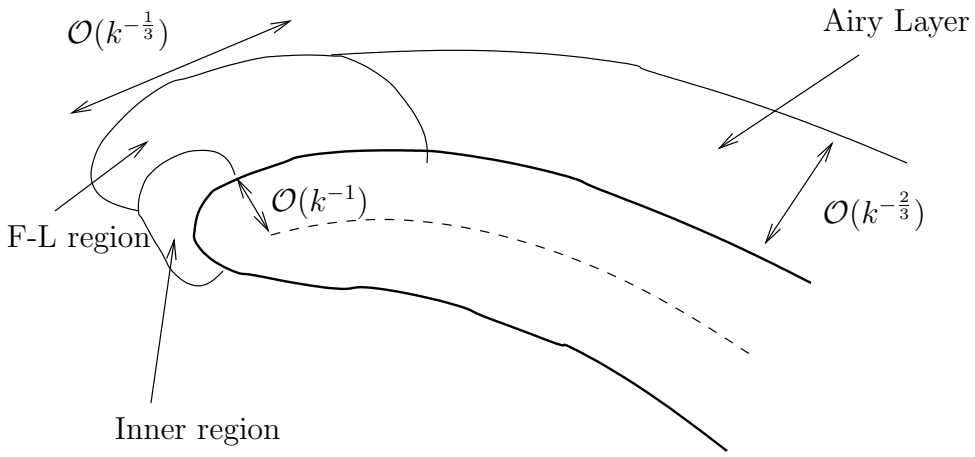


**Figure 4.11:** Asymptotic regions for a thin scatterer with curved midline.

We will only consider the problem of scattering by a parabola, rather than that for a general thin obstacle. For a general obstacle there will be a region about the point of tangency for which the scatterer will appear locally parabolic, and we expect that only those rays meeting the surface in this region will match with those from the tip region in the thin edge approximation.

### 4.5.1 Large curvature limit of the GTD approximation

The shape of a parabola is uniquely defined by the curvature $\kappa_0$ at its tip. By choosing our length scale to be the radius of curvature $R_0 = \frac{1}{\kappa_0}$ there, we see that the two-dimensional scalar problem of scattering of a plane wave by a parabola depends only upon the ratio of the incident wavelength to the radius of curvature of the tip, and the angle of incidence.

Using this rescaling the various asymptotic regions (in terms of the original coordinate system) for the blunt body diffraction problem are found to depend on curvature in the manner shown in Figure 4.12. Most of these regions were described in Chapter 3, but in addition we will find that the distant far field region is significant. This is the region, at a distance much greater than $k\kappa^{-2}$ away from a compact body ($\kappa$ being a typical curvature of the body), where the scattered field is approximately a system of rays propagating away from a point. In the case of a parabola, which is not compact, those rays which meet the body at points near the tip (of the same order of magnitude away as the radius of curvature at the tip) form such a system of rays in their distant far field. We will find that these match with the diffracted fields in the thin case. However the other rays reflect from points at which the curvature of the parabola is small, and so where the body is approximately flat. These will be found to match with the reflected field of the sharp

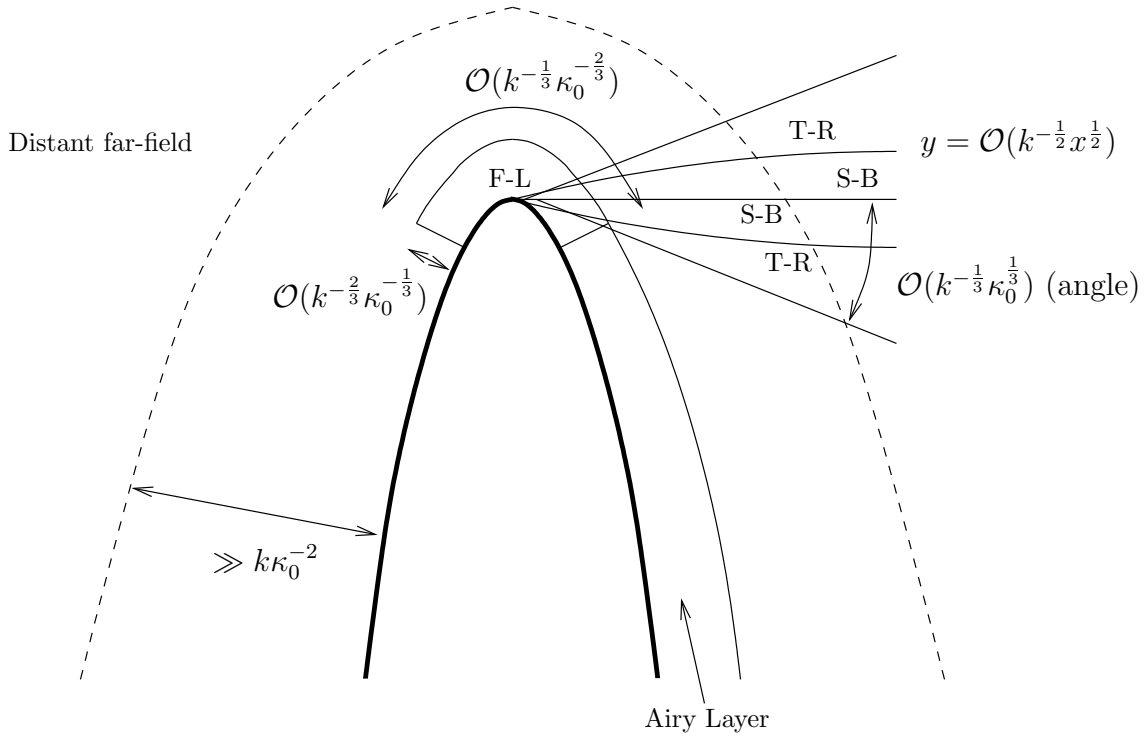


**Figure 4.12:** Asymptotic regions for the GTD analysis of diffraction by a parabola, showing the dependence of the size of these regions upon the curvature $\kappa_0$ at the tip.

edge solution.

### 4.5.2 Large-$\beta$ limit of the tightly-curved edge solution

We may also examine the behaviour of the approximation for a thin parabola as the radius of curvature at the tip becomes large. Our exact integral solutions (4.30), (4.31) are still valid in this case, and in fact the GTD solution for a blunt parabola may be found by careful analysis of these integrals when $\beta = \mathcal{O}(r^{\frac{1}{2}})$ [66], [103], [113]. However, in the earlier analysis of these integrals we have assumed that $\beta$ is independent of $r$, and so our asymptotic expansion for the fields is not necessarily valid. We have noted the necessary relationships between $r$ and $\beta$ for the analysis to be valid, and find in each region that this corresponds to the point of observation being in the distant far field of the GTD solution.

We note here that the GO field for a parabola is best calculated using the parametrisation used in [44], namely

$$(x, y) = \frac{\beta^2}{2\sin^2\frac{1}{2}\Theta}(\cos\Theta, \sin\Theta) \tag{4.161}$$

(in the inner coordinate system).

When the observation angle lies in the region $0 < \phi < 2\pi - \phi_0$ we see that our analysis is valid provided that $r \gg k^{-1}\beta^4$ (on the outer length scale), and expressed in terms of the tip curvature this condition becomes $r \gg k\kappa_0^{-2}$. This may be seen to be the same condition as for the distant far field of GTD approximation for the blunt problem. The diffraction coefficient is given in integral form by (4.65) (4.66), and we may further approximate these integrals for large $\beta$.

When $0 < \phi < \phi_0$ integrals (4.65) and (4.66) may (as we discussed when $\beta = \mathcal{O}(1)$) be completed by an arc at infinity in the left hand half plane, and the fields expressed as series over the poles of the $\beta$- dependent PCFs. The first few poles are sufficiently near the turning point $\hat{\nu} = \frac{i\beta^2}{2}$ of the PCFs that we may approximate the $\beta$- dependent PCFs by their approximations [44, (B14)-(B17)] in terms of Airy functions. The poles then, as noted in [44], have approximate locations

$$\nu_m \sim -\frac{1}{2} + i\left(\frac{\beta^2}{2} + \frac{a_m e^{-\frac{2\pi i}{3}}\beta^{\frac{2}{3}}}{2^{\frac{1}{3}}} + \mathcal{O}(\beta^{-\frac{1}{3}})\right), \tag{4.162}$$

$$\nu'_m \sim -\frac{1}{2} + i\left(\frac{\beta^2}{2} + \frac{a'_m e^{-\frac{2\pi i}{3}}\beta^{\frac{2}{3}}}{2^{\frac{1}{3}}} + \mathcal{O}(\beta^{-\frac{1}{3}})\right), \tag{4.163}$$

where $a_m$ and $a'_m$ are the roots of $\mathrm{Ai}(z)$ and $\mathrm{Ai}'(z)$ respectively. After approximating the remaining PCFs in the terms of the series using their Airy function approximations we find that the diffracted fields become

$$\Psi_d \sim -\frac{e^{ir-\frac{\pi i}{12}}\sqrt{\pi}2^{-\frac{5}{6}}\beta^{\frac{2}{3}}}{\sqrt{r}\sin\frac{\phi_0}{2}\cos\frac{\phi}{2}}\sum_{m=0}^{\infty}\left(\frac{\tan\frac{\phi_0}{2}}{\tan\frac{\phi}{2}}\right)^{\nu_m}\frac{\mathrm{Ai}(e^{-\frac{2\pi i}{3}}a_m)}{\mathrm{Ai}'(a_m)}, \tag{4.164}$$

$$\Psi_n \sim \frac{e^{ir+\frac{\pi i}{4}}\sqrt{\pi}2^{-\frac{5}{6}}\beta^{\frac{2}{3}}}{\sqrt{r}\sin\frac{\phi_0}{2}\cos\frac{\phi}{2}}\sum_{m=0}^{\infty}\left(\frac{\tan\frac{\phi_0}{2}}{\tan\frac{\phi}{2}}\right)^{\nu'_m}\frac{\mathrm{Ai}'(e^{-\frac{2\pi i}{3}}a'_m)}{a'_m\mathrm{Ai}(a'_m)}, \tag{4.165}$$

and as in [44] it is possible to show that these match with the distant far field of the shed creeping rays in the GTD approximation.

For $\phi_0 < \phi < 2\pi - \phi_0$ the integral form for the directivity may be approximated by the method of steepest descents. The details of this are somewhat involved, but we find that the integral has a saddle point contribution, and this may be seen to agree with the reflected field of the blunt case, in the distant far field region.

For $\phi_0$ near $\phi$ we find that the dominant contribution to the integral form of the directivity is from near $\nu = \frac{i\beta^2}{2}$ (along with a contribution from near $\nu = -\frac{1}{2}$, which cancels with the diffracted contribution supplied by $I_i$). We may again approximate the

$\beta$- dependent PCFs in terms of Airy functions, and find that the far field is approximately

$$\Psi_d \sim -\frac{e^{ir+\frac{\pi i}{12}}\beta^{\frac{2}{3}}}{\sqrt{2\pi r}\sin\phi_0}e^{-\frac{i\beta^{\frac{4}{3}}\tilde{\phi}}{2\sin\phi_0}}\int_{-\infty}^{\infty}e^{\frac{ip\tilde{\phi}}{\sin\phi_0}}\frac{\mathrm{Ai}(-2^{\frac{1}{3}}p)}{\mathrm{Ai}(-2^{\frac{1}{3}}e^{\frac{2\pi i}{3}}p)}dp+\chi(\tilde{\phi})\Psi_i, \quad (4.166)$$

$$\Psi_n \sim \frac{e^{ir+\frac{5\pi i}{12}}\beta^{\frac{2}{3}}}{\sqrt{2\pi r}\sin\phi_0}e^{-\frac{i\beta^{\frac{4}{3}}\tilde{\phi}}{2\sin\phi_0}}\int_{-\infty}^{\infty}e^{\frac{ip\tilde{\phi}}{\sin\phi_0}}\frac{\mathrm{Ai}'(-2^{\frac{1}{3}}p)}{\mathrm{Ai}'(-2^{\frac{1}{3}}e^{\frac{2\pi i}{3}}p)}dp+\chi(\tilde{\phi})\Psi_i, \quad (4.167)$$

where $\phi=\phi_0+\beta^{-\frac{2}{3}}\tilde{\phi}$, and $\chi(s)$ is again the Heaviside function. After laborious conversion of coordinate systems these may be seen to agree with the results of [140] for the incident transition region in the GTD approximation.

In the region $2\pi-\phi_0<\phi<2\pi$ the reflected field is present. This can be seen to agree with the reflected field for the blunt case provided that $r\gg k^{-1}\beta^6=k^2\kappa_0^{-3}=k^2\kappa^{-6}$. This condition is, however, related to the approximations of Appendix C for the ratio of $\beta$- dependent PCFs. If more terms are retained we find that the reflected fields agree provided that $r\gg k^{-1}\beta^2$.

In $2\pi-\phi_0<\phi<2\pi$ there is also a diffracted field. Again the roots of the PCFs may be approximated in terms of the roots of Airy functions, and find that the fields may be written as

$$\Psi_d \sim -\frac{e^{ir-\frac{\pi i}{12}}\sqrt{\pi}2^{-\frac{5}{6}}\beta^{\frac{2}{3}}}{\sqrt{r}\sin\frac{\phi_0}{2}\cos\frac{\phi}{2}}\sum_{m=0}^{\infty}\left(\frac{\tan\frac{\phi_0}{2}}{|\tan\frac{\phi}{2}|}\right)^{\nu_m}e^{\nu_m\pi i}\frac{\mathrm{Ai}(e^{-\frac{2\pi i}{3}}a_m)}{\mathrm{Ai}'(a_m)}, \quad (4.168)$$

$$\Psi_n \sim \frac{e^{ir+\frac{\pi i}{4}}\sqrt{\pi}2^{-\frac{5}{6}}\beta^{\frac{2}{3}}}{\sqrt{r}\sin\frac{\phi_0}{2}\cos\frac{\phi}{2}}\sum_{m=0}^{\infty}\left(\frac{\tan\frac{\phi_0}{2}}{|\tan\frac{\phi}{2}|}\right)^{\nu'_m}e^{\nu'_m\pi i}\frac{\mathrm{Ai}'(e^{-\frac{2\pi i}{3}}a'_m)}{a'_m\mathrm{Ai}(a'_m)}, \quad (4.169)$$

where

$$e^{\nu_n\pi i}\sim\exp\left(-\frac{\pi i}{2}-\frac{\pi\beta^2}{2}-\pi a_m e^{-\frac{2\pi i}{3}}\beta^{\frac{2}{3}}2^{-\frac{1}{3}}\right). \quad (4.170)$$

As noted in [44] this corresponds to the distant far-field of the field shed by a creeping ray travelling "backwards" around the parabola, which is not found in the standard GTD analysis. This field has an $\mathcal{O}(e^{-\frac{\pi\beta^2}{2}})$ pre-factor, so is exponentially small for large $\beta$.

## 4.6 Comparison of exact and asymptotic results

### 4.6.1 Evaluation of Parabolic Cylinder Functions

Practically-minded methods for evaluation of PCFs [139] [13] involve summation of the (hypergeometric) power series of the function about the origin for small values of order and argument, and application of an appropriate asymptotic expansion when one or both of these parameters are large. However, the asymptotic approach is inherently limited

in accuracy, and unfortunately we will often need to evaluate the functions to quite high precision. This proves to be moderately costly in time, and one of the potential benefits of an asymptotic approach for diffraction problems, rather than a finite element or boundary integral method, is that the diffracted fields may be evaluated far more quickly.

Apart from summation of the power series, a number of alternative approaches are possible. As discussed in [49], it is possible to evaluate the PCFs by quadrature of their integral representations (A.3) or (A.5). Another possibility would be to use the exact expansion of the PCFs in terms of cylindrical Bessel functions discussed in [105, Appendix], and these expansions are also asymptotic for large order (see Appendix A.4.1). This has been implemented (for confluent hypergeometric functions) in [1], but unfortunately the series converge very slowly when the argument is much larger than 1. The PCFs may be expressed in terms of hypergeometric functions [3, §19.12], and so methods for evaluating these may be employed, such as those built into Maple or Mathematica, or the rational approximations of [87]. Again, these are rather slow to calculate.

On a more positive note, it is reasonably straightforward to calculate the values of the PCFs at the integers using the explicit expressions (4.81) for $D_0(z)$ and $D_{-1}(z)$, and the recurrence relations (A.6) and (A.7). The recurrence relation applied forward is numerically unstable for the recessive solutions, and so we must either perform the calculations to extremely high accuracy, or employ backwards recursion. (See [122] for algorithms for real positive values of the argument.)

### 4.6.2 Calculation of the exact fields

The exact fields in this problem may be calculated by direct quadrature of (4.30) and (4.31), or by summation of the residue series.

Direct quadrature of integrals (4.30) and (4.31) is difficult. The integrands are highly oscillatory, (and also become large near the turning points of the PCFs) which makes accurate evaluation difficult as the values of the integrands must be computed at a very large number of points for each observation angle. Such problems may be slightly ameliorated by performing the integrations along (or at least near to) the contours of steepest descent. However this still requires evaluation of the PCFs at a large number of values (as the location of the steepest descent paths varies with the observation angle). In addition the deformation of the integrals will give a number of residue contributions, at the same poles as for the asymptotic method, but with exact rather than approximate values for the PCFs.

The series forms for the exact fields are easier to calculate, as provided $\phi$ is not equal to

$\frac{\pi}{2}$ the method of calculation does not vary with the angle of observation. From our earlier analysis we recall that the diffracted field may be expressed as a series of approximate residues to the left of the original contour when $0 < \phi < \phi_0$, and to the right when $\phi_0 < \phi < 2\pi - \phi_0$, and that these pole contributions decay exponentially (after at most $\mathcal{O}(r^{\frac{1}{2}})$ terms). However the behaviour of the far-field of the exact integrands does not vary with $\phi$, so we complete the exact contour to the same side regardless of the observation angle. When this is the opposite direction to that used for the diffracted fields the terms initially grow exponentially, and do not decay until after $\mathcal{O}(r)$ terms. When $0 < \phi_0 < \frac{\pi}{2}$ this may be overcome by the use of variable precision arithmetic. However, when $\frac{\pi}{2} < \phi_0 < \pi$, calculating the series requires accurate evaluation of the poles (and residues) of the PCFs, which is more difficult.

### 4.6.3 Calculation of the asymptotic approximations

The asymptotic approximations to the field may be computed more quickly (for large $r$) than the exact solutions, apart from within the transition region, but some care must still be taken.

Outside the transition region we will use the asymptotic approximations listed in Section 4.2.4.8; these consist of a diffracted fan of rays along with a reflected field (where present). The diffracted field may be calculated by summation of the residue series forms (4.110) and (4.116). In $0 < \phi < 2\pi - \phi_0$ the diffraction coefficients may also be found by numerical integration of (4.113) and (4.117). Where possible these integral forms are preferred, as the series solutions converge increasingly slowly as we approach the incident shadow boundary ($\phi = \phi_0$). These integrals decay exponentially when we are sufficiently far from $\nu = -\frac{1}{2}$ on the contours of integration, and so the contour may be truncated to a finite section (from our earlier discussion the size of this must be large compared to both 1 and $\beta^2$). In $0 < \phi < \pi$ the contour of integration is just a section of the line $\mathrm{Re}\ \nu = -\frac{1}{2}$. If we choose the contour in $\pi < \phi < 2\pi - \phi_0$ to consist of part of the line segment from $\infty e^{-\frac{\pi i}{4}}$ to $-\frac{1}{2}$ and part of the line segment from $-\frac{1}{2}$ to $-\frac{1}{2} + i\infty$ then the integration contours do not depend upon the angle of observation. Although this quadrature requires the evaluation of the ratio of $\beta$- dependent PCFs at a large number of points, their values may be tabulated on these fixed contours, and the same values used for all angles of observation.

Near the reflected shadow boundary the integral form for the diffraction coefficient has a saddle point (4.140), which causes the integrand to grow before eventually decaying along the fixed contour of integration. This causes the integrand to become large, which

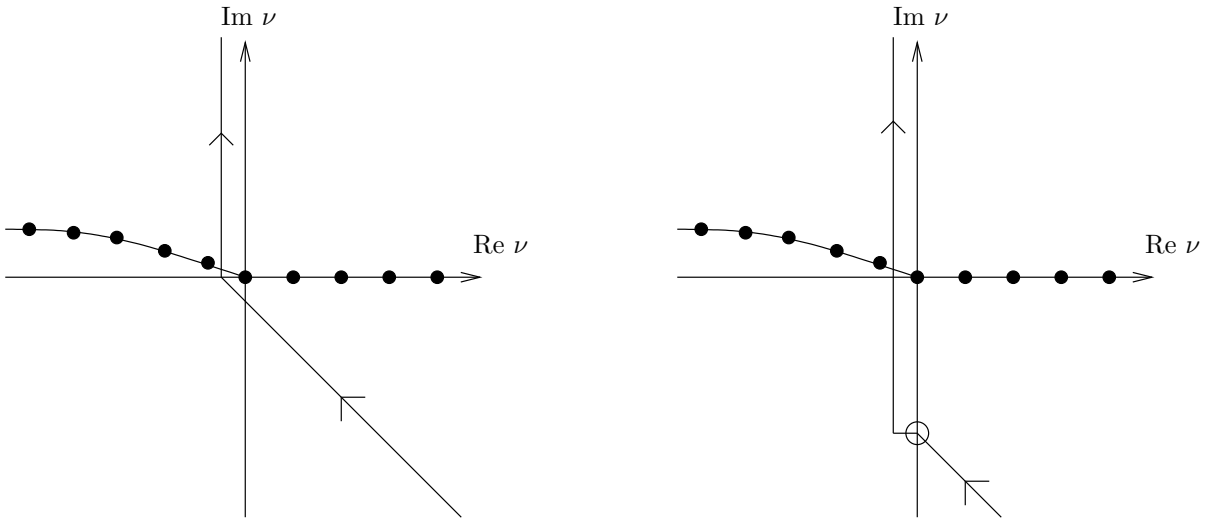


**Figure 4.13:** Contours of integration for the numerical evaluation of the diffracted field (using the integral expressions (4.113) or (4.117) for the diffraction coefficients) when $\pi < \phi < 2\pi - \phi_0$. The left hand diagram shows the contour consisting of the lines from $e^{-\frac{\pi i}{4}}\infty$ to $-\frac{1}{2}$ to $i\infty$ used away from the reflected boundary (although the numerical integration is only be performed on a finite part of this contour). Near the shadow boundary the integral has a saddle point at (4.140), and we instead use the contour on the right, which passes through (or at least near to) the saddle point. The integrand is $\mathcal{O}(1)$ and oscillatory on the section of the contour from the saddle to the real axis.

means that we must evaluate the PCFs more precisely, and also must extend the finite range of our integration. We may instead choose to perform the integration over a contour which follows the steepest descent path (found numerically) from infinity to the saddle, consists of two straight lines from the saddle to $-\frac{1}{2}$, and then runs parallel to the imaginary axis to $+i\infty$ (see Figure 4.13). This method gives improved values for the diffraction coefficients as we approach the reflected shadow boundary. However as $\phi$ approaches $2\pi - \phi_0$ from below the saddle point tends towards $-i\infty$, and so this method becomes impractical, and in that case the diffraction coefficient must instead be approximated by the saddle point contribution (4.141). This problem is not restricted to the integral forms, as the series form of the diffraction coefficient converges increasingly slowly as we approach the boundary.

In the region $2\pi - \phi_0 < \phi < 2\pi$ the reflected field is present. In Section 4.2.4.8 we simply listed the leading-order contribution to the saddle point approximation, the error in which is $\mathcal{O}(r^{-\frac{1}{2}})$. It is possible to calculate the next order correction term to the reflected field by keeping higher-order terms in the analysis for a perturbed saddle point contribution discussed in Appendix D, but to obtain an approximation accurate

to $\mathcal{O}(r^{-\frac{1}{2}})$ we must also retain additional terms in our approximation of the ratio of $\beta$-dependent PCFs (see Appendix A.4.1 and Appendix C). This leads to the expressions becoming rather unwieldy, and in a practical implementation the reflected field would be found by the standard geometrical optics method. Instead, we use the observation from Appendix D that, for such a perturbed saddle point, it is possible to find the fields up to and including the $\mathcal{O}(r^{-\frac{1}{2}})$ terms by simply considering the perturbation as part of the leading-order phase, and then directly applying the standard saddle point formula. For $0 < \phi_0 < \frac{\pi}{2}$ this gives the approximation

$$R \sim \sqrt{\frac{2\pi}{|u''(\hat{x}_0)|}} A(\hat{x}_0) e^{u(\hat{x}_0)} e^{\frac{3\pi i}{4}} \tag{4.171}$$

where

$$A(\hat{x}) = -\frac{e^{\frac{\pi i}{4}}}{2\sqrt{\pi}\cos\frac{\phi_0}{2}(\hat{\xi}^2 - 2\hat{x})^{\frac{1}{4}}(\hat{\eta}^2 + 2\hat{x})^{\frac{1}{4}}} \frac{((\hat{\eta}^2 + 2\hat{x})^{\frac{1}{2}} - \hat{\eta})^{\frac{1}{2}}}{(\hat{\xi} - (\hat{\xi}^2 - 2\hat{x})^{\frac{1}{2}})^{\frac{1}{2}}} \left(1 - \frac{i\beta^3}{r^{\frac{1}{2}} 3\sqrt{2\hat{x}}} + \frac{\beta}{r^{\frac{1}{2}}\sqrt{2\hat{x}}}\right) \tag{4.172}$$

$$\begin{aligned} u(\hat{x}) = {} & \frac{i\,|\hat{\xi}|}{2}(\hat{\xi}^2 - 2\hat{x})^{\frac{1}{2}} + i\hat{x}\log\left(|\hat{\xi}| - (\hat{\xi}^2 - 2\hat{x})^{\frac{1}{2}}\right) + \frac{i\hat{\eta}}{2}(\hat{\eta}^2 + 2\hat{x})^{\frac{1}{2}} \\ & -ix\log\left(\hat{\eta} - (\hat{\eta}^2 + 2\hat{x})^{\frac{1}{2}}\right) - i\hat{x}\log\left(\tan\frac{\phi_0}{2}\right) - r^{-\frac{1}{2}} i2\beta\sqrt{2\hat{x}} \end{aligned} \tag{4.173}$$

and $x_0$ is the real positive saddle point $u'(x_0) = 0$, which is found numerically (by the Newton-Raphson method). The reflected field may also be approximated by direct application of the geometrical optics formula (3.40), using the parametrisation (4.161).

In the transition region we will plot the approximations (4.134) to the field in the shadow boundary. As the phase-amplitude approximations for the PCFs are also valid for small $\nu$ we find that we may also approximate the saddle point contribution using formula (4.171), and this gives a higher-order (and uniformly valid) approximation to the saddle point contribution. When $\beta$ is small we also plot the approximations (4.144) to the transition region field, integrated along a very similar contour to that shown in Figure 4.13.

### 4.6.4 Discussion of results

In the following we will compare the exact and asymptotic results for the scalar diffraction problem. We will only plot $I_d$ and its approximations, as the incident field is large and interferes with the reflected and diffracted fields, which makes it difficult to see the behaviour of the diffracted fields. Where we have only listed approximations for the total

fields it is easy to find the approximations of $I_d$ by subtracting from these the exact representation (4.36) for $I_s$.

We choose to plot the real and imaginary parts of the fields against observation angle, rather than compare the diffraction coefficients. The reflected field from the parabola does not decay like $1/\sqrt{r}$ for large $r$, as it is not a compact obstacle, and our approach will allow us to examine the approximations in the shadow boundary region. In Figures 4.14 to 4.17 we compare the exact values for $I_d$ with their asymptotic approximations. In $0 < \phi < 2\pi - \phi_0$ we plot the diffracted field given by (4.113), and in $2\pi - \phi_0 < \phi < 2\pi$ we plot the diffracted field found using the series form (4.110), along with the approximation (4.171) for the reflected field.

We see from Figure 4.14 that for $r = 20$, and $\beta = 1$, the approximations are very accurate away from the reflected boundary. The approximation in $0 < \phi < 2\pi - \phi_0$ becomes inaccurate as we approach the shadow boundary (the diffracted field plotted was found by numerical integration on a fixed contour, but use of the saddle point approximation makes no improvement). In $2\pi - \phi_0 < \phi < 2\pi$ the approximations are seen to be very close to the exact result and the approximation in this region appears good right up to the shadow boundary; it should be noted that for $\beta$ not small the contribution to the approximation from the diffracted residue series is numerically very small. Further away from the scatterer, as in Figure 4.15 where $r = 50$, the approximations are more accurate, and we notice that the region near the reflected boundary where the diffracted field is a poor approximation becomes smaller.

The approximations are also quite accurate for a wide range of $\beta$. In Figure 4.16 we plot the real and imaginary parts of the fields for $r = 20$ and $\beta = \frac{1}{10}$. Again the approximations are seen to be good away from the shadow boundary; however the diffracted field in $2\pi - \phi_0 < \phi < 2\pi$ is now not negligible, and we see that it becomes large as we approach the shadow boundary from both sides.

In Figure 4.17 we plot the fields for $\beta = \frac{3}{2}$, and see similar behaviour as when $\beta = 1$, except that the region near the reflected boundary where the approximation is poor is larger. Calculating the fields for larger $\beta$ is possible, but more difficult. Locating the poles of the PCFs (used to give the diffracted field in $2\pi - \phi_0 < \phi < 2\pi$) becomes harder, as the expansions (4.63) for the poles are only good for very large $n$, and we must instead track the paths of the poles as $\beta$ varies. Another difficulty is that the expansions are only valid for $r \gg \beta^4$, and this becomes very large even for moderate $\beta$.

In Figure 4.18 we compare the asymptotic approximations to the field found using the leading-order approximation (4.112) to the saddle point contribution, and the uniform

approximation (4.171). We see that the leading-order approximation is a poor estimate of the exact field, but becomes better for larger $r$, which is to be expected as the error in the leading-order approximation is $\mathcal{O}(r^{-\frac{1}{2}})$. We also see that the leading-order estimate becomes progressively worse as we approach the shadow boundary. The qualitative behaviour of the leading-order approximation is also rather different to the exact field; due to the term of the form

$$\exp\left(-i\beta^2 \sin\phi_0 \left(\frac{x\cos\phi_0 - y\sin\phi_0}{x\sin\phi_0 + y\cos\phi_0}\right)\right) \tag{4.174}$$

the phase of the leading-order approximation varies very rapidly as we approach the reflected boundary, and it can also be seen in Figure 4.19 that the amplitude of the leading-order approximation does not diminish as we approach the boundary.

In Figure 4.20 we consider the behaviour near the reflected boundary when $\beta = 1$ and $r = 20$. In this case we have the approximate solution (4.134) for the field in the transition region, and we find that this is indeed a reasonably good approximation. It can also be seen that approximation found by using the uniform approximation (4.171) for the saddle point contribution is good even in the transition region, and that in fact it gives a slightly more accurate approximation.

In Figure 4.21 we see, as predicted, that the saddle point approximation in the transition region is not at all good when $\beta$ is small (here $\beta = \frac{1}{5}$). Instead we find that the integral approximation (4.144) gives a reasonable approximation to the fields, although this leading-order approximation is only valid to $\mathcal{O}(r^{-\frac{1}{2}})$. In this case the diffracted field supplied by the residue series is larger, and it is much more noticeable that the approximation (4.134) is in fact discontinuous, because we truncate the residue series for the diffracted field at a point which varies with the observation angle. For large $r$ the series are terminated at a point where the terms are exponentially small, but for finite $r$ this gives finite discontinuities in the approximations. Standard (and formal) methods for finding a uniform approximation to the fields when the steepest descent contour crosses a pole (such as those in [127]) may not be directly applied here, as there are a large number of poles which are near each other in the $\tilde{\nu}$ plane. As this is an exponentially small effect a much more delicate analysis of the problem is necessary to deduce the exact way that in which these discontinuities are smoothed. If higher-order terms in the approximation of the $\xi$- and $\eta$- dependent PCFs for the residue contributions are retained we find that these discontinuities are smaller in magnitude, although still present.

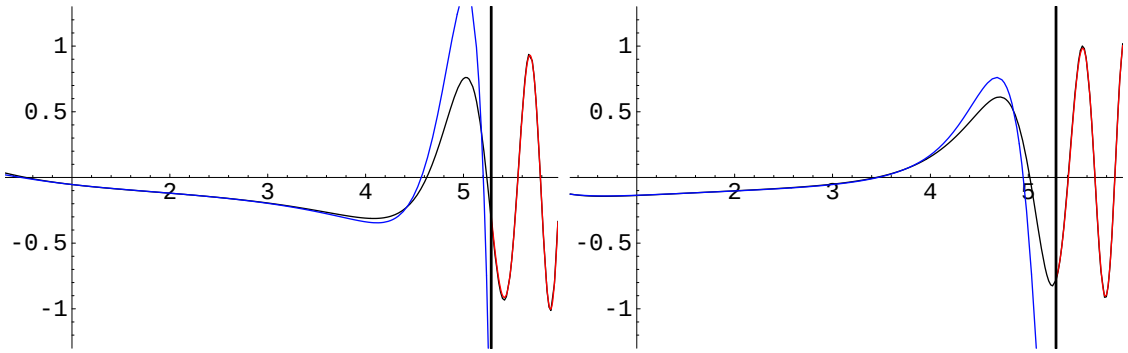


**Figure 4.14:** Plots of the real (left) and imaginary (right) parts versus observation angle for the exact expression for $I_d$ (black), and the asymptotic approximation (red/blue), when $r = 20$, $\phi_0 = 1$ and $\beta = 1$. The blue curve is the approximation to the diffracted part of the field, calculated using the integral representations (4.113). The red curve is the approximation to the reflected and the part of the diffracted field which is not supplied by $I_i$. The function plotted for the red curve consists of the uniform approximation (4.171) to the saddle point contribution along with the residue series (4.113) for the diffracted field. The position of the reflected shadow boundary ($\phi = 2\pi - \phi_0$) is indicated by the thick vertical line.

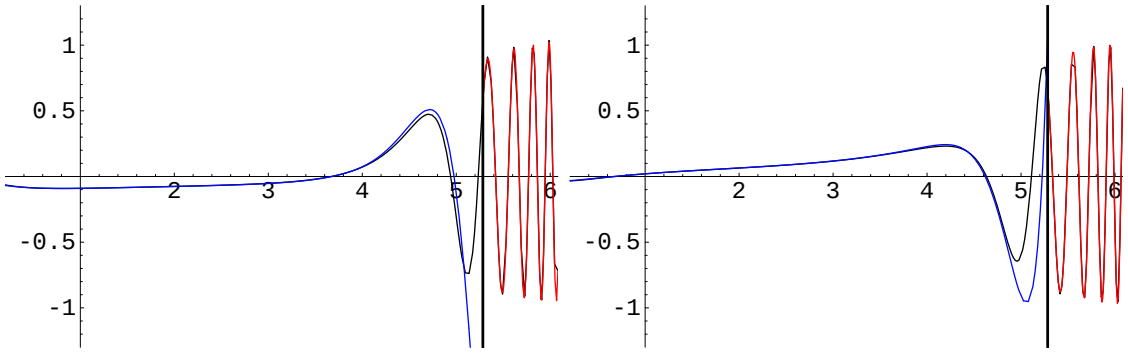


**Figure 4.15:** As for Figure 4.14 but with $r = 50$.

## 4.7 Summary and conclusions

In this chapter we have considered the problem of scattering by a thin, perfectly conducting body. The edges of such a body have a radius of curvature which is comparable to the wavelength of the incident field, and so the diffracted fields differ from both those for a blunt body and those for a sharp edge.

The inner problem reduced to the case of oblique E-M plane wave incidence upon a perfectly conducting parabolic cylinder. The solution to this was expressed as integrals of parabolic cylinder functions, and we have found the far-field expansions of these solutions. This allowed the directivity of the edge-diffracted fields to be found. Our results corrected

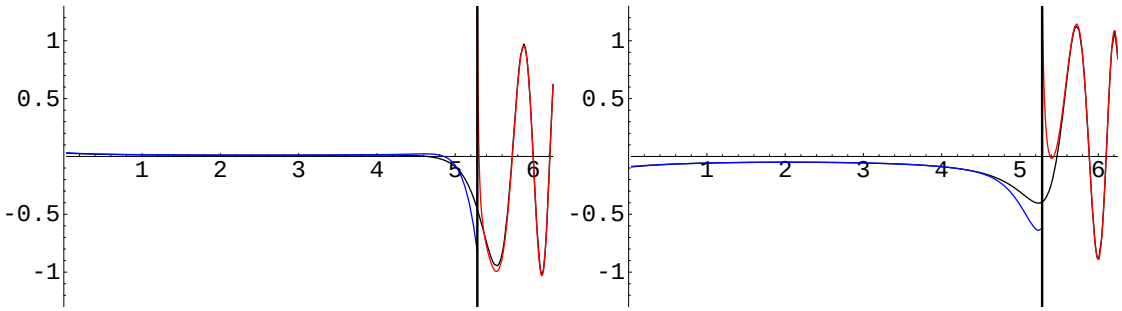


**Figure 4.16:** As for Figure 4.14 but with $\beta = \frac{1}{10}$.

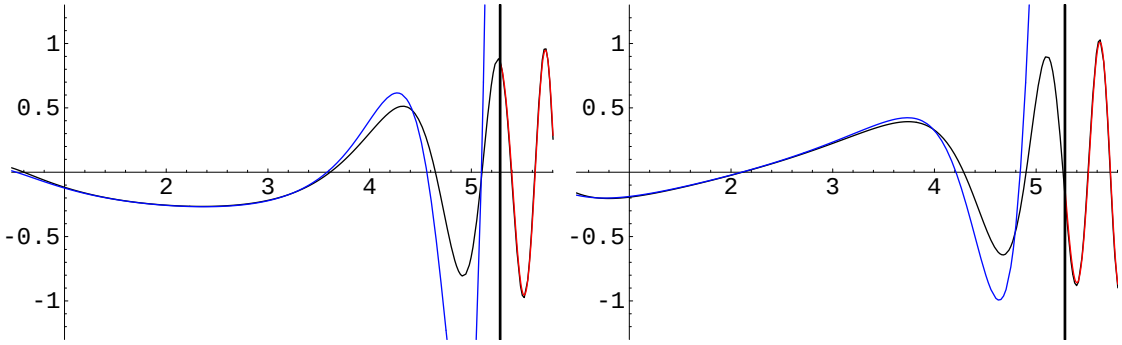


**Figure 4.17:** As for Figure 4.14 but with $\beta = \frac{3}{2}$.

a number of inaccuracies in the results of [44], both for the values of the diffraction coefficients, and in some of the details of the analysis. We have also made a detailed examination of the behaviour of the solutions in the regions near the shadow boundaries. The region in the vicinity of the reflected shadow boundary was of particular interest, and was seen to have an unusual structure.

We then discussed the difficulties with the standard creeping ray analysis for a body which is asymptotically flat, as the usual Airy layer analysis is not valid. In an attempt to find a useful expression for the creeping fields we considered the case of a thin body with curved mid-line. For such a body the curvature of the boundary is not small away from the tip, and so we may find a standard creeping ray or whispering gallery solution near the surface. However the launch coefficients for these modes must be determined by the numerical solution of the partial differential equation (4.152).

We also briefly considered the behaviour of our asymptotic solution as the curvature at the tip of the parabola became small. We noted that the solution matches with the far-field region of the GTD solution, as our analysis for a parabola with large curvature proved to be valid even in the blunt case, provided the observation point was sufficiently far from

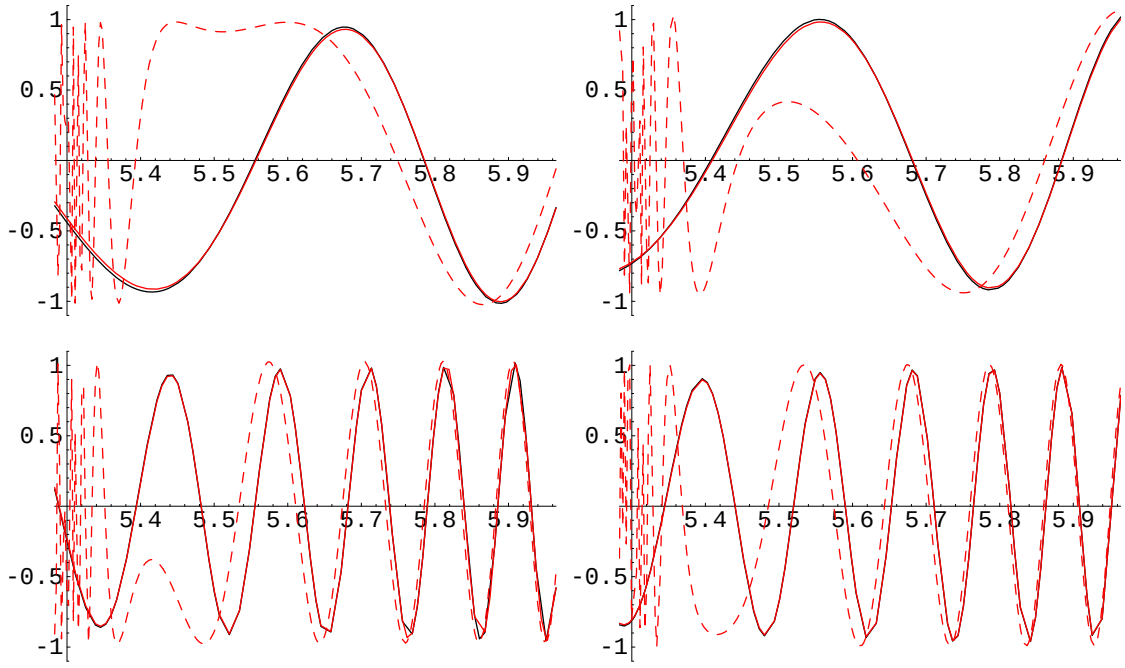


**Figure 4.18:** Plots of the real (left) and imaginary (right) parts of the exact value of $I_d$ (black), and its asymptotic approximations using the series form (4.110) for the diffracted field along with either the leading-order approximation (from Section 4.2.4.8) for the reflected field (dashed red), or the uniform approximation (4.171) (solid red). The upper plot is for $r = 20$ and the lower plot is for $r = 100$.

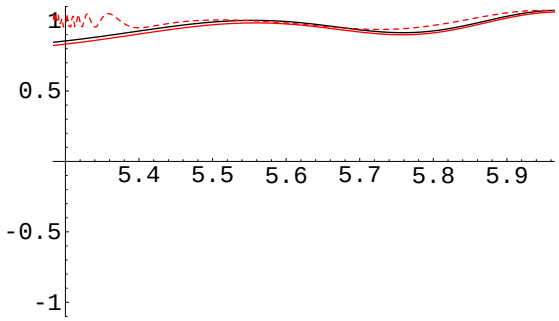


**Figure 4.19:** As for Figure 4.18, but showing the absolute values of the exact value of $I_d$ (black) and its approximations (red, as described for Figure 4.18) when $r = 20$.

the parabola. We did not resolve the problem of the initiation of the exponentially small backwards-creeping ray field, as to do that would require an analysis of the integral solutions for both $r$ and $\beta$ large which was exponentially accurate. However we note here that our analysis of the reflected transition region suggests the possibility that the backwards-creeping fields are switched on by the reflected field.

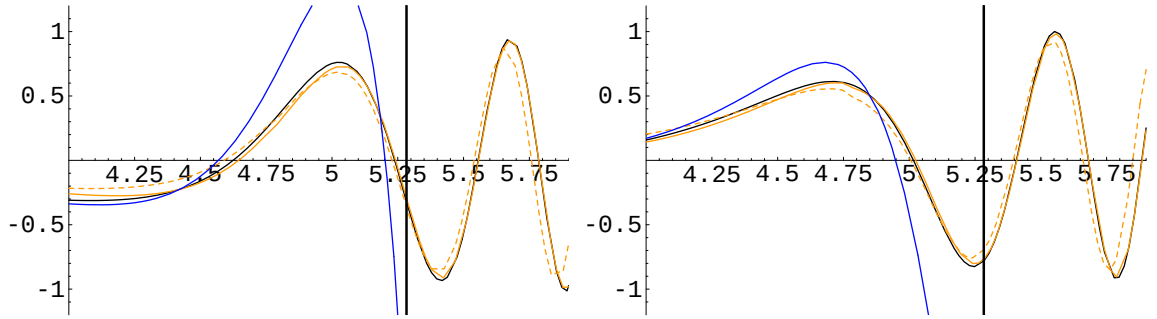


**Figure 4.20:** Plots of the real (left) and imaginary (right) parts of the exact value of $I_d$ (black) near the reflected boundary, the transition region approximations (yellow), and the diffracted field in $\pi < \phi_0 < 2\pi - \phi_0$ (blue) from the integral representation (4.113). The approximations in the reflected transition region consist of the series (4.129) for the diffracted field, truncated just before its smallest term, along with an approximation of the saddle point contribution; the dotted yellow line is its leading-order approximation (4.128), and the solid yellow line is the uniform approximation (4.171). Here $r = 20$ and $\beta = 1$.

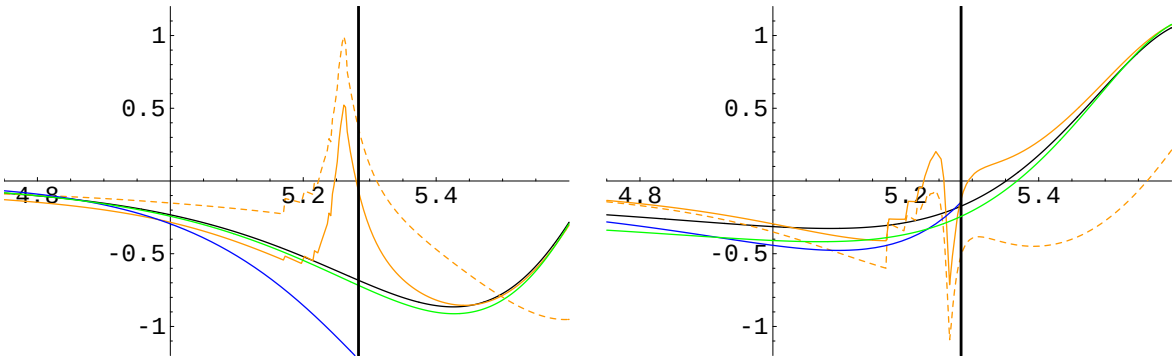


**Figure 4.21:** As for Figure 4.20, but with $\beta = \frac{1}{5}$. Here we also plot the small-$\beta$ transition region function (4.144), which is the solid green line.

Finally, we considered the process of numerical evaluation of the functions appearing in the far-field directivities, and compared the exact and approximate expressions for the scattered fields.

# Chapter 5

# Dielectric Structures

In this chapter we will discuss the propagation of electromagnetic waves in the presence of dielectric structures. In particular we will consider obstacles which consist of a thin layer of dielectric material. Such structures are commonly used to protect radar arrays physically, without significantly impeding their operational performance. The main difference between dielectric and perfectly conducting obstacles is that the fields within the structure may be non-zero for a dielectric structure, and so waves may propagate through the obstacle. If a wave is incident upon the interface between two materials, neither of which are perfect conductors, then along with the usual reflected wave there is a wave transmitted into the other material. This transmitted wave may reflect many times at the interior boundary of the scatterer, and at each reflection a wave is transmitted into the exterior material. Unless the material is lossy, or the reflection coefficient small, we must consider a large number of these reflections to obtain a good approximation to the scattered fields.

It would be preferable to avoid consideration of the fields within the dielectric material, and instead approximate the effects of propagation within the structure by boundary conditions on the exterior fields at the surface of the scatterer. Such an approach assumes that the interaction between the external fields and the structure is local in nature; this is not the case for an arbitrary dielectric body. However in the special case of a thin dielectric layer with high refractive index we may approximate the effects of the layer by transition conditions which relate the fields and their derivatives on either side of the layer.

We will find approximate transition conditions for planar and curved layers, and use these to find the fields scattered by the layer. If the layer has a small "tip" region, within which the curvature is large, we will find a leading-order approximation to the directivity

of the fields diffracted from this tip (provided certain conditions are satisfied). We will also examine waves which propagate almost tangentially to the layer, and will find modes which are of a similar form to whispering gallery and creeping rays for an impenetrable boundary. These are initiated by tangential incidence upon the layer, and we will find the launch amplitudes for these modes.

## 5.1 Formulation of problem (and numerical solution methods)

In the presence of electric and magnetic current sources $\mathbf{J}_c$ and $\mathbf{M}_c$, the electric and magnetic fields satisfy Maxwell's equations

$$\nabla \wedge \mathbf{E} - ik\hat{\mu}\mathbf{H} = -\mathbf{M}_c, \tag{5.1}$$

$$\nabla \wedge \mathbf{H} + ik\hat{\epsilon}\mathbf{E} = \mathbf{J}_c, \tag{5.2}$$

where the relative permittivity $\hat{\epsilon}$ and permeability $\hat{\mu}$ are now functions of position. If two materials with different E-M properties meet at a smooth boundary then we require that the tangential components of both fields are continuous across the interface; if the surface has an edge or vertex then suitable local conditions [66] must also be satisfied there. In the remainder of this chapter we will consider a uniform dielectric body in free space, so $\hat{\epsilon}$ and $\hat{\mu}$ are constant in each medium.

If the incident fields are generated by distant sources then the current source terms will vanish within the region of interest. However, when the permittivity and permeability vary from their free space values we see that (5.1) and (5.2) may be written in the form

$$\nabla \wedge \mathbf{E} - ik\mathbf{H} = ik(\hat{\mu} - 1)\mathbf{H}, \tag{5.3}$$

$$\nabla \wedge \mathbf{H} + ik\mathbf{E} = -ik(\hat{\epsilon} - 1)\mathbf{E}, \tag{5.4}$$

and so the field scattered by the structure is the same as that which would be generated by the equivalent currents [11]

$$\mathbf{J}_{eq} = -ik(\hat{\epsilon} - 1)\mathbf{E}, \qquad \mathbf{M}_{eq} = -ik(\hat{\mu} - 1)\mathbf{H}, \tag{5.5}$$

radiating in free space. Such a solution also has continuous tangential field components across the boundaries between materials. If vector potentials are introduced for both the electric and magnetic fields then these scattered fields may be readily expressed in terms of the fields within the dielectric [11]; this allows us to write the problem as a volume

integral equation. Such an equation is readily discretised [114], but yields a large and dense system of linear equations.

An alternative method is to consider each of the Cartesian components of the fields separately [72] (see [108] for the acoustic case). The field components each satisfy

$$(\nabla^2 + k^2)\phi = k^2(1 - N^2)\phi, \tag{5.6}$$

and so the scattered field may be considered to be generated by equivalent point sources radiating in free space. However, the tangential field components of this scattered field are not continuous across the interfaces between materials. This causes there to be additional contributions from surface currents distributed upon the interfaces.

In the case of a homogeneous dielectric body the problem may instead be formulated as a surface integral equation [91] [50] [143] [151], which is often preferred for numerical purposes as the region to be discretised has one fewer spatial dimension. In the simplest case of a closed, compact dielectric body with no "holes" the scattered fields may be postulated as those due to initially unknown electric and/or magnetic surface currents. These are in the same position as the surface of the scatterer but radiate in free space. The total external fields may be found in terms of these currents, and so, by using the continuity conditions at the boundary, the internal fields at the interface may be found as functions of the unknown currents. The interior problem with all tangential field components given on the boundary is over-specified, and so an integral equation may be obtained for the currents by demanding that the interior problem is self-consistent.

## 5.2 GTD for dielectric structures

If the wavelength of the incident field is small compared to a typical length scale of the structure, which corresponds to large $k$, then the GTD may be used to give an approximation to the scattered fields. This is more complicated than the perfectly conducting or impedance cases as waves may now propagate within the obstacle.

When a plane wave is incident upon a locally planar interface between two different materials there is a (possibly evanescent) wave transmitted into the second material, and a wave reflected back into the first. The directions of propagation of these three waves lie in a plane containing the normal to the surface. The angles made by the incident and reflected waves with the normal to the surface are equal, whereas the transmitted wave obeys Snel's law

$$N_1 \sin\theta_i = N_2 \sin\theta_t \tag{5.7}$$

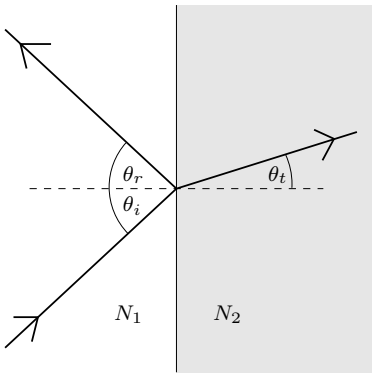


**Figure 5.1:** Reflection and refraction at the interface between two materials with refractive indices $N_1$ and $N_2$. In the three-dimensional case the directions of propagation of all three of these waves lie in a plane which also contains the normal to the surface.

where here $N_1$ and $N_2$ are the refractive indices of the two materials, $\theta_i$ is the angle made by the direction of incidence with the normal to the surface, and $\theta_t$ is the corresponding angle for the transmitted wave, as shown in Figure 5.1. If $\theta_i$ and $\theta_t$ differ then the wave is said to undergo refraction at the interface.

As the problem is linear the incident plane wave may be decomposed into two plane waves, whose electric and magnetic fields respectively are normal to the plane of incidence. The continuity conditions for the tangential fields at the interface allow the amplitudes of the reflected and transmitted waves (often referred to as the Fresnel coefficients) to be found for each polarization [66, p. 316] [14, §1.5.2]. The total reflected and transmitted fields may then be found by recombining the fields for the two polarizations.

For a wave incident upon the boundary from the material with larger refractive index, and with $\theta_i$ greater than the critical angle $\theta_c = \sin^{-1}\left(\frac{N_2}{N_1}\right)$, there is no real solution for $\theta_t$. Instead within the second material there is a plane wave for which the normal component of the wavenumber is complex, which therefore decays exponentially away from the interface. Such evanescent waves are best described by complex rays [27]. For an infinite planar half space such rays transmit no energy away from the surface, and the reflection coefficient is of unit magnitude. However when the interface is curved then these complex rays may have a caustic, and there is an exponentially small loss of energy in the form of real rays [135] [55]. Losses may also occur if another dielectric body is placed within the evanescent wave, as at the interface between two media the complex rays may be refracted to become real rays.

These planar reflection and refraction coefficients may be used to find the geometrical optics solution for a general dielectric obstacle [75] [28]. Exactly as in the case of scattering by an impenetrable obstacle it is necessary to perform a local analysis of the fields

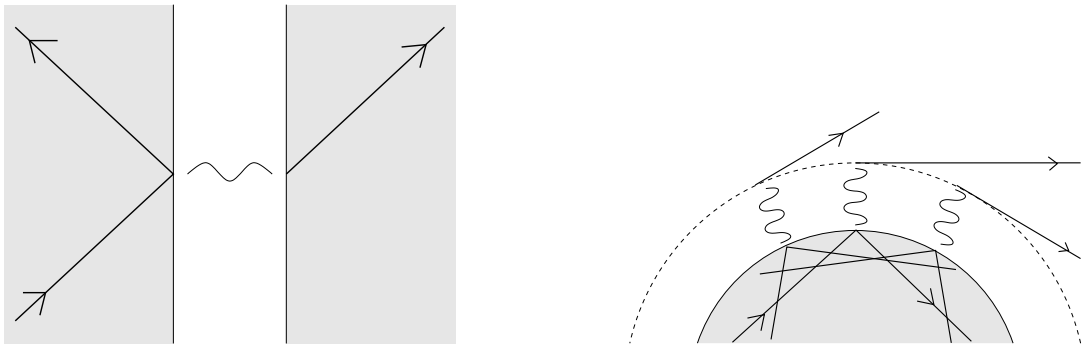

**Figure 5.2:** Conversion between evanescent and real rays. In the left hand diagram we see an evanescent wave generated by total internal reflection in the material at the left undergoing refraction at the interface between free space and the second material, and so becoming real rays. Similarly, in the right hand diagram an evanescent wave is generated by total internal reflection at a curved interface. The resulting complex rays possess a complex caustic, and across this line the evanescent wave becomes real, shedding real rays tangentially to the caustic.

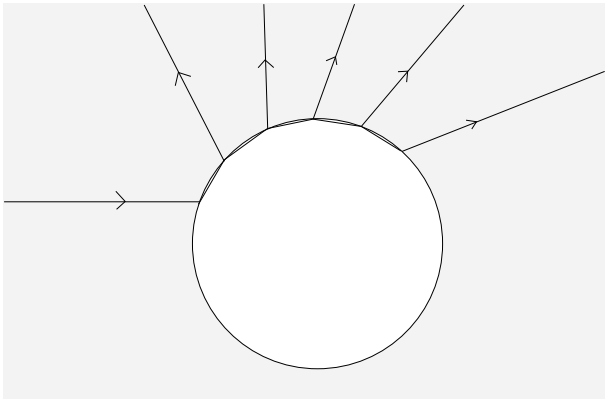

**Figure 5.3:** Critical incidence upon a convex object with lower refractive index than the surrounding medium, showing the rays which are reflected multiple times at the interface.

near caustics, cusps and other singularities of the ray solution; for a dielectric obstacle such singularities may be present even in the simple case of a convex obstacle illuminated by a plane wave (such as in Figure 5.4, where a caustic of the transmitted rays can be seen).

As for an impenetrable body, the GO solution is not smooth in the vicinity of points of tangency, and is not smooth across the shadow boundary as the incident field switches off there. Provided the difference between the refractive indices of the two materials is not asymptotically small then the local effect of propagation within the dielectric material may be approximated by (vector) impedance boundary conditions upon the external

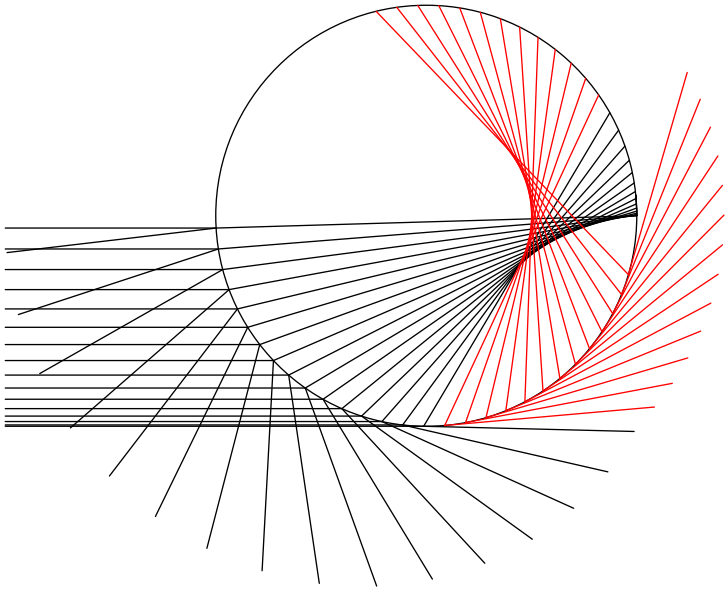

**Figure 5.4:** Tangential incidence upon a dielectric cylinder. The black lines are the incident, reflected and transitted rays (not including any internally reflected rays). The red lines show the rays shed into both materials by creeping fields initiated at the point of tangency.

fields. This impedance depends upon the angle of incidence; in the Fock region, and for creeping waves or whispering gallery modes, the external fields propagate almost tangentially to the interface, and so this impedance is approximately constant [119]. Explicitly, for a two-dimensional dielectric obstacle in free space the TE mode satisfies the impedance boundary condition

$$\frac{\partial E_z}{\partial n} = -ik\sqrt{\frac{\hat{\epsilon}}{\hat{\mu}}}\sqrt{1-\frac{\sin^2\theta_0}{N^2}}E_z \tag{5.8}$$

and the TM mode satisfies the boundary condition

$$\frac{\partial H_z}{\partial n} = -ik\sqrt{\frac{\hat{\mu}}{\hat{\epsilon}}}\sqrt{1-\frac{\sin^2\theta_0}{N^2}}H_z \tag{5.9}$$

where $\hat{\epsilon}$, $\hat{\mu}$ and $N=\sqrt{\hat{\epsilon}\hat{\mu}}$ are the (relative) E-M properties of the dielectric material, and $\theta_0$ is the angle of incidence. By introducing the Fock region or Airy layer scaling $n = k^{-\frac{2}{3}}\hat{n}$ for the normal coordinate, we see that when $\hat{\epsilon}$ and $\hat{\mu}$ are both $\mathcal{O}(1)$ the external fields satisfy Dirichlet conditions, to leading order, at the interface. The impedance affects the problem for the $\mathcal{O}(k^{-\frac{1}{3}})$ correction, but does not change the amplitude of the leading-order field; this problem is considered in more detail in [5] [82]. In the three-dimensional electromagnetic case it is found, in [5] and [16], that the amplitudes of the TE and TM

modes are coupled upon geodesics which have non-zero torsion (by which we mean that the geodesic is not contained within a plane).

For the surface impedance to substantially affect the exponential decay rates (see (3.53) and (3.55)) of these Airy layer modes, then $\eta = \sqrt{\frac{\hat{\mu}}{\hat{\epsilon}}}$ must be either $\mathcal{O}(k^{\frac{1}{3}})$ for TE polarization, or $\mathcal{O}(k^{-\frac{1}{3}})$ for TM polarization. From the plane wave reflection and transmission coefficients it can be seen that the these parameter regimes correspond to the transmission coefficient (for the appropriate polarization) being $\mathcal{O}(1)$ when the incident angle $\theta_0$ differs from $\frac{\pi}{2}$ by an $\mathcal{O}(k^{-\frac{1}{3}})$ amount.

Another distinguished limit is obtained when the difference between the refractive indices of the two materials is small, specifically when $N - 1 = \mathcal{O}(k^{-\frac{1}{3}})$ with $\hat{\epsilon}, \hat{\mu} = \mathcal{O}(1)$. However, near the point of tangency for the external fields the internal fields are also near tangency, and so we cannot use impedance boundary conditions. Instead, it is found that the fields on both sides of the interface near the point of tangency have asymptotic approximations in terms of Airy functions [5].

The GO solution is also not smooth near points of critical incidence upon the interface (from within the dielectric) and near the critically reflected ray. The reflection coefficient is not differentiable with respect to the incident angle at the critical angle, and a "lateral wave" is switched on across the critically reflected ray. If the surface is convex when viewed from the material with higher refractive index then the fields refracted twice at the interface, along with the fields which are refracted and internally reflected multiple times, as shown in Figure 5.3, will also be switched on across this line.

For a planar interface this problem has been widely studied, for instance in [75], [20], [141] and [27]. A lateral wave is initiated at the point of critical incidence, which propagates along the boundary, decaying algebraically and shedding rays at the critical angle into the medium with higher refractive index. Suitable transition functions (in terms of the parabolic cylinder function of order $\frac{1}{2}$) valid in the vicinity of the critically reflected ray have also been found. However, when the interface has $\mathcal{O}(1)$ curvature (on the outer length scale), such an algebraically decaying surface wave cannot be found, and instead the wave propagating along the surface consists of a series of exponentially decaying surface modes. These modes propagate almost tangentially to the boundary in the fast medium, and so may again be studied by an Airy-layer analysis with suitable impedance boundary conditions. They shed rays at the critical angle into the slower medium, and in the fast medium resemble whispering gallery or creeping ray modes depending upon the sign of the curvature of the interface. Even the modes of whispering gallery type decay exponentially as they propagate along the boundary, as rays are transmitted into the

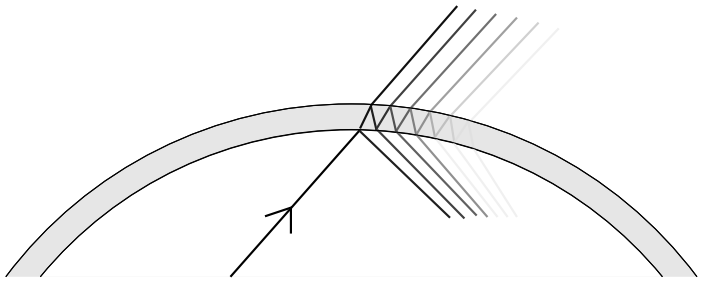

**Figure 5.5:** Path of a ray through a thin dielectric layer, showing the multiple internal reflections within the layer. The shading illustrates the decay in the amplitude of the rays with each reflection.

slow medium. Comparison with the asymptotic behaviour of the separable problems in a cylindrical geometry [28] [86], and a spherical geometry [97], has allowed the appropriate launch coefficients for these surface modes to be found. In the spherical case further analysis has been made of the behaviour of the scattered far field near the critically reflected ray [34] [45], and the fields in this region may be approximated in terms of Fresnel-Fock and Pearcey-Fock integrals. The transition region in the cylindrical case is considered in [118], [56] and [54], where the fields near the surface are also studied.

Along with the problems of critical incidence and tangency, local analysis must also be performed near points where the boundary is not smooth. Unfortunately the problem of diffraction by a dielectric wedge of arbitrary angle has proved intractable in general, except in special cases, such as for a diaphanous (or iso-refractive) wedge [77]. Approximate solutions have been found in the case when the difference between the two refractive indices is small [111], [70], or large [88]. Other approximate solutions may be found when the angle made at the tip of the wedge is approximately $\pi$ [69], or when the angle is small [70].

## 5.3 Approximate methods for thin layers

The GTD framework discussed above may be used to find the fields scattered by a dielectric body. However, unless the reflection coefficients are small, or the dielectric is significantly lossy, then to obtain a good approximation to the scattered fields the rays must be traced as they undergo a large number of reflections at the interface. For a general structure this ray tracing procedure may be quite numerically demanding, and for some geometries the path of the $n$-fold reflected ray, for large $n$, is very sensitive to the position of the initial ray. In the particular case of a dielectric layer which is highly

transmissive because of interference between multiply reflected rays, the location of the ray paths is not particularly sensitive to the position of the initial incident ray. However a large number of reflections within the layer must still be included in the calculation to give an adequate approximation to the scattered fields.

Within the GTD framework many authors have used the reflection and transmission coefficients for a plane wave incident upon a planar slab to account for these multiply reflected rays [142] [23] [22]. Heuristic diffraction coefficients are also used in [23] to find the field diffracted by the edge of such a layer.

Motivated by the exact solution to the two-dimensional problem of a (line) source radiating in the presence of a constant thickness cylindrical layer [43], reflection and transmission coefficients were introduced in [42], which incorporate the effects of multiple reflection and curvature of the layer. This method was also applied to a tapered layer. This work also contained an attempt to account for surface/propagating modes of the dielectric layer by Poisson (re-)summation of those ray fields which have undergone a large number of reflections at the interface. Complex rays have also been used to study the propagation of a Gaussian beam through a two-dimensional radome [48].

An alternative approach which can be used to find the effect of a radome on the radiation pattern of an antenna is to first calculate the (near) fields of the antenna radiating in free space, and either use these expressions exactly [104] or the plane wave decomposition of the antenna fields [148] to give the fields on the inside surface of the dielectric layer. The planar-slab plane-wave transmission coefficients are then used to find the field components on the outer surface of the radome. The fields outside the radome may be expressed as an integral over the exterior surface of the radome, using Helmholtz' integral in the scalar case or the Stratton-Chu integral formula in the vector case. This integral may be approximated further to give the directivity of the emitted fields. The field components on the exterior surface of the radome may also be found by the method of [26] for a two-dimensional structure. At each point on the layer the antenna fields may be expanded in terms of cylindrical harmonics, in a coordinate system centred upon the centre of curvature of the layer. The reflection and transmission coefficients for cylindrical waves incident upon a cylinder of constant thickness may then be used to find the field on the outer surface of the radome at that point.

Another method related to those above applies the principle of reciprocity upon some surface which is within the radome and encloses the antenna. The fields on this surface generated by antenna currents, or from a plane wave incident upon the radome from outside, are found separately by some exact or approximate method, such as ray tracing

with planar slab reflection and diffraction coefficients [129] [101], or the Physical Theory of Diffraction (PTD) with heuristic diffraction coefficients [112]. This allows the antenna currents induced by an incident plane wave to be found, or equivalently the far field pattern radiated by an antenna.

Other approximate methods for planar layers involve approximation of the volume integrals discussed in section 5.1. For a layer which is thin compared to the wavelength of the fields both in free space and within the dielectric material such an analysis is performed in [72]. In that work, the volume and surface integrals found by applying (5.6) to each of the Cartesian components of the fields are approximated in this limit. The reflected field and the correction to the transmitted field are small, and so an expression for the leading-order scattered field may be found in terms of the incident field. Similar methods have also been applied to the standard volume integral formulation of the problem [124] [126], where the effect of the layer is expressed in terms of a simplified integral equation, or equivalently as approximate transition conditions.

A large number of numerical techniques have also been used for problems of this type, including discretization of the boundary integral formulations [9] [153], finite element methods [52], volume integral approaches [138] [85], and finite-difference time-domain methods [8]. These dielectric structures are often electrically large, and so these numerical methods are often either quite computationally expensive or multi-level methods (such as the fast multi-pole method) must be employed. One promising approach [2] combines a physical optics approximation (using curvature-corrected slab reflection and transmission coefficients) with a boundary integral equation method in a small region where the layer has large curvature.

For a few special geometries, such as a confocal spheroidal configuration [83] or a cylindrical geometry [4] solutions may be found by separation of variables. However this technique is even more limited than in the case of an impenetrable body, as both the inner and outer surfaces must be confocal, which limits the thickness profiles which are possible (a uniform layer may only be considered in a planar, cylindrical or spherical geometry).

## 5.4 Approximate boundary conditions

The approach that we will employ in this chapter is to approximate the effect of propagation within the dielectric material by boundary conditions on the fields and their derivatives at the interface. Such boundary conditions (commonly known as Leontovich

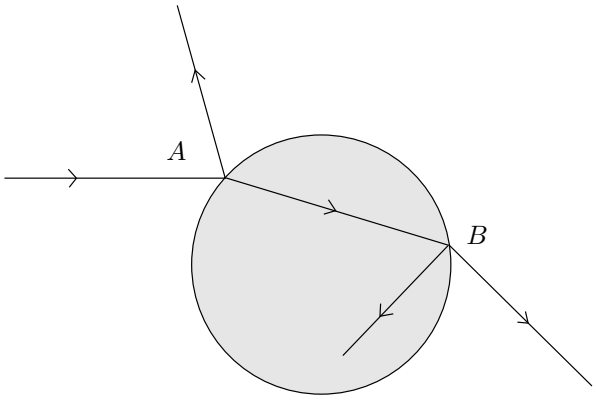


**Figure 5.6:** Transmission of rays through a dielectric structure. The behaviour of the exterior fields near $B$ can be seen to depend on the fields near $A$.

boundary conditions; see [106] for some historical discussion) were first introduced by Rytov [120] for highly conducting materials, and subsequently used to model the propagation of radio waves along the surface of the Earth and near conducting obstacles [46, Ch. 5, 11]. Subsequently, similar conditions have been used to model a number of different types of obstacles, including metal-backed dielectric layers [71] and periodic surfaces [58]. Approximate boundary conditions are also useful for computational purposes; absorbing boundary conditions ([128] and references within) are used to impose outgoing radiation conditions at the edge of the domain in finite element calculations, and on-surface radiation conditions [78] [67] [7] [25] applied to the scattered fields on the surface may be used to give (rather counter-intuitive) approximations to the scattered fields for a convex obstacle. For a review of many applications of impedance boundary conditions, and related results, we refer the reader to [127] and [59].

The fundamental assumption made in each of these approximations is that the interaction between the incident field and the structure is (approximately) local in nature. This is not the case in general for non-lossy dielectric materials, for a ray incident upon the interface may be transmitted into the body and travel some distance through the body, before exiting the structure at a different point, as shown in Figure 5.6. There are a few special situations where the transmitted rays cannot leave the structure at a point within the region of interest, such as a (slightly perturbed) dielectric half space, or when we are only concerned with the local behaviour of the fields near the interface (away from critical incidence).

In the case of a thin dielectric layer (and also for a wire grid) it is possible to find transition conditions which relate the fields at points on opposite sides of the layer. If the layer is thin compared to the exterior wavelength then these may be expressed as

transition conditions on the external fields at the midline of the layer.

### 5.4.1 Derivation of approximate boundary or transition conditions

A number of different methods may be used to derive approximate boundary conditions. One approach [71] [110] is to pose the approximate conditions as a number of linear relationships between the fields and their derivatives at the boundary or midline of the layer, where the coefficients are initially unknown. In the case of a planar layer modelled by second-order transition conditions these are of the form

$$\prod_{m=1}^{2}\left(\frac{\partial}{\partial y}+ik\gamma_m\right)\phi(x,0+)-\prod_{m=1}^{2}\left(\frac{\partial}{\partial y}-ik\gamma_m\right)\phi(x,0-)=0, \tag{5.10}$$

$$\prod_{m=1}^{2}\left(\frac{\partial}{\partial y}+ik\Gamma_m\right)\phi(x,0+)+\prod_{m=1}^{2}\left(\frac{\partial}{\partial y}-ik\Gamma_m\right)\phi(x,0-)=0, \tag{5.11}$$

for some constants $\gamma_1$, $\gamma_2$, $\Gamma_1$, $\Gamma_2$ (after [125]). In some cases the coefficients in the boundary conditions are allowed to depend upon the angle of incidence [110].

The plane wave reflection (and transmission) coefficients are then found in the exact and approximate cases, and the coefficients of the conditions are chosen to make these approximately equal.

Another somewhat related method is to consider the problem of a planar boundary, and to take the Fourier transform(s) of the fields in the transverse direction(s) [59]. The plane wave reflection and transmission coefficients may then be used to find exact boundary conditions on the transformed fields, where the coefficients in these conditions depend upon the transverse wavenumbers. These coefficients are then approximated by polynomials in the transverse wavenumbers (at this point implicitly assuming that the interaction with the dielectric is local in nature) and these conditions may then be expressed as boundary conditions on the untransformed fields and their derivatives. The effects of constant curvature may also be included in this method if we instead consider the problem in a cylindrical geometry, and take the Fourier transform in the angular variable.

A third method is to use the volume integral formulation of the problem discussed earlier, which expresses the scattered fields in terms of the fields within the dielectric obstacle. An approximation may be found for the internal fields as a function of the external fields on the boundary; using this we can deduce the scattered fields in terms of the fields on the boundary, and so the approximate boundary conditions [124] [126] [127].

We note here that when the geometry is discontinuous, due to the layer having a sharp edge or a discontinuity in thickness, then for transition or impedance conditions which include second or higher derivatives of the fields (such as those discussed below), extra local conditions [125] [127, pp. 175–180] must be imposed near the discontinuity to ensure uniqueness, in addition to the usual edge conditions.

With most of the above methods the limits of validity for the approximation are not immediately apparent. We will instead proceed in a similar manner to the derivation of the boundary conditions for a highly conducting obstacle outlined in Chapter 2. The fields within the layer will be asymptotically expanded in terms of a small parameter (the reciprocal of the refractive index of the layer) and this will allow us to find conditions upon the exterior fields and their derivatives at the midline of the layer.

### 5.4.2 Transition conditions for a high contrast dielectric layer

We will now seek approximate transition conditions for a layer of dielectric material which has a high refractive index, and which is of the same order of thickness as the internal wavelength, so is thin compared with the free space wavelength. Similar boundary conditions may be found for a layer of arbitrary refractive index which is thin compared to the wavelength both inside and outside the layer [117] [127]. In that case both the external fields and the fields within the dielectric layer are expanded as power series in the normal coordinate, centred at the midline of the layer. The continuity conditions are applied at each of the interfaces, and this gives transition conditions relating the external fields on the two sides.

In our case the layer is not necessarily thin compared to the interior wavelength, and so the (first term of) the power series will give a poor approximation to the interior fields. However the refractive index is large, and so a ray incident upon the layer will be refracted and propagate through the layer almost normally to the midline. This will allow us to proceed in a similar manner to the analysis for highly conducting obstacles discussed in Chapter 2; versions of such impedance boundary conditions which are accurate to higher order and which include the effects of curvature can be found in [127], [128]. Somewhat similar conditions, for multiple-layer structures were found in [115]. In that paper higher order conditions were obtained, but only for planar structures. Our conditions will be second-order, and only for a single layer, but will include the effects of curvature of the layer.

In this section we will choose our length scale to be $1/(2\pi)$ times the wavelength of the incident field; Maxwell's equations are then (5.1) and (5.2), but with $k = 1$. In the

two-dimensional case we may consider the two polarizations of the field separately, and they each reduce to scalar problems. For transverse electric polarization we set

$$\mathbf{E} = \phi\,\mathbf{e}_z. \tag{5.12}$$

The planar dielectric layer occupies the region $-\frac{d}{2N} < x < \frac{d}{2N}$, and we denote the external fields to the left of the layer by $\phi^L$, the fields within the layer by $\phi^C$ and the fields to the right of the layer by $\phi^R$. Then

$$(\nabla^2 + 1)\phi^L = 0, \qquad (\nabla^2 + N^2)\phi^C = 0, \qquad (\nabla^2 + 1)\phi^R = 0, \tag{5.13}$$

in each of the respective regions. We seek an asymptotic expansion of the fields in each of the regions of the form

$$\phi \sim \phi_0 + \frac{1}{N}\phi_1 + \dots. \tag{5.14}$$

As the refractive index is large we expect that the incident waves will be strongly refracted at the interface and propagate almost normally through the layer, so we scale $x = N^{-1}\hat{x}$, but only for the internal fields. The equation within the layer then becomes

$$\frac{\partial^2\phi^C}{\partial\hat{x}^2} + \frac{1}{N^2}\frac{\partial^2\phi^C}{\partial y^2} + \phi^C \;=\; 0, \tag{5.15}$$

and to leading order the solutions of this equation are

$$\phi_0 \;\sim\; \alpha_0(y)\cos\hat{x} + \beta_0(y)\sin\hat{x}. \tag{5.16}$$

If we assume that we may analytically continue the external fields from the interface up to the midline of the layer, and then asymptotically expand $\phi^L$ and $\phi^R$ in power series about the midline $x = 0$, we find that

$$\phi^L\left(-\frac{d}{2N}, y\right) \;\sim\; \phi_0^L(0,y) - \frac{d}{2N}\frac{\partial\phi_0^L}{\partial x} + \frac{1}{N}\phi_1^L(0,y) + \dots, \tag{5.17}$$

$$\phi^R\left(\frac{d}{2N}, y\right) \;\sim\; \phi_0^R(0,y) + \frac{d}{2N}\frac{\partial\phi_0^R}{\partial x} + \frac{1}{N}\phi_1^R(0,y) + \dots, \tag{5.18}$$

and similar expansions may be found for the normal derivatives of the field at the interfaces. Continuity of the tangential components of the electric field at the interface requires that

$$\phi^L = \phi^C \quad \text{on } y = -\frac{d}{2N}, \qquad \phi^C = \phi^R \quad \text{on } y = \frac{d}{2N}, \tag{5.19}$$

at the respective interfaces, and continuity of the tangential components of the magnetic field becomes

$$\frac{\partial\phi^L}{\partial x} = \frac{N}{\hat{\mu}}\frac{\partial\phi^C}{\partial\hat{x}} \quad \text{on } y = -\frac{d}{2N}, \qquad \frac{\partial\phi^R}{\partial x} = \frac{N}{\hat{\mu}}\frac{\partial\phi^C}{\partial\hat{x}} \quad \text{on } y = -\frac{d}{2N}. \tag{5.20}$$

Applying the continuity conditions for the magnetic field to (5.16) gives at leading order

$$0 = \beta_0(y)\cos\left(-\frac{d}{2}\right) - \alpha_0(y)\sin\left(-\frac{d}{2}\right), \tag{5.21}$$

$$0 = \beta_0(y)\cos\left(\frac{d}{2}\right) - \alpha_0(y)\sin\left(\frac{d}{2}\right). \tag{5.22}$$

This pair of equations has no non-trivial solution unless $\sin(d) = 0$, which corresponds to the thickness of the layer being an integer multiple of half the internal wavelength. If this condition is not satisfied then the leading-order external fields satisfy Dirichlet conditions on the midline of the layer, and so the layer is approximately impenetrable. If $d = \pi$ then the boundary condition (5.19) gives

$$\phi_0^C(\hat{x}, y) = -\phi_0^L(0, y)\sin\hat{x}, \tag{5.23}$$

and so we have that

$$\phi_0^L(0, y) + \phi_0^R(0, y) = 0. \tag{5.24}$$

The next order interior equation is the same as that for the leading-order fields, and so has solution

$$\phi_1^C = \alpha_1(y)\cos\hat{x} + \beta_1(y)\sin\hat{x}, \tag{5.25}$$

and on applying the continuity conditions at the interfaces we find that

$$\phi_1^L - \frac{\pi}{2}\frac{\partial\phi_0^L}{\partial x} = -\beta_1(y) = -\left(\phi_1^R + \frac{\pi}{2}\frac{\partial\phi_0^R}{\partial x}\right), \tag{5.26}$$

and

$$\hat{\mu}\frac{\partial\phi_0^L}{\partial x} = \alpha_1(y) = -\hat{\mu}\frac{\partial\phi_0^R}{\partial x}. \tag{5.27}$$

Finally we consider the equation within the layer at $\mathcal{O}(N^{-2})$

$$\frac{\partial^2\phi_2^C}{\partial\hat{x}^2} + \phi_2^C = -\frac{\partial^2\phi_0^C}{\partial y^2}, \tag{5.28}$$

which has solutions of the form

$$\phi_2 = \alpha_2(y)\cos\hat{x} + \beta_2(y)\sin\hat{x} - \frac{1}{2}\frac{\partial^2\phi_0^L}{\partial y^2}\hat{x}\cos\hat{x}. \tag{5.29}$$

Applying the continuity conditions upon the normal derivatives then gives

$$\frac{\partial\phi_1^L}{\partial x} + \frac{\partial\phi_1^R}{\partial x} = \frac{\pi}{2}\left(\frac{\partial^2\phi_0^L}{\partial x^2} - \frac{\partial^2\phi_0^R}{\partial x^2}\right) + \frac{\pi}{2\hat{\mu}}\frac{\partial^2\phi_0^L}{\partial y^2}. \tag{5.30}$$

Equations (5.24) and (5.27) are transition conditions for the leading-order field, and equations (5.26) and (5.30) are inhomogeneous transition conditions for the first order correction to the fields.

We may also continue this analysis to higher order. The conditions for the $\mathcal{O}(N^{-2})$ fields are

$$\phi_2^L + \phi_2^R = \frac{\pi}{2}\left(\frac{\partial \phi_1^L}{\partial x} - \frac{\partial \phi_1^R}{\partial x}\right) \tag{5.31}$$

$$\frac{\partial \phi_2^L}{\partial x} + \frac{\partial \phi_2^R}{\partial x} = \frac{\pi}{2}\left(\frac{\partial^2 \phi_1^L}{\partial x^2} - \frac{\partial^2 \phi_1^R}{\partial x^2}\right) + \frac{\pi}{2\hat{\mu}}\frac{\partial^2}{\partial y^2}\left(\phi_1^L - \frac{\pi}{2}\frac{\partial \phi_0^L}{\partial x}\right) \tag{5.32}$$

For transverse magnetic polarization we write

$$\mathbf{H} = \phi\, \mathbf{e}_z, \tag{5.33}$$

and replace $\hat{\mu}$ in the continuity condition for the derivatives by $\hat{\epsilon}$. For most (non-magnetic) materials $\hat{\mu}$ is very close to 1, and so we rescale $\hat{\epsilon} = N^2\epsilon^*$. The continuity conditions for the electric field become

$$\frac{\partial \phi^L}{\partial x} = \frac{1}{\epsilon^* N}\frac{\partial \phi^C}{\partial \hat{x}} \quad \text{on } y = -\frac{d}{2N}, \qquad \frac{\partial \phi^R}{\partial x} = \frac{1}{\epsilon^* N}\frac{\partial \phi^C}{\partial \hat{x}} \quad \text{on } y = \frac{d}{2N}, \tag{5.34}$$

and so we must rescale $\phi^C = N\hat{\phi}^C$. Again the layer is impenetrable (now with Neumann boundary conditions on each side) unless $d$ is approximately a multiple of $\pi$. When $d = \pi$ we obtain the conditions

$$\phi_0^L + \phi_0^R = 0, \tag{5.35}$$

$$\frac{\partial \phi_0^L}{\partial x} + \frac{\partial \phi_0^R}{\partial x} = 0, \tag{5.36}$$

$$\frac{\partial \phi_1^L}{\partial x} + \frac{\partial \phi_1^R}{\partial x} = \pi\frac{\partial^2 \phi_0^L}{\partial x^2}, \tag{5.37}$$

$$\phi_1^L + \phi_1^R = \pi\frac{\partial \phi_0^L}{\partial x} - \frac{\pi\epsilon^*}{2}\frac{\partial^2}{\partial y^2}\frac{\partial \phi_0^L}{\partial x}, \tag{5.38}$$

by a very similar procedure to the TE case.

The above calculations are valid provided the radius of curvature of the layer is much greater than the external wavelength. When the layer is curved on the scale of the exterior wavelength, but is approximately flat on the scale of the interior wavelength, we may repeat the analysis above but in orthogonal curvilinear coordinates $s$ and $n$ centred upon the midline of the layer. Helmholtz' equation within the layer in this coordinate system is approximately

$$\left(\frac{\partial^2}{\partial s^2} + N^2\frac{\partial^2}{\partial \hat{n}^2} + N\kappa(1 - N^{-1}\hat{n}\kappa)\frac{\partial}{\partial \hat{n}} + N^2\right)\phi^C = 0, \tag{5.39}$$

and following a rather similar analysis to that outlined above we obtain the boundary

conditions

$$\begin{aligned}
\phi_0^L + \phi_0^R &= 0, && (5.40)\\
\frac{\partial \phi_0^L}{\partial n} + \frac{\partial \phi_0^R}{\partial n} &= 0, && (5.41)\\
\phi_1^L + \phi_1^R &= \pi \frac{\partial \phi_0^L}{\partial n} + \frac{\pi\kappa}{2}\phi_0^L, && (5.42)\\
\frac{\partial \phi_1^L}{\partial n} + \frac{\partial \phi_1^R}{\partial n} &= \pi \frac{\partial^2 \phi_0^L}{\partial n^2} + \frac{\pi}{2\hat{\mu}}\frac{\partial^2 \phi_0^L}{\partial s^2} + \frac{\pi\kappa}{2}\frac{\partial \phi_0^L}{\partial n} - \frac{3\pi\kappa^2\phi_0^L}{8\hat{\mu}}, && (5.43)
\end{aligned}$$

for transverse electric polarization, and

$$\begin{aligned}
\phi_0^L + \phi_0^R &= 0, && (5.44)\\
\frac{\partial \phi_0^L}{\partial n} + \frac{\partial \phi_0^R}{\partial n} &= 0, && (5.45)\\
\phi_1^L + \phi_1^R &= \pi \frac{\partial \phi_0^L}{\partial n} - \frac{\pi\epsilon^*}{2}\frac{\partial^2}{\partial s^2}\frac{\partial \phi_0^L}{\partial n} + \frac{\pi\kappa}{2}\phi_0^L - \frac{\pi\epsilon^*\kappa^2}{8}\frac{\partial \phi_0^L}{\partial n}, && (5.46)\\
\frac{\partial \phi_1^L}{\partial n} + \frac{\partial \phi_1^R}{\partial n} &= \pi \frac{\partial^2 \phi_0^L}{\partial n^2} + \frac{\pi\kappa}{2}\frac{\partial \phi_0^L}{\partial n}, && (5.47)
\end{aligned}$$

for transverse magnetic polarization.

This approach may also be extended to the three-dimensional acoustic case. Helmholtz' equation within the layer is approximately

$$\left(\nabla_{s/f}^2 + N\left((\kappa_1+\kappa_2) - N^{-1}(\kappa_1^2+\kappa_2^2)\hat{n}\right)\frac{\partial}{\partial \hat{n}} + N^2\frac{\partial^2}{\partial \hat{n}^2} + N^2\right)\phi = 0, \quad (5.48)$$

where $\kappa_1$ and $\kappa_2$ are the two principal curvatures of the midline of the layer. Solving the same *scalar* problems as in the two-dimensional cases we find that

$$\begin{aligned}
\phi_0^L + \phi_0^R &= 0, && (5.49)\\
\frac{\partial \phi_0^L}{\partial n} + \frac{\partial \phi_0^R}{\partial n} &= 0, && (5.50)\\
\phi_1^L + \phi_1^R &= \frac{\pi}{2}\left(\frac{\partial \phi_0^L}{\partial n} - \frac{\partial \phi_0^R}{\partial n}\right) + \frac{\pi\phi_0^L(\kappa_1+\kappa_2)}{2}, && (5.51)\\
\frac{\partial \phi_1^L}{\partial n} + \frac{\partial \phi_1^R}{\partial n} &= \frac{\pi}{2}\left(\frac{\partial^2 \phi_0^L}{\partial n^2} - \frac{\partial^2 \phi_0^R}{\partial n^2}\right) + \frac{\pi(\kappa_1+\kappa_2)}{2}\frac{\partial \phi_0^L}{\partial n} + \frac{\pi}{2\hat{\mu}}\nabla^2\phi_0^L - \frac{\pi(\kappa_1+\kappa_2)^2}{8\hat{\mu}}\phi_0^L - \frac{\pi(\kappa_1^2+\kappa_2^2)}{4\hat{\mu}}\phi_0^L, && (5.52)
\end{aligned}$$

for the analogue of the TE problem, and

$$\begin{aligned}
\phi_0^L + \phi_0^R &= 0, && (5.53)\\
\frac{\partial \phi_0^L}{\partial n} + \frac{\partial \phi_0^R}{\partial n} &= 0, && (5.54)\\
\phi_1^L + \phi_1^R &= \frac{\pi}{2}\left(\frac{\partial \phi_0^L}{\partial n} - \frac{\partial \phi_0^R}{\partial n}\right) - \frac{\pi\epsilon^*}{2}\nabla^2\frac{\partial \phi_0^L}{\partial n} + \frac{\pi(\kappa_1+\kappa_2)}{2}\phi_0^L + \frac{\pi\epsilon^*(\kappa_1+\kappa_2)^2}{8}\frac{\partial \phi_0^L}{\partial n} - \frac{\pi\epsilon^*(\kappa_1^2+\kappa_2^2)}{4}\frac{\partial \phi_0^L}{\partial n}, && (5.55)\\
\frac{\partial \phi_1^L}{\partial n} + \frac{\partial \phi_1^R}{\partial n} &= \frac{\pi}{2}\left(\frac{\partial^2 \phi_0^L}{\partial n^2} - \frac{\partial^2 \phi_0^R}{\partial n^2}\right) + \frac{\pi(\kappa_1+\kappa_2)}{2}\frac{\partial \phi_0^L}{\partial n}, && (5.56)
\end{aligned}$$

for the analogue of the TM problem.

### 5.4.3 Integral form of the scattered field

(In this section we will again work on the scale of the external wavelength - we will return to the original outer length scale in the stationary phase analysis of the next section.)

We will now consider a dielectric layer whose centre-line is an infinite curve which divides the region of interest into two components $L$ and $R$, within which the fields are $\phi^L$ and $\phi^R$ respectively. If we set

$$\psi = \begin{cases} \phi^L & \text{in } L \\ -\phi^R & \text{in } R \end{cases} \tag{5.57}$$

then the leading-order transition conditions become

$$[\psi_0] = \left[\frac{\partial \psi_0}{\partial n}\right] = 0. \tag{5.58}$$

where the square brackets denote the jump in $\psi$ from $L$ to $R$; in terms of the original fields $[\psi] = -(\phi^L + \phi^R)$. From this we see that if a field is incident upon the layer then to leading order it passes through the layer unchanged except for a phase shift of $\pi$, which we introduced by the change of sign in $R$. However, for the first-order correction we find that

$$[\psi_1] = a\left(s, \psi_0, \frac{\partial \psi_0}{\partial n}, \frac{\partial^2 \psi_0}{\partial n^2}, \frac{\partial^2 \psi_0}{\partial s^2}\right), \qquad \left[\frac{\partial \psi_1}{\partial n}\right] = b\left(s, \psi_0, \frac{\partial \psi_0}{\partial n}, \frac{\partial^2 \psi_0}{\partial n^2}, \frac{\partial^2 \psi_0}{\partial s^2}\right), \tag{5.59}$$

where the functions $a$ and $b$ depend on the polarisation of the field, and can be found easily from the previous section. Thus we see that $\psi$ and its normal derivative have discontinuities across the layer, whose size depends only upon the geometry of the layer and the incident field $\psi_0$. Such a discontinuity in the normal derivative of the fields may be generated by a surface density of point sources on the midline of the layer. Similarly a discontinuity in the fields may be generated by a surface density of dipoles (whose dipole axes are normal to the layer). The properties of such surface distributions of point sources and dipoles are well known, as they are commonly encountered in the formulation of integral equations for scattering problems [32], where they are referred to as single and double layer potentials. The fields generated by such surface charge distributions are smooth (and outgoing) everywhere away from the surface.

The problem may instead be expressed in terms of distributions as

$$(\nabla^2 + 1)\psi_1 \;=\; a(s)\delta'(n) + b(s)\delta(n) \tag{5.60}$$

or alternatively the fields may be found by applying Helmholtz' integral on both sides of the layer. In any case, the field scattered by the layer is found to be

$$\psi_1 \;=\; \int a(s)\nabla_{\boldsymbol{x}} G(r).\mathbf{n} + b(s)G(r)ds, \tag{5.61}$$

where $\boldsymbol{x}$ is the point of observation, $\tilde{\boldsymbol{x}}(s)$ is the midline of the layer, parametrized by arc-length $s$, and $r = |\,\boldsymbol{x} - \tilde{\boldsymbol{x}}\,|$. The Green's function used here is the two-dimensional solution of

$$(\nabla^2 + 1)G(\boldsymbol{x}, \tilde{\boldsymbol{x}}) = \delta(\boldsymbol{x} - \tilde{\boldsymbol{x}}), \tag{5.62}$$

namely

$$G(\boldsymbol{x}, \tilde{\boldsymbol{x}}) = -\frac{i}{4}H_0^{(1)}(r). \tag{5.63}$$

## 5.5 Plane wave incidence on a thin dielectric layer

We now wish to find the asymptotic behaviour of this integral representation of the scattered field when a plane wave is incident upon the layer.

Returning to our original (outer) length scale we write $\tilde{\boldsymbol{x}} = k\tilde{\boldsymbol{x}}'$, $\boldsymbol{x} = k\boldsymbol{x}'$, $r = kr'$ and $s = ks'$, and subsequently omit the primes from these new variables. For an incident plane wave $\phi_0 = e^{ikx}$ we find that the transition conditions are of the form

$$a = \hat{a}(s)e^{ik\tilde{x}(s)}, \qquad b = \hat{b}(s)e^{ik\tilde{x}(s)}, \tag{5.64}$$

where $\hat{a}(s)$ and $\hat{b}(s)$ are functions which vary on the outer length scale. For observation points at an $\mathcal{O}(1)$ distance from the layer we find that

$$\psi^1 \;=\; -\frac{k^{\frac{1}{2}}}{2\sqrt{2\pi}}\int\left(i\hat{a}(s)\frac{(\boldsymbol{x}-\tilde{\boldsymbol{x}}).\tilde{\mathbf{n}}}{r} + \hat{b}(s)\right)\frac{e^{ikr+ik\tilde{x}(s)+\frac{\pi i}{4}}}{\sqrt{r}}ds, \tag{5.65}$$

where we have used the large argument expansions of the Hankel functions to approximate

$$G(kr) \sim -\frac{e^{ikr+\frac{\pi i}{4}}}{2\sqrt{2\pi kr}}, \qquad G'(kr) \sim -\frac{ie^{ikr+\frac{\pi i}{4}}}{2\sqrt{2\pi kr}}. \tag{5.66}$$

We first consider the case of plane wave incidence upon a layer which has small curvature on the length scale of the outer wavelength, so the curvature-dependent terms in the transition conditions may be ignored. This integral is of an appropriate form to apply the method of stationary phase, with phase $v = \tilde{x} + r$. The dominant contributions to the integral are from regions near those points at which $\frac{dv}{ds} = 0$, and in general these correspond to local minima[1] of $v$.

The stationary phase contributions are

$$\psi^1 \;\sim\; \frac{1}{2\sqrt{r}}\left(\hat{a}(s_0)\frac{(\boldsymbol{x}-\tilde{\boldsymbol{x}}(s_0)).\tilde{\mathbf{n}}(s_0)}{r} - i\hat{b}(s_0)\right)\frac{e^{ikr(s_0)+ik\tilde{x}(s_0)}}{\sqrt{r_{ss}(s_0)+\tilde{x}_{ss}(s_0)}} \tag{5.67}$$

[1] If this is not the case the reflected rays have passed through a caustic or focus.

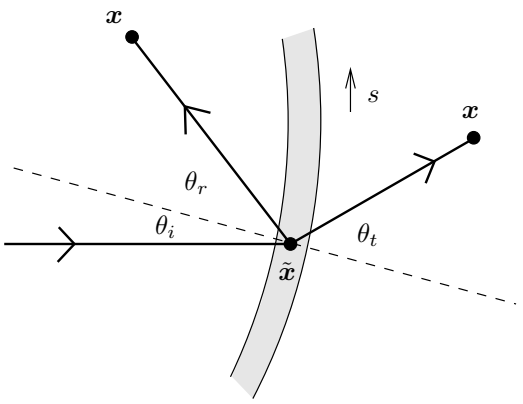


**Figure 5.7:** Reflection and transmission at a curved shell. The plane wave is incident from the left, and positive $\kappa$ corresponds to the layer being concave when viewed from that side. The angles $\theta_i$, $\theta_r$ and $\theta_t$ are defined such that they are positive when the direction of the incident plane wave (or the reflected/transmitted wave) makes an acute angle with the direction of increasing $s$ along the layer, as shown here.

to leading order. In order to evaluate this it is helpful to note that

$$r_s = -\frac{\tilde{\boldsymbol{x}}_s.(\boldsymbol{x}-\tilde{\boldsymbol{x}})}{r} \qquad r_{ss} = \frac{1}{r}\left(1+\kappa\tilde{\boldsymbol{n}}.(\boldsymbol{x}-\tilde{\boldsymbol{x}})-(r_s)^2\right) \tag{5.68}$$

with our current choice of sign for the curvature $\kappa(s)$, as shown in Figure 5.7, for which $\tilde{\boldsymbol{x}}_{ss} = -\kappa\tilde{\boldsymbol{n}}$, and positive $\kappa$ corresponds to the layer being concave when viewed from $L$. For points on the opposite side of the layer to the incident plane wave

$$r_s(s_0) = -\sin\theta_t, \qquad r_{ss}(s_0) = \kappa\cos\theta_t + \frac{\cos^2\theta_t}{r}, \qquad \frac{(\boldsymbol{x}-\tilde{\boldsymbol{x}}(s_0)).\tilde{\mathbf{n}}(s_0)}{r} = \cos\theta_t, \tag{5.69}$$

and on the same side

$$r_s(s_0) = -\sin\theta_r, \qquad r_{ss}(s_0) = -\kappa\cos\theta_r + \frac{\cos^2\theta_r}{r}, \qquad \frac{(\boldsymbol{x}-\tilde{\boldsymbol{x}}(s_0)).\tilde{\mathbf{n}}(s_0)}{r} = -\cos\theta_r, \tag{5.70}$$

where the angles $\theta_t$ and $\theta_r$ are shown in Figure 5.7 (and are defined for all points $\boldsymbol{x}(s)$). We also have that

$$\tilde{x}_s = \sin\theta_i, \qquad \tilde{x}_{ss} = \cos\theta_i\frac{d\theta_i}{ds} = -\kappa\cos\theta_i, \tag{5.71}$$

and so the integrand of (5.65) has stationary phase points where $\sin\theta_i = \sin\theta_r$, or $\sin\theta_i = \sin\theta_t$. The transmitted field is found to be

$$\psi^1 \sim \frac{1}{2}\left(\hat{a}(s_0) - \frac{i\hat{b}(s_0)}{\cos\theta_i}\right)e^{ikx}, \tag{5.72}$$

and the reflected field is

$$\psi^1 \sim -\frac{1}{2}\left(\hat{a}(s_0) + \frac{i\hat{b}(s_0)}{\cos\theta_i}\right)\left(\frac{\cos\theta_i}{\cos\theta_i - 2\kappa r}\right)^{\frac{1}{2}} e^{ik\tilde{x}(s_0)+ikr} \tag{5.73}$$

Now

$$\hat{a}(s) = -\pi i \cos\theta_i \qquad \hat{b}(s) = \pi \cos^2\theta_i + \frac{\pi}{2\hat{\mu}} \sin^2\theta_i \tag{5.74}$$

and so we find for the reflected field

$$\psi^1 \sim -\frac{\pi i}{4\hat{\mu}} \frac{\sin^2\theta_i}{\cos\theta_i} \left( \frac{\cos\theta_i}{\cos\theta_i - 2\kappa r} \right)^{\frac{1}{2}} e^{ik\tilde{x}(s_0)+ikr}, \tag{5.75}$$

and for the transmitted field

$$\psi^1 \sim \left( -\pi i \cos\theta_i - \frac{\pi i}{4\hat{\mu}} \frac{\sin^2\theta_i}{\cos\theta_i} \right) e^{ikx}, \tag{5.76}$$

which (when we account for the change of sign between $\phi$ and $\psi$ in $R$) agrees with the reflected and transmitted fields found using the plane wave reflection and transmission coefficients (5.101) and (5.102). This stationary phase analysis may be extended to an arbitrary incident field, provided that $\theta_i$ is slowly varying on the scale of the exterior wavelength, by use of the appropriate expression for $\frac{d\theta_i}{ds}$. It is also possible to apply this method to the three-dimensional problem, in a similar manner to that discussed in [108]. In this case the scattered fields are expressed in the form of an integral over a two-dimensional surface, and so the method of stationary phase for a two-dimensional integral [147] must be used.

## 5.6 Plane wave scattering from a tightly curved tip

We now consider the case of an infinite dielectric layer which has $\mathcal{O}(1)$ or smaller curvature (on the outer length scale) everywhere except in a "tip" region which is small in comparison to the free-space wavelength, but large compared to the wavelength within the dielectric material (and so the thickness of the layer). Within this region the direction of the midline of the layer changes by a finite amount, and so the curvature is large there.

As the curvature is large in this tip region we must use the boundary conditions (5.40) to (5.43), or (5.44) to (5.47), which include the effects of such curvature. These were found under the assumption that the layer has $\mathcal{O}(1)$ curvature on a wavelength scale. However, from the derivation of these conditions, we expect that they will be valid within our tip region (to leading order at least), provided that the radius of curvature is large compared with the wavelength within the dielectric material.

We proceed in the same manner as the previous section, and obtain expression (5.65) for $\psi^1$, but with the addition of the curvature-dependent terms from the transition con-

ditions. In the TE case we find that

$$\hat{a}(s) = -\pi i \cos\theta_i - \frac{\pi\kappa}{2k}, \tag{5.77}$$

$$\hat{b}(s) = \pi i \cos^2\theta_i + \frac{\pi}{2\hat{\mu}}\sin^2\theta_i + \frac{\pi\kappa i}{2k\hat{\mu}}\cos\theta_i - \frac{\pi\kappa i}{2k}\cos\theta_i + \frac{3\pi\kappa^2}{8\hat{\mu}k^2}, \tag{5.78}$$

where $\kappa(s)$ is the curvature of the midline of the layer on the outer length scale. The integral for the scattered field then becomes

$$\psi^1 \sim -\frac{k^{\frac{1}{2}}}{2\sqrt{2\pi}}\int\left(\left(\pi\cos\theta_i - \frac{\pi\kappa i}{2k}\right)\frac{(\boldsymbol{x}-\tilde{\boldsymbol{x}}).\tilde{\boldsymbol{n}}}{r} + \pi\cos^2\theta_i + \frac{\pi}{2\hat{\mu}}\sin^2\theta_i \right.$$
$$\left. + \frac{\pi\kappa i}{2k}\left(\frac{1}{\hat{\mu}} - 1\right)\cos\theta_i + \frac{3\pi\kappa^2}{8k^2\hat{\mu}}\right)\frac{e^{ikr+ik\tilde{x}+\frac{\pi i}{4}}}{\sqrt{r}}ds. \tag{5.79}$$

The tip region is $\mathcal{O}(k^{-1}\epsilon)$ in size, where $N^{-1} \ll \epsilon \ll 1$. In order for the change in direction to subtend a finite angle, $\kappa$ must be $\mathcal{O}(k\epsilon^{-1})$ in this region.

We may rewrite (5.79) as $\psi^1 \sim I_1 + I_2 + I_3$, where $I_1$ is the integral of that part of the integrand which is independent of $\kappa$, and where $I_2$ and $I_3$ are the integrals of those parts which are proportional to $\kappa$ and $\kappa^2$ respectively. We find that

$$I_1 = -\frac{k^{\frac{1}{2}}}{2\sqrt{2\pi}}\int\left(\pi\cos\theta_i\frac{(\boldsymbol{x}-\tilde{\boldsymbol{x}}).\tilde{\boldsymbol{n}}}{r} + \pi\cos^2\theta_i + \frac{\pi}{2\hat{\mu}}\sin^2\theta_i\right)\frac{e^{ikr+ik\tilde{x}+\frac{\pi i}{4}}}{\sqrt{r}}ds. \tag{5.80}$$

The contribution from the tip region to $I_1$ is $\mathcal{O}(k^{-\frac{1}{2}}\epsilon)$ and so small. The dominant contributions to the expansion of this integral consist of any stationary phase points (provided that these are at a distance from the tip which is much further than $k^{-\frac{1}{2}}$ from the tip) and as discussed in the previous sections these yield the reflected and transmitted fields. In addition there are (lower order) end point contributions from near the tip region. The variation of the amplitude of the integrand is sufficiently rapid in the tip region that these end point contributions are to leading order the same as would be found if the tip, rather than being tightly curved, was a wedge which subtended the same angle. Hence we find that

$$I_1 \sim \text{st.pts.} + \frac{e^{ik\rho-\frac{\pi i}{4}}}{2\sqrt{2\pi k\rho}}\left[\frac{\pi\cos\theta_i\cos(\theta+\theta_i) + \pi\cos^2\theta_i + \frac{\pi}{2\hat{\mu}}\sin^2\theta_i}{\sin\theta_i - \sin(\theta+\theta_i)}\right]_-^+ \tag{5.81}$$

where here st.pts. denotes the contributions from stationary points, $[]_-^+$ denotes the change in the quantity across the tip region (in the direction of increasing $s$), and $(\rho,\theta)$ are cylindrical polar coordinates centred on the tip, with $\theta = 0$ corresponding to the direction of propagation of the incident plane wave. If any stationary phase point is at an $\mathcal{O}(k^{-\frac{1}{2}})$ distance from the tip then this discontinuity modifies the stationary point contribution.

The contributions from both the end point and the stationary point may be expressed in terms of a Fresnel (or complementary error) function.

The integral containing terms proportional to the curvature of the layer is

$$I_2 = -\frac{k^{\frac{1}{2}}}{2\sqrt{2\pi}} \int \frac{\pi\kappa i}{2k} \left( -\frac{(\boldsymbol{x} - \tilde{\boldsymbol{x}}).\tilde{\boldsymbol{n}}}{r} + \left( \frac{1}{\hat{\mu}} - 1 \right) \cos\theta_i \right) \frac{e^{ikr + ik\tilde{x} + \frac{\pi i}{4}}}{\sqrt{r}} ds. \tag{5.82}$$

The integrand is large within the tip region, but small outside, because of the behaviour of the curvature function. In the tip region $e^{ikr+ik\tilde{x}} \sim e^{ik\rho}$, and using the fact that $\kappa(s) = \frac{d\theta_i}{ds}$ we find that

$$I_2 \sim \frac{e^{ik\rho - \frac{\pi i}{4}}\sqrt{\pi}}{4\sqrt{2k\rho}} \left[ \sin(\theta + \theta_i) - \left( \frac{1}{\hat{\mu}} - 1 \right) \sin\theta_i \right]_-^+. \tag{5.83}$$

The integral containing terms proportional to the square of the curvature of the layer is

$$I_3 = -\frac{k^{\frac{1}{2}}}{2\sqrt{2\pi}} \int \frac{3\pi\kappa^2}{8k^2\hat{\mu}} \frac{e^{ikr + ik\tilde{x} + \frac{\pi i}{4}}}{\sqrt{r}} ds. \tag{5.84}$$

Again, the dominant contribution to this integral is from the tip region, and expanding the phase gives

$$I_3 \sim -\frac{3\sqrt{\pi} e^{ik\rho + \frac{\pi i}{4}}}{16\sqrt{2\rho} k^{\frac{3}{2}} \hat{\mu}} \int_{-\infty}^{\infty} \kappa^2 \, ds. \tag{5.85}$$

Despite the $k^{-\frac{3}{2}}$ algebraic factor the contribution from this integral is in fact $\mathcal{O}(k^{-\frac{1}{2}}\epsilon^{-1})$ (as the tip region is of $\mathcal{O}(k^{-1}\epsilon)$ in length, and the curvature must be $\mathcal{O}(k\epsilon^{-1})$ in this region for the change in angle at the tip to be finite). Therefore the contribution to the fields diffracted by the tip from $I_3$ is slightly larger than the contributions from $I_1$ and $I_2$, which are $\mathcal{O}(k^{-\frac{1}{2}})$.

The result is somewhat unwieldy in this form, and so we rewrite the diffracted fields in terms of the coordinate system shown in Figure 5.8. The wedge subtends an angle $\alpha$, the angle of incidence is $\beta$, and $(\rho, \theta^*)$ is a polar coordinate system centred at the tip, but now with $\theta^* = 0$ corresponding to the axis of symmetry of the wedge. We then find that the tip diffracted field is approximately

$$\begin{aligned}
&- \frac{3\sqrt{\pi} e^{ik\rho + \frac{\pi i}{4}}}{16\sqrt{2\rho} k^{\frac{3}{2}} \hat{\mu}} \int_{-\infty}^{\infty} \kappa^2 \, ds \\
&\quad + \frac{e^{ik\rho - \frac{\pi i}{4}}}{2\sqrt{2\pi k\rho}} \left\{ \frac{\pi}{2\hat{\mu}} \left( \frac{\cos(\theta^* + \frac{\alpha}{2})\cos(\beta + \frac{\alpha}{2})}{\cos(\theta^* + \frac{\alpha}{2}) - \cos(\beta + \frac{\alpha}{2})} - \frac{\cos(\theta^* - \frac{\alpha}{2})\cos(\beta - \frac{\alpha}{2})}{\cos(\beta - \frac{\alpha}{2}) - \cos(\theta^* - \frac{\alpha}{2})} \right) \right. \\
&\qquad + \pi \left( \frac{\sin(\beta + \frac{\alpha}{2})\sin(\theta^* + \frac{\alpha}{2})}{\cos(\theta^* + \frac{\alpha}{2}) - \cos(\beta + \frac{\alpha}{2})} - \frac{\sin(\beta - \frac{\alpha}{2})\sin(\theta^* - \frac{\alpha}{2})}{\cos(\beta - \frac{\alpha}{2}) - \cos(\theta^* - \frac{\alpha}{2})} \right) \\
&\quad \left. + \frac{\pi}{2} \left( \frac{1 + \sin^2(\beta + \frac{\alpha}{2}) - \cos^2(\theta^* + \frac{\alpha}{2})}{\cos(\theta^* + \frac{\alpha}{2}) - \cos(\beta + \frac{\alpha}{2})} - \frac{1 + \sin^2(\beta - \frac{\alpha}{2}) - \cos^2(\theta^* - \frac{\alpha}{2})}{\cos(\beta - \frac{\alpha}{2}) - \cos(\theta^* - \frac{\alpha}{2})} \right) \right\}
\end{aligned} \tag{5.86}$$

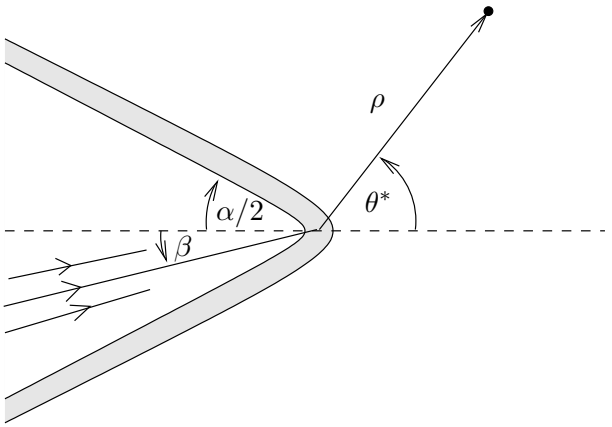


**Figure 5.8:** Coordinate system for tip diffracted field.

and this can be seen to satisfy reciprocity, as it is invariant under the transformation $\beta \to \pi + \theta^*$, $\theta^* \to \pi + \beta$. (This expression is found by substituting $\theta = \theta^* - \beta$, $\theta_i^- = \frac{\pi}{2} - \frac{\alpha}{2} + \beta$, $\theta_i^+ = \frac{\alpha}{2} - \frac{\pi}{2} + \beta$ into (5.81), (5.83) and (5.85)).

This approximation is valid when the radius of curvature in the tip region is small compared with the wavelength in free space, but large compared to the wavelength within the dielectric material (and so the thickness of the layer). As the radius of curvature decreases, the contribution from integral $I_3$ increases. When the radius of curvature is comparable with the internal wavelength, $\epsilon = N^{-1}$, and the contribution to $\psi_1$ from $I_3$ is $\mathcal{O}(k^{-\frac{1}{2}}N)$. We see that the asymptotic expansion for $\psi$ in inverse powers of $N$ has broken down at this point. The analysis for the approximate transition conditions also becomes invalid when the radius of curvature is comparable to the internal wavelength, as we can no longer assume that the external fields are slowly varying in the tangential direction on the scale of the internal wavelength. When the radius of curvature at the tip is comparable to the internal wavelength we must instead solve the full Maxwell equations in the vicinity of the tip, both inside and outside the dielectric material. Such an approach was employed in [2], where a boundary integral equation for the tip region was combined with a physical optics approximation away from the tip.

## 5.7 Tangential incidence upon thin layers

We now consider the problem of an externally incident plane wave impinging almost tangentially upon a half-wavelength dielectric layer with high refractive index. The analysis of Sections 5.5 and 5.6 breaks down near the point of tangency, and we instead find that we will have to consider a Fock region near the point of tangency, as in the case of an

impenetrable obstacle. This will initiate Airy layer modes, which propagate almost tangentially to the layer, and are similar to the creeping ray and whispering gallery modes on an impenetrable boundary.

We will first examine the modes which propagate along a dielectric layer, both in the flat and curved cases. We will find that, in the curved case, there are modes which propagate along the layer, and these are not simply perturbed versions of the flat layer modes. However, the leading-order transition conditions (5.24) and (5.27) do not support propagating modes. This suggests that our approximate transition conditions have become invalid for near-tangential incidence upon the layer. We will confirm this fact by examining the plane wave reflection and transmission coefficients for a planar slab. We will obtain suitable transition conditions in this case, and use them to find the Airy-layer type modes. In addition, we will use these modified transition conditions to find the solution within the Fock region. This solution will be matched with the outer geometrical optics fields, and we will obtain the launch coefficients for the Airy layer modes.

### 5.7.1 Propagating and leaky modes in thin layers

As is well known, waves may propagate along such a dielectric layer, guided by internal reflection at the interfaces – such a planar layer is also known as a symmetric dielectric slab waveguide [21].

Those modes which are totally internally reflected at the interfaces are known as guided modes. For a planar slab of constant thickness $\frac{d}{Nk}$ (on the outer length scale), and with the $x$-axis directed along the layer, a guided mode with $x$-dependence of the form $e^{ik\beta x}$ may propagate provided that

$$\tan\left(\sqrt{N^2-\beta^2}\frac{d}{N}\right) = \frac{2}{\frac{\sqrt{N^2-\beta^2}}{\hat{\mu}\sqrt{\beta^2-1}}-\frac{\hat{\mu}\sqrt{\beta^2-1}}{\sqrt{N^2-\beta^2}}}, \tag{5.87}$$

in the case of TE polarization (the modes for TM polarization satisfy the same condition, but with $\hat{\mu}$ replaced by $\hat{\epsilon}$). Such modes are either even or odd about the midline of the layer; the condition satisfied by even modes is

$$\tan\left(\sqrt{N^2-\beta^2}\frac{d}{2N}\right) = \frac{\hat{\mu}\sqrt{\beta^2-1}}{\sqrt{N^2-\beta^2}}, \tag{5.88}$$

and the condition for odd modes is

$$\tan\left(\sqrt{N^2-\beta^2}\frac{d}{2N}\right) = -\frac{\sqrt{N^2-\beta^2}}{\hat{\mu}\sqrt{\beta^2-1}}. \tag{5.89}$$

These equations must be solved numerically in general. For a layer with $d < \frac{\pi N}{\sqrt{N^2-1}}$ only the lowest-order even modes for each polarization may propagate. For large $N$, this lowest TE mode propagates with $\beta \sim N\hat{\beta}$, where $\hat{\beta}$ is the solution of

$$\tan\left(\sqrt{1-\hat{\beta}^2}\frac{d}{2}\right) = \frac{\hat{\mu}\hat{\beta}}{\sqrt{1-\hat{\beta}^2}}. \tag{5.90}$$

For TM polarization, as for the transition conditions we scale $\epsilon = N^2\hat{\epsilon}$. Then for $d < \pi$ the lowest-order even mode is given approximately by

$$\beta \sim 1 + \frac{\tan^2\left(\frac{d}{2}\right)}{2N^2\epsilon^{*2}}, \tag{5.91}$$

but when $d = \pi$

$$\beta \sim \left(\frac{4N}{\pi\epsilon^*}\right)^{\frac{1}{3}}. \tag{5.92}$$

There are also other modes, known as leaky modes, which correspond to waves which reflect at less than the critical angle within the layer. These are such that $\beta$ has a positive imaginary part, and so decay exponentially in the direction of propagation. In the region outside the layer they correspond to an outwards propagating wave. Such modes may be found by replacing $\sqrt{\beta^2-1}$ by $-i\sqrt{1-\beta^2}$ in the formulas listed above. We find that, for the range of parameters under consideration, these leaky modes have rapid decay.

We will find that the leaky modes modes play little part in the problem of tangential incidence. These modes decay sufficiently rapidly that they do not affect the solution (and are accounted for by the approximate transition conditions). The propagating modes decay slowly, but consist of plane waves which are totally internally reflected at the internal interfaces, and so cannot be set up by an externally incident real ray (although they may be initiated by a complex ray). As $\beta \gg 1$ for large $N$ our steepest descent contours, for the analysis of the Fock region near the point of tangency, will not encounter the poles related to these propagating modes, and so they are not initiated.

### 5.7.2 Propagating and surface modes for cylindrical layers

We now wish to consider modes which propagate in or near a curved dielectric layer. Along with the guided modes considered above we expect there to be modes which propagate almost tangentially to the layer. These do not decay exponentially away from the layer, but are instead guided above or below the layer in a similar manner to creeping or whispering gallery modes on an impenetrable boundary.

We consider the two-dimensional problem in a circular cylindrical geometry, with a dielectric layer of thickness $\frac{d}{Nk}$, and midline $r = 1$ (both on an outer length-scale). Following [149], and motivated by the separable solutions of this problem, we seek solutions for TE polarization of the form

$$\phi = \begin{cases} C_1 J_\beta(kr)e^{i\beta\theta} & 0 < r < 1 - \frac{d}{2Nk} \\ A_2 H_\beta^{(1)}(Nkr)e^{i\beta\theta} + B_2 H_\beta^{(2)}(Nkr)e^{i\beta\theta} & 1 - \frac{d}{2Nk} < r < 1 + \frac{d}{2Nk} \\ A_3 H_\beta^{(1)}(kr)e^{i\beta\theta} & r > 1 + \frac{d}{2Nk} \end{cases}, \tag{5.93}$$

where $\beta$ is a possibly-complex constant. The solution in $r > 1 + \frac{d}{2Nk}$ is outgoing as $r \to \infty$, and we have chosen the separable solution in $r < 1 - \frac{d}{2Nk}$ which is bounded as $r \to 0$. For real $\beta$, with $\beta < k$, this solution in $r < 1 - \frac{d}{2Nk}$ consists of cylindrically incoming and outgoing waves, with caustic at $r = \frac{\beta}{k}$.

Continuity of the tangential field components at the interface yields the four linear equations

$$C_1 J_\beta\left(k - \frac{d}{2N}\right) = A_2 H_\beta^{(1)}\left(Nk - \frac{d}{2}\right) + B_2 H_\beta^{(2)}\left(Nk - \frac{d}{2}\right), \tag{5.94}$$

$$C_1 J_\beta'\left(k - \frac{d}{2N}\right) = \frac{N}{\hat{\mu}}\left(A_2 H_\beta^{(1)\prime}\left(Nk - \frac{d}{2}\right) + B_2 H_\beta^{(2)\prime}\left(Nk - \frac{d}{2}\right)\right), \tag{5.95}$$

$$A_3 H_\beta^{(1)}\left(k + \frac{d}{2N}\right) = A_2 H_\beta^{(1)}\left(Nk + \frac{d}{2}\right) + B_2 H_\beta^{(2)}\left(Nk + \frac{d}{2}\right), \tag{5.96}$$

$$A_3 H_\beta^{(1)\prime}\left(k + \frac{d}{2N}\right) = \frac{N}{\hat{\mu}}\left(A_2 H_\beta^{(1)\prime}\left(Nk + \frac{d}{2}\right) + B_2 H_\beta^{(2)\prime}\left(Nk + \frac{d}{2}\right)\right), \tag{5.97}$$

for $C_1$, $A_2$, $B_2$ and $C_3$, and the permissible values of $\beta$ are determined by the condition that the determinant of this system vanishes. The zero lines of the real and imaginary parts of this determinant are plotted in Figure 5.9.

In Figure 5.9 the lines on which both the real and imaginary parts of the determinant of the system (5.94) - (5.97) vanish are plotted in the complex $\hat{\beta} = \beta/k$ plane. The determinant of the system vanishes at the intersection of these lines, at which points non-trivial solutions of the system of equations, and so propagating modes, may be found. Three types of such solutions are found: the "whispering gallery" modes near the real axis, the "creeping ray" modes near the line $\arg(\hat{\beta} - 1) = \frac{\pi}{3}$, and also the internally propagating mode of the slab. The internally propagating mode is given approximately by (5.90), but with a small and positive imaginary part (for the two plots with $N = 3$ and $N = 20$ this solution lies outside the region shown). The other poles can be seen to move away from the real axis, or the line $\arg(\hat{\beta} - 1) = \frac{\pi}{3}$, as $N$ increases (from (5.144) and (5.142) it is found that initially this movement is proportional to $\log N$). We expect

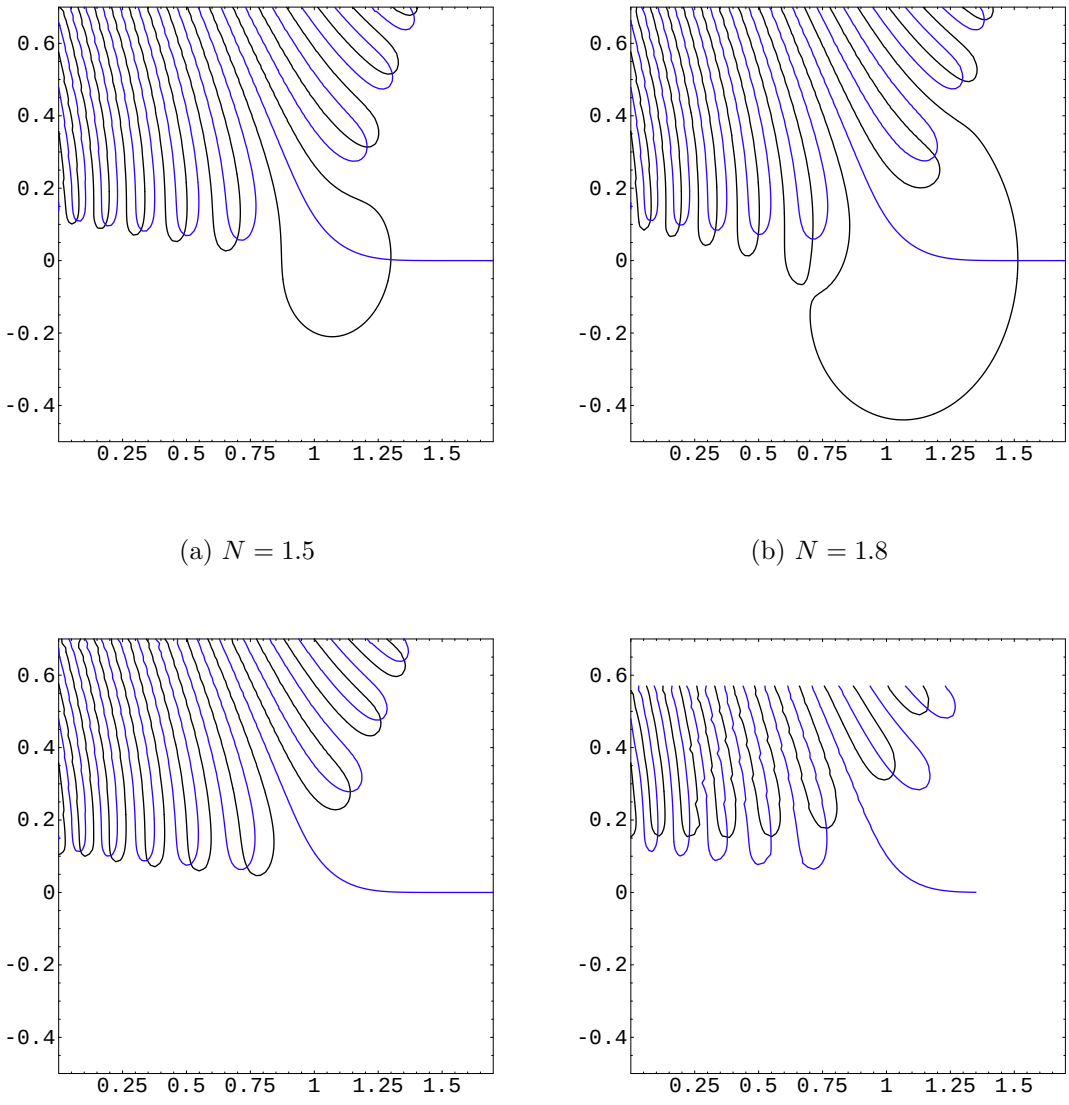


(a) $N = 1.5$ (b) $N = 1.8$

(c) $N = 3.0$ (d) $N = 20.0$

**Figure 5.9:** Propagating and surface modes for a cylindrical layer in the TE polarization case. The black lines are the lines in the complex $\hat{\beta} = \beta/k$ plane on which the real part of the determinant of (5.94) - (5.97) vanishes, and the blue lines are the zero lines for the imaginary part. Propagating modes may be found when $\hat{\beta}$ is at one of the intersections between these two systems of lines. For all of these plots $k = 16$, $d = \pi$ and $\hat{\mu} = 1$, and $N$ varies as indicated above. (The region of computation is slightly restricted in the $N = 20$ case because of numerical accuracy).

that those modes for which $\hat{\beta} - 1 = \mathcal{O}(k^{-\frac{1}{3}})$ may be initiated by tangential incidence, and so $N$ must not be overly large, otherwise there will be no solutions in this region.

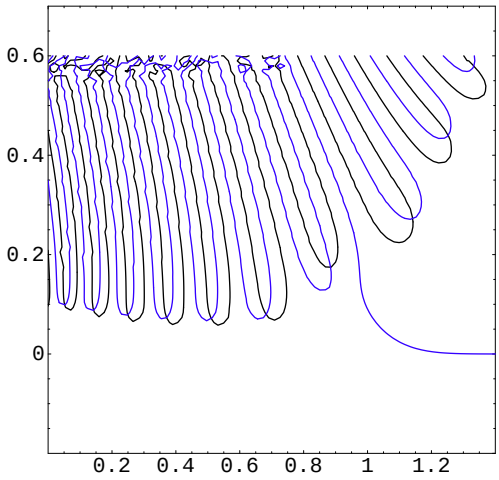


**Figure 5.10:** Propagating and surface modes for a cylindrical layer in the TM polarization case. The plot is as for Figure 5.9, but with $N = 3.0$ and $k = 20$.

### 5.7.3 Comparison between approximate and exact reflection and transmission coefficients

We now compare the reflection and transmission coefficients for plane-wave incidence upon a planar layer obtained both by consideration of the exact problem and by using the approximate transition conditions. This allows us to examine the accuracy of the approximations; in particular we are interested in the validity of these approximations for near-tangential incidence.

By considering plane wave propagation in each material, along with the continuity conditions, the reflection and transmission coefficients for a planar layer of thickness $d/N$ (which corresponds to $d/(Nk)$ on the outer length scale) are found to be

$$R = \frac{(\lambda^2-1)(e^{i\alpha}-e^{-i\alpha})e^{-\frac{id}{N}\cos\theta}}{-(\lambda^2+1)(e^{i\alpha}-e^{-i\alpha})+2\lambda(e^{i\alpha}+e^{-i\alpha})}, \tag{5.98}$$

$$T = \frac{4\lambda e^{-\frac{id}{N}\cos\theta}}{-(\lambda^2+1)(e^{i\alpha}-e^{-i\alpha})+2\lambda(e^{i\alpha}+e^{-i\alpha})}, \tag{5.99}$$

for transverse electric polarization, where

$$\alpha = \frac{d}{N}\sqrt{N^2-\sin^2\theta}, \qquad \lambda = \frac{\sqrt{N^2-\sin^2\theta}}{\hat{\mu}\cos\theta}. \tag{5.100}$$

The reflection and transmission coefficients[2] for transverse magnetic polarization are

[2]The reflection coefficients so obtained are for the amplitude of the magnetic field, as this is the scalar quantity under consideration; in other situations it is customary to write the reflection coefficients in the TM case in terms of the amplitude of the electric field. As the region to either side of the layer is free space this simply results in a change of sign for the reflection coefficient

found by replacing $\hat{\mu}$ by $\hat{\epsilon} = N^2\epsilon^*$ in (5.98) and (5.99). For both polarizations we consider the reflected and transmitted waves as emanating from the midline of the layer.

When we use the approximate boundary conditions (5.26) and (5.30) to find the $\mathcal{O}(N^{-1})$ scattered fields we find that

$$R \sim -\frac{\pi i}{4N\hat{\mu}}\frac{\sin^2\theta}{\cos\theta}, \tag{5.101}$$

$$T \sim -1 + \frac{\pi i\cos\theta}{N} + \frac{\pi i}{4N\hat{\mu}}\frac{\sin^2\theta}{\cos\theta}, \tag{5.102}$$

for transverse electric polarization, and using (5.37) and (5.38) we obtain

$$R \sim \frac{\pi\epsilon^* i}{4N}\cos\theta\sin^2\theta, \tag{5.103}$$

$$T \sim -1 + \frac{\pi i}{N}\cos\theta + \frac{\pi\epsilon^* i}{4N}\cos\theta\sin^2\theta, \tag{5.104}$$

for transverse magnetic polarization. We may manipulate the expressions for the boundary conditions to give

$$\phi^L + \phi^R = \frac{\pi}{2N}\left(\frac{\partial\phi^L}{\partial n} - \frac{\partial\phi^R}{\partial n}\right) + \mathcal{O}(N^{-2}), \tag{5.105}$$

$$\frac{\partial\phi^L}{\partial n} + \frac{\partial\phi^R}{\partial n} = \frac{\pi}{2N}\left(\frac{\partial^2\phi^L}{\partial n^2} - \frac{\partial^2\phi^R}{\partial n^2}\right) + \frac{\pi}{4\hat{\mu}N}\left(\frac{\partial^2\phi^L}{\partial s^2} - \frac{\partial^2\phi^R}{\partial s^2}\right) + \mathcal{O}(N^{-2}), \tag{5.106}$$

where we have taken care to ensure that the resulting boundary conditions are unchanged when $L$ is exchanged with $R$, and the direction of the normal reversed. Using these we obtain the reflection and transmission conditions

$$R = -\frac{1 - \frac{\pi i\cos\theta}{2N}}{2\left(1 + \frac{\pi i\cos\theta}{2N}\right)} + \frac{1 - \frac{\pi i\cos\theta}{2N} - \frac{\pi i\sin^2\theta}{4\hat{\mu}N\cos\theta}}{2\left(1 + \frac{\pi i\cos\theta}{2N} + \frac{\pi i\sin^2\theta}{4\hat{\mu}N\cos\theta}\right)}, \tag{5.107}$$

$$T = -\frac{1 - \frac{\pi i\cos\theta}{2N}}{1 + \frac{\pi i\cos\theta}{2N}} - R. \tag{5.108}$$

For the TM case we similarly have

$$\phi^L + \phi^R = \frac{\pi}{2N}\left(\frac{\partial\phi^L}{\partial n} - \frac{\partial\phi^R}{\partial n}\right) - \frac{\pi\epsilon^*}{4N}\frac{\partial^2}{\partial s^2}\left(\frac{\partial\phi^L}{\partial n} - \frac{\partial\phi^R}{\partial n}\right) + \mathcal{O}(N^{-2}), \tag{5.109}$$

$$\frac{\partial\phi^L}{\partial n} + \frac{\partial\phi^R}{\partial n} = \frac{\pi}{2N}\left(\frac{\partial^2\phi^L}{\partial n^2} - \frac{\partial^2\phi^R}{\partial n^2}\right) + \mathcal{O}(N^{-2}), \tag{5.110}$$

and these give reflection and transmission coefficients

$$R = \frac{1 - \frac{\pi i\cos\theta}{2N}}{2\left(1 + \frac{\pi i\cos\theta}{2N}\right)} - \frac{1 - \frac{\pi i\cos\theta}{2N} - \frac{\pi\epsilon^* i}{4N}\sin^2\theta\cos\theta}{2\left(1 + \frac{\pi i\cos\theta}{2N} + \frac{\pi\epsilon^* i}{4N}\sin^2\theta\cos\theta\right)}, \tag{5.111}$$

$$T = -\frac{1 - \frac{\pi i\cos\theta}{2N}}{1 + \frac{\pi i\cos\theta}{2N}} + R. \tag{5.112}$$

We compare the argument and phase of the reflection and transmission coefficients obtained from these approximate conditions with the exact results in Figures 5.11 and 5.12. There we can see that for moderately large $N$ the approximate boundary conditions give reasonable approximations to $R$ and $T$ for near-normal incidence, but the accuracy of the approximations becomes worse as the angle of incidence increases, and they are poor near tangency.

It should be noted that some of the plots in Figure 5.11 are somewhat misleading as to the accuracy of the approximations (5.101) and (5.103), as the phase of the reflection coefficient is constant and the amplitude of the transmission coefficient is greater than unity. For the phase of reflection coefficient we see that the leading-order approximation is pure imaginary; the $\mathcal{O}(N^{-2})$ correction is found to be real, and so results in the phase being non-constant. The approximation of the transmission coefficient is somewhat inconsistent, as the $\mathcal{O}(N^{-2})$ correction is in fact real. As the imaginary part of (5.104) supplies an $\mathcal{O}(N^{-2})$ contribution to the magnitude of the transmission coefficient, to be consistent to $\mathcal{O}(N^{-1})$ we must approximate the transmission coefficient as $-1$. The leading-order approximations supply adequate approximations to the fields themselves, but if this behaviour for the reflection and transmission coefficients is unacceptable we must proceed to higher order. In the TE case, using the transition conditions (5.31) and (5.32) for the $\mathcal{O}(N^{-2})$ fields we obtain the reflection and transmission coefficients

$$R \sim -\frac{\pi i}{4N\hat{\mu}}\frac{\sin^2\theta}{\cos\theta} - \frac{\pi^2\sin^2\theta}{4N^2\hat{\mu}} - \frac{\pi^2\sin^4\theta}{16N^2\hat{\mu}^2\cos^2\theta}, \tag{5.113}$$

$$T \sim -1 + \frac{\pi i\cos\theta}{N} + \frac{\pi i}{4N\hat{\mu}}\frac{\sin^2\theta}{\cos\theta} + \frac{\pi^2\cos^2\theta}{2N^2} + \frac{\pi^2\sin^2\theta}{4N^2\hat{\mu}} + \frac{\pi^2\sin^4\theta}{16N^2\hat{\mu}^2\cos^2\theta}, \tag{5.114}$$

which are accurate to $\mathcal{O}(N^{-2})$.

### 5.7.4 Approximate boundary conditions near tangency

As noted above, the approximations (5.101), (5.102), and (5.103), (5.104), to the transmission and reflection coefficients appear not to be valid near tangency, and this suggests that the approximate boundary conditions (in the form derived in Section 5.4.2, and so expanded in powers of $N^{-1}$) must break down for angles of incidence in this region. By comparing the expansions for large $N$ of the exact and approximate coefficients it is found that they do not agree when $\frac{\pi}{2} - \theta = \mathcal{O}(N^{-1})$, for when this is the case $\frac{\sin^2\theta}{N\cos\theta}$ is no longer small. For such angles of incidence $\frac{\partial\phi}{\partial n} = \mathcal{O}(N^{-1})$, and so the analysis of Section 5.4.2 must be modified. In the TE case we find that the reflection and transition coefficients (5.107), (5.108), obtained from the combined transition conditions (5.105) and (5.106),

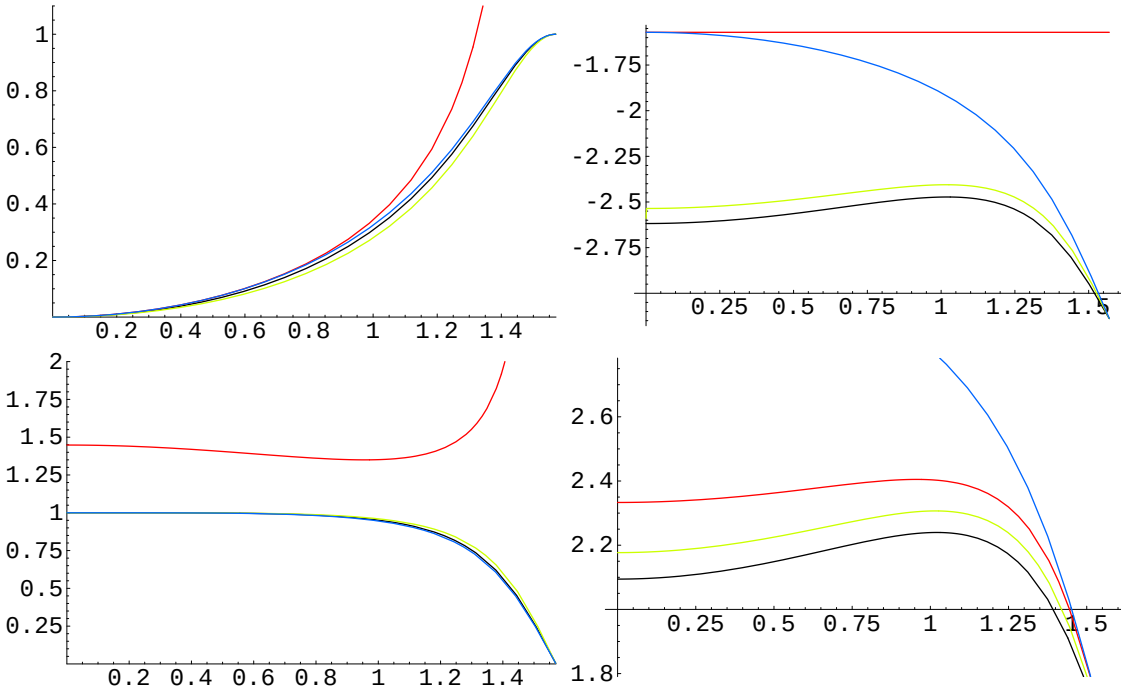


**Figure 5.11:** Comparison between exact and approximate reflection and transmission coefficients for TE polarization. The upper left and upper right plots compare the magnitude and phase against angle of incidence (in radians) for the reflection coefficients, and the lower plots are for the transmission coefficients. In each case the black line is the exact value from (5.98) or (5.99), the red line is the value (5.101) or (5.102) from the expanded approximate transition conditions, the yellow line is the value (5.107) or (5.108) from the combined transition conditions, and the blue line is (5.117) from the approximate transition conditions valid near tangency. These values are calculated with $N = 3$ and $\hat{\mu} = 1$.

are valid even near tangency. We therefore expect suitable leading-order transition conditions to consist of those terms in the combined transition conditions which are not small for such angles of incidence.

By a similar analysis to that in Section 5.4.2, but now noting that $\frac{\partial \phi}{\partial n} = \mathcal{O}(N^{-1})$, we obtain the transition conditions

$$\phi^L + \phi^R = \mathcal{O}(N^{-2}), \tag{5.115}$$

$$\frac{\partial \phi^L}{\partial n} + \frac{\partial \phi^R}{\partial n} = \frac{\pi}{2\hat{\mu}N}\frac{\partial^2 \phi^L}{\partial s^2} + \mathcal{O}(N^{-2}), \tag{5.116}$$

and these give reflection and transmission coefficients

$$R = -\frac{\frac{\pi i \sin^2\theta}{4\hat{\mu}N\cos\theta}}{1 + \frac{\pi i \sin^2\theta}{4\hat{\mu}N\cos\theta}}, \qquad T = -\frac{1}{1 + \frac{\pi i \sin^2\theta}{4\hat{\mu}N\cos\theta}}. \tag{5.117}$$

For TM polarization the situation is slightly different, as the reflection coefficient

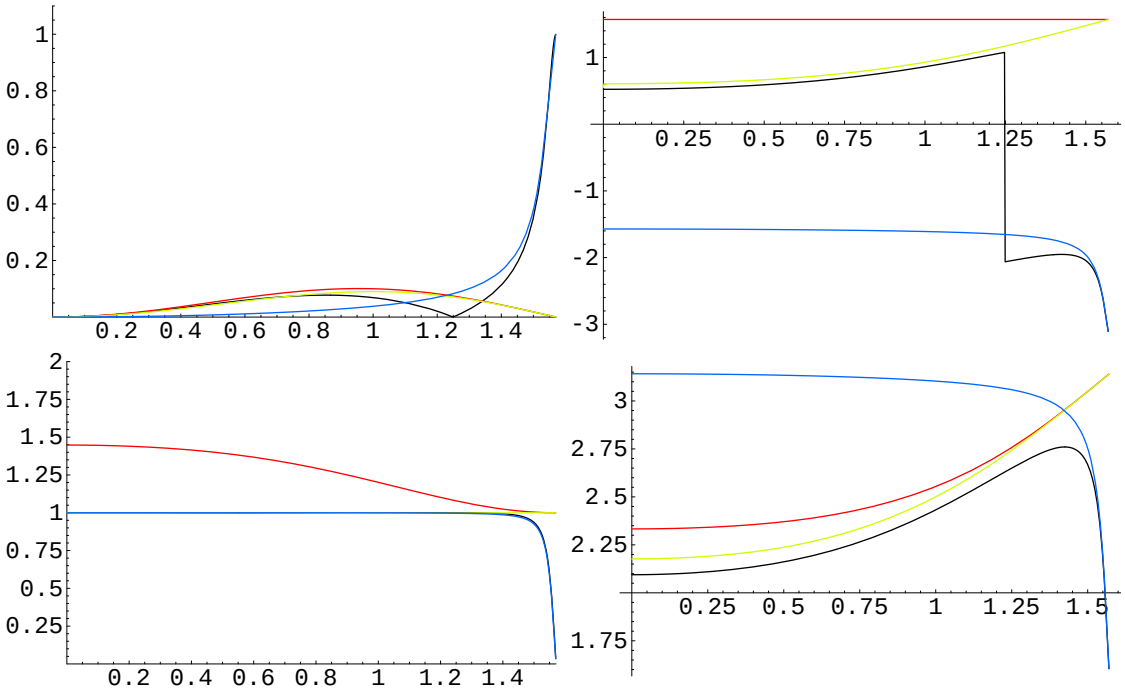


**Figure 5.12:** As for Figure 5.11 except for TM polarization, again with $N = 3$, $\hat{\epsilon} = N^2$ and $\hat{\mu} = 1$.

is small even compared to $N^{-1}$ when $N^{-2} \ll \frac{\pi}{2} - \theta \ll 1$, and becomes $\mathcal{O}(1)$ when $\frac{\pi}{2} - \theta = \mathcal{O}(N^{-3})$. This behaviour is related to the small reflectivity at the first interface near the Brewster angle ($\tan\theta = \frac{N}{\hat{\mu}}\sqrt{\frac{N^2-\hat{\mu}^2}{N^2-1}}$). When $\frac{\pi}{2} - \theta = \mathcal{O}(N^{-3})$ we obtain the same boundary conditions as for TE polarization, but with $\hat{\mu}$ replaced by $N^2\epsilon^*$.

### 5.7.5 Airy layer fields

We now wish to consider modes which propagate almost tangentially to the boundary, in a similar manner to creeping waves and whispering gallery modes on a perfectly conducting or impedance surface. These solutions will be somewhat similar to tangentially propagating modes upon the interface between two dielectric materials with refractive indices which differ by an $\mathcal{O}(k^{-\frac{1}{3}})$ amount, as studied in [5].

We expect that these Airy layer modes will correspond to waves propagating in a direction for which $\frac{\pi}{2} - \theta = \mathcal{O}(k^{-\frac{1}{3}})$, and the distinguished limit occurs when both $R$ and $1 - T$ are $\mathcal{O}(1)$ quantities for angles of incidence in this region. This corresponds to a refractive index $N = \mathcal{O}(k^{\frac{1}{3}})$ for TE polarization, and $N = \mathcal{O}(k^{\frac{1}{9}})$ for TM polarization. Thus in the subsequent analysis of tangential incidence and tangentially propagating fields we will scale $N = k^{\frac{1}{3}}\hat{N}$ or $N = k^{\frac{1}{9}}\hat{N}$ depending upon the polarization, and then obtain the same problems in either case.

By comparison with the perfectly conducting and impedance cases we introduce the scaling

$$n = k^{-\frac{2}{3}}\hat{n}, \tag{5.118}$$

for the normal coordinate, and seek a solution of the form

$$\phi = A(s,\hat{n})e^{iks+ik^{\frac{1}{3}}v(s)}. \tag{5.119}$$

The transition conditions then become

$$\begin{aligned} A(s,0+) + A(s,0-) &= 0, & (5.120)\\ \frac{\partial A}{\partial \hat{n}}(s,0+) + \frac{\partial A}{\partial \hat{n}}(s,0-) &= -\frac{\pi}{2\hat{\mu}\hat{N}}A(s,0-), & (5.121) \end{aligned}$$

(for both the leading-order term and the first-order correction).

We pose an asymptotic expansion for the amplitude

$$A \sim A_0(s,\hat{n}) + k^{-\frac{1}{3}}A_1(s,\hat{n}) + \ldots, \tag{5.122}$$

and Helmholtz' equations in $s$–$n$ coordinates become

$$\begin{aligned} \frac{\partial^2 A_0}{\partial \hat{n}^2} - 2v'(s)A_0 + 2\hat{n}\kappa(s)A_0 &= 0, & (5.123)\\ \frac{\partial^2 A_1}{\partial \hat{n}^2} - 2v'(s)A_1 + 2\hat{n}\kappa(s)A_1 &= -2i\frac{\partial A_0}{\partial s}, & (5.124) \end{aligned}$$

where both $A_0$ and $A_1$ satisfy the transition conditions above. We also require that these solutions match into an outgoing field as $\hat{n} \to \infty$, and are bounded as $\hat{n} \to -\infty$. Following [121] we introduce the new variable

$$\eta = \kappa(s)^{-\frac{2}{3}}(\kappa\hat{n} - v'), \tag{5.125}$$

and the equations become

$$\begin{aligned} \frac{\partial^2 A_0}{\partial \eta^2} + 2\eta A_0 &= 0, & (5.126)\\ \frac{\partial^2 A_1}{\partial \eta^2} + 2\eta A_1 &= -\frac{2i}{\kappa^{\frac{2}{3}}}\left(\frac{\partial A_0}{\partial s} + \left(\frac{1}{3}\frac{\kappa'}{\kappa}\eta + \frac{2}{3}\frac{\kappa'}{\kappa^{\frac{5}{3}}}\frac{dv}{ds} - \frac{1}{\kappa^{\frac{2}{3}}}\frac{d^2v}{ds^2}\right)\frac{\partial A_0}{\partial \eta}\right). & (5.127) \end{aligned}$$

Using the matching conditions at infinity we see that the leading-order solution is of the form

$$A_0 = \begin{cases} \alpha(s)\mathrm{Ai}(-2^{\frac{1}{3}}e^{\frac{2\pi i}{3}}\eta) & \eta > -\kappa^{-\frac{2}{3}}(s)v'(s) \\ \beta(s)\mathrm{Ai}(-2^{\frac{1}{3}}\eta) & \eta < -\kappa^{-\frac{2}{3}}(s)v'(s) \end{cases}, \tag{5.128}$$

and to satisfy the transition conditions we demand that

$$\begin{aligned} u_1(\eta_0)\alpha(s) + u_0(\eta_0)\beta(s) &= 0, & (5.129)\\ u_1'(\eta_0)\alpha(s) + (u_0'(\eta_0) + lu_0(\eta_0))\beta(s) &= 0, & (5.130)\end{aligned}$$

where

$$\begin{aligned} \eta_0(s) = -\kappa^{-\frac{2}{3}}(s)v'(s), \qquad l(s) = \frac{\pi}{2\kappa^{\frac{1}{3}}(s)\hat{\mu}\hat{N}},\\ u_1(\eta) = \mathrm{Ai}(-2^{\frac{1}{3}}e^{\frac{2\pi i}{3}}\eta), \qquad u_0(\eta) = \mathrm{Ai}(-2^{\frac{1}{3}}\eta). \end{aligned} \tag{5.131}$$

This system of linear equations for $\alpha(s)$, $\beta(s)$ has a solution provided that

$$W[u_1, u_0](\eta_0) + lu_0u_1 = 0, \tag{5.132}$$

where $W$ denotes the Wronskian of the two functions. Explicitly this condition is

$$\begin{aligned} 0 &= \frac{e^{-\frac{\pi i}{6}}}{2^{\frac{2}{3}}\pi} + \frac{\pi}{2\kappa^{\frac{1}{3}}(s)\hat{\mu}\hat{N}}\mathrm{Ai}(-2^{\frac{1}{3}}\eta_0(s))\mathrm{Ai}(-2^{\frac{1}{3}}e^{\frac{2\pi i}{3}}\eta_0(s))\\ &= \frac{e^{-\frac{\pi i}{6}}}{2^{\frac{2}{3}}\pi} + \frac{\pi}{2\kappa^{\frac{1}{3}}(s)\hat{\mu}\hat{N}}\mathrm{Ai}(2^{\frac{1}{3}}\kappa^{-\frac{2}{3}}(s)v'(s))\mathrm{Ai}(2^{\frac{1}{3}}e^{\frac{2\pi i}{3}}\kappa^{-\frac{2}{3}}(s)v'(s)), \end{aligned} \tag{5.133}$$

and this gives a relationship between the curvature of the layer $\kappa(s)$ and the correction to the phase $v'(s)$ (or equivalently $\eta_0(s)$). Unlike the perfectly conducting case it is not possible to find an explicit expression for the roots of (5.133), and the distribution of these will be discussed later.

From (5.129) it may be seen that

$$A_0 = \begin{cases} a(s)\mathrm{Ai}(-2^{\frac{1}{3}}\eta_0(s))\mathrm{Ai}(-2^{\frac{1}{3}}e^{\frac{2\pi i}{3}}\eta) & \eta > \eta_0(s)\\ -a(s)\mathrm{Ai}(-2^{\frac{1}{3}}e^{\frac{2\pi i}{3}}\eta_0(s))\mathrm{Ai}(-2^{\frac{1}{3}}\eta) & \eta < \eta_0(s) \end{cases}, \tag{5.134}$$

where the amplitude $a(s)$ is currently unknown. As in the perfectly conducting case we must consider the solvability condition for the first-order correction equation to find the behaviour of $a(s)$. The solution to the adjoint of the leading-order problem is just $\bar{A}_0$. However we cannot apply the Fredholm alternative immediately as the inhomogeneous term on the right hand side of (5.127) is not integrable because of the $\eta\frac{\partial A_0}{\partial \eta}$ term. By direct calculation it is possible to see that $\frac{1}{4}\eta^2 A_0$ satisfies

$$\left(\frac{\partial^2}{\partial\eta^2} + 2\eta\right)\frac{1}{4}\eta^2 A_0 = \eta\frac{\partial A_0}{\partial\eta} + \frac{1}{2}A_0. \tag{5.135}$$

Subtracting this from the left hand side we are now left with a suitably well behaved function[3]. The solvability condition then becomes

$$\int_{-\infty}^{\infty} A_0 \left( \frac{\partial A_0}{\partial s} - \frac{1}{6}\frac{\kappa'}{\kappa} A_0 + \left( \frac{\kappa'}{\kappa^{\frac{5}{3}}}\frac{dv}{ds} - \frac{1}{\kappa^{\frac{2}{3}}}\frac{d^2v}{ds^2} \right) \frac{\partial A_0}{\partial \eta} \right) d\eta \;\; = \;\; 0. \tag{5.136}$$

Since

$$\int_{-\infty}^{\infty} A_0 \frac{\partial A_0}{\partial \eta} d\eta = 0 \tag{5.137}$$

this simplifies to

$$\frac{1}{2}\frac{d}{ds}\left( \int_{-\infty}^{\infty} A_0^2 d\eta \right) - \frac{1}{6}\frac{\kappa'}{\kappa} \int_{-\infty}^{\infty} A_0^2 d\eta \;\; = \;\; 0, \tag{5.138}$$

with solution

$$\kappa^{-\frac{1}{6}} \left( \int_{-\infty}^{\infty} A_0^2 d\eta \right)^{\frac{1}{2}} \;\; = \;\; \text{const.} \tag{5.139}$$

The integral of $A_0^2$ does not only depend on $s$ through $a(s)$, but also varies with $\eta_0(s)$. The integrals of $A_0^2$ may be calculated explicitly[4], and using the propagation relation (5.133) and the Wronskian of the Airy functions we have that

$$a(s) \;\; = \;\; a_0 \kappa^{\frac{1}{6}}(s) \left( 1 + \frac{2^{\frac{7}{3}} e^{\frac{2\pi i}{3}} \kappa^{\frac{1}{3}}(s) \hat{\mu}\hat{N}}{\pi} \frac{\mathrm{Ai}'(-2^{\frac{1}{3}} e^{\frac{2\pi i}{3}} \eta_0(s))}{\mathrm{Ai}(-2^{\frac{1}{3}} e^{\frac{2\pi i}{3}} \eta_0(s))} \right)^{-\frac{1}{2}}. \tag{5.140}$$

The constant $a_0$ is not determined at this point, but may be found by matching this solution with the fields in the local region within which the Airy layer modes are initiated; in the current case this is the Fock-Leontovich region near the point of tangency.

### 5.7.6 Location of solutions of the propagation relation

The behaviour of the perturbation to the phase $v(s)$, and so the rate of exponential decay of the Airy layer solutions, is given by equation (5.133). We expect there to be countably many roots, and these will lie in the sector $\frac{\pi}{3} < \arg v'(s) < \pi$, or equivalently $-\frac{2\pi}{3} < \arg \eta_0 < 0$. (It is preferable to express these results in terms of $\eta_0$, as the locations of the solutions for $\eta_0$ are exactly the same as the poles of the integrand for the Fock region solution (5.164)).

[3] Its improper integral exists, at least.

[4] Integration by parts gives

$$\int \mathrm{Ai}^2(ax)dx = x\mathrm{Ai}^2(ax) - \frac{1}{a}\left(\mathrm{Ai}'(ax)\right)^2$$

For the solutions with large modulus we may replace the Airy functions by their asymptotic expansions for large argument, and use these to find approximations for the locations of the poles. Equation (5.133) for $\eta_0$ in the above-mentioned sector of the complex plane is then approximately

$$0 = 1 + \frac{l}{2^{\frac{3}{2}}\eta_0^{\frac{1}{2}}}\left(e^{\frac{4i\sqrt{2}}{3}\eta_0^{\frac{3}{2}}} + i\right), \tag{5.141}$$

which has solutions near (but not on) the anti-Stokes lines $\arg\eta_0 = 0, -\frac{2\pi}{3}$. The series of poles near the real axis have locations given by the solution of

$$\eta_0 \sim x_m - \frac{i}{2\sqrt{2x_m}}\log\left(\frac{2^{\frac{3}{2}}\sqrt{x_m}}{l}\right) \tag{5.142}$$

to leading order, $m$ is a large positive integer, and

$$x_m \sim \left(\frac{3\pi}{4\sqrt{2}}(2m+1)\right)^{\frac{2}{3}}. \tag{5.143}$$

The set of poles near the line $\arg\ \eta_0 = -\frac{2\pi}{3}$ satisfy the same equation, and their locations are given by

$$\eta_0 \sim x_m e^{-\frac{2\pi i}{3}} + \frac{e^{-\frac{\pi i}{6}}}{2\sqrt{2x_m}}\log\left(\frac{2^{\frac{3}{2}}\sqrt{x_m}}{l}\right), \quad x_m = \left(\frac{3\pi}{4\sqrt{2}}(2m+\frac{4}{3})\right)^{\frac{2}{3}}. \tag{5.144}$$

The members of the first series of solutions may be identified with whispering gallery modes, and those in the second series identified with creeping ray modes. However all these modes decay exponentially as they propagate along the surface. The transmission coefficient at the interface is non-zero, and so even for the whispering gallery modes we expect energy to be lost in the form of shed transmitted rays. Those solutions which are at an $\mathcal{O}(1)$ distance from the origin may not be cleanly divided into creeping and whispering gallery modes. When $\hat{N}$ is small, $l$ is large, and so the condition for $\eta_0(s)$ is approximately

$$\mathrm{Ai}(-2^{\frac{1}{3}}\eta_0(s))\mathrm{Ai}(-2^{\frac{1}{3}}e^{\frac{2\pi i}{3}}\eta_0(s)) = 0 \tag{5.145}$$

(where this approximation is valid provided that $|\,\eta_0\,| \ll l^{\frac{1}{2}}$). In this case the roots are seen to agree with those for creeping ray modes on the convex side, and whispering gallery modes on the concave side, where the external fields satisfy Dirichlet boundary conditions at the midline of the layer.

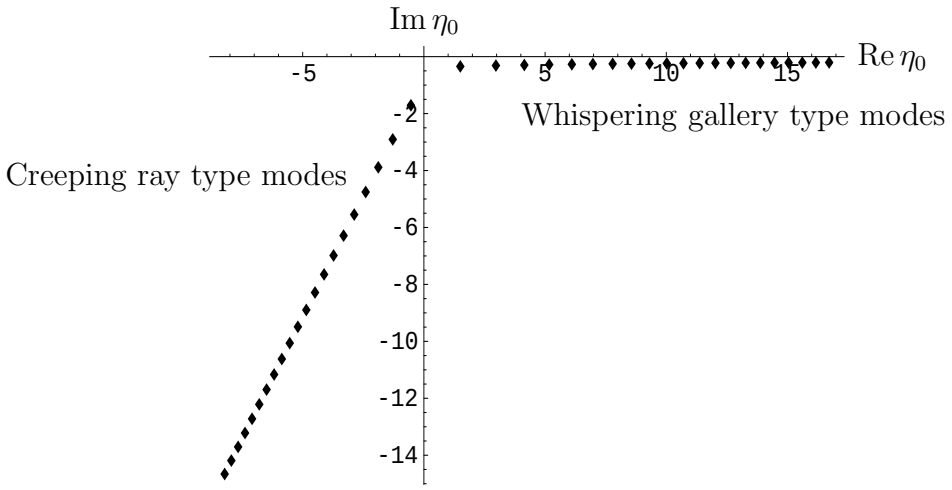


**Figure 5.13:** Locations of solutions of the propagation relation (5.133) for Airy layer modes, in the complex $\eta_0$ plane. This plot is for TE polarization, with $k = 40$ and $N = 5$.

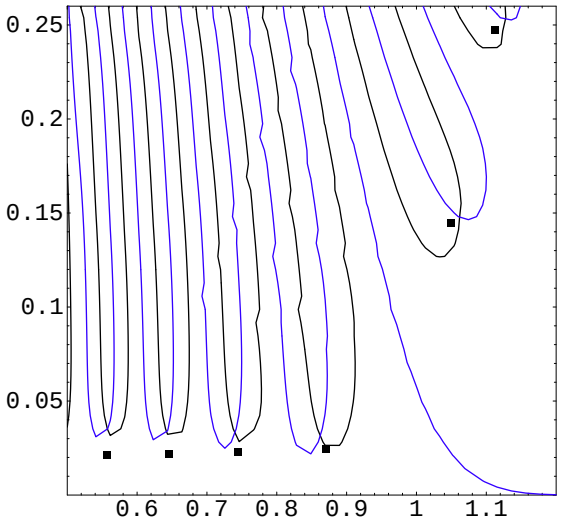


**Figure 5.14:** Comparison between the exact and approximate solutions for the propagation constants for near tangential modes. As in Figure 5.9 we plot in the complex $\hat{\beta} = \beta/k$ plane the zero lines of the real and imaginary parts of the determinant of (5.94) - (5.97), and compare these with the approximate solutions from (5.144) and (5.142), which are shown by filled squares. The above plot is for TE polarization, with $k = 40$, $N = 4$ and $\hat{\mu} = 1$.

### 5.7.7 Fock region

We now wish to examine the initiation of the above Airy layer solutions by a ray impinging tangentially upon the layer. The analysis in the Fock region near the point of tangency is similar to that for a perfectly conducting obstacle, but just as in the Airy layer we must now consider the fields on both sides of the layer.

Following [121] we write

$$\phi = A(\hat{s}, \hat{n})e^{iks}, \tag{5.146}$$

where we have introduced the usual scalings

$$s = k^{-\frac{1}{3}}\hat{s}, \qquad n = k^{-\frac{2}{3}}\hat{n}. \tag{5.147}$$

The leading-order amplitude then satisfies the Fock equation

$$\frac{\partial^2 A}{\partial \hat{n}^2} + 2i\frac{\partial A}{\partial \hat{s}} + 2\kappa_0 \hat{n} A \;=\; 0, \tag{5.148}$$

along with the transition conditions (5.121) on $n = 0$. We take the Fourier transform in $\hat{s}$

$$\bar{A} \;=\; \int_{-\infty}^{\infty} A(\hat{s}, \hat{n})e^{i\lambda\hat{s}}ds, \tag{5.149}$$

and make the substitution

$$\eta \;=\; \kappa_0^{-\frac{2}{3}}(\lambda + \kappa_0\hat{n}). \tag{5.150}$$

The equation for the transformed amplitude is then

$$\frac{\partial^2 \bar{A}}{\partial \eta^2} + 2\eta A = 0 \tag{5.151}$$

and the transition conditions become

$$\bar{A}(\lambda, \eta_0-) + \bar{A}(\lambda, \eta_0+) \;=\; 0, \tag{5.152}$$

$$\frac{\partial \bar{A}}{\partial \eta}(\lambda, \eta_0-) + \frac{\partial \bar{A}}{\partial \eta}(\lambda, \eta_0+) \;=\; -\frac{\pi}{2\hat{\mu}\hat{N}\kappa_0^{\frac{1}{3}}}\bar{A}(\lambda, \eta_0-), \tag{5.153}$$

to leading order, where

$$\eta_0 = \kappa_0^{-\frac{2}{3}}\lambda. \tag{5.154}$$

As for the Airy layer we desire that the solution in this region matches with the outer GO field, but now require that this GO field consists of the incident plane wave along with a wave which is outgoing as $\hat{n} \to \infty$. Thus the solution is of the form

$$\bar{A} = \begin{cases} \alpha^+(\lambda)\mathrm{Ai}(-2^{\frac{1}{3}}\eta) + \beta^+(\lambda)\mathrm{Ai}(-2^{\frac{1}{3}}e^{\frac{2\pi i}{3}}\eta) & \eta > \eta_0, \\ \alpha^-(\lambda)\mathrm{Ai}(-2^{\frac{1}{3}}\eta) & \eta < \eta_0. \end{cases} \tag{5.155}$$

The Fourier transform of the Airy function is

$$\int_{-\infty}^{\infty} \mathrm{Ai}(t)e^{i\lambda t}dt = e^{-\frac{i\lambda^3}{3}}, \tag{5.156}$$

so we have that

$$2^{\frac{1}{3}}\kappa_0^{-\frac{2}{3}}e^{iks}\int_{-\infty}^{\infty}\mathrm{Ai}(-2^{\frac{1}{3}}\kappa_0^{-\frac{2}{3}}(\lambda+\kappa_0\hat{n}))e^{-i\lambda\hat{s}}d\lambda = e^{iks}e^{i\kappa_0\tilde{s}\tilde{n}-\frac{i\kappa_0^2\tilde{s}^3}{6}} \sim e^{ikx}. \tag{5.157}$$

Therefore the solution matches to leading order with the incident plane wave above the layer provided that

$$\alpha^+(\lambda) = 2\pi 2^{\frac{1}{3}}\kappa_0^{-\frac{2}{3}}, \tag{5.158}$$

which is a constant. The transition conditions become

$$\alpha^- u_0 + \alpha^+ u_0 + \beta^+ u_1 = 0, \tag{5.159}$$

$$\alpha^- u_0' + \alpha^+ u_0' + \beta^+ u_1' = -l_0\alpha^- u_0, \tag{5.160}$$

(where $u_1$ and $u_0$ are defined in (5.131), and $l_0$ is the value of $l$ at the point of tangency) with solution

$$\alpha^- = \frac{\alpha^+ W[u_0,u_1]}{\frac{2^{\frac{1}{3}}e^{-\frac{\pi i}{6}}}{2\pi}+l_0u_0u_1}, \qquad \beta^+ = -\frac{\alpha^+ l_0 u_0^2}{\frac{2^{\frac{1}{3}}e^{-\frac{\pi i}{6}}}{2\pi}+l_0u_0u_1}. \tag{5.161}$$

Explicitly, the transform of the field in the Fock region is

$$\bar{A} = \begin{cases} 2^{\frac{4}{3}}\pi\kappa_0^{-\frac{2}{3}}\left(\mathrm{Ai}(-2^{\frac{1}{3}}\eta) - \dfrac{l_0\mathrm{Ai}^2(-2^{\frac{1}{3}}\eta_0)\mathrm{Ai}(-2^{\frac{1}{3}}e^{\frac{2\pi i}{3}}\eta)}{\frac{2^{\frac{1}{3}}e^{-\frac{\pi i}{6}}}{2\pi}+l_0\mathrm{Ai}(-2^{\frac{1}{3}}\eta_0)\mathrm{Ai}(-2^{\frac{1}{3}}e^{\frac{2\pi i}{3}}\eta_0)}\right) & \hat{n}>0, \\ 2^{\frac{4}{3}}\pi\kappa_0^{-\frac{2}{3}}\left(-\dfrac{\frac{2^{\frac{1}{3}}e^{-\frac{\pi i}{6}}}{2\pi}\mathrm{Ai}(-2^{\frac{1}{3}}\eta)}{\frac{2^{\frac{1}{3}}e^{-\frac{\pi i}{6}}}{2\pi}+l_0\mathrm{Ai}(-2^{\frac{1}{3}}\eta_0)\mathrm{Ai}(-2^{\frac{1}{3}}e^{\frac{2\pi i}{3}}\eta_0)}\right) & \hat{n}<0. \end{cases} \tag{5.162}$$

The fields within the Fock region may be found by applying the inverse Fourier transform

$$A = \frac{1}{2\pi}\int_{-\infty}^{\infty}\bar{A}(\lambda,\hat{n})e^{-i\lambda\hat{s}}d\lambda, \tag{5.163}$$

and in the next section we will consider matching between this solution and the outer GO field.

### 5.7.8 Matching with scattered fields

We now match between the solution found above in the Fock region, and the outer geometrical optics fields. We will find the launch coefficients for Airy layer modes, and an approximation valid in the transition region near the shadow boundary.

If we introduce the new integration variable $p = \kappa_0^{-\frac{2}{3}}\lambda$, and scale $\hat{n} = \kappa_0^{-\frac{1}{3}}\tilde{n}$, $\hat{s} = \kappa_0^{-\frac{2}{3}}\tilde{s}$, then the solution in the Fock region is

$$\phi = 2^{\frac{1}{3}}e^{iks}\int_{-\infty}^{\infty}\left\{\mathrm{Ai}(-2^{\frac{1}{3}}(p+\tilde{n})) - \frac{l_0\mathrm{Ai}^2(-2^{\frac{1}{3}}p)\mathrm{Ai}(-2^{\frac{1}{3}}e^{\frac{2\pi i}{3}}(p+\tilde{n}))}{\frac{2^{\frac{1}{3}}e^{-\frac{\pi i}{6}}}{2\pi}+l_0\mathrm{Ai}(-2^{\frac{1}{3}}p)\mathrm{Ai}(-2^{\frac{1}{3}}e^{\frac{2\pi i}{3}}p)}\right\}e^{-i\tilde{s}p}dp \tag{5.164}$$

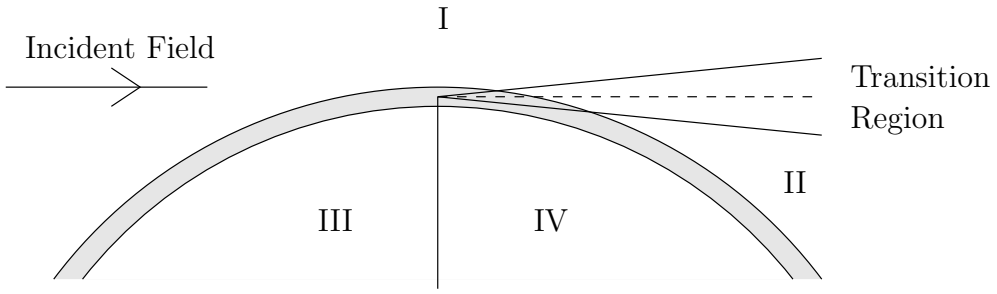


**Figure 5.15:** Regions for matching between the Fock solution and the GO field.

above the layer ($\tilde{n} > 0$), and

$$\phi = -2^{\frac{1}{3}} e^{iks} \int_{-\infty}^{\infty} \frac{\frac{2^{\frac{1}{3}} e^{-\frac{\pi i}{6}}}{2\pi} \mathrm{Ai}(-2^{\frac{1}{3}}(p+\tilde{n}))}{\frac{2^{\frac{1}{3}} e^{-\frac{\pi i}{6}}}{2\pi} + l_0 \mathrm{Ai}(-2^{\frac{1}{3}} p)\mathrm{Ai}(-2^{\frac{1}{3}} e^{\frac{2\pi i}{3}} p)} e^{-i\tilde{s}p} dp \tag{5.165}$$

below the layer ($\tilde{n} < 0$).

To perform the matching we need to find the asymptotic expansion of these integrals when one or both of $|\,\tilde{s}\,|$ and $|\,\tilde{n}\,|$ are large, which will be obtained by the method of steepest descent/stationary phase. These integrals have contributions from a number of saddle/stationary points, which correspond to reflected or transmitted rays, and residue contributions from the poles of the integrands, which correspond to Airy layer modes. The poles of the integrands are in the same locations (in the $p$ plane) as the solutions $\eta_0$ to the propagation relation (5.133) discussed earlier.

The number and type of poles and saddles obtained, and so the ray fields and modes present, varies significantly with the point of observation. We will therefore consider the approximation of the integral in each of the regions shown in Figure 5.15 separately. For the sake of brevity we will omit some of the details of these calculations.

#### 5.7.8.1 Region I

In I, the region above the layer which is directly illuminated by the incident field, we will find that the Fock solution matches with the incident wave and the reflected field. From equation (5.157) we recall that the first part of the integrand of (5.164) is a (leading-order) approximation to the incident plane wave. For the remainder of (5.164) we note that the asymptotic expansion of $\mathrm{Ai}(-2^{\frac{1}{3}}p)$ for $p \gg 1$ consists of the sum of two exponential terms. Therefore we use the connection formula

$$\mathrm{Ai}(z) + e^{\frac{2\pi i}{3}} \mathrm{Ai}(e^{\frac{2\pi i}{3}} z) + e^{-\frac{2\pi i}{3}} \mathrm{Ai}(e^{-\frac{2\pi i}{3}} z) = 0, \tag{5.166}$$

to rewrite (5.164) as

$$\phi = 2^{\frac{1}{3}} e^{iks} \int_{-\infty}^{\infty} \mathrm{Ai}(-2^{\frac{1}{3}}(p+\tilde{n})) e^{-i\tilde{s}p} dp + I_1 + I_2 + I_3, \tag{5.167}$$

where

$$I_1 = -2^{\frac{1}{3}} e^{iks} \int_{-\infty}^{\infty} l_0 e^{\frac{4\pi i}{3}} \mathrm{Ai}^2(-2^{\frac{1}{3}} e^{\frac{2\pi i}{3}} p) \mathrm{Ai}(-2^{\frac{1}{3}} e^{\frac{2\pi i}{3}}(p+\tilde{n})) \frac{e^{-i\tilde{s}p}\, dp}{D(p)}, \tag{5.168}$$

$$I_2 = -2^{\frac{1}{3}} e^{iks} \int_{-\infty}^{\infty} 2 l_0 \mathrm{Ai}(-2^{\frac{1}{3}} e^{\frac{2\pi i}{3}} p) \mathrm{Ai}(-2^{\frac{1}{3}} e^{-\frac{2\pi i}{3}} p) \mathrm{Ai}(-2^{\frac{1}{3}} e^{\frac{2\pi i}{3}}(p+\tilde{n})) \frac{e^{-i\tilde{s}p}\, dp}{D(p)}, \tag{5.169}$$

$$I_3 = -2^{\frac{1}{3}} e^{iks} \int_{-\infty}^{\infty} l_0 e^{-\frac{4\pi i}{3}} \mathrm{Ai}^2(-2^{\frac{1}{3}} e^{-\frac{2\pi i}{3}} p) \mathrm{Ai}(-2^{\frac{1}{3}} e^{\frac{2\pi i}{3}}(p+\tilde{n})) \frac{e^{-i\tilde{s}p}\, dp}{D(p)}, \tag{5.170}$$

and

$$D(p) = \frac{2^{\frac{1}{3}} e^{-\frac{\pi i}{6}}}{2\pi} + l_0 \mathrm{Ai}(-2^{\frac{1}{3}} p) \mathrm{Ai}(-2^{\frac{1}{3}} e^{\frac{2\pi i}{3}} p). \tag{5.171}$$

By using the asymptotic expansions of the Airy function for large argument [100, Ch. 11] we find that, in the region

$$|p| \gg 1, \quad |\arg p| < \frac{\pi}{3}, \quad |p+\tilde{n}| \gg 1, \quad |\arg(p+\tilde{n})| < \frac{\pi}{3}, \tag{5.172}$$

the integrand of $I_1$ has asymptotic expansion

$$-\frac{e^{iks} l_0 e^{-\frac{\pi i}{4}}}{2^{\frac{1}{4}} 4\pi^{\frac{1}{2}} p^{\frac{1}{2}} (p+\tilde{n})^{\frac{1}{4}}} \frac{e^{\frac{i2\sqrt{2}}{3}(p+\tilde{n})^{\frac{3}{2}} + \frac{i4\sqrt{2}}{3} p^{\frac{3}{2}} - i\tilde{s}p}}{1 + \frac{l_0}{p^{\frac{1}{2}} 2^{\frac{3}{2}}} (e^{\frac{4i\sqrt{2}}{3} p^{\frac{3}{2}}} + i)}, \tag{5.173}$$

the integrand of $I_2$ has asymptotic expansion

$$-\frac{e^{iks} l_0 e^{-\frac{\pi i}{4}}}{2^{\frac{1}{4}} 4\pi^{\frac{1}{2}} p^{\frac{1}{2}} (p+\tilde{n})^{\frac{1}{4}}} \frac{2i e^{\frac{i2\sqrt{2}}{3}(p+\tilde{n})^{\frac{3}{2}} - i\tilde{s}p}}{1 + \frac{l_0}{p^{\frac{1}{2}} 2^{\frac{3}{2}}} (e^{\frac{4i\sqrt{2}}{3} p^{\frac{3}{2}}} + i)}, \tag{5.174}$$

and the integrand of $I_3$ has asymptotic expansion

$$\frac{e^{iks} l_0 e^{-\frac{\pi i}{4}}}{2^{\frac{1}{4}} 4\pi^{\frac{1}{2}} p^{\frac{1}{2}} (p+\tilde{n})^{\frac{1}{4}}} \frac{e^{\frac{i2\sqrt{2}}{3}(p+\tilde{n})^{\frac{3}{2}} - \frac{i4\sqrt{2}}{3} p^{\frac{3}{2}} - i\tilde{s}p}}{1 + \frac{l_0}{p^{\frac{1}{2}} 2^{\frac{3}{2}}} (e^{\frac{4i\sqrt{2}}{3} p^{\frac{3}{2}}} + i)}. \tag{5.175}$$

The phase of each of these terms is of the form

$$u = \frac{2\sqrt{2}}{3}(p+\tilde{n})^{\frac{3}{2}} + m\frac{4\sqrt{2}}{3} p^{\frac{3}{2}} - \tilde{s}p \tag{5.176}$$

where $m = 1, 0, -1$ for $I_1$, $I_2$ and $I_3$ respectively. In region I we find that out of these three integrals only $I_3$ has a saddle/stationary point on the positive real $p$ axis. Provided that $\tilde{n} > \tilde{s}^2/2$, there is a single saddle point $p_0$, given by

$$p_0^{\frac{1}{2}} = \frac{1}{\sqrt{2}} \left( -\frac{2\tilde{s}}{3} + \frac{1}{3}\sqrt{\tilde{s}^2 + 6\tilde{n}} \right), \tag{5.177}$$

or equivalently

$$p_0 = \frac{5}{18}\tilde{s}^2 + \frac{\tilde{n}}{3} - \frac{2\tilde{s}}{9}\sqrt{\tilde{s}^2 + 6\tilde{n}}. \tag{5.178}$$

As we cannot approximate the Airy functions when $|\,p\,|$ is bounded we deform the contours of the integrals in the manner shown in Figure 5.16, such that the contour for $I_3$ follows the path of steepest descent up to $p_0$, and then proceeds along the real axis to $+\infty$. (As in Chapter 4 each of the integrands, considered individually, grows exponentially as $p \to -\infty$, and so we recombine the three integrals on the section of the contour from $-\infty$ to some point $A$ which is to the right of the line $\arg p = \frac{2\pi}{3}$.) We expect the dominant contribution to the integrals to be the contribution from near $p_0$ for $I_3$. However the integrand of $I_3$ is still not in an appropriate form for the method of steepest descents/stationary phase to be used, as the denominator contains a rapidly varying exponential. For large $|p|$ this exponential is algebraically small compared to the rest of the denominator, and so we find that it does not affect the leading-order saddle point contribution.

To see this more clearly, and to introduce a method which will prove essential for the analysis in regions II and IV, we instead use the connection formula for the Airy functions to write

$$D = \left\{ \frac{2^{\frac{1}{3}}e^{-\frac{\pi i}{6}}}{2\pi} - l_0 e^{-\frac{2\pi i}{3}}\mathrm{Ai}(-2^{\frac{1}{3}}e^{\frac{2\pi i}{3}}p)\mathrm{Ai}(-2^{\frac{1}{3}}e^{-\frac{2\pi i}{3}}p) \right\} - l_0 e^{\frac{2\pi i}{3}}\mathrm{Ai}^2(-2^{\frac{1}{3}}e^{\frac{2\pi i}{3}}p). \tag{5.179}$$

If we now approximate the Airy functions for $p \gg 1$ we see that the part of the RHS which is contained in brackets has an asymptotic expansion which is non-oscillatory, whereas the remaining part has an expansion which consists of a single exponential term. This remaining part is small near $p_0$, and so we can expand

$$D(p)^{-1} = D_0(p)^{-1}\sum_{m=0}^{\infty}(r(p))^m \tag{5.180}$$

where

$$D_0(p) = \frac{2^{\frac{1}{3}}e^{-\frac{\pi i}{6}}}{2\pi} - l_0 e^{-\frac{2\pi i}{3}}\mathrm{Ai}(-2^{\frac{1}{3}}e^{\frac{2\pi i}{3}}p)\mathrm{Ai}(-2^{\frac{1}{3}}e^{-\frac{2\pi i}{3}}p), \tag{5.181}$$

$$r(p) = \frac{l_0 e^{\frac{2\pi i}{3}}\mathrm{Ai}^2(-2^{\frac{1}{3}}e^{\frac{2\pi i}{3}}p)}{\frac{2^{\frac{1}{3}}e^{-\frac{\pi i}{6}}}{2\pi} - l_0 e^{-\frac{2\pi i}{3}}\mathrm{Ai}(-2^{\frac{1}{3}}e^{\frac{2\pi i}{3}}p)\mathrm{Ai}(-2^{\frac{1}{3}}e^{-\frac{2\pi i}{3}}p)}. \tag{5.182}$$

This method is also used in [86] and [62] to resolve a similar difficulty.

If we expand the denominator of the integrand of $I_3$ in this manner on the section of the integral from $A$ to $p_0$ to $+\infty$ then this series is convergent. The asymptotic expansion

of the integrand of the first term in the series is just (5.175), but without the $e^{\frac{i4\sqrt{2}}{3}p^{\frac{3}{2}}}$ term in the denominator, and in the region (5.172)

$$r(p) \sim \frac{l_0}{p^{\frac{1}{2}}2^{\frac{3}{2}}} \frac{e^{\frac{i4\sqrt{2}}{3}p^{\frac{3}{2}}}}{1+\frac{il_0}{p^{\frac{1}{2}}2^{\frac{3}{2}}}}. \tag{5.183}$$

From this we see $r(p)$ is exponentially small for $0 < \arg p < \frac{2\pi}{3}$ and $|\,p\,| \gg 1$, and so the integrals for $m \geq 1$ can be deformed to paths which are similar to those shown for $I_1$ and $I_2$ in Figure 5.16, and so give exponentially small contributions.

We may then evaluate the contribution to $I_3$ from near $p_0$, and despite the change of direction in the contour, this is just the usual saddle/stationary point contribution (We should, more formally, rescale $\tilde{s} = K\tilde{s}'$, $\tilde{n} = K^2\tilde{n}'$, $\tilde{p} = K^2\tilde{p}'$ for some large parameter $K$, before evaluating the saddle point contribution). After some algebraic manipulation to convert between surface and ray coordinate systems we find that the contribution from this stationary point matches with a ray reflected from above the layer, with reflection coefficient

$$R \;=\; -\frac{\frac{\pi i \sin^2\theta}{4\hat{\mu}\hat{N}\cos\theta}}{1+\frac{\pi i \sin^2\theta}{4\hat{\mu}\hat{N}\cos\theta}}. \tag{5.184}$$

It is helpful to note that the leading-order relationship between $\theta$ and our surface coordinate system is

$$\frac{\pi}{2} - \theta \;\sim\; -\frac{2\tilde{s}}{3} + \frac{\sqrt{\tilde{s}^2+6\tilde{n}}}{3}. \tag{5.185}$$

If we were to expand the outer geometrical optics field in powers of $k$, and then take the limit of this field as the angle of incidence approaches tangency, we would obtain a reflected field with the reflection coefficient (5.101). The expression (5.184) is the same as the plane wave reflection coefficient (5.117) obtained from the transition conditions (5.115) and (5.116). These agree to leading order with (5.101), for angles of incidence in the range $k^{-\frac{1}{3}} \ll \frac{\pi}{2} - \theta \ll 1$. However the reflection coefficient (5.184) is in fact valid to higher order in this region, and we recall from our earlier discussion that it is also valid for plane-wave incidence upon a planar slab, even for near-tangential incidence. We will find for all the ray fields that the Fock region matches with the inner limit of the geometrical optics fields, with the reflection and transmission coefficients approximated by those of (5.117).

#### 5.7.8.2 Region II

In II, which is the region above the layer where the incident field has been transmitted by the layer twice (if the layer was impenetrable this would be the shadow region),

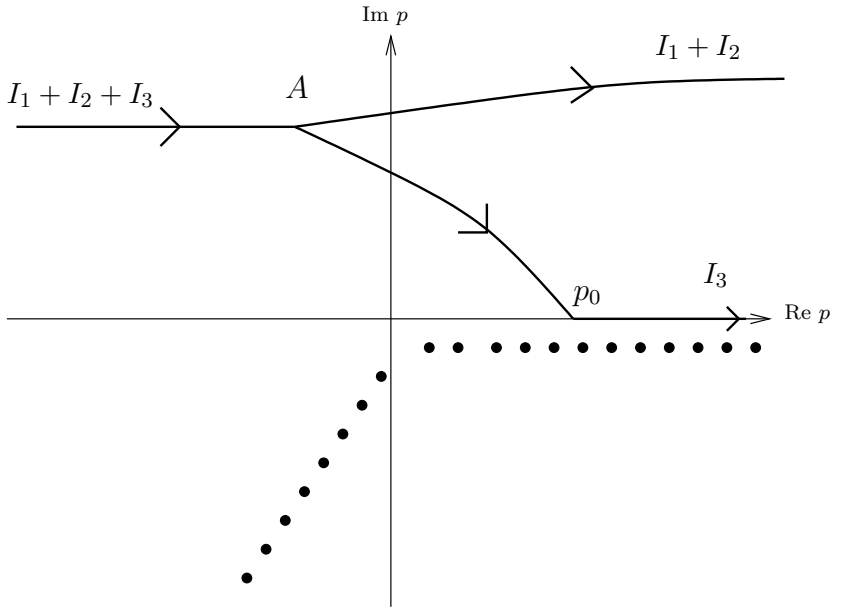


**Figure 5.16:** Contours of integration in region I.

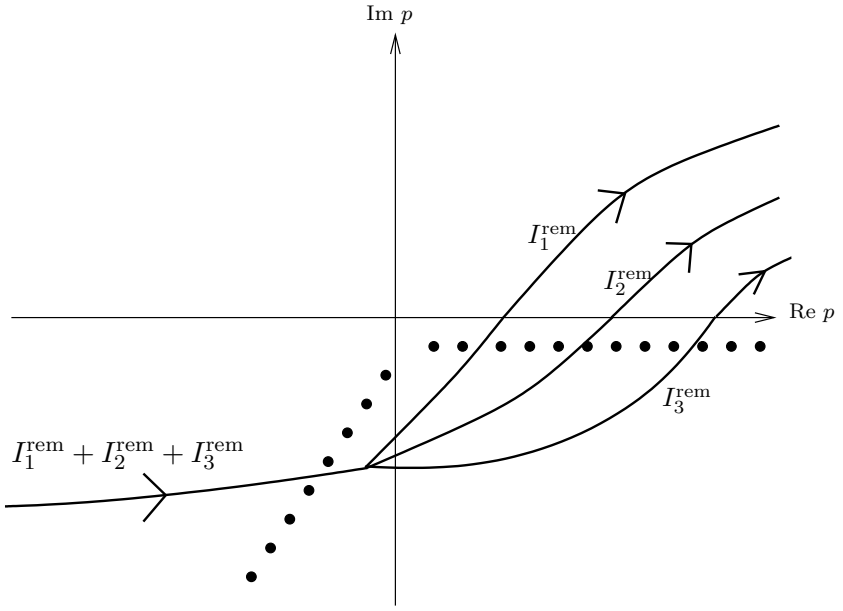


**Figure 5.17:** Contours of integration for remainder integrals in region II.

then the situation is considerably more complicated. Along with the field that has been transmitted straight through the layer twice, there are an infinite series of ray fields which correspond to those rays which are first transmitted through the layer, before being reflected $m$ times below the layer, and then finally transmitted through the layer into region II. The paths of these multiply-reflected rays can be seen in Figure 5.18. Each of these $m$-fold reflected ray fields has caustics, but these lie in region IV below the layer.

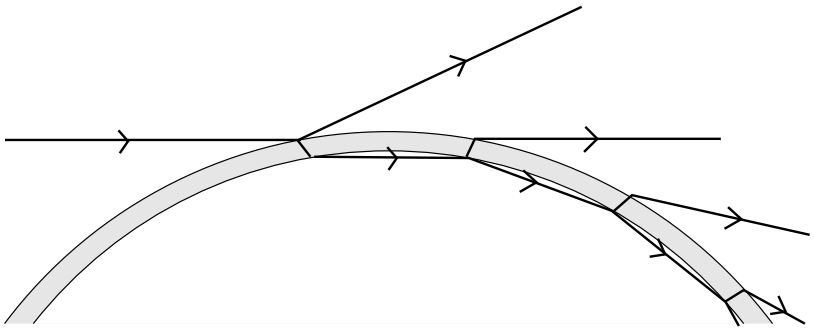

**Figure 5.18:** Multiply-reflected fields near tangential incidence.

In addition to these rays we expect that there will be Airy layer modes initiated at the point of tangency which propagate almost tangentially to the layer. As discussed earlier, those Airy layer modes which are of whispering gallery type may be associated with rays which are guided by multiple reflections below the layer. As these modes have a very similar behaviour to the reflected rays we expect that there will be some indeterminacy in the representation of the fields in this region, and it will be possible to write these in a number of different ways as combinations of rays and modes. A similar problem is obtained for near critical incidence upon a convex scatterer with a lower refractive index than its surroundings [86], and for a point source in the presence of a convex boundary [61], [62].

If we simply replace $D$ by $D_0$ in $I_1$, $I_2$ and $I_3$, and approximate the Airy functions by their expansions for large argument, then the contributions obtained from the stationary points match to leading order with the directly transmitted field, and the field reflected once below the layer. However, both the approximation of $D$ by $D_0$, and the expansion of the Airy functions, are not valid for bounded $|\,p\,|$. The approximated integrands do not have any poles, and so we do not obtain any residue contributions.

Instead, we deform the contours of integration in the complex plane, and use the series approximation (5.180) for $D$. This series is not (necessarily) convergent on the whole real axis, and we will deform the contours of integration into the region $-\frac{\pi}{3} < \arg p < 0$, $|\,p\,| \gg 1$, within which the series certainly does not converge. In order to deal with this we expand the denominator $D(p)$ of each of $I_1$, $I_2$ and $I_3$ as

$$D^{-1} = D_0^{-1} \sum_{m=0}^{M-1} (r(p))^m + \frac{D_0^{-1}(r(p))^M}{1 - r(p)} = D_0^{-1} \sum_{m=0}^{M-1} (r(p))^m + D^{-1}(r(p))^M \qquad (5.186)$$

which is the same geometrical series as before, but terminated after $M$ terms. We write

$$I_q = \sum_{m=0}^{M-1} I_q^m + I_q^{\mathrm{rem(M)}} \qquad (5.187)$$

for $q = 1, 2, 3$, where $I_q^m$ is the integral over the real line of the same function as $I_q$, but with $D^{-1}$ replaced by $D_0^{-1}(r(p))^m$, and where $I_n^{\mathrm{rem(M)}}$ has $D^{-1}$ replaced by $D^{-1}(r(p))^M$. Each of the $I_q^m$ are now in an appropriate form to be approximated by the method of steepest decent, and the phase of the asymptotic expansion of the integrand for $p \gg 1$ is

$$u_q^m = \frac{2\sqrt{2}}{3}(p+\tilde{n})^{\frac{3}{2}} + \frac{4\sqrt{2}}{3}p^{\frac{3}{2}}\,(q-2+m) - \tilde{s}p. \tag{5.188}$$

We see that each of the integrals, except $I_3^0$, has a single saddle on the real axis, and so we obtain a large number of saddle point contributions. In order to evaluate the saddle point contribution we need to approximate the Airy functions by their asymptotic expansions, and for this to be valid we require that the saddle point is at a point for which $p \gg 1$. By examining (5.188) we see that, for large $\tilde{s}$, $M$ must be much smaller than $\tilde{s}$ for all the saddle point contributions to be approximated. When we match into the outer coordinate system $\tilde{s} = \mathcal{O}(k^{\frac{1}{3}})$, so $M$ must be much smaller than $k^{\frac{1}{3}}$. By expanding the denominators we have removed the poles from all these integrals, apart from the remainder integrals. The dominant contribution to each of the integrals is from the saddle point, and when we calculate the saddle point contributions we find that $I_1^0$ matches with the inner limit of the once reflected ray field, with amplitude

$$-\frac{\frac{\pi i \sin^2\theta}{4\hat{\mu}\hat{N}\cos\theta}}{1+\frac{\pi i \sin^2\theta}{4\hat{\mu}\hat{N}\cos\theta}}, \tag{5.189}$$

and $I_2^0$ matches with the (correction to the) ray field which is directly transmitted twice through the layer, with amplitude

$$-\frac{\frac{\pi i \sin^2\theta}{2\hat{\mu}\hat{N}\cos\theta}}{1+\frac{\pi i \sin^2\theta}{4\hat{\mu}\hat{N}\cos\theta}}. \tag{5.190}$$

(The leading order transmitted field is supplied by the first part of (5.167)). We also find that $I_1^m$, for $m \geq 1$, matches with the leading order $m$-fold reflected ray field, with amplitude

$$\left(-\frac{\frac{\pi i \sin^2\theta}{4\hat{\mu}\hat{N}\cos\theta}}{1+\frac{\pi i \sin^2\theta}{4\hat{\mu}\hat{N}\cos\theta}}\right)^m. \tag{5.191}$$

These all match, to leading order, with the leading order geometrical optics field. However, we also find that the integral $I_3^1$ supplies a higher-order correction to the directly-transmitted field, and the integrals $I_3^{m+1}$ and $I_2^m$, for $m \geq 1$, supply higher-order corrections to the $m$-fold reflected fields. If we denote the reflection and transmission coefficients (5.117) by $R$ and $T$, then we find that the correction from $I_3^1$ accounts for the difference in

amplitude between the saddle point contribution from $I_2^0$, and correction to the directly transmitted field with amplitude $T^2-1$. The corrections from $I_3^{m+1}$ and $I_2^m$ also account for the difference in amplitude between the contribution from $I_1^m$ and the $m$-fold reflected field with amplitude $R^mT^2$.

We are then left with the remainder integrals, which have poles in the same locations as the original integrals. At these poles $r(p)=1$, and so we see that the residues of the remainder integrals are exactly the same as those for the original integrals $I_1$, $I_2$ and $I_3$. The expansions of the remainder integrals consist of a contribution from a saddle point on the real axis (the phases of the remainder integrals on the real axis are $u_n^M$), along with residue contributions from those poles. This saddle point contribution is modified by the fact that the approximation for $p \gg 1$ of the denominator of the integrand contains a rapidly varying exponential term. On the line on which the poles reside this exponential term is of the same size as the rest of the denominator, and unlike the analysis in region I the contour of integration must cross this line. As in section 4.2.3.3, we may expand the denominator of the integrand in a binomial series. The nature of this expansion is different on either side of the line of poles, as the exponential term changes between being much smaller and much larger than the rest of the denominator. We then find that the leading-order contribution to the saddle point in this case is half that which would be obtained if the denominator was $D_0$ rather than $D$ (and so does not contain an oscillatory part). The steepest descents paths for these integrals can be seen in Figure 5.17, and we find that the expansions of the integrals consist of the (half) saddle point contributions plus those poles which lie between the real axis and the new contours.

For those residues obtained from all three integrals the total contributions are

$$\begin{aligned}
&-2\pi i\sum_m \frac{\mathrm{Ai}^2(-2^{\frac{1}{3}}p_m)\mathrm{Ai}(-2^{\frac{1}{3}}e^{\frac{2\pi i}{3}}(p_m+\tilde{n}))e^{-i\tilde{s}p_m}}{\mathrm{Ai}'(-2^{\frac{1}{3}}p_m)\mathrm{Ai}(-2^{\frac{1}{3}}e^{\frac{2\pi i}{3}}p_m)+e^{\frac{2\pi i}{3}}\mathrm{Ai}(-2^{\frac{1}{3}}p_m)\mathrm{Ai}'(-2^{\frac{1}{3}}e^{\frac{2\pi i}{3}}p_m)} \\
&\quad = 4\pi^2 e^{\frac{2\pi i}{3}}e^{iks}\sum_m \mathrm{Ai}^2(-2^{\frac{1}{3}}p_m)e^{-ip_n\tilde{s}}\left(1+\frac{2^{\frac{7}{3}}e^{\frac{2\pi i}{3}}\kappa_0^{\frac{1}{3}}\hat{\mu}\hat{N}}{\pi}\frac{\mathrm{Ai}'(-2^{\frac{1}{3}}e^{\frac{2\pi i}{3}}p_m)}{\mathrm{Ai}(-2^{\frac{1}{3}}e^{\frac{2\pi i}{3}}p_m)}\right)^{-1} \qquad (5.192)
\end{aligned}$$

and corresponding results can be found for those residues which contribute to only one or two of these integrals.

#### 5.7.8.3 Region III

In region III below the layer, which corresponds to $\tilde{s}<0$ and $\tilde{n}<0$, we may proceed in a similar manner to region I, and find that the Fock solution matches with the transmitted field.

#### 5.7.8.4 Region IV

In region IV, below the layer with $\tilde{s} > 0$ and $\tilde{n} < 0$, the situation is similar to region II as each of the $m$-fold reflected wave fields switches on across a caustic in this region. There are also curves across which the coordinate system is such that $\tilde{n}$ changes from being decreasing to increasing across the ray, and although there is no discontinuity in the fields there this changes the exponential which contains the saddle point. For example, the once-reflected ray is switched on across the caustic $\tilde{n} = -\frac{\tilde{s}^2}{6}$, and the ray outgoing from this caustic changes its behaviour when $\tilde{n} = -\frac{\tilde{s}^2}{8}$. By a similar analysis to that in region II we find that the solution matches with this complicated geometrical optics field. In addition to these reflected ray fields we also obtain residue contributions from the integrals, which match with Airy layer modes as discussed in region II.

It must be noted that the solution in the Fock region is only valid to leading order, and in particular the phases for all these geometrical optics fields are only correct to leading order. Higher-order corrections are obtained from the solution to the $\mathcal{O}(k^{\frac{1}{3}})$ Fock-Leontovich problem, which in particular includes the (leading-order) effects of the derivative of the curvature of the layer at the point of tangency.

#### 5.7.8.5 Transition region

The above matching fails to be valid in the vicinity of the border between regions I and II, near the continuation of the tangentially incident ray. This is a consequence of those saddle/stationary phase points which supply the reflected field being at an $\mathcal{O}(1)$ distance from the origin, and so the large argument approximation of the Airy functions is invalid. Instead, as for an impenetrable obstacle, we find a transition region solution near the shadow boundary. We recall from Section 3.1.4.4 that this region corresponds to $y = \mathcal{O}(k^{-\frac{1}{3}}\kappa_0^{\frac{1}{3}}x)$ and $x = \mathcal{O}(1)$, where $x$ and $y$ are as shown in Figure 3.3.

In this region we expect the dominant contribution to the integral to be from the vicinity of the origin, but there may also be a saddle point (away from the origin) which supplies the directly-transmitted field. At any rate, these contributions will be from parts of the integral for which $|p+\tilde{n}| \gg 1$, and so we may employ the asymptotic expansion for $\mathrm{Ai}(-2^{\frac{1}{3}}e^{\frac{2\pi i}{3}}(p+\tilde{n}))$. This expansion is not valid for $p+n<0$, but the error introduced by this is exponentially small. If we introduce a polar coordinate system $(r,\xi)$ centred at the point of tangency, with $\xi = 0$ along the shadow boundary, and such that $\xi > 0$ corresponds to the directly lit region, then we find that the Fock solution matches into a

system of rays given by

$$-\frac{2^{\frac{1}{6}}l_0\pi^{\frac{1}{2}}e^{ikr-\frac{i\hat{\xi}^3}{6}+\frac{\pi i}{4}}}{k^{\frac{1}{6}}\kappa_0^{\frac{1}{3}}\sqrt{r}}\int_{-\infty}^{\infty}\frac{\mathrm{Ai}^2(-2^{\frac{1}{3}}p)e^{i\hat{\xi}p}}{1+2^{\frac{2}{3}}\pi l_0 e^{\frac{\pi i}{6}}\mathrm{Ai}(-2^{\frac{1}{3}}p)\mathrm{Ai}(-2^{\frac{1}{3}}e^{\frac{2\pi i}{3}}p)}dp, \tag{5.193}$$

where we have scaled $\xi = k^{-\frac{1}{3}}\kappa^{\frac{1}{3}}\hat{\xi}$. In the region $\xi < 0$ we must add onto this the correction to the transmitted field. This solution is not valid in an inner region near the shadow boundary, as the correction to the transmitted field switches on at this point. An inner solution in terms of a complementary error function may be found in this region.

#### 5.7.8.6 Launch coefficients for Airy layer modes

We recall that each of the Airy layer modes has the form (5.134), where the amplitude $a(s)$ is given by (5.140). The amplitude of these modes may be found by matching with the residue series (5.192). We find for the mode associated with the pole $p_m$ that

$$a_0 = 4\pi^2 e^{\frac{2\pi i}{3}}\mathrm{Ai}^2(-2^{\frac{1}{3}}p_m)\kappa_0^{-\frac{1}{6}}\left(1+\frac{2^{\frac{7}{3}}e^{\frac{2\pi i}{3}}\kappa_0^{\frac{1}{3}}\hat{\mu}\hat{N}}{\pi}\frac{\mathrm{Ai}'(-2^{\frac{1}{3}}e^{\frac{2\pi i}{3}}p_m)}{\mathrm{Ai}(-2^{\frac{1}{3}}e^{\frac{2\pi i}{3}}p_m)}\right)^{-\frac{1}{2}}. \tag{5.194}$$

The residue series (5.192) is only valid for the fields above the layer. However the residue of (5.165), from the same pole $p_m$, gives a field below the layer which matches with the same Airy layer mode, and with the same launch coefficient.

## 5.8 Summary and conclusions

In this chapter we have examined the problem of scattering by a thin dielectric layer with high refractive index. We have formulated approximate transition conditions which account for multiple reflections and the curvature of the layer. These we used to find the fields scattered by a region of a layer which was tightly curved compared to the external wavelength, but had a large radius of curvature compared to the wavelength within the dielectric material. We also examined the problem of tangential incidence upon such a thin layer. The approximate transition conditions were modified to be valid for waves propagating almost tangentially to the layer, and we found Airy layer modes which are similar to whispering gallery and creeping modes upon an impenetrable boundary. We then considered the local problem in the Fock region near the point of tangency. This was found to match with the outer geometrical optics field, and we found the launch coefficients for the Airy layer modes initiated at the point of tangency.

There are a number of possible extensions to this work. We found approximate transition conditions for both polarizations in the two-dimensional E-M case, and transition

conditions valid for three-dimensional scalar problems. It appears possible, with some rather involved calculations, to extend this analysis to the three-dimensional E-M case, in a similar manner to the analysis in the appendix of [127] for a curved, highly conducting boundary. It also seems possible to find higher-order approximations to the boundary conditions. This has been performed in the planar case [117] [115], but when the layer is curved the higher-order equations become increasingly complicated. It may also be possible to extend these approximate transition conditions to the case of a thin layer whose thickness varies over a length scale which is large compared to the internal wavelength. We expect that the analysis for a tightly curved tip region may be extended to these more general transition conditions, but with correspondingly more complicated results.

It may also be possible to extend the analysis for near-tangential incidence to the three-dimensional electromagnetic case. As in the perfectly conducting case we expect that the problem near the point of tangency will decompose into two separate problems for TE and TM polarizations, as the electric and magnetic fields are (to leading order) perpendicular to the direction of propagation, and near tangency the direction of propagation is almost in the tangent plane to the surface. If this is the case, then it seems likely that the problems in the Fock region for these two polarizations will reduce to the two-dimensional problem which we have studied here. It should also be possible to find Airy layer solutions in the three-dimensional case by a similar analysis to the perfectly conducting case.

# Chapter 6

# Obstacle Scattering

In this chapter we will present a practical interpretation of the scattering theory of Lax and Phillips [80] for the Helmholtz equation in the exterior of an obstacle. Instead of following their abstract development, we will define the scattering matrix to be the operator which relates the incoming and outgoing radiation patterns for solutions of the exterior Helmholtz problem. We will find that this operator is connected in a simple manner to the definition employed by Lax and Phillips. We will then examine the behaviour for large wavenumber of a function related to the determinant of the scattering matrix, which is known as the (total) scattering phase. This will be seen to have asymptotic behaviour for large wavenumber which is similar to the counting function for the eigenvalues of Helmholtz' equation in the interior of the scatterer. We will then discuss the work of Smilansky [38] [36], and mention some of the insights into the relationship between the internal and external problems developed in that work.

The purpose of this chapter is primarily to give a straightforward and explicit exposition of the various different versions of the scattering matrix. We will also use the asymptotic solutions discussed in Chapter 3 to verify the known results for the high frequency behaviour of the scattering phase, using a significantly simpler mathematical method.

## 6.1 The exterior Helmholtz problem

We will consider solutions of Helmholtz' equation

$$(\nabla^2 + k^2)\psi = 0 \tag{6.1}$$

outside an obstacle $\Omega \subset \mathbb{R}^n$, along with the Dirichlet condition $\psi = 0$ on the boundary $\partial\Omega$. As in the remainder of the thesis the fields will be considered to have time-dependence of

the form[1] $e^{-i\omega t}$. For the purposes of this work we will consider the obstacle to be a smooth, strictly convex, compact body. This will allow us to approximate the scattered field using the asymptotic results developed in [134], [140] and [121]. This also ensures that the body is non-trapping. A rigorous definition of this may be found in [93]; informally it means that for any ray which is multiply reflected from the obstacle, the distance along the ray between any two reflections is bounded. For a strictly convex obstacle there are no multiply reflected rays.

## 6.2 The scattering matrix

We will now study the various different methods used to define a linear operator known as the scattering matrix, and discuss the relationship between the different scattering matrices so defined.

### 6.2.1 Physically-motivated definition

Let $\psi$ be a solution of (6.1), and suppose the far field of $\psi$ in polar coordinates[2] $(r, \boldsymbol{\theta})$ , is of the form

$$\psi(r, \boldsymbol{\theta}) \sim r^{-\left(\frac{n-1}{2}\right)} e^{ikr} a(\boldsymbol{\theta}) + r^{-\left(\frac{n-1}{2}\right)} e^{-ikr} b(\boldsymbol{\theta}), \tag{6.2}$$

so that it consists of an outgoing cylindrical wave with radiation pattern $a(\boldsymbol{\theta})$, and an incoming cylindrical wave with radiation pattern $b(\boldsymbol{\theta})$. Such a cylindrical incoming field is not commonplace in studies of diffraction, but may be constructed by considering a Herglotz wave function [31], which is of the form

$$\psi_g(\boldsymbol{x}; k) \;=\; \int_{S^{n-1}} e^{ik\boldsymbol{x}.\boldsymbol{\omega}} g(\boldsymbol{\omega}) d\boldsymbol{\omega} \;=\; \int_{S^{n-1}} e^{ikr\boldsymbol{\theta}.\boldsymbol{\omega}} g(\boldsymbol{\omega}) d\boldsymbol{\omega} \tag{6.3}$$

for some function $g(\boldsymbol{\theta})$. This is clearly a solution of the Helmholtz equation in free space, and it is possible to find its leading-order asymptotic behaviour, for large radial distance

[1] This differs from the usual convention for mathematical scattering theory, where the fields have time-dependence of the form $e^{i\omega t}$, and $\lambda$ is used instead of $k$. However, despite this fact, the plane waves considered are of the form $e^{i\lambda\boldsymbol{\omega}.\boldsymbol{x}}$ (where the vectors are generally printed in ordinary, rather than bold type), for which the direction of propagation is now $-\boldsymbol{\omega}$. Such notational differences are essentially trivial, but it can become relatively difficult to translate between the two systems.

[2] In this section we wish not to restrict ourselves to a specific number of dimensions, and so consider the angle $\boldsymbol{\theta}$ to be a vector of unit length in $\mathbb{R}^n$. The set of all such vectors in $\mathbb{R}^n$ is known as the unit sphere, and denoted by $S^{n-1}$. Our position vector $\boldsymbol{x} \in \mathbb{R}^n$ is then related to these polar coordinates by $\boldsymbol{x} = r\boldsymbol{\theta}$

$r$, by the method of stationary phase. The exponent has stationary points at $\boldsymbol{\omega} = \pm\boldsymbol{\theta}$, and so we find that

$$\psi_g(\boldsymbol{x}; k) \quad \sim \quad \left(\frac{2\pi}{kr}\right)^{\frac{n-1}{2}} \left(e^{ikr} e^{-\frac{\pi i}{4}(n-1)} g(\boldsymbol{\theta}) + e^{-ikr} e^{\frac{\pi i}{4}(n-1)} g(-\boldsymbol{\theta})\right), \tag{6.4}$$

as $r \to \infty$. If we choose $g(\boldsymbol{\theta})$ such that

$$g(\boldsymbol{\theta}) = \left(\frac{k}{2\pi}\right)^{\frac{n-1}{2}} e^{-\frac{\pi i}{4}(n-1)} b(-\boldsymbol{\theta}), \tag{6.5}$$

then the far-fields of $\psi$ and $\psi_g$ have the same incoming radiation pattern. In fact, this ensures that $\psi - \psi_g$ satisfies an outgoing radiation condition, and this is a sufficient condition for $\psi$ to be unique (see, for instance [133]). Therefore, for any given incoming radiation pattern $b(\boldsymbol{\theta})$ there is an unique solution $\psi$, and by examining the far field of $\psi$ we may determine $a(\boldsymbol{\theta})$. In the particular case where no scatterer is present, $\psi$ must in fact be identically equal to $\psi_g$, and so

$$a(\boldsymbol{\theta}) = e^{-\frac{\pi i}{2}(n-1)} b(-\boldsymbol{\theta}). \tag{6.6}$$

Since there is a unique outgoing field for each choice of incoming field, and the problem is linear, there exists a linear operator $\mathcal{S}^P(k)$ such that

$$a \quad = \quad \mathcal{S}^P(k)\, b. \tag{6.7}$$

This operator is known as the absolute scattering matrix[3]. (Some authors use the notation $A_H$ rather than $\mathcal{S}^P$ for this operator.) When there is no obstacle present we see from (6.6) that the absolute scattering operator in free space $\mathcal{S}_0^P$ is

$$\mathcal{S}_0^P(k) \quad = \quad e^{-\frac{\pi i}{2}(n-1)} \mathcal{R}, \tag{6.8}$$

where $\mathcal{R}$ denotes reflection on $S^{n-1}$, that is

$$\mathcal{R}\phi(\boldsymbol{\xi}) \quad = \quad \phi(-\boldsymbol{\xi}), \tag{6.9}$$

for all functions $\phi(\boldsymbol{\xi})$.

To find $\mathcal{S}^P$ explicitly when an obstacle is present (this analysis follows [47]) we will consider the functions $\psi_+(\boldsymbol{x}, \boldsymbol{\omega}; k)$ defined as follows. For each unit vector $\boldsymbol{\omega}$, $\psi_+(\boldsymbol{x}, \boldsymbol{\omega}; k)$ is the solution to the exterior Helmholtz problem, with a plane wave $e^{ik\boldsymbol{\omega}.\boldsymbol{x}}$ incident upon

[3]This is not, in fact, a matrix except in the one-dimensional case. However, the term scattering operator is used for a different linear operator, which we will discuss very briefly in the next section.

the obstacle, and outgoing radiation conditions at infinity. The far fields of such solutions are of the form

$$\psi_+ \quad \sim \quad e^{ik\boldsymbol{\omega}.\boldsymbol{x}} + r^{-\left(\frac{n-1}{2}\right)} e^{ikr} A_+(\boldsymbol{\theta}, \boldsymbol{\omega}; k), \tag{6.10}$$

where the function $A_+(\boldsymbol{\theta}; \boldsymbol{\omega}; k)$ is known as the directivity, diffraction coefficient, scattering amplitude or radiation pattern.

In a distributional sense

$$\begin{aligned} \psi_+(r\boldsymbol{\theta}, \boldsymbol{\omega}; k) \quad \sim \quad & \left(\frac{2\pi}{k}\right)^{\frac{n-1}{2}} \left( r^{-\left(\frac{n-1}{2}\right)} e^{ikr} e^{-\frac{\pi i}{4}(n-1)} \delta_{\boldsymbol{\omega}}(\boldsymbol{\theta}) + r^{-\left(\frac{n-1}{2}\right)} e^{-ikr} e^{\frac{\pi i}{4}(n-1)} \delta_{-\boldsymbol{\omega}}(\boldsymbol{\theta}) \right) \\ & + r^{-\left(\frac{n-1}{2}\right)} e^{ikr} A_+(\boldsymbol{\theta}, \boldsymbol{\omega}; k) \end{aligned} \tag{6.11}$$

for large $r$, where $\delta_{\boldsymbol{\omega}}(\boldsymbol{\xi})$ is the delta function on the unit sphere, defined by

$$\int_{S^{n-1}} \delta_{\boldsymbol{\omega}}(\boldsymbol{\xi}) \phi(\boldsymbol{\xi}) d\boldsymbol{\xi} \quad = \quad \phi(\boldsymbol{\omega}) \tag{6.12}$$

for any smooth function $\phi$. This expression for $\psi_+$ comes from consideration of the action of $e^{ikr\boldsymbol{\theta}.\boldsymbol{\omega}}$ upon a smooth function for large $r$, which is the same calculation we performed earlier to find the far field expansion of $\psi_g$. Examining the incoming and outgoing parts of the far field of $\psi_+$, we see it must be the case that

$$\mathcal{S}^P(k) \left(\delta_{\boldsymbol{\omega}}(\boldsymbol{\xi})\right) \quad = \quad e^{-\frac{\pi i}{2}(n-1)} \delta_{-\boldsymbol{\omega}}(\boldsymbol{\xi}) + \left(\frac{k}{2\pi}\right)^{\frac{n-1}{2}} e^{-\frac{\pi i}{4}(n-1)} A_+(\boldsymbol{\xi}, -\boldsymbol{\omega}, k). \tag{6.13}$$

Thus, since $\mathcal{S}^P(k)$ is a linear operator,

$$\mathcal{S}^P(k) \quad = \quad e^{-\frac{\pi i}{2}(n-1)} \mathcal{R} + \left(\frac{k}{2\pi}\right)^{\frac{n-1}{2}} e^{-\frac{\pi i}{4}(n-1)} \mathcal{A}\mathcal{R}, \tag{6.14}$$

where $\mathcal{A}$ is the integral operator with kernel $A(\boldsymbol{\xi}, \boldsymbol{\omega}, k)$, that is

$$\mathcal{A}\phi(\boldsymbol{\xi}) \quad = \quad \int_{S^{n-1}} A_+(\boldsymbol{\xi}, \boldsymbol{\omega}, k) \phi(\boldsymbol{\omega}) d\boldsymbol{\omega} \tag{6.15}$$

for any function $\phi(\boldsymbol{\xi})$. Alternatively, to find the scattering matrix we could use (6.5) to find the Herglotz function $\psi_g$ which has the desired incoming far-field pattern $b(\boldsymbol{\theta})$. This function $\psi_g$ can be considered as a linear combination of plane waves, and so by the linearity of the problem we could find the outgoing far field in terms of the $A_+$. This method is essentially equivalent to that above.

We note here that the operator

$$\left(\frac{k}{2\pi}\right)^{\frac{n-1}{2}} e^{-\frac{\pi i}{4}(n-1)} \mathcal{A}\mathcal{R} \tag{6.16}$$

(or sometimes its kernel) is sometimes known as the relative scattering matrix, and denoted by $A'_H$.

### 6.2.2 Lax and Phillips's definition

Lax and Phillips take a considerably more abstract approach towards defining the scattering matrix in their theory [80], as they are interested in its application to the time domain problem, and also for problems other than the wave equation. Unfortunately this results in an operator with slightly different form to that considered above, and it is the scattering matrix defined by their method whose properties have been examined subsequently. However, we will find that the two definitions result in very similar explicit forms for the scattering matrix.

For the time-dependent[4] problem, we consider the set of initial data $f = \{f_1, f_2\}$ for functions $f_1$ and $f_2$ defined outside the obstacle. Then there exists a unique solution $\phi(\boldsymbol{x}, t)$ to the initial value problem $\phi(\boldsymbol{x}, 0) = f_1$, $\phi_t(\boldsymbol{x}, 0) = f_2$. We may then consider the operators $U(t)$ (for some real $t$), which take initial data at time 0 to initial data at time $t$. These conserve energy (provided we impose suitable boundary conditions on the obstacle). We can also define the operators $U_0(t)$, which are the same as $U(t)$, but for the wave equation in the absence of the obstacle. In order to define the scattering operator Lax and Phillips [80] define the wave operators $W_+$ and $W_-$ by

$$W_\pm f = \lim_{t \to \pm\infty} U(-t)U_0(t) \tag{6.17}$$

and the scattering operator $S$ is then defined by $S = W_+^{-1}W_-$. It can be found [80] that $U(t)f$ tends to $U_0(t)W_-^{-1}f$ as $t \to -\infty$, and to $U_0(t)W_+^{-1}f$ as $t \to \infty$. Therefore the scattering operator relates the behaviour of a solution of the initial value problem for large negative times to its behaviour for large positive times.

We note here that there are some differences between the problem in even and odd dimensions, related to the different properties of the time-dependent problem (Huygens' principle does not hold in two dimensions). For the frequency-domain problem the scattering matrix can be defined in exactly the same manner in even and odd dimensions, but the scattering matrix (and so the scattering phase), when considered as a function of $k$, will have a branch cut along the negative real $k$ axis.

Lax and Phillips [80] then proceed to relate this to the frequency domain problem by a rather abstract route, and we will simply consider the explicit definitions. We consider the functions $\psi_+(\boldsymbol{x}, \boldsymbol{\omega}, k)$ as introduced before. We may similarly construct a related family $\psi_-$, which are defined as for the $\psi_+$ except that, whereas $\psi_+ - e^{ik\boldsymbol{x}.\boldsymbol{\omega}}$ is purely outgoing, $\psi_- - e^{ik\boldsymbol{x}.\boldsymbol{\omega}}$ has a purely incoming far-field. Thus, for large $r$,

$$\psi_-(\boldsymbol{x}, \boldsymbol{\omega}; k) \quad \sim \quad e^{ik\boldsymbol{x}.\boldsymbol{\omega}} + A_-(\boldsymbol{\theta}, \boldsymbol{\omega}; k)\frac{e^{-ikr}}{r^{\frac{n-1}{2}}}. \tag{6.18}$$

[4] In this chapter we will choose $c$ to be 1 for the time-dependent problem.

These solutions $\psi_+$ and $\psi_-$ are sometimes referred to as distorted plane waves.

For arbitrary initial data $f$, we consider the functions $\tilde{f}_\pm(\omega)$

$$\tilde{f}_\pm(\boldsymbol{\omega}) = \langle f(\boldsymbol{x}), \psi_\mp(\boldsymbol{x}, \boldsymbol{\omega}; k)\rangle_E \tag{6.19}$$

$$= \frac{1}{2}\int_{\mathbb{R}^n - \Omega} \left\{ \boldsymbol{\nabla} f_1(\boldsymbol{x}).\overline{\boldsymbol{\nabla}\psi_\mp(\boldsymbol{x}, \boldsymbol{\omega}; k)} + f_2(\boldsymbol{x})\overline{(-ik\psi_\mp(\boldsymbol{x}, \boldsymbol{\omega}; k))} \right\} d\boldsymbol{x} \tag{6.20}$$

where the angled brackets denote the inner product on the space of initial data for the wave equation, related to the energy norm. Lax and Phillips' [80] definition of the scattering matrix, which we will denote $\mathcal{S}^L(k)$, is that map from $L^2(S^{n-1})$ to $L^2(S^{n-1})$ for which

$$\tilde{f}_+(\boldsymbol{\omega}) = \mathcal{S}^L(k)\tilde{f}_-(\boldsymbol{\omega}). \tag{6.21}$$

It is not obvious that such a map should exist, so we will paraphrase Lax and Phillips' derivation of the explicit form of the scattering matrix, which additionally shows that (6.21) is a valid definition. Assume for the moment that the scattering matrix is of the form $\mathcal{S}^L = I + T$, where $I$ is the identity, and $T$ an integral operator with kernel $K(\boldsymbol{\xi}, \boldsymbol{\omega}; k)$. Then Lax and Phillips show that the desired operator has the property that

$$\psi_-(\boldsymbol{x}, \boldsymbol{\xi}; k) \;=\; \psi_+(\boldsymbol{x}, \boldsymbol{\xi}; k) + \int_{S^{n-1}} \overline{K(\boldsymbol{\xi}, \boldsymbol{\omega}; k)}\psi_+(\boldsymbol{x}, \boldsymbol{\omega}; k) d\boldsymbol{\omega}. \tag{6.22}$$

We need this to hold for all $\boldsymbol{x}$, so we may replace the $\psi_\pm$ with their asymptotic expansions for large $r$, and then our condition is that

$$A_-(\boldsymbol{\theta}, \boldsymbol{\xi}; k)\frac{e^{-ikr}}{r^{\frac{n-1}{2}}} - A_+(\boldsymbol{\theta}, \boldsymbol{\xi}; k)\frac{e^{ikr}}{r^{\frac{n-1}{2}}} \;\sim\; \int \overline{K(\boldsymbol{\xi}, \boldsymbol{\omega}; k)} \left\{ e^{ikr\boldsymbol{\theta}.\boldsymbol{\omega}} + A_+(\boldsymbol{\theta}, \boldsymbol{\omega}; k)\frac{e^{ikr}}{r^{\frac{n-1}{2}}} \right\} d\boldsymbol{\omega} \tag{6.23}$$

in the limit as $r \to \infty$. As before, by the method of stationary phase,

$$\int_{S^{n-1}} \overline{K(\boldsymbol{\xi}, \boldsymbol{\omega}; k)} e^{ikr\boldsymbol{\theta}.\boldsymbol{\xi}} d\boldsymbol{\xi} \;\sim\; \left(\frac{2\pi}{kr}\right)^{\frac{n-1}{2}} \left( e^{ikr} e^{-\frac{\pi i}{4}(n-1)} \overline{K(\boldsymbol{\xi}, \boldsymbol{\theta}; k)} + e^{-ikr} e^{\frac{\pi i}{4}(n-1)} \overline{K(\boldsymbol{\xi}, -\boldsymbol{\theta}; k)} \right) \tag{6.24}$$

for large $r$. If (6.22) is to hold, then both the $e^{ikr}$ and $e^{-ikr}$ dependent parts of the far field of (6.23) must vanish. Just considering the $e^{-ikr}$ dependent terms, we see that we require that

$$A_-(\boldsymbol{\theta}, \boldsymbol{\xi}; k) \;=\; \left(\frac{2\pi}{k}\right)^{\frac{n-1}{2}} e^{\frac{\pi i}{4}(n-1)} \overline{K(\boldsymbol{\xi}, -\boldsymbol{\theta}; k)}, \tag{6.25}$$

so the kernel must be of the form

$$K(\boldsymbol{\xi}, \boldsymbol{\omega}; k) \;=\; \left(\frac{ik}{2\pi}\right)^{\frac{n-1}{2}} \overline{A_-(\boldsymbol{\xi}, -\boldsymbol{\omega}; k)}. \tag{6.26}$$

We have not shown that such a kernel does in fact yield condition (6.22). However, consider the function

$$\psi \quad = \quad \psi_-(\boldsymbol{x},\boldsymbol{\omega};k) - \psi_+(\boldsymbol{x},\boldsymbol{\omega};k) - \int \overline{K(\boldsymbol{\xi},\boldsymbol{\omega};k)}\psi_+(\boldsymbol{x},\boldsymbol{\omega};k)d\boldsymbol{\omega}. \tag{6.27}$$

Then $\psi$ satisfies the Helmholtz equation and the boundary equations, but has no outgoing part. For all real $k$ (and all but a countable number of complex $k$) it follows by uniqueness that $\psi$ must be identically zero. Hence the identity (6.22) does indeed hold.

We now wish to write this kernel in terms of $A_+$. We note that

$$\psi_+(\boldsymbol{x},\omega;k) = \overline{\psi_-(\boldsymbol{x},-\boldsymbol{\omega};k)}, \tag{6.28}$$

so

$$A_+(\boldsymbol{\theta},\boldsymbol{\omega};k) = \overline{A_-(\boldsymbol{\theta},-\boldsymbol{\omega};k)}, \tag{6.29}$$

and using this identity we find that

$$K(\boldsymbol{\xi},\boldsymbol{\omega};k) = \left(\frac{ik}{2\pi}\right)^{\frac{n-1}{2}} A_+(\boldsymbol{\xi},\boldsymbol{\omega};k) \tag{6.30}$$

Note that this formula differs from that of Lax and Phillips [80], and also of other workers, as we have both written the matrix in the appropriate form for $e^{-i\omega t}$ time dependence, and the integral operator consists of an integration over the second variable in the kernel, rather than the first.

The operator $\mathcal{S}^L$ does not initially appear related to the physical problem, especially as the functions $\psi_-$ are not realisable in practice. By directly comparing their explicit forms, we see that

$$\mathcal{S}^P(k) \quad = \quad \mathcal{S}^L(k)e^{-\frac{\pi i}{2}(n-1)}\mathcal{R}, \tag{6.31}$$

and so $\mathcal{S}^L = \mathcal{S}^P(\mathcal{S}_0^P)^{-1}$. If we let $a(\boldsymbol{\theta})$ be an arbitrary incoming radiation pattern, $b_0(\boldsymbol{\theta})$ be the corresponding outgoing radiation in free space, and $b(\boldsymbol{\theta})$ be the outgoing radiation pattern with the obstacle present, then

$$b(\boldsymbol{\theta}) = \mathcal{S}^L b_0(\boldsymbol{\theta}). \tag{6.32}$$

We see from this that $\mathcal{S}^L$ is a measure of the effect of the obstacle on the exterior Helmholtz problem.

### 6.2.3 High frequency approximation of the scattering matrix

We now wish briefly to discuss the approximation of the scattering matrix for large $k$; in the physics literature this is referred to as the semi-classical approximation. One useful technique (for a bounded obstacle), noted in [38] and [36], is to expand the fields in terms of cylindrical harmonics; this is equivalent to considering the Fourier series of the incoming and outgoing directivities $a(\boldsymbol{\theta})$ and $b(\boldsymbol{\theta})$. When we do this to the fields themselves we note that, for large but finite $k$, there are only a finite number of modes which are substantially affected by the presence of the obstacle (as $H_n^{(1)}(r)$ and $H_n^{(2)}(r)$ are exponentially small for large $n$ and $r < n$). This approximation of the scattering matrix is then a finite matrix, and it is far easier to consider the properties of such a matrix than an (infinite) operator. It is also possible to obtain a reasonably simple expression for the elements of the (approximate) scattering matrix by this method [36].

The directivity $A_+(\boldsymbol{\theta}, \boldsymbol{\omega}; k)$ can be approximated by the ray methods of Chapter 3. For $\boldsymbol{\theta} \not\simeq \boldsymbol{\omega}$ the dominant contribution will be from reflected rays, and as the obstacle is convex there is a single such ray path. There are also exponentially small contributions from creeping rays. However for $\boldsymbol{\theta} \simeq \boldsymbol{\omega}$ (that is, the forward scattering direction) we find that we are within the transition regions of the tangency points, and for $\boldsymbol{\theta} = \boldsymbol{\omega}$ we are in fact within the shadow boundary regions. For $r \gg k$ it is found that the shadow boundaries from all points on the horizon merge, as discussed in [140], [30]. In order to find the leading-order directivity in this region we must, in fact, consider the shadow boundary fields to higher order than that discussed in Chapter 3. In the three-dimensional case there may be additional complications in this direction, as we note that, in the case of axial incidence upon an axisymmetric body, the forwards scattering direction is a caustic of the fields.

We will be interested in determining the behaviour of the eigenvalues of the scattering matrix as the wavenumber varies. However, it is not clear how to directly obtain these eigenvalues from the above high-frequency approximation of the scattering matrix. Instead, we will study the properties of these eigenvalues by defining a function known as the scattering phase. We will be able to find the derivative of this function in terms of integrals over the surface of the scatterer of those solutions obtained when a plane wave is incident upon the scatterer. These integrals may then be approximated for large $k$ using the asymptotic results outlined in Chapter 3.

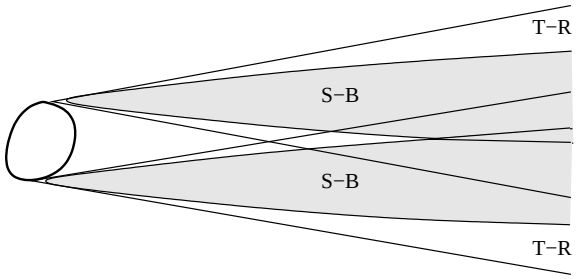


**Figure 6.1:** Far-field of a compact obstacle, showing the merging of the shadow boundary and transition regions far from the obstacle. The parabolic shadow boundary regions are shaded (and indicated by S-B), and the transition regions to either side of each of the shadow boundary regions (indicated by T-R). In the two dimensional case the fields in the merged region are just the sum of those due to the upper and lower tangency regions. In the three dimensional case there may be an axial caustic of the rays.

## 6.3 Large-wavenumber asymptotics of the scattering phase

Using the relative scattering matrix $\mathcal{S}^L$ we may define a function known as the scattering phase. It has been shown, for a wide class of obstacles [131], that the asymptotic behaviour of this function agrees to leading order with the asymptotic behaviour of the counting function for the number of eigenvalues of the Helmholtz equation in the interior of the obstacle.

In the case of a strictly convex obstacle it was conjectured by [24] that the first two terms in the expansion of the scattering phase with Dirichlet boundary conditions agree with the first two terms for the interior eigenvalues with Neumann boundary conditions. This motivated [92] and [107], to find the first two terms in the expansion of the scattering phase with Dirichlet boundary conditions. However, the method of proof in these works is rather theoretical, drawing on the work of [64], and involves relating the asymptotic behaviour of the scattering phase to various results regarding the kernel of the heat equation. Instead we will follow the route begun in [89], and express the derivative of the scattering phase in terms of an integral over the surface of the scatterer of the functions $\psi_+$ considered earlier. For large $k$ we may approximate these functions, and so obtain the first two terms of the asymptotic behaviour of the scattering phase in a reasonably straightforward manner.

### 6.3.1 The scattering phase

Here we intend to briefly state some of the properties of the scattering matrix needed to define the scattering phase; for proofs see [80], [89]. For both Dirichlet and Neumann boundary conditions on the obstacle, it is possible to show that $\mathcal{S}^L(k)$ is a unitary operator for all real $k$. This means that that $\mathcal{S}^L(\mathcal{S}^L)^* = (\mathcal{S}^L)^*\mathcal{S}^L = I$, where $(\mathcal{S}^L)^*$ is the adjoint operator to $\mathcal{S}^L$. All the eigenvalues of $\mathcal{S}^L$ are therefore of unit modulus, and so of the form $e^{-i\beta_j(k)}$ for real-valued $\beta_j(k)$. These $\beta_j$ are known as the phase shifts of the problem. If we let $f_j(\boldsymbol{\theta})$ be an eigenfunction of $\mathcal{S}^L$, with associated phase shift $\beta_j$, and consider the Herglotz wave function $\psi_{f_j}$ incident upon our obstacle, then the outgoing far field pattern is found to be $e^{-i\beta_j(k)}$ times that which would be expected were the obstacle not present.

We will define the scattering phase[5]

$$s(k) \quad = \quad \frac{i}{2\pi}\log\det\mathcal{S}^L(k). \tag{6.33}$$

As $\mathcal{T}(k) = \mathcal{S}^L - \mathcal{I}$ is an integral operator of trace class[6], it can be found that the scattering phase function is related to the phase shifts by

$$s(k) \quad = \quad \frac{1}{2\pi}\sum_j \beta_j(k) \pmod{2\pi}. \tag{6.34}$$

### 6.3.2 Exact calculation for a circular scatterer

In this part we will calculate the exact scattering phase for a circular obstacle in two dimensions. We will then find the asymptotic behaviour of the scattering phase for large wavenumber.

Let the obstacle be the disk $r \leq 1$. The Helmholtz equation is separable in polar coordinates, and has solutions of the form

$$\psi_n \quad = \quad \left(a_n H_n^{(1)}(kr) + b_n H_n^{(2)}(kr)\right) e^{in\theta}, \tag{6.35}$$

[5]By choosing the time-dependence to be of the form $e^{-i\omega t}$, we find that our scattering matrix (as a function of $k$) is the Schwartz reflection in the real axis of that obtained for $e^{i\omega t}$ time-dependence. In the definition (6.33) we therefore define the phase shifts and scattering phase with the other sign to that in [93], and we then find that the scattering phase agrees with that for the other form of time-dependence. We also choose to divide the scattering phase by $2\pi$, in order to emphasise the similarity between it and the counting function for the interior eigenvalues.

[6]A trace class operator [116] is a bounded operator $\mathcal{T}$ such that, for any orthonormal system $\{\phi_j | j \in J\}$, we have $\sum_{j\in J} |< \mathcal{T}\phi_j, \phi_j >| < \infty$.

for integer $n$, and constants $a_n$ and $b_n$. These solutions will satisfy the Dirichlet boundary condition on $r = 1$ provided that

$$a_n H_n^{(1)}(k) + b_n H_n^{(2)}(k) = 0. \tag{6.36}$$

Expanding the Hankel functions for large $r$ we see that

$$\psi_n \sim \sqrt{\frac{2}{\pi k r}} \left( a_n e^{ikr - \frac{n\pi i}{2} - \frac{\pi i}{4}} + b_n e^{-ikr + \frac{n\pi i}{2} + \frac{\pi i}{4}} \right) e^{in\theta}, \tag{6.37}$$

and so, by examining the incoming and outgoing parts of the far field and using the definition of the absolute scattering matrix $\mathcal{S}^P$, we find that

$$a_n e^{-\frac{n\pi i}{2} - \frac{\pi i}{4}} e^{in\theta} = \mathcal{S}^P(k) b_n e^{\frac{in\pi}{2} + \frac{\pi i}{4}} e^{in\theta}. \tag{6.38}$$

Using the relationship (6.31) between the two definitions of the scattering matrix we have

$$a_n e^{in\theta} = \mathcal{S}^L(k) b_n e^{in\theta}. \tag{6.39}$$

Therefore the functions $e^{in\theta}$ are a complete basis of eigenfunctions for the Lax-Phillips scattering matrix, and have associated eigenvalues and phase shifts

$$\lambda_n(k) = \frac{a_n}{b_n} = -\frac{H_n^{(2)}(k)}{H_n^{(1)}(k)}, \qquad \beta_n(k) = \frac{1}{i} \log \left( -\frac{H_n^{(2)}(k)}{H_n^{(1)}(k)} \right). \tag{6.40}$$

We may use these to find an exact expression for the scattering phase

$$s(k) = \frac{i}{2\pi} \sum_{-\infty}^{\infty} \log \left( -\frac{H_n^{(2)}(k)}{H_n^{(1)}(k)} \right). \tag{6.41}$$

We wish to compute the asymptotic expansion of this sum in the limit $k \gg 1$. Despite the fact that $k$ is big, in the sum $n$ becomes arbitrarily large, so we cannot simply replace all the Hankel functions by their expansions for large argument. Instead we must apply the expansions of Debye type [3]. Bessel's equation has a turning point at $n = k$, so the Debye expansions have different forms on each side of this point. For $0 \leq n < k$ we may use the approximation

$$\frac{H_n^{(2)}(n \sec \gamma)}{H_n^{(1)}(n \sec \gamma)} \sim \exp \left\{ -2i \left( n \tan \gamma - n\gamma - \frac{\pi}{4} \right) \right\}, \tag{6.42}$$

which is valid for $0 < \gamma < \frac{\pi}{2}$. For $n > k$ we must first use the fact that

$$\frac{H_n^{(2)}(k)}{H_n^{(1)}(k)} = \frac{J_n(k) - iY_n(k)}{J_n(k) + iY_n(k)}, \tag{6.43}$$

and then the appropriate Debye-type expansions for $J_n(k)$ and $Y_n(k)$ are

$$J_n(n\,\mathrm{sech}\,\alpha) \sim \frac{e^{n(\tanh\alpha-\alpha)}}{\sqrt{2\pi n\tanh\alpha}} \qquad Y_n(n\,\mathrm{sech}\,\alpha) \sim -\frac{2e^{n(\alpha-\tanh\alpha)}}{\sqrt{2\pi n\tanh\alpha}}. \tag{6.44}$$

From these we have that if $n > k$ then $Y_n(k)$ is exponentially large compared with $J_n(k)$, and so $\beta_n(k)$ is exponentially small, and this allows us to ignore these terms in the sum. The expansions for the Bessel and Hankel functions are not valid for $k$ within $\mathcal{O}(n^{\frac{1}{3}})$ of the turning point at $k = n$, but omitting these terms in the sum will again yield an error which is small compared with $k$.

When we rearrange our sum, and apply the above approximation for the phase shifts, we find that

$$\begin{aligned}\sum_{n=-\infty}^{\infty}\beta_n(k) &= 2\sum_{n=0}^{\infty}\beta_n(k) - \beta_0(k)\\ &\sim \left\{2i\sum_{n=0}^{k}\log\left(-e^{-2i(n\tan\gamma-n\gamma-\frac{\pi}{4})}\right)\right\} - (2k+\frac{\pi}{2})\\ &= 4k\left\{\sum_{n=0}^{k}\cos\gamma\,(\tan\gamma-\gamma)\right\} + \pi(k+1) - (2k+\frac{\pi}{2})\end{aligned} \tag{6.45}$$

where $\gamma$ is given by $k = n\sec\gamma$, with $0 < \gamma < \frac{\pi}{2}$. We now approximate the sum remaining by the trapezium rule for integration, and this gives us that

$$\begin{aligned}\sum_{n=0}^{k}\cos\gamma(\tan\gamma-\gamma) &\sim \frac{1}{2} + \int_0^k \cos\gamma(\tan\gamma-\gamma)\,dn + \mathcal{O}(k^{-1})\\ &= \frac{k\pi}{8} + \frac{1}{2} + \mathcal{O}(k^{-1}).\end{aligned} \tag{6.46}$$

Therefore the asymptotic behaviour of our scattering phase is

$$s(k) = \frac{1}{2\pi}\sum_{n=-\infty}^{\infty}\beta_n(k) \sim \frac{k^2}{4} + \frac{k}{2} + \mathcal{O}(1). \tag{6.47}$$

### 6.3.3 An integral formula for the scattering phase

We now wish to summarise the results of Helton, Majda and Ralston [53], [109] and [89], which express the derivative of the scattering phase in terms of integrals of the functions $\psi_+$ over the surface of the obstacle. As the scattering matrix is in the form $\mathcal{S}^L(k) = \mathcal{I} + \mathcal{T}(k)$, where $\mathcal{T}$ is of trace class, it is known [51] that

$$\frac{d}{dk}\log\det\mathcal{S}^L(k) = -\mathrm{Tr}\left(\mathcal{S}^L(k)\frac{d\mathcal{S}^{L*}(k)}{dk}\right) \tag{6.48}$$

and so

$$\frac{ds}{dk}(k) \quad = \quad -\frac{i}{2\pi}\,\mathrm{Tr}\left(\mathcal{S}^L(k)\frac{d\mathcal{S}^{L*}(k)}{dk}\right). \tag{6.49}$$

We wish to compute the kernel of $\mathcal{S}^L\frac{d\mathcal{S}^{L*}}{dk}$ (for a star-shaped obstacle various properties of this operator can be proved [109]), from which we can calculate the trace of the operator and so the behaviour of the scattering phase.

Here we summarise [53], specialising to the case of an obstacle in a medium of constant refractive index. We find an expression for the directivity of the problem where a plane wave is incident upon the obstacle in terms of integrals of the field. Let the $\psi_+$ be as defined previously, and set $U(x,w;k)=\psi_+(x,w;k)-e^{ikx.w}$. By a stationary phase expansion very similar to those employed before, they found that

$$c_k A_+(-\boldsymbol{\omega},\boldsymbol{\xi};k) = J = \lim_{r\to\infty}\int_{|x|=r} U(\boldsymbol{x},\boldsymbol{\xi};k)\frac{\partial e^{ik\boldsymbol{x}.\boldsymbol{\omega}}}{\partial n} - e^{ik\boldsymbol{x}.\boldsymbol{\omega}}\frac{\partial}{\partial n}U(\boldsymbol{x},\boldsymbol{\xi};k)dS \tag{6.50}$$

where $c_k = 2^{\frac{n+1}{2}}\pi^{\frac{n-1}{2}}e^{\frac{\pi i(n-3)}{4}}k^{-\frac{n-3}{2}}$. Using (6.30) we may therefore find the kernel $K_T$ of $\mathcal{T}(k)=\mathcal{S}^L(k)-\mathcal{I}$ to be

$$K_T(-\boldsymbol{\omega},\boldsymbol{\xi};k) = \left(\frac{ik}{2\pi}\right)^{\frac{n-1}{2}}\frac{1}{c_k}J. \tag{6.51}$$

Unfortunately, we need the kernel of $\frac{d\mathcal{S}^*}{dk}$, and directly differentiating the above integral with respect to the wavenumber is not at all straightforward. However, we can use the fact noted in [53] that if $\phi(\boldsymbol{x})$ is a solution to the Helmholtz equation with wavenumber $\lambda k$ outside an obstacle $\Omega$, then $\phi(\frac{\boldsymbol{x}}{\lambda})$ satisfies the Helmholtz equation with wavenumber $k$ outside an obstacle $\lambda\Omega=\{\lambda x \mid x\in\Omega\}$. If we consider the series of problems parametrised by a variable $t$, with fixed $k$ but varying obstacle $\Omega(t)=t\,\Omega$, then the operator $K_T$ for $\lambda=1$ and $k=k_1$ is the same as the operator $K_T$ with $\lambda=\frac{k_1}{k_0}$ and $k=k_0$, and so we find that

$$\frac{\partial K_T}{\partial k} \quad = \quad \frac{1}{k}\frac{\partial K_T}{\partial t}. \tag{6.52}$$

We now need to calculate the variation of $K$ for fixed $k$ and varying $t$ (that is, varying the boundary but not the wavenumber). From (6.50) we find that

$$\frac{\partial K_T}{\partial t}(-\boldsymbol{\omega},\boldsymbol{\xi};k) = \left(\frac{ik}{2\pi}\right)^{\frac{n-1}{2}}\frac{1}{c_k}\frac{\partial J}{\partial t} \tag{6.53}$$

and so we simply need to find $\frac{\partial J}{\partial t}$. By differentiating (6.50) with respect to $s$ for fixed $r$ (where $r$ is much larger than the diameter of the obstacle), and then using Green's theorem to deform the surface integral to the boundary of the obstacle, we find that

$$\frac{\partial J}{\partial t} = \int_{\partial\Omega}\frac{\partial U}{\partial t}(\boldsymbol{x},\boldsymbol{\xi};k)\frac{\partial}{\partial n}\left(e^{ik\boldsymbol{x}.\boldsymbol{\omega}}\right) - e^{ik\boldsymbol{x}.\boldsymbol{\omega}}\frac{\partial}{\partial n}\frac{\partial U}{\partial t}(\boldsymbol{x},\boldsymbol{\xi};k)dS. \tag{6.54}$$

By using the boundary conditions and another application of Green's theorem we find that

$$\frac{\partial J}{\partial t} = \int_{\partial\Omega} \frac{\partial U}{\partial t}(\boldsymbol{x}, \boldsymbol{\xi}; k) \frac{\partial \psi_+}{\partial n}(\boldsymbol{x}, \boldsymbol{\omega}; k) dS. \tag{6.55}$$

Differentiating the boundary condition with respect to $t$ we find that

$$\frac{\partial U}{\partial t}(\boldsymbol{x}, \boldsymbol{\xi}; k) = -(\boldsymbol{n}.\boldsymbol{x}) \frac{\partial \psi_+}{\partial n}(\boldsymbol{x}, \boldsymbol{\xi}; k), \tag{6.56}$$

and so

$$\frac{\partial K}{\partial k}(\boldsymbol{\xi}, \boldsymbol{\omega}; k) = -\left(\frac{ik}{2\pi}\right)^{\frac{n-1}{2}} \frac{1}{kc_n} \int_{\partial\Omega} \frac{\partial \psi_+}{\partial n}(-\boldsymbol{\xi}) \frac{\partial \psi_+}{\partial n}(\boldsymbol{\omega})(\boldsymbol{x}.\boldsymbol{n})\, dS. \tag{6.57}$$

The kernel of $\frac{d\boldsymbol{S}^{L*}}{dk}$ is the conjugate transpose of $\frac{\partial K_T}{\partial k}$, and so given by

$$\frac{i}{8\pi^2}\left(\frac{k}{2\pi}\right)^{n-3} \int_{\partial\Omega} \overline{\frac{\partial \psi_+}{\partial n}(\boldsymbol{\xi}) \frac{\partial \psi_+}{\partial n}(-\boldsymbol{\omega})} dS. \tag{6.58}$$

From our discussion of the Lax-Phillips definition of the scattering operator we recall (6.22), and so when $\psi_+(\boldsymbol{x}, \boldsymbol{\omega}; k)$ is considered as a function of $\boldsymbol{\omega}$ (for each fixed point $\boldsymbol{x}$) we find that

$$\mathcal{S}^L(k)\overline{\psi_+(\boldsymbol{x}, \boldsymbol{\xi}; k)} = \overline{\psi_-(\boldsymbol{x}, \boldsymbol{\xi}; k)} = \psi_+(\boldsymbol{x}, -\boldsymbol{\xi}; k). \tag{6.59}$$

As this holds for all $\boldsymbol{x}$ we can take the normal derivative of this relationship, and so by considering the composition of $\mathcal{S}^L$ and $\frac{dS^*}{dk}$ we find that

$$\mathrm{Tr}\left(\mathcal{S}^L(k)\frac{d\mathcal{S}^{L*}}{dk}\right) = \frac{i}{8\pi^2}\left(\frac{k}{2\pi}\right)^{n-3} \int_{S^{n-1}} \int_{\partial\Omega} (\boldsymbol{x}.\boldsymbol{n}) \left|\frac{\partial \psi_+(\boldsymbol{\omega})}{\partial n}\right|^2 dS d\boldsymbol{\omega}. \tag{6.60}$$

We therefore obtain the result

$$\frac{ds}{dk}(k) = \frac{1}{16\pi^3}\left(\frac{k}{2\pi}\right)^{n-3} \int_{S^{n-1}} \int_{\partial\Omega} (\boldsymbol{x}.\boldsymbol{n}) \left|\frac{\partial \psi_+}{\partial n}(\boldsymbol{\omega})\right|^2 dS d\boldsymbol{\omega}, \tag{6.61}$$

and as in [90] we will proceed to approximate this integral, and so obtain the asymptotic behaviour of the scattering phase.

### 6.3.4 Approximating the surface integral

The remainder of this section will involve finding approximations in the limit as $k \gg 1$ to the multiple integral (6.61). The functions $\psi_+$ comprising the integrand are just the solutions found when scalar plane waves are incident upon a strictly convex, smooth obstacle. Thus we may approximate their derivatives on the surface using the asymptotic framework outlined in [140].

The strict convexity of the body is important, as it means that each point on the surface can be considered to be either directly illuminated by the plane wave, or in the geometrical shadow of the body; there are no rays which after reflection from the surface intersect the scatterer again. Moreover, the problems of tangential incidence at a point on a body at which the curvature vanishes, and diffraction from a point where the curvature also changes sign are unsolved analytically to date.

We will interchange the order of integration, and first examine the inner integral

$$\int_{S^{n-1}} \left| \frac{\partial \psi_+}{\partial n}(\boldsymbol{x}, \boldsymbol{\omega}; k) \right|^2 d\boldsymbol{\omega} \tag{6.62}$$

at some fixed point $\boldsymbol{x}$ on $\partial\Omega$. As the body is smooth there are no points at which diffraction occurs because of a discontinuity in the tangent to the surface, or in its derivatives. We therefore expect that the expansion of this integral for large $k$ will have essentially the same form at every point, with the exact value depending only on the curvature and its derivatives at that point.

For the sake of simplicity we will initially consider the case of a two-dimensional obstacle. As in [89], by local geometrical optics considerations we find that the leading order approximation to the normal derivative of the field is given by

$$\frac{\partial \psi_+}{\partial n} \sim 2ik(\boldsymbol{n}.\boldsymbol{\omega})e^{ik\boldsymbol{\omega}.\boldsymbol{x}} \tag{6.63}$$

if the incident direction $\boldsymbol{\omega}$ is such that the point on the surface would be directly illuminated, and

$$\frac{\partial \psi_+}{\partial n} \simeq 0 \tag{6.64}$$

for those points in the geometrical shadow. Note that this is only the leading order term in the geometrical optics approximation; there are higher order terms which depend upon the curvature and its derivatives on the surface. As the body is convex and smooth it is easy to see that the point is directly illuminated if $\boldsymbol{\omega}.\boldsymbol{n} < 0$, and in shadow if $\boldsymbol{\omega}.\boldsymbol{n} > 0$. This approximation becomes invalid when the incident field is almost tangentially incident at $\boldsymbol{x}$ (in fact, when $\boldsymbol{\omega}.\boldsymbol{n} = \mathcal{O}(k^{-\frac{1}{3}}\kappa_0^{\frac{1}{3}})$), but as we will see shortly the contributions from these near-tangential directions yield higher-order corrections.

Using these approximations our inner integral becomes

$$\begin{aligned} \int_{S^1} \left| \frac{\partial \psi_+}{\partial n} \right|^2 d\boldsymbol{\omega} &\simeq \int_{\boldsymbol{\omega}.\boldsymbol{n}<0} 4k^2(\boldsymbol{\omega}.\boldsymbol{n})^2 d\boldsymbol{\omega} \\ &= 2\pi k^2 \end{aligned} \tag{6.65}$$

and this is independent of the point $\boldsymbol{x}$ chosen on the boundary. Thus we may substitute this into (6.61), and obtain

$$\begin{aligned}\frac{ds}{dk} &= \frac{1}{8\pi^2 k}\int_{\partial\Omega}(\boldsymbol{x}.\boldsymbol{n})\int_{S^{n-1}}\left|\frac{\partial\psi_+}{\partial n}\right|^2 d\boldsymbol{\omega}\; dS \\ &\sim \frac{k}{4\pi}\int_{\partial\Omega}(\boldsymbol{x}.\boldsymbol{n})\; dS \\ &= \frac{k}{4\pi}\int_{\Omega}\nabla.\boldsymbol{x}\; dV \\ &= \frac{k}{2\pi}\;\mathrm{Area}(\Omega). \end{aligned} \tag{6.66}$$

Integrating this, we find that

$$s(k) \;\sim\; \frac{k^2}{4\pi}\;\mathrm{Area}(\Omega) \tag{6.67}$$

for large $k$, and this agrees with the result (6.47) for the unit disk.

#### 6.3.4.1 $\mathcal{O}(k)$ correction from regions of near-tangential incidence

The calculation above only gives the leading order behaviour of the scattering phase. We will improve[7] upon the work of Majda and Ralston [89], by considering the contributions from those incident angles which are almost tangential to the surface at the point under consideration. At such angles of incidence, the geometrical optics approximation is invalid, and the point under consideration on the surface is within the Fock-Leontovich asymptotic region introduced in Section 3.1.4.1. From (3.47) we find that the normal derivative on the body of the solution for plane-wave incidence in this region is given by

$$\frac{\partial\psi_+}{\partial n} \;\simeq\; e^{ik\boldsymbol{x}.\boldsymbol{\omega}}k^{\frac{2}{3}}\kappa_0^{\frac{1}{3}}B(\hat{s}) \tag{6.68}$$

with

$$B(\hat{s}) \;=\; i\hat{s} - 2^{\frac{2}{3}}e^{\frac{2\pi i}{3}}e^{\frac{i\hat{s}^3}{6}}\int_{-\infty}^{\infty}\mathrm{Ai}(-2^{\frac{1}{3}}p)\frac{\mathrm{Ai}'(-2^{\frac{1}{3}}e^{\frac{2\pi i}{3}}p)}{\mathrm{Ai}(-2^{\frac{1}{3}}e^{\frac{2\pi i}{3}}p)}e^{-i\hat{s}p}d\hat{s}. \tag{6.69}$$

Here $s$ is the distance measured along the surface from the point of tangency (also known as the horizon) to $\boldsymbol{x}$, $\hat{s} = k^{\frac{1}{3}}\kappa_0^{\frac{2}{3}}s$ is the same distance but on the Fock-Leontovich length scale, and $\kappa_0(\boldsymbol{\omega})$ is the curvature of the body at the horizon. This formula is valid for $\hat{s} = \mathcal{O}(1)$, but we find that it matches with the leading-order term of the geometrical

[7] Majda and Ralston appear to estimate the order of magnitude of this contribution in [89]. However its value is not explicitly calculated, and the work is presented in the framework of micro-local analysis.

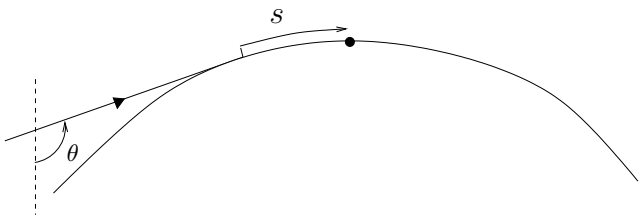


**Figure 6.2:** Coordinate system for the Fock-Leontovich solution used to estimate the contributions from near-tangential incidence.

optics approximation when $\hat{s} \to -\infty$, and an exponentially-decaying creeping-wave field as $\hat{s} \to \infty$.

We will parametrise the incident direction $\boldsymbol{\omega}$ by the angle $\omega$ made between the direction of propagation and the inwards-pointing normal to the surface at $\boldsymbol{x}$. The directions for which the incoming wave is tangent to the surface at $\boldsymbol{x}$ are $\omega = \frac{\pi}{2}$, and $\omega = -\frac{\pi}{2}$. Using the definition of curvature in terms of the derivative of the tangent to the surface we see that the point $\boldsymbol{x}$ is within the Fock-Leontovich region when $\omega - (\pm\frac{\pi}{2}) = O(k^{-\frac{1}{3}}\kappa_0^{\frac{1}{3}})$.

We wish to write the integrand of (6.62) in terms of the properties of the surface at the point $\boldsymbol{x}$ alone. In the Fock-Leontovich region $s$ is small, and so we will introduce an error of higher order by replacing the curvature at the horizon $\kappa_0$ by that at the point under consideration on the surface $\kappa(\boldsymbol{x})$.

We divide the range of integration in (6.62) into a number of sections

$$I = \int_{-\pi}^{\pi} \left| \frac{\partial \psi_+}{\partial n}(x, \omega; k) \right|^2 d\omega = \int_{-\pi}^{-\frac{\pi}{2}-\delta} + \int_{-\frac{\pi}{2}-\delta}^{\frac{\pi}{2}+\delta} + \int_{-\frac{\pi}{2}+\delta}^{\frac{\pi}{2}-\delta} + \int_{\frac{\pi}{2}-\delta}^{\frac{\pi}{2}+\delta} + \int_{\frac{\pi}{2}+\delta}^{\pi}, \tag{6.70}$$

where we have chosen $\delta$ such that $k^{-\frac{1}{3}}\kappa_0^{\frac{1}{3}} \ll \delta \ll 1$. For the first and last integrals the incident angle is such that the point $\boldsymbol{x}$ on the surface is within the geometrical shadow. Here the integrand is exponentially small and we may discard the contributions from these integrals. For the third integral the range of incident angles is such that the point $\boldsymbol{x}$ is directly illuminated by the incident plane wave, and sufficiently far from the horizon so that the geometrical optics approximation used in the previous section is still valid. However in the second and fourth integrals the incident plane wave is nearly tangent to the surface at $\boldsymbol{x}$, and so $\boldsymbol{x}$ is sufficiently near the horizon that we may approximate the integrand by the Fock-Leontovich solution given above. Let $\frac{\partial \psi_{GO}}{\partial n}$ denote the normal derivative of the leading order geometrical optics approximation, and $\frac{\partial \psi_{FL}}{\partial n}$ the normal derivative of the Fock-Leontovich approximation. Then our approximation of (6.62) can

be written as

$$I \sim \int_{-\frac{\pi}{2}-\delta}^{-\frac{\pi}{2}+\delta} \left|\frac{\partial\psi_{FL}}{\partial n}\right|^2 d\omega + \int_{-\frac{\pi}{2}+\delta}^{\frac{\pi}{2}-\delta} \left|\frac{\partial\psi_{GO}}{\partial n}\right|^2 d\omega + \int_{\frac{\pi}{2}-\delta}^{\frac{\pi}{2}+\delta} \left|\frac{\partial\psi_{FL}}{\partial n}\right|^2 d\omega. \quad (6.71)$$

We now wish to rewrite this expression as the integral (6.65), which we used to find the leading-order behaviour of the scattering phase, and a remainder which will supply the next order correction. We subtract the geometrical optics approximation from the first and third integrands, but only on the region $-\frac{\pi}{2} < \omega < \frac{\pi}{2}$ where the point $\boldsymbol{x}$ is directly illuminated. This gives

$$\begin{aligned} I \simeq & \int_{-\frac{\pi}{2}-\delta}^{-\frac{\pi}{2}+\delta} \left\{ \left|\frac{\partial\psi_{FL}}{\partial n}\right|^2 - \left|\frac{\partial\psi_{GO}}{\partial n}\right|^2 \chi(\omega+\frac{\pi}{2}) \right\} d\omega + \int_{-\frac{\pi}{2}}^{\frac{\pi}{2}} \left|\frac{\partial\psi_{GO}}{\partial n}\right|^2 d\omega \\ & + \int_{\frac{\pi}{2}-\delta}^{\frac{\pi}{2}+\delta} \left\{ \left|\frac{\partial\psi_{FL}}{\partial n}\right|^2 - \left|\frac{\partial\psi_{GO}}{\partial n}\right|^2 \chi(\frac{\pi}{2}-\omega) \right\} d\omega, \end{aligned} \quad (6.72)$$

where $\chi(x)$ is the Heaviside function. If we denote the last of these three integrals by $I_3$, and rescale $\omega = \frac{\pi}{2} + k^{-\frac{1}{3}}\kappa_0^{\frac{1}{3}}\hat{s}$, we find that

$$I_3 = k^{-\frac{1}{3}}\kappa_0^{\frac{1}{3}} \int_{-\delta k^{\frac{1}{3}}\kappa_0^{-\frac{1}{3}}}^{\delta k^{\frac{1}{3}}\kappa_0^{-\frac{1}{3}}} \left|\frac{\partial\psi_{FL}}{\partial n}(\frac{\pi}{2}+k^{-\frac{1}{3}}\kappa_0^{\frac{1}{3}}\hat{s})\right|^2 - \left|\frac{\partial\psi_{GO}}{\partial n}(\frac{\pi}{2}+k^{-\frac{1}{3}}\kappa_0^{\frac{1}{3}}\hat{s})\right|^2 \chi(-\hat{s})d\hat{s}. \quad (6.73)$$

As $\omega$ is very near $\frac{\pi}{2}$ we may replace the geometrical optics solution by its approximation for $\omega - \frac{\pi}{2} \ll 1$, which is

$$\left|\frac{\partial\psi_{GO}}{\partial n}\right|^2 = 4k^2(\boldsymbol{\omega}.\boldsymbol{n})^2 = 4k^2\cos^2\omega \sim 4k^{\frac{4}{3}}\kappa_0^{\frac{2}{3}}\hat{s}^2 \quad (6.74)$$

and so obtain

$$I_3 \sim k\kappa_0 \int_{-\delta k^{\frac{1}{3}}\kappa_0^{-\frac{1}{3}}}^{\delta k^{\frac{1}{3}}\kappa_0^{-\frac{1}{3}}} |B(\hat{s})|^2 - 4\chi(-\hat{s})\hat{s}^2\, d\hat{s}. \quad (6.75)$$

We have chosen $\delta$ to be sufficiently large such that we may replace the limits of integration by $\pm\infty$, introducing only higher order errors , and so find that

$$I_3 \sim k\kappa_0 \int_{-\infty}^{\infty} |B(\hat{s})|^2 - 4\chi(-\hat{s})\hat{s}^2\, d\hat{s}. \quad (6.76)$$

This integral has proved intractable analytically, but it is reasonably easy to compute numerically, and we find that

$$\int_{-\infty}^{\infty} |B(\hat{s})|^2 - 4\chi(-\hat{s})\hat{s}^2 d\hat{s} \approx \pi \quad (6.77)$$

so $I_3 = \pi k\kappa_0(\boldsymbol{x})$. In fact, since the multiplicative constant is independent of the body under consideration we know that it must be $\pi$ by comparison with the result (6.47) for

the special case of the unit disc. By symmetry we see that the first integral in 6.72 has the same asymptotic behaviour, and the second integral is exactly (6.65) so we have that

$$I \;=\; \int_{-\pi}^{\pi} \left| \frac{\partial \psi_+}{\partial n}(\boldsymbol{x}, \omega; k) \right|^2 d\omega \quad \sim \quad 2\pi k^2 + 2\pi\kappa(\boldsymbol{x})k. \tag{6.78}$$

Substituting this into (6.61) gives us that

$$\begin{aligned} \frac{ds}{dk} \;&=\; \frac{1}{8\pi^2 k} \int_{\partial\Omega} (\boldsymbol{x}.\boldsymbol{n}) \int_{-\pi}^{\pi} \left| \frac{\partial \psi_+}{\partial n} \right|^2 d\boldsymbol{\omega}\; dS \\ &\sim\; \frac{k}{4\pi} \int_{\partial\Omega} (\boldsymbol{x}.\boldsymbol{n})\; dS + \frac{1}{4\pi} \int_{\partial\Omega} \kappa(\boldsymbol{x})(\boldsymbol{x}.\boldsymbol{n})\; dS. \end{aligned} \tag{6.79}$$

The first integral is the leading order term from before. To evaluate the second integral we note that, from the Serret-Frenet relations[8] for a curve in the plane, $\frac{d\boldsymbol{t}}{ds} = -\kappa\boldsymbol{n}$, where $s$ is arc length along the boundary in a clockwise sense, and $\boldsymbol{t}(s)$ is the tangent to the boundary. Thus

$$\int_{\partial\Omega} \kappa(\boldsymbol{x}.\boldsymbol{n})\; ds \;=\; -\int_{\partial\Omega} \boldsymbol{x}.\frac{d\boldsymbol{t}}{ds} ds \;=\; -[\boldsymbol{x}.\boldsymbol{t}] + \int_{\partial\Omega} \frac{d\boldsymbol{x}}{ds}.\boldsymbol{t}\; ds \;=\; \text{Length}(\partial\Omega), \tag{6.80}$$

and on integrating (6.79), and applying this result, we have that

$$s(k) \quad \sim \quad \frac{k^2}{4\pi}\,\text{Area}(\Omega) + \frac{k}{4\pi}\,\text{Length}(\partial\Omega). \tag{6.81}$$

This expression now agrees to two terms with the result (6.47) for the unit disk.

### 6.3.5 Three dimensional case

In the three dimensional case we find that the estimate of the leading order geometrical optics field is the same as before, and so we find that

$$\int_{S^2} \left| \frac{\partial \psi_+}{\partial n} \right|^2 d\boldsymbol{w} \simeq \int_{\boldsymbol{\omega}.\boldsymbol{n}<0} 4k^2(\boldsymbol{\omega}.\boldsymbol{n})^2\; d\boldsymbol{\omega} = 8\pi k^2 \int_0^{\frac{\pi}{2}} \cos^2\omega \sin\omega\; d\omega = \frac{8\pi k^2}{3} \tag{6.82}$$

and so

$$\frac{ds}{dk} = \frac{1}{16\pi^3} \int_{\partial\Omega} (\boldsymbol{x}.\boldsymbol{n}) \int_{S^{n-1}} \left| \frac{\partial \psi_+}{\partial n} \right|^2 d\boldsymbol{\omega}\; dS = \frac{k^2}{6\pi^2} \int_{\partial\Omega} (\boldsymbol{x}.\boldsymbol{n})\; dS = \frac{k^2}{2\pi^2}\text{Vol}(\Omega). \tag{6.83}$$

Thus

$$s(k) \quad \sim \quad \frac{k^3}{6\pi^2}\text{Vol}(\Omega). \tag{6.84}$$

[8]Here we have chosen $\kappa$ to be positive for the unit circle traversed in a clockwise direction, and where $\boldsymbol{n}$ is the outwards-pointing unit normal.

The contribution from the Fock-Leontovich region to the next-order term may be considered in a similar manner, as from [30] it can be seen that the amplitude of the field within the Fock-Leontovich region is the same as in the three-dimensional case. However, we must now consider $s$ to be the distance from the horizon to the point $\boldsymbol{x}$, measured along a geodesic which is parallel to the incident field at the horizon. The curvature $\kappa_0$ then must be taken to be the normal curvature of this geodesic at the point of tangency, which we approximate by the curvature $\kappa(\boldsymbol{x}, \boldsymbol{\omega})$ of the geodesic at the point $\boldsymbol{x}$.

At any point on a smooth surface there are two principal directions, orthogonal to each other, for which geodesics through the point attain maximum and minimum curvatures $\kappa_1$ and $\kappa_2$. It is then possible to write the curvature of a geodesic through this point in the form $\kappa_1 \cos^2\phi + \kappa_2 \sin^2\phi$, where $\phi$ is the angle the geodesic makes with the first principal direction.

To approximate the integral (6.62) we introduce a polar coordinate system $(\omega, \phi)$ for the direction of the incident plane wave, with pole $\omega = 0$ along the inwards-pointing normal. Then integral (6.62) becomes

$$\int\int \left| \frac{\partial \psi_+(\boldsymbol{x}, \omega, \phi; k)}{\partial n} \right|^2 \sin\omega \; d\omega \; d\phi. \tag{6.85}$$

For near-tangential incidence $\sin\omega \simeq 1$, and therefore the contribution from the Fock-Leontovich region to the integral for constant $\phi$ is the same as in the two-dimensional case. Hence

$$\int \left| \frac{\partial \psi_+(\boldsymbol{x}, \omega, \phi; k)}{\partial n} \right|^2 \sin\omega \; d\omega \sim \frac{4\pi k^2}{3} + \pi\kappa(\phi)k, \tag{6.86}$$

and so we find that

$$\int\int \left| \frac{\partial \psi_+(\boldsymbol{x}, \omega, \phi; k)}{\partial n} \right|^2 \sin\omega \; d\omega \; d\phi \sim \frac{8\pi k^2}{3} + 2\pi^2 H(\boldsymbol{x})k, \tag{6.87}$$

where $H = \frac{1}{2}(\kappa_1 + \kappa_2)$ is known as the mean curvature of the surface.

If, as in Section 6.3.3, we let $\Omega(t) = t\Omega$, and $\partial\Omega(t)$ be the corresponding boundary, then we have that

$$\frac{d}{dt}(\text{Area}(\partial\Omega(t)))\bigg|_{t=1} = 2\int_{\partial\Omega} H(\boldsymbol{x})(\boldsymbol{x}.\boldsymbol{n})dS. \tag{6.88}$$

By similarity

$$\text{Area}(\partial\Omega(t)) = t^2 \text{Area}(\partial\Omega(1)), \tag{6.89}$$

and so

$$\int_{\partial\Omega} H(\boldsymbol{x})(\boldsymbol{x}.\boldsymbol{n})dS = \text{Area}(\partial\Omega). \tag{6.90}$$

Using this result we find that

$$\frac{ds}{dk} = \frac{1}{16\pi^3}\int_{\partial\Omega}(\boldsymbol{x}.\boldsymbol{n})\int_{S^{n-1}}\left|\frac{\partial\psi_+}{\partial n}\right|^2 d\boldsymbol{\omega}\; dS \tag{6.91}$$

$$= \frac{k^2}{6\pi^2}\int_{\partial\Omega}(\boldsymbol{x}.\boldsymbol{n})\; dS + \frac{k}{8\pi}\int_{\partial\Omega}H(\boldsymbol{x})(\boldsymbol{x}.\boldsymbol{n})dS \tag{6.92}$$

$$= \frac{k^2}{2\pi^2}\mathrm{Vol}(\Omega) + \frac{k}{8\pi}\mathrm{Area}(\partial\Omega). \tag{6.93}$$

Therefore

$$s(k) \sim \frac{k^3}{6\pi^2}\mathrm{Vol}(\Omega) + \frac{k^2}{16\pi}\mathrm{Area}(\partial\Omega), \tag{6.94}$$

and this agrees to two terms with the known results for the asymptotic behaviour of the scattering phase in three dimensions [41], [92], [131], [90].

## 6.4 Counting function for the interior eigenvalues

We will now briefly discuss the asymptotic behaviour of the average internal spectral density, and so the smooth part of the counting function for the internal eigenvalues. This analysis is explained at greater length in [15], and we will closely follow the development there.

We consider the interior Helmholtz problem with Dirichlet boundary conditions for a compact region. For general values of $k$ no non-trivial solution exists, but at particular values of $k$, known as the eigenvalues of the problem ($-k^2$ is an eigenvalue of the Laplacian operator $\nabla^2$) there are non-zero solutions. We denote the values of $k$ by $k_j$, and the corresponding (normalised) solutions by $\psi_j(\boldsymbol{x})$. Multiple eigenvalues are repeated according to their multiplicity, and the corresponding $\psi_j$ chosen to be an orthonormal basis of the eigenspace. As usual, defining the Green's function $G(\boldsymbol{x},\boldsymbol{x}';k^2)$ to be the solution of

$$(\nabla^2_{\boldsymbol{x}} + k^2)G = \delta(\boldsymbol{x}-\boldsymbol{x}') \tag{6.95}$$

with $G=0$ on $\partial\Omega$, we find that it has expansion

$$G = \sum_j \frac{\psi_j(\boldsymbol{x})\psi_j(\boldsymbol{x}')}{k^2-k_j^2} \tag{6.96}$$

in terms of the eigenfunctions $\psi_j(\boldsymbol{x})$. We define $N(k) = \#\{k_n | \, 0 \le k_n \le k\}$ to be the counting functions for the eigenvalues, and $d(k)$ to be the spectral density, so that

$$d(k) = \sum_j \delta(k-k_j), \qquad N(k) = \int_0^k d(k')dk'. \tag{6.97}$$

We also define the function

$$\rho(k^2) = \sum_j \delta(k^2 - k_j^2). \tag{6.98}$$

Using the expansion (6.96) for the Green's function in terms of the eigenfunctions we find (following [15]) that

$$\begin{aligned}\rho(k^2) = \sum_j \delta(k^2 - k_j^2) &= \lim_{\epsilon\to 0+} \frac{1}{2\pi i} \sum_j \left( \frac{1}{k^2 - k_j^2 + i\epsilon} - \frac{1}{k^2 - k_j^2 - i\epsilon} \right) \\ &= \lim_{\epsilon\to 0+} \frac{1}{2\pi i} \int_\Omega \lim_{\boldsymbol{x}\to\boldsymbol{x}'} \left( G(\boldsymbol{x},\boldsymbol{x}';k^2+i\epsilon) - G(\boldsymbol{x},\boldsymbol{x}';k^2-i\epsilon) \right) d\Omega \\ &= -\frac{1}{\pi} \int_\Omega \lim_{\epsilon\to 0+} \operatorname{Im} G(\boldsymbol{x},\boldsymbol{x}';k^2) d\Omega, \end{aligned} \tag{6.99}$$

and so

$$d(k) = 2k\rho(k^2) = -\frac{2}{\pi} \int_\Omega \lim_{\boldsymbol{x}\to\boldsymbol{x}'} \operatorname{Im} G(\boldsymbol{x},\boldsymbol{x}';k^2)\, d\boldsymbol{x} = -\frac{2}{\pi} \operatorname{Im} \operatorname{Tr} \left[ G(\boldsymbol{x},\boldsymbol{x}';k^2) \right]. \tag{6.100}$$

Despite the fact that $d(k)$ is not continuous (as it is a sum of delta functions), it is possible to write

$$d(k) = \bar{d}(k) + d_{\text{osc}}(k) \tag{6.101}$$

where $\bar{d}$ is the averaged spectral density, and $d_{\text{osc}}$ is the oscillatory remainder.

In order to evaluate the mean behaviour for the counting function $\bar{d}$ we must estimate the integral (6.100). The dominant contribution is due to the direct ray from $\boldsymbol{x}$ to $\boldsymbol{x}'$, so to leading order we may approximate $G$ by the free space Green's function. We now specialize to the two dimensional case, for which the free space Green's function is

$$G_0 = -\frac{i}{4} H_0^{(1)}(k\,|\boldsymbol{x} - \boldsymbol{x}'\,|). \tag{6.102}$$

As $\operatorname{Im} G_0(\boldsymbol{x},\boldsymbol{x}') \sim \frac{1}{4} J_0(k\,|\boldsymbol{x} - \boldsymbol{x}'\,|)$, we find that

$$\bar{d}(k) \sim \frac{\text{Area}(\Omega) k}{2\pi} \tag{6.103}$$

and so

$$\bar{N}(k) \sim \frac{\text{Area}(\Omega) k^2}{4\pi}. \tag{6.104}$$

Higher-order terms in the expansion of the smooth part of the counting function are generally calculated by first subtracting this leading order contribution from the trace formula, and then examining the asymptotic expansion of the function for $s \gg 1$, when $k = is$. Only points which are near the boundary contribute (as the Greens function for imaginary $k$ decays exponentially with distance), and we then find that

$$\bar{N}(k) \sim \frac{k^2}{4\pi} \text{Area}(\Omega) \mp \frac{k}{4\pi} \text{Length}(\partial\Omega), \tag{6.105}$$

where the upper and lower signs are for Dirichlet and Neumann boundary conditions respectively. A large number of terms in this expansion may be found by this method [94]. The oscillatory part of the spectral density $d_{\mathrm{OSC}}$ can be found to be related to the periodic orbits of the interior problem. These are finite, closed ray paths within $\Omega$, and are discussed further in [15] and its references.

## 6.5 Internal-external duality

In the previous sections we have determined the behaviour of the scattering phase, and the counting function for the eigenfunctions. It can be seen that the first two terms in the asymptotic expansion of the scattering phase (in the exterior of an obstacle) for Dirichlet boundary conditions are the same as the first two terms in the asymptotic expansion of the counting function for eigenvalues for Neumann boundary data (and in fact the same result holds true with the boundary conditions interchanged). It might be conjectured that this is indicative of a significant connection between these these two problems. There is indeed a connection between the internal and external problems, but it is not as straightforward as this result connecting the scattering phase and counting function might suggest.

In section 6.2.3 we discussed the high-frequency approximation of the scattering matrix. We noted that the kernel of $\mathcal{T} = \mathcal{S}^L - \mathcal{I}$, which is proportional to the directivity $A_+(\boldsymbol{\theta}, \boldsymbol{\omega}; k)$, could be approximated to leading order by considering the geometrical optics reflected field. It was realised in [36], [38] that there is an inherent relationship (at least for a convex obstacle) between the reflection of rays in the internal problem, and the reflection of rays in the external problem. In Figure 6.3 we see that the reflection of a ray at the internal boundary is equivalent to an external ray path. This allows a relationship to be found between trajectories of rays reflected inside the obstacle, and the scattering of rays outside the obstacle. However it is not directly obvious how this relates the scattering operator and the interior eigenvalues. The relationship is made more explicit in the work Smilansky and others [36], [38], and formalised in a rigorous sense by Eckmann and Pillet [40], [39], [41].

### 6.5.1 Eigenvalues of the internal problem and the scattering phase

From the explicit calculation of the eigenvalues for the scattering phase for the unit circle, we find that at an eigenvalue of the internal problem (with Dirichlet boundary

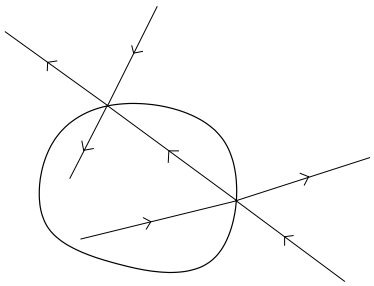

**Figure 6.3:** Relationship between interior and exterior ray-paths.

conditions) the scattering matrix has an eigenvalue 1. This solution corresponds to the analytic continuation of the internal eigenfunction to the whole of space. Moreover, any external solution can be expressed (via the relevant Herglotz function) in terms of a superposition of plane waves, and so it is easy to see that if the scattering matrix has eigenvalue 1 this external solution can be extended to a solution of the interior problem.

However for more general boundaries it is not possible to continue the eigenfunctions in this way, and so we find that the scattering matrix does not ever attain the eigenvalue 1. Instead it was found that, as the wavenumber approaches the eigenvalue of the interior problem, one of the phase shifts $\beta_j$ approaches $2\pi$ from below. There are infinitely many phase shifts which accumulate at 0 from above, and it is found that there is a sequence of avoided crossings as $k$ passes through the internal eigenvalue. If we consider the exterior fields for the eigenfunction associated with the phase shift which approaches $2\pi$, it is found [36] that the field vanishes pointwise outside the obstacle. This result has been made more precise by Eckmann and Pillet [40], where it was noted that the scattering matrix can be related to the operator which takes the field due to a distribution of point sources on the boundary of the obstacle to its values on the boundary. It is well known (from its application to boundary integral equations) that this operator has eigenvalues at the internal eigenvalues of the Dirichlet problem [98] [144]. This relationship is discussed in a more practical manner in [36], and numerical studies have been made [35].

It also proves possible to relate the behaviour of the scattering phase to the spectral density of the interior problem. If $d(k)$ is the interior spectral density, then

$$d(k) = \sum_{n=1}^{\infty} \delta(k - k_n) = \lim_{\epsilon \to 0+} \sum_{j}^{\infty} \delta_{2\pi}(\beta_j(k) + \epsilon)\beta_j'(k) \tag{6.106}$$

where the second equality follows from the approach of one of the scattering phases to $2\pi$ as $k$ approaches an eigenvalue of the internal problem. By applying the Poisson

summation formula (or alternatively the Fourier series of the delta function) it is found[9], at least formally, that

$$d(k) = s'(k) + \frac{1}{\pi}\mathrm{Im}\sum_{m=1}^{\infty}\frac{1}{m}\mathrm{Tr}\left[\frac{d}{dk}S^{*m}(k)\right] \tag{6.107}$$

where the second term is related to the periodic orbits of the interior problem. (This expression relating the scattering phase and spectral density can also be obtained by formally considering the behaviour of $Z(k) = \det(I - S(k))$, where $S$ is the finite dimensional approximation of $\mathcal{S}$, as discussed in [38].) In [132] they examine the approximation of the "smooth" part of the phase shift, which they find from applying the trace formula

$$\frac{1}{2k}\frac{\partial s}{\partial k} = \frac{1}{\pi}\mathrm{Im}\lim_{\epsilon\to 0+}\mathrm{Tr}\left(G(k+i\epsilon) - G_0(k+i\epsilon)\right)] \tag{6.108}$$

where $G_0$ is the free space Green's function[10], $G$ is the exterior Greens function with Dirichlet boundary conditions (and is taken to be zero within the obstacle). The definition of $G$ is the same as (6.95) for the interior problem, but with outgoing radiation conditions imposed at infinity. This is a similar procedure to that used to find the smooth part of the scattering density for the internal problem. This is then evaluated when $k$ is a pure imaginary number, and using methods similar to those for the internal problem it is possible to compute a large number of terms in the expansion of the (smooth part of the) scattering phase. Apart from the leading order term, the dominant contributions are those from points near the boundary. It is found that the only change between the internal and external problems is the change in the sign of the curvature. It is found that, for the first 13 correction terms, the coefficients in the asymptotic expansions of the smooth part of the scattering phase and the (suitably smoothed) internal spectral density simply differ in sign.

In a more rigorous setting, various zeta functions which relate the internal spectral density and the scattering phase are found, both in the case when the boundary conditions are Dirichlet for both the internal and external problems [40], and when each of the internal and external problems may have Dirichlet and Neumann boundary conditions independently [41]. Various other properties of the scattering matrix are proved in [39].

[9] In deducing this relationship it is useful to note that [53], if $v_j(k)$ is the eigenfunction associated with the eigenvalue $e^{-i\beta_k(k)}$, then $e^{i\beta_j(k)} = (v(k), S(k_0)S^*(k)v(k))$ and differentiating this with respect to $k$ and setting $k = k_0$ we find that $i\beta_j'(k_0) = \left(v(k_0), S(k_0)\frac{dS^*}{dk}(k_0)v(k_0)\right)$ and so, in the finite dimensional approximation, if the eigenvectors of the scattering matrix span the whole space then (6.107) follows relatively simply.

[10] There is a sign change between this and [132], as we have used an alternative definition for the Green's function in this thesis.

## 6.6 Physical significance of the scattering phase

We now briefly discuss the significance of the scattering phase to the properties of the exterior problem. The relationship between the exterior problem and the scattering phase is not as direct as the relationship between the interior problem and the counting functions for the eigenvalues. Initially, the motivation for this work was that, in an odd number of space dimensions, the scattering phase (and the scattering matrix) can be analytically continued to a meromorphic function for all complex $k$. The function $s(k)$ has zeros in the half plane $\operatorname{Im} k > 0$, and poles in the half plane $\operatorname{Im} k < 0$. We recall from (6.33) that

$$s(k) = -\frac{1}{2\pi} \arg \det \mathcal{S}^L. \tag{6.109}$$

Therefore, if we could find the behaviour in the complex plane of $s(k)$ we could count the zeros and poles of $\det \mathcal{S}^L$ by examining the change in $s(k)$ around a suitable contour. However, our asymptotic estimate of the behaviour of $s$ is only valid on the real line, and so this is not possible.

In the frequency-domain, the region of the wavenumber plane $\operatorname{Re} k > 0$, $\operatorname{Im} k > 0$ corresponds to a medium which damps waves propagating through it, whereas the region $\operatorname{Re} k > 0$, $\operatorname{Im} k < 0$ corresponds to a medium which amplifies waves propagating through it. It can be found that [80], at a pole of $s(k)$, there exists an outgoing solution to the exterior Helmholtz problem with no incoming part. Such solutions grow exponentially at infinity, and so make little sense for the time-harmonic problem. However if we examine the time-domain problem then we note that these poles also correspond to solutions of the wave equation. Those modes with $k$ purely imaginary were examined in [79]. Asymptotic expansions of other modes can be constructed [10, §7.5], essentially by considering creeping ray fields for complex $k$, but imposing periodicity on creeping waves which have circled the obstacle (these do not decay as $k$ has negative imaginary part). The poles with small imaginary part are of most interest, as they correspond to solutions to the time-dependent problem which decay slowly.

The function $s(k)$ is also related to the Wigner delay time in quantum scattering [132] and a very thorough discussion can be found in [33].

## 6.7 Summary

In this chapter we have discussed the various different versions of the scattering matrix used in the mathematical and physical literature, and discussed the relationship between

them. We then defined the phase shifts and the scattering phase, which are related to the eigenvalues of the scattering matrix. These were directly calculated in the simple case of scattering by the unit disc, and we found the asymptotic behaviour for large $k$ of the scattering phase. In order to find the asymptotic behaviour of the scattering phase for a general smooth, strictly convex obstacle we followed the procedure of [53], [89]. This allowed us to express the derivative of the scattering phase in terms of (integrals of) the normal derivative of the fields on the obstacle when plane waves were incident. We then used the methods of Chapter 3 to find approximations for large $k$ to the fields, and so the scattering phase. This was found to agree to two terms with the result for the unit disc, and agrees with the known [92] results for the behaviour of the scattering phase found by more mathematically involved methods. We then recounted the behaviour of the counting function for the eigenvalues in the internal problem (following the simple exposition of [15]). The relationship between the internal and external problems has been studied by Smilansky (and other collaborators), and we discussed some of their findings. We finally gave a brief discussion of the physical significance of the scattering phase.

# Chapter 7

# Discussion and Further Work

## 7.1 Thesis summary

In Chapter 1 we described the background to our study of these diffraction and scattering problems, and in particular the industrial motivation for the problems which we have attempted to address.

Chapter 2 introduced Maxwell's equations, which govern the behaviour of electromagnetic waves, and the various boundary and radiation conditions that we employ in the remainder of the work.

In Chapter 3 we then outlined the Geometrical Theory of Diffraction (GTD). In particular we discussed the results for scattering by a convex body which were placed in a modern asymptotic framework in [121]. These results were used throughout the remainder of the thesis, and the work of Chapters 4 and 5 was motivated by the need to extend this theory to more general geometries and materials.

In Chapter 4 we discussed the problem of scattering of electromagnetic waves by a body which is thin, of aspect ratio $\mathcal{O}(k^{-\frac{1}{2}})$. The inner problem near the edge of such a body reduced to the scattering by an electromagnetic plane wave by a parabolic cylinder. Generalizing, correcting and extending the work of [44], we examined the integral solutions to this inner problem. We found the far fields of these integrals, and in particular examined the behaviour of the fields in the transition regions, near shadow boundaries. We discussed the problems with creeping ray fields on bodies which have small curvature, and we examined the case of a thin body with curved mid-line in Section 4.4. We then discussed the behaviour of our solution as the radius of curvature at the tip of the parabola became large, and saw that it matched smoothly with the analysis of Chapter 3 for a blunt obstacle.

Chapter 5 consisted of a study of diffraction by a radome, which is a thin layer of material used to physically protect an antenna. We considered the case of a half-wavelength-thick layer of high refractive-index dielectric material, and developed transition conditions, which included curvature-correction terms. These allowed us to find an integral expression for the fields scattered by the layer in Section 5.5. We then examined this integral solution to find an expression for the fields scattered by a tightly curved "tip" region in Section 5.6, where the radius of curvature of the layer was large compared with the wavelength within the dielectric, but small compared to the wavelength in free space. We then proceeded in Section 5.7 to examine the analogue of creeping waves and whispering gallery modes propagating almost tangentially to such a thin layer. By examining the problem near the point of tangency, we determined the launch coefficients for these modes.

In Chapter 6 we discussed a more theoretical aspect of wave propagation, namely scattering theory. We gave a clear and explicit exposition of the various definitions of the scattering matrix. Using the methods of Chapter 3 we then in Section 6.3.3 found an asymptotic expansion for a function known as the scattering phase. This was seen to have similar behaviour to the counting function for the eigenvalues of the interior problem. We then finally discussed the work of Smilansky and others on the relationship between the scattering problem in the exterior of an obstacle and the eigenvalue problem in the interior.

## 7.2 Further work

### 7.2.1 Chapter 3

The results of Chapter 3 have been extended to the three-dimensional electromagnetic case, but only for a perfectly conducting obstacle. These have been studied [81] [6], but it would be useful for the sake of completeness to place these in the asymptotic framework of Coats [30].

### 7.2.2 Chapter 4

In Chapter 4 we only considered diffraction by thin, perfectly conducting bodies, and it would be desirable to extend this work to impedance boundary conditions (which can be used to model imperfectly conducting or dielectric-coated obstacles), or to penetrable bodies. However, in all these cases, the inner problems near the edges will reduce to the

problem of diffraction by a parabolic cylinder. Unfortunately, as noted in Section 4.1, there is not a reasonably simple expression for the scattered fields in either of these cases. The solutions can be obtained (implicitly) in series form, but unless some approximations to the coefficients of these series can be made it seems unlikely that we could make any further approximation of these solutions.

We have also only considered plane wave incidence for the inner problem. For a point source at an $\mathcal{O}(1)$ distance from the edge will be approximately a plane wave; however we expect that the behaviour of the solution will differ from that in the plane wave case in the shadow boundary regions. There are solutions [17] [84] (in the form of integrals of PCFs) to the two dimensional problem of a line source parallel to a perfectly conducting parabolic cylinder. By means of a Fourier transform in the axial variable we should be able to find from this the solution to a scalar point source in the three dimensional case, and with Dirichlet or Neumann boundary conditions upon the cylinder. The analysis for a line source would be similar to the plane wave problem but slightly more complicated; the point source problem would have additional difficulties due to the extra integration involved. Using the same solutions we could also consider the problem of a line source in the inner region near the edge. In this case we expect that the fields outside the inner region will consists of a system of rays propagating away from the edge, along with fields propagating along the surface of the body. The case of a line source actually on the body is likely to prove the easiest case, especially as the integral form of the solution has been examined by the method of stationary phase for a parabola which has radius of curvature which is much larger than the wavelength [18].

Another related problem is scattering by a wedge with an edge which is curved on the order of a wavelength, rather than sharp. A solution can be found to the problem of plane wave scattering by a perfectly conducting hyperbolic cylinder [17], and this could be used to study the problem near the edge (although there is no reason why the profile in the inner region should take this form). However the special functions within the solution would now be Mathieu functions, rather than PCFs, and the general form of the integral analysis may be significantly different. We also note that a hyperbola with a tightly curved edge is necessarily flat away from the edge, and so similar difficulties with regards to the creeping ray fields will occur.

### 7.2.3 Chapter 5

There are a number of extensions possible to the work of Chapter 5, in addition to the extensions discussed at the end of Chapter 5; there we mentioned the possibility of

extending the approximate transition conditions and the analysis of the tightly curved tip and tangential incidence to the three dimensional E-M case, and to the case of more complicated material layers. For a thin dielectric layer with high refractive index we found that the propagating modes of the layer could be ignored. However, for a general thin layer it is possible to find propagating (or slowly decaying) modes within the layer, and it would be interesting mathematically to consider the problem of initiation of such modes. It also would be interesting to examine the problem of incidence of a complex wave or Gaussian beam upon a high refractive index layer, as this could potentially excite the propagating modes. Such modes could also be initiated by a source near or within the layer.

Much of the study of approximate transition conditions has been on their applications to diffraction at discontinuities, such as diffraction by a dielectric-coated wedge, or diffraction by a jump in thickness of a dielectric slab. It is assumed that the impedance boundary conditions hold up to the discontinuity, and the scattered fields are found by the usual transform methods (generally Wiener-Hopf or Malyuzhinets's method [102]). However these solutions contain unknown parameters, which have to be determined by extra conditions upon the fields near the discontinuity [127]; failure to impose the correct conditions often results in solutions which do not satisfy reciprocity. It would be interesting to compare our solution for a tightly curved "tip" region with that obtained for a sharp edge from transform methods.

### 7.2.4 Chapter 6

The work of Chapter 6 serves as an introduction to scattering theory, and discusses the developments of Smilansky. There are number of possible extensions, including generalization to the electromagnetic case. The theory can also be used to study the problem of an obstacle within a waveguide, which is an open problem of particular interest.

## 7.3 Other questions arising

In both Chapters 4 and 5 we examined the asymptotic behaviour of integrals by the method of steepest descent. There were two situations in particular where we were interested in terms in the expansion which were exponentially subdominant to the main contribution to the integral, namely the backwards creeping field in the case of a parabola with $\mathcal{O}(1)$ curvature, and the Airy layer modes initiated by tangential incidence upon a thin layers (both these were residue contributions in regions for which a geometrical

ray field was also present). In both situations the integrand contained special functions, and after deforming the contours to the paths of steepest descent, we had to first approximate the integrands, before approximating the local contributions from the saddle point(s). These approximations involve discarding a number of exponentially small terms, which could be larger than the contributions of interest. The analysis of the errors made in these integrals for an exact integrand is reasonably well studied [12], and it is possible to find expansions for these exponentially small errors. Studies have been made of the exponentially small contributions to multiple integrals of exponential functions [60]; however, for integrals with poles generated by the zeros of special functions it is generally not possible to rewrite the integral in this form. In general the saddle point contribution from the approximate integral (both expanded to all terms) can formally be identified with the Poincaré asymptotic expansion of the geometrical optics field [18]. However it seems difficult to make further progress with this analysis.

For the exponentially small backwards-creeping field it may be possible to examine the process of initiation by similar considerations to those in [27], examining the lines of equal phase for the various contributions. Alternatively it may be possible to find these backwards propagating fields by considering the problem of a creeping wave travelling along a body with varying curvature, as it is thought [44] that when the curvature of the body varies, the forward propagating creeping ray mode initiates the backwards creeping field through mode conversion.

Another significant problem arising is that of diffraction by bodies which have small ($\mathcal{O}(k^{-\frac{1}{2}})$) curvature, as discussed briefly in Section 4.3.1. In this case we find that the Fock problem near tangency is now of $\mathcal{O}(1)$ in length, and $\mathcal{O}(k^{-\frac{1}{2}})$ in height, and we are unable to find Airy layer solutions on the body of the usual form. As the problem (4.146) in the region near the surface contains an arbitrary function we are unable to solve this problem exactly, but some insight may be gained by considering plane wave incidence upon (or a point source near) a parabolic cylinder with small curvature.

In Chapter 5 we also discussed the general problem of the application of the GTD to a dielectric body, where we noted that, in addition to the problem near points of tangential incidence, local analysis needed to be performed near points of critical incidence upon the layer. Both of these problems have been studied in various different cases, and it may be worthwhile to compile the various different solutions, extending them if necessary to the three dimensional E-M case (some steps towards this may have been performed in the very recent book [6]).

# Appendix A

# Parabolic Cylinder Functions

Here we describe summarise some of the properties of parabolic cylinder functions. In particular we will set out the various asymptotic expansions used in the analysis of the thin edge problem.

## A.1 Definition

The parabolic cylinder (or Weber) function $D_\nu(z)$ is the solution of the ordinary differential equation

$$\frac{d^2 D_\nu}{dz^2} + \left(\nu + \frac{1}{2} - \frac{z^2}{4}\right) D_\nu = 0, \tag{A.1}$$

along with initial conditions

$$D_\nu(0) = \frac{2^{\frac{\nu}{2}}\sqrt{\pi}}{\Gamma(\frac{1}{2} - \frac{\nu}{2})}, \quad D'_\nu(0) = -\frac{2^{\frac{\nu+1}{2}}\sqrt{\pi}}{\Gamma(-\frac{\nu}{2})} \tag{A.2}$$

[3, §19.3.1, §19.3.5], [66, pp. 85-86]. It is entire as a function of both order $\nu$ and argument $z$.

## A.2 Integral form

Following Whittaker and Watson [146, §16.6] we may represent the PCFs in integral form as

$$D_\nu(z) = \frac{\Gamma(\nu+1)e^{-\frac{z^2}{4}}}{2\pi i}\int_C \exp\left(-\frac{1}{2}s^2 + zs - (\nu+1)\log s\right) ds, \tag{A.3}$$

$$= \frac{\Gamma(\nu+1)e^{-\frac{z^2}{4}}2^{-\frac{\nu}{2}}}{2\pi i}\int_C \exp\left(-t^2 + \sqrt{2}zt - (\nu+1)\log t\right) dt. \tag{A.4}$$

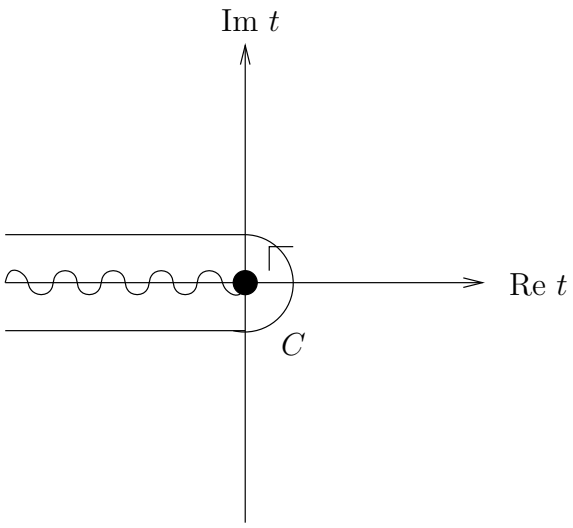


**Figure A.1:** Contour of integration for the integral representations (A.3) and (A.4). Here the wavy line denotes the branch cut of the logarithm.

Here we take the logarithm to be the usual principal branch on $-\pi < \arg t < \pi$. The contour C is as shown in Figure A.1; it comes in from $-\infty$ below the branch cut, encircles the branch point at zero in a counter-clockwise sense, and then returns to $-\infty$ above the branch cut[1]. These integrals may be shown to satisfy both the parabolic cylinder equation (A.1) and the initial conditions (A.2). There is an alternative representation due to Cherry [29],

$$D_\nu(z) = \frac{1}{\sqrt{2\pi}} e^{\frac{z^2}{4}} e^{-\frac{\nu\pi i}{2}} \int_{ci-\infty}^{ci+\infty} \exp\left(-\frac{t^2}{2} + izt + \nu \log t\right) dt, \tag{A.5}$$

where $c$ is an arbitrary positive constant.

## A.3 Recurrence relations, reflection and connection formulae

### A.3.1 Recurrence relations

By using the integral representations of the PCFs it can be shown that [146, §16.61], [3, §19.6]

$$D_{\nu+1}(z) - zD_\nu(z) + \nu D_{\nu-1}(z) = 0, \tag{A.6}$$

$$D'_\nu(z) + \frac{1}{2} zD_\nu(z) - \nu D_{\nu-1}(z) = 0. \tag{A.7}$$

[1] In older literature an integral along this contour would be denoted by $\int_{-\infty}^{(0+)}$.

### A.3.2 Reflection formula

The parabolic cylinder functions are entire in both order and argument, and real-valued when both order and argument are real. Thus by reflection in the real axis we have that

$$\overline{D_{\bar{\nu}}(\bar{z})} = D_\nu(z). \tag{A.8}$$

### A.3.3 Connection formulae

It is easy to see that $D_\nu(-x)$, $D_{-1-\nu}(ix)$, $D_{-1-\nu}(-ix)$ are all solutions of (A.1). However this is a second order linear equation, and so has only two linearly independent solutions. From the initial values of these functions it may be seen that [3, §19.4], [44, §B1]

$$D_\nu(z) = \frac{\Gamma(\nu+1)}{\sqrt{2\pi}}\left(e^{\frac{1}{2}\nu\pi i}D_{-1-\nu}(iz) + e^{-\frac{1}{2}\nu\pi i}D_{-1-\nu}(-iz)\right), \tag{A.9}$$

$$D_\nu(z) = e^{-\nu\pi i}D_\nu(-z) + \frac{\sqrt{2\pi}}{\Gamma(-\nu)}e^{-\frac{1}{2}(1+\nu)\pi i}D_{-1-\nu}(iz), \tag{A.10}$$

$$D_\nu(z) = e^{\nu\pi i}D_\nu(-z) + \frac{\sqrt{2\pi}}{\Gamma(-\nu)}e^{\frac{1}{2}(1+\nu)\pi i}D_{-1-\nu}(-iz). \tag{A.11}$$

## A.4 Asymptotic expansion of the functions

The PCFs have a number of different asymptotic expansions, each valid for different ranges of order and argument. In general these expansions become more complicated as they become more widely applicable.

### A.4.1 Expansion for large $\nu$, with $z = \mathcal{O}(1)$

These may be found in [63], and they are listed in [3, §19.9], although it is not explicitly stated that they are valid for complex $\nu$ and $z$. We have

$$D_\nu(z) \sim \sqrt{2}e^{-\frac{\nu}{2}}\nu^{\frac{\nu}{2}}\cos\left(z\sqrt{\nu} - \frac{\nu\pi}{2}\right), \tag{A.12}$$

$$D_{-1-\nu}(z) \sim \frac{1}{\sqrt{2\nu}}e^{\frac{\nu}{2}}\nu^{-\frac{\nu}{2}}\exp\left(-z\sqrt{\nu}\right), \tag{A.13}$$

valid for $|\arg\nu| < \pi$. However these are merely the leading-order terms in the expansions. Higher-order terms may be found either by considering the expansions of Appendix A.4.3 for very large $|\nu|$, or alternatively by the using the expansions discussed in [105, Appendix], which express the PCFs in terms of spherical Bessel functions. This latter method actually results in a convergent sequence. When we do this we find that

$$D_{-1-\nu}(z) \sim \frac{1}{\sqrt{2\nu}}e^{\frac{\nu}{2}}\nu^{-\frac{\nu}{2}}\exp\left(-z\sqrt{\nu}\right)\left(1 - \frac{z}{4\sqrt{\nu}} - \frac{z^3}{24\sqrt{\nu}} + \mathcal{O}\left(\frac{z^4}{\nu}\right)\right), \tag{A.14}$$

where higher order coefficients may be found from the discussion in [105] and [130, p. 69]. It may be noted (from numerical comparisons) that for $|z|>1$ this approximation requires $|\nu|$ to be very large, as the numerators of the terms in the expansion contain progressively larger powers of $z$.

### A.4.2 Expansion for large $z$, with $\nu = \mathcal{O}(1)$

These are given in [44, Sec. B2], and again restricted versions of these expansions are listed in [3, §19.8].

$$D_\nu(z) \sim z^\nu e^{-\frac{1}{4}z^2}, \quad |\arg z|< \frac{\pi}{2}, \tag{A.15}$$

$$D_\nu(z) \sim z^\nu e^{-\frac{1}{4}z^2} - \frac{\sqrt{2\pi}}{\Gamma(-\nu)} e^{\nu\pi i} z^{-1-\nu} e^{\frac{1}{4}z^2}, \quad \frac{\pi}{2} < \arg z < \pi \tag{A.16}$$

$$D_\nu(z) \sim z^\nu e^{-\frac{1}{4}z^2} - \frac{\sqrt{2\pi}}{\Gamma(-\nu)} e^{-\nu\pi i} z^{-1-\nu} e^{\frac{1}{4}z^2}, \quad -\pi < \arg z < -\frac{\pi}{2}. \tag{A.17}$$

These expansions may be found either by considering the large $x$ expansions of the results in the following section, or a steepest descents analysis of integral (A.5). By the latter method it is relatively straightforward to calculate these expansions to higher orders, and we find that

$$D_\nu(z) \sim z^\nu e^{-\frac{1}{4}z^2} \left\{ 1 - \frac{\nu(\nu-1)}{2z^2} + \frac{\nu(\nu-1)(\nu-2)(\nu-3)}{24z^4} + \cdots \right\} \tag{A.18}$$

for $|\arg z|< \frac{\pi}{2}$. By further analysis of these saddle point contributions (using the method of Appendix D for the contribution from a perturbed saddle point) we may also find expansions valid when $\nu$ is large, but small compared to $|z|^2$.

When $\nu = \mathcal{O}(|z|)$, $|\arg z|< \frac{\pi}{2}$ we find that

$$D_\nu(z) \sim z^\nu e^{-\frac{1}{4}z^2 - \frac{\nu^2}{2z^2}} \left\{ 1 + \frac{\nu}{2z^2}\left(1 - \frac{\nu^2}{z^2}\right) + \cdots \right\} \tag{A.19}$$

and when $\nu = \mathcal{O}(|z|^{\frac{4}{3}})$, $|\arg z|< \frac{\pi}{2}$, we have

$$D_\nu(z) \sim z^\nu e^{-\frac{1}{4}z^2 - \frac{\nu^2}{2z^2} - \frac{\nu^3}{2z^4}} \left\{ 1 + \frac{\nu}{2z^2} - \frac{5\nu^4}{6z^6} + \cdots \right\}. \tag{A.20}$$

### A.4.3 Expansion for large $\nu$ and $z$, with $z = \sqrt{2}e^{-\frac{\pi i}{4}}x$, $x > 0$ and $\nu$ not near $-ix^2/2$

Here we follow Rice [113], where a number of expansions similar to those that we list here can be found, and use the integral representation (A.4), which we write in the form

$$D_\nu(\bar{p}x) = \frac{\Gamma(1+\nu)e^{\nu\pi i}e^{\frac{ix^2}{2}}2^{-\frac{\nu}{2}}}{2\pi i} \int_C \frac{\exp\left(-t^2 + 2e^{-\frac{\pi i}{4}}xt - \nu\log t\right)}{t} dt. \tag{A.21}$$

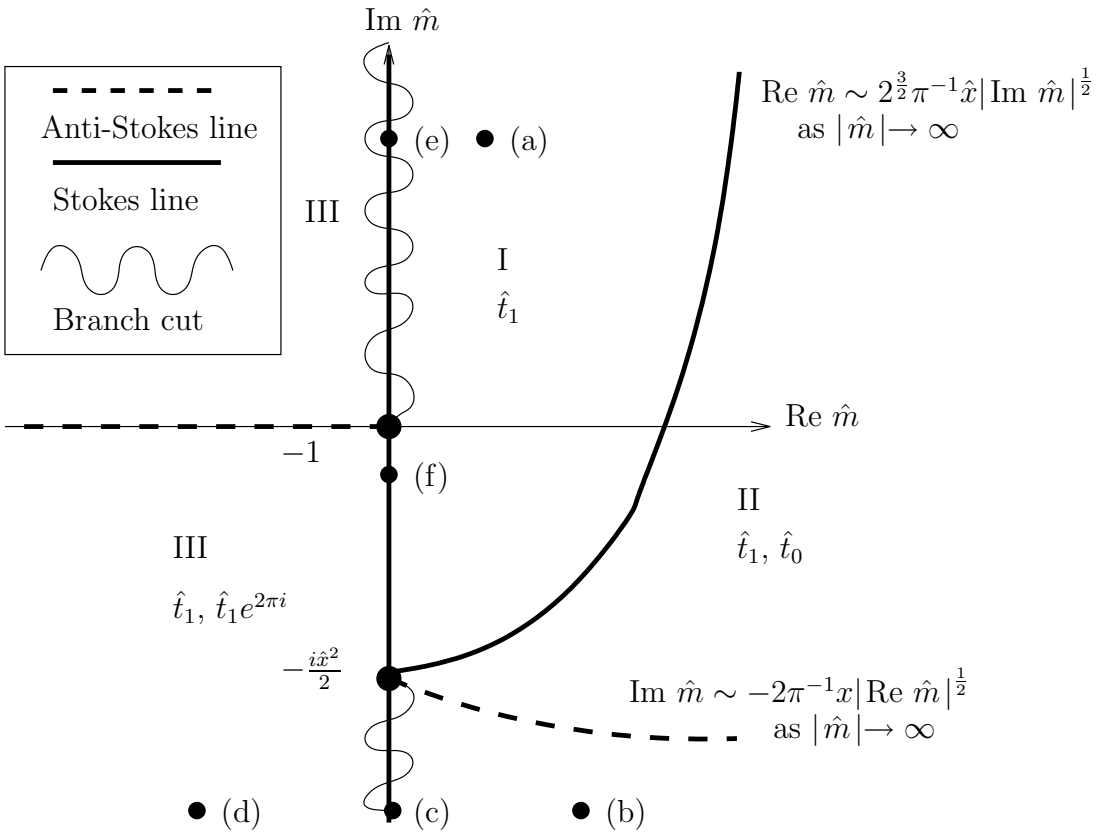


**Figure A.2:** Stokes lines, anti-Stokes lines and branch cuts for the asymptotic expansions of $D_\nu(\bar{p}\xi)$. The points (a) to (f) correspond to the values of $\hat{m}$ for the steepest descent paths shown in Figures A.3 and A.4.

We introduce the scalings $x = \sqrt{k}\hat{x}$, $m = \nu = k\hat{m}$ and $t = \sqrt{k}\hat{t}$ for some large parameter $k$, and this gives

$$D_\nu(\bar{p}x) = \frac{\Gamma(1+k\hat{m})e^{\frac{ik\hat{x}^2}{2}}(2k)^{-\frac{k\hat{m}}{2}}}{2\pi i}\int_C \frac{1}{\hat{t}}\exp\left\{k(-\hat{t}^2 + 2e^{-\frac{\pi i}{4}}\hat{x}\hat{t} - \hat{m}\log\hat{t})\right\}d\hat{t}. \qquad \text{(A.22)}$$

The asymptotic expansion of this integral for large $k$ may be found by the method of steepest descents. The phase of the integrand is $\hat{u} = -\hat{t}^2 + 2e^{-\frac{\pi i}{4}}\hat{x}\hat{t} - \hat{m}\log\hat{t}$, so saddle points are given by the solutions of $0 = d\hat{u}/\hat{t} = -2\hat{t} + 2e^{-\frac{\pi i}{4}}\hat{x} - \hat{m}/\hat{t}$, namely

$$\hat{t}_0 = \frac{1}{2}\left\{e^{-\frac{\pi i}{4}}\hat{x} + (-i\hat{x}^2 - 2\hat{m})^{\frac{1}{2}}\right\}, \quad \hat{t}_1 = \frac{1}{2}\left\{e^{-\frac{\pi i}{4}}\hat{x} - (-i\hat{x}^2 - 2\hat{m})^{\frac{1}{2}}\right\}. \qquad \text{(A.23)}$$

Here we follow [113] and choose the square root to be the principal branch for $-\frac{3\pi}{2} \le \arg(-i\hat{x}^2 - 2\hat{m}) < \frac{\pi}{2}$. This causes $\hat{t}_0$ to lie in the half plane $-\frac{3\pi}{4} \le \arg(\hat{t} - \frac{e^{-\frac{\pi i}{4}}\hat{x}}{2}) < \frac{\pi}{4}$, and $\hat{t}_1$ to lie in the complementary half plane. We also take the branch cut in the logarithm to be along the line $\arg\hat{t} = \frac{3\pi}{4}$, and consider the phase $\hat{u}$ as a multi-function. The contour of integration joins the valley at $e^{-\pi i}\infty$ to the valley at $e^{\pi i}\infty$, and so there is also the

possibility that the saddle point at $e^{2\pi i}\hat{t}_1$ (on the next sheet of the Riemann surface of the logarithm) is switched on.

The asymptotic expansion may only be discontinuous across lines where the phases of two of the saddle point contributions have equal imaginary part, and these are known as Stokes lines. By considering the nature of the paths of steepest decent in each of the regions bounded by these lines, we find that the active Stokes lines (those where a contribution is actually switched on or off) are as in Figure A.2. Typical forms of the steepest descent paths in each of these regions can be seen in Figure A.3.

Starting in region I at the point (a) (shown in Figure 4.4) the contour of integration passes through the saddle $\hat{t}_1$ but not $\hat{t}_0$, as can be seen in the top row of Figure A.3. As we cross the Stokes line and move into region II the integration contour passes through $\hat{t}_0$, and at point (b) in region II and we pick up both saddle point contributions as shown in the middle row of Figure A.3. As we cross the imaginary axis below $-\frac{i\hat{x}}{2}$, and move into region III, we cross a branch cut and a double Stokes line. The branch cut is associated with the square root in (A.23) and is a result of the labels $\hat{t}_0$ and $\hat{t}_1$ switching, as illustrated in the top row of Figure A.4 (at the point (c)). At the same time the steepest descent contour from $e^{-\pi i}\infty$ through $\hat{t}_1$ passes through $\hat{t}_0$ and through $\hat{t}_1 e^{2\pi i}$. Thus the contribution from $\hat{t}_1$ (which is relabelled as $\hat{t}_0$ when we cross the branch cut) is turned off and the contribution from $t_0 e^{2\pi i}$ (which is relabelled as $\hat{t}_1 e^{2\pi i}$ is turned on as we cross this line). The steepest descent contours at the point (d) in region III may be seen in the bottom row of Figure A.3.

If we complete the circuit in the complex $\hat{m}$ plane we again meet a branch cut and a Stokes line along the positive imaginary axis (at the point (e)), which lies between regions III and I. The branch cut here corresponds to the saddle point $\hat{t}_1$ passing through the branch cut of the logarithm, so that $\hat{t}_1 e^{2\pi i}$ on the left of the branch cut (in the $\hat{m}$ plane) becomes $\hat{t}_1$ on the right. At the same time the steepest descent path through $\hat{t}_1$ passes through $\hat{t}_1 e^{2\pi i}$, so that as we cross the Stokes line (from left to right) the contribution from $\hat{t}_1$ disappears. The steepest descent contours at the point (e) on this line are shown on the middle row of Figure A.4. Finally, let us check what happens as we cross the imaginary axis from region I to region III between 0 and $-\frac{ix^2}{2}$ we cross the same Stokes line as on 0 to $i\infty$, but not the branch cut. The steepest descent contours at the point (f) on this line may be seen in the bottom row of Figure A.4, and we see that this is just a standard Stokes line.

Evaluating the saddle point contributions we find that [113]

$$D_\nu(\bar{p}x) \sim \frac{\Gamma(1+\nu)2^{\frac{\nu}{2}}}{\sqrt{2\pi}(-ix^2-2\nu)^{\frac{1}{4}}} \begin{cases} A_1 & \text{in I} \\ A_1 + A_0 & \text{in II} \\ A_1(1-e^{-2\pi i\nu}) & \text{in III} \end{cases} \tag{A.24}$$

where

$$A_1 = \exp\left(-\frac{e^{-\frac{\pi i}{4}}x}{2}(-ix^2-2\nu)^{\frac{1}{2}} + \frac{\nu}{2} - (\nu+\frac{1}{2})\log\left(e^{-\frac{\pi i}{4}}x - (-ix^2-2\nu)^{\frac{1}{2}}\right)\right), \tag{A.25}$$

$$A_0 = -i\exp\left(\frac{e^{-\frac{\pi i}{4}}x}{2}(-ix^2-2\nu)^{\frac{1}{2}} + \frac{\nu}{2} - (\nu+\frac{1}{2})\log\left(e^{-\frac{\pi i}{4}}x + (-ix^2-2\nu)^{\frac{1}{2}}\right)\right). \tag{A.26}$$

To evaluate $D_{-1-\nu}(\bar{p}x)$ we write

$$D_{-1-\nu}(\bar{p}x) = \frac{\Gamma(-\nu)e^{\frac{ix^2}{2}}2^{\frac{1}{2}+\frac{\nu}{2}}}{2\pi i}\int_C \exp\left(-t^2 + 2e^{-\frac{\pi i}{4}}xt + \nu\log t\right)dt \tag{A.27}$$

and if we make the same scalings as before, but with $\nu = -k\hat{m}$, we find that the integral has the same phase as before, but with different amplitude. This gives

$$D_{-1-\nu}(\bar{p}x) \sim \frac{\Gamma(-\nu)2^{-\frac{\nu}{2}}}{2\sqrt{\pi}(-ix^2+2\nu)^{\frac{1}{4}}} \begin{cases} B_1 & \text{in I} \\ B_1 + B_0 & \text{in II} \\ B_1(1-e^{2\pi i\nu}) & \text{in III} \end{cases} \tag{A.28}$$

where

$$B_1 = \exp\left(-\frac{e^{-\frac{\pi i}{4}}x(-ix^2+2\nu)^{\frac{1}{2}}}{2} - \frac{\nu}{2} + (\nu+\frac{1}{2})\log\left(e^{-\frac{\pi i}{4}}x - (-ix^2+2\nu)^{\frac{1}{2}}\right)\right), \tag{A.29}$$

$$B_0 = -i\exp\left(\frac{e^{-\frac{\pi i}{4}}x(-ix^2+2\nu)^{\frac{1}{2}}}{2} - \frac{\nu}{2} + (\nu+\frac{1}{2})\log\left(e^{-\frac{\pi i}{4}}x + (-ix^2+2\nu)^{\frac{1}{2}}\right)\right). \tag{A.30}$$

with regions I, II and III as before in the $\hat{m}$ plane (so the regions in the $\nu$ plane are as for $D_\nu(\bar{p}x)$, but rotated by a half turn about the origin).

By this method we may also compute the asymptotic expansion of the derivatives of $D_\nu$, as

$$\frac{\partial D_\nu}{\partial z}(z) = \frac{\Gamma(\nu+1)e^{-\frac{z^2}{4}}2^{-\frac{\nu}{2}}}{2\pi i}\int_C (\sqrt{2}t - 2z)\exp\left(-t^2 + \sqrt{2}zt - (\nu+1)\log t\right)dt, \tag{A.31}$$

so the saddle point contributions are as before, but multiplied by a $-2z+\sqrt{2}t$ prefactor, and we may also perform a very similar procedure to find the expansion of the derivative with respect to $\nu$.

We note here that the above asymptotic expansions are asymptotic for fixed $x$ and $|\,\nu\,|\gg 1$. The expressions are however not asymptotic for fixed $\mu$ and $x\to\infty$, as the saddle point $t_1$ approaches the logarithmic singularity of the phase at $t=0$. In this case the saddle point contributions may be calculated by Bleistein's method [100] [139], and it is found that they are the same as those above, but with the gamma functions replaced by their asymptotic approximations for large $|\,\nu\,|$. This result may also be seen by considering the steepest descent analysis of (A.5), as the saddle point analysis of this integral is still valid for bounded $|\,\nu\,|$.

### A.4.4 Expansion for small $|\,z\,|$

The power series for the PCFs converges everywhere, and by using the first two terms we find that

$$D_\nu(z)\sim\frac{2^{\frac{\nu}{2}}\sqrt{\pi}}{\Gamma(\frac{1}{2}-\frac{\nu}{2})}\left(1-\frac{z\sqrt{2}\Gamma(\frac{1}{2}-\frac{\nu}{2})}{\Gamma(-\frac{\nu}{2})}\right), \tag{A.32}$$

$$D'_\nu(z)\sim-\frac{2^{\frac{\nu+1}{2}}\sqrt{\pi}}{\Gamma(-\frac{\nu}{2})}\left(1+\frac{z(\nu+\frac{1}{2})\Gamma(-\frac{\nu}{2})}{\sqrt{2}\Gamma(\frac{1}{2}-\frac{\nu}{2})}\right), \tag{A.33}$$

for small $|\,z\,|$.

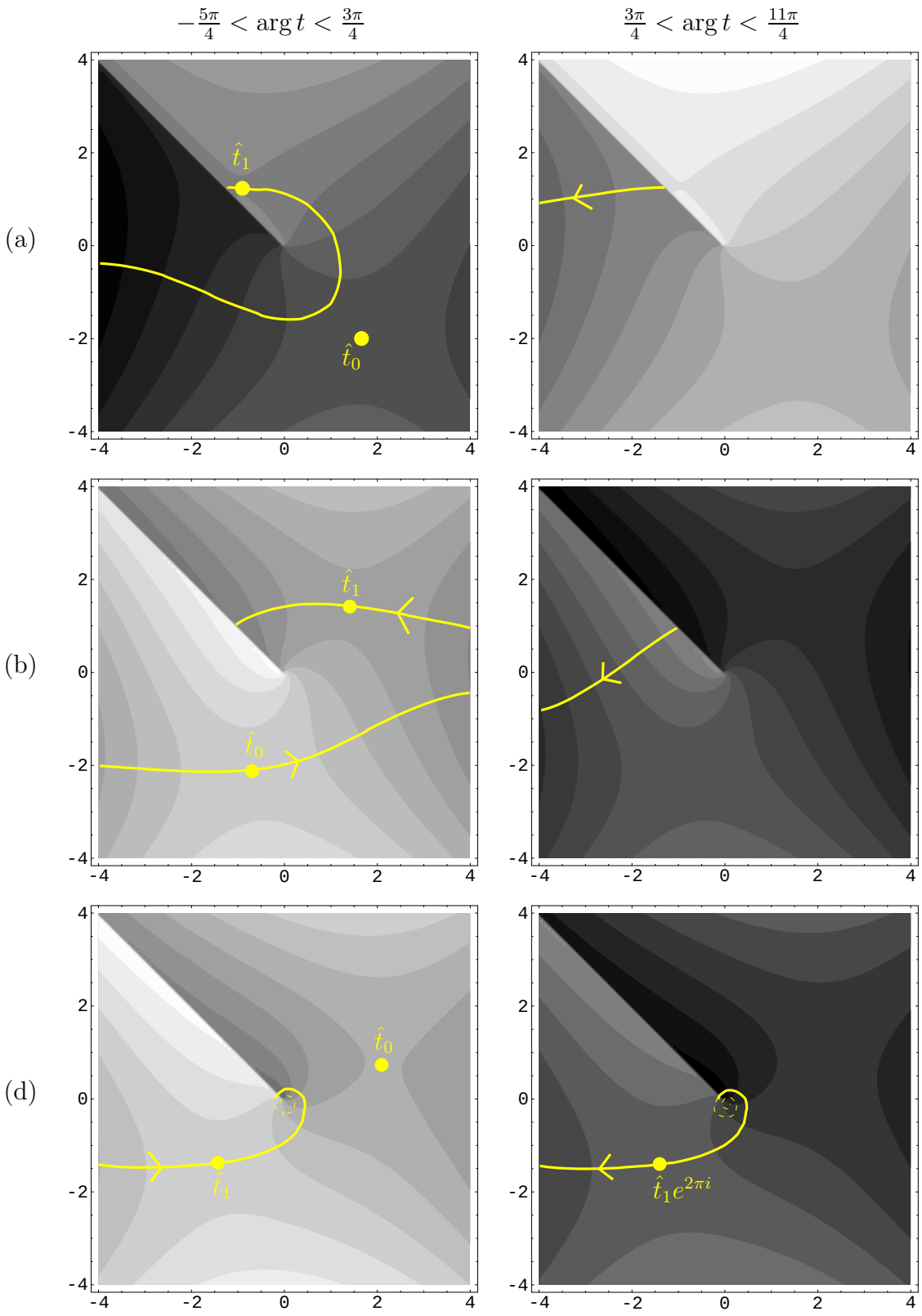


**Figure A.3:** Saddle points and paths of steepest descent in the complex $\hat{t}$ plane for the integral representations of the PCFs, which each row corresponding to regions I, II and III respectively. The circles indicate the saddle points, and the shading shows the behaviour of the real part of the phase (with lighter shading indicating a greater real part). In each case the left hand figure is for the sheet of the logarithm $-\frac{5\pi}{4} < \arg\ t < \frac{3\pi}{4}$ and the right hand figure is for the sheet $\frac{3\pi}{4} < \arg\ t < \frac{11\pi}{4}$. (The specific values of the parameters used were $\hat{x} = 1$, and $\hat{m} = 2 + 8i$, $\hat{m} = 4 - 8i$ and $\hat{m} = -4 - 8i$ respectively.)

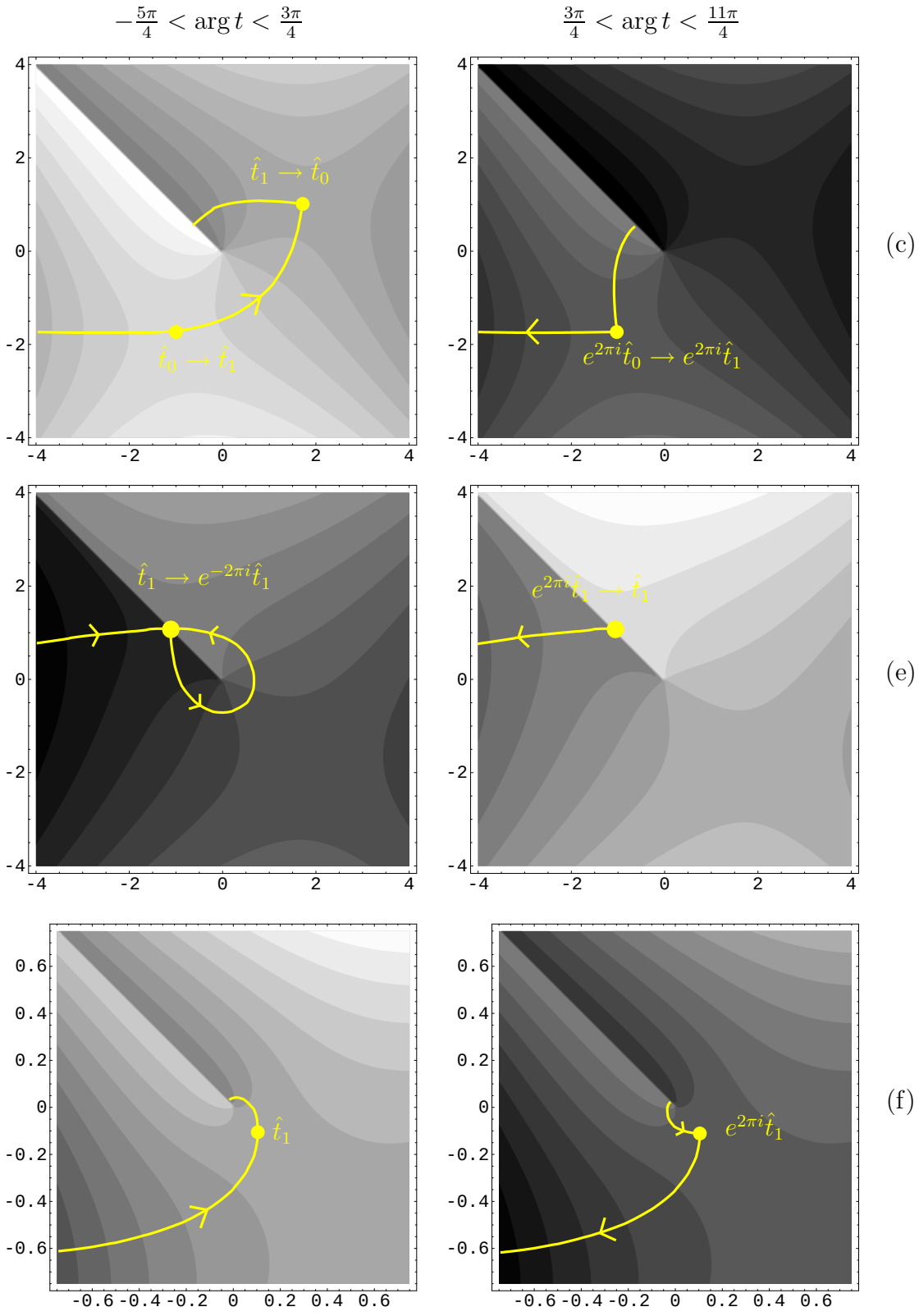


**Figure A.4:** Steepest descent paths on the boundaries between the regions in Figure (A.2). The first row shows the change in integration contours when we pass from region II into region III (between $-i\hat{x}^2/2$ and $-i\infty$); the second row shows the contours when we pass from region III into region I (across the positive imaginary axis); and the third row is when we pass from region I into region III between 0 and $-i\hat{x}^2/2$. (Again $\hat{x} = 1$ for all these plots, and $\hat{m} = -8i$, $\hat{m} = 8i$ and $\hat{m} = -\frac{i}{4}$ respectively.)

# Appendix B

# Discussion of Behaviour of the Integrands in the Thin Edge Problem

In Section (4.2) we discussed the approximation of a number of integrals related to the problem of diffraction by a thin body, and here we will set out the phase-amplitude expansions for the integrands of $I_s$, $I_s^1$, and $I_s^2$. We will discuss the behaviour of these integrands for large $\hat{\nu}$, including the location of any saddle points .

## B.1 Phase-amplitude expansions

We introduce the scalings (4.41), and use the expansions of section A.4.3 to approximate the $\xi$ and $\eta$ dependent PCFs in our integrands. When we do this, we find that the integrand of the initial integral $I_s$ has asymptotic expansion of the form

$$\frac{-i\sqrt{r}}{8\sqrt{\pi}\cos\frac{\phi_0}{2}}\frac{\exp(r\hat{\nu}\log\tan\frac{\phi_0}{2})}{\sin^2(r\hat{\nu}\pi)(-i\hat{\xi}^2-2\hat{\nu})^{\frac{1}{4}}(-i\hat{\eta}^2+2\hat{\nu})^{\frac{1}{4}}}J(\hat{\xi},\hat{\eta},\hat{\nu}). \tag{B.1}$$

for large $r$. Because of the Stokes lines of the constituent PCFs, the expansion of the integrand has different forms in the different regions of the complex $\hat{\nu}$ plane, and these are shown in Figure B.1. The behaviour of $J$ in each of these regions is

| Region | $J$ |
|---|---|
| (i) | $(1-e^{-2r\pi\hat{\nu}i})R_1S_1$ |
| (ii) | $(1-e^{2r\pi\hat{\nu}i})R_1S_1$ |
| (iii) | $(1-e^{-2r\pi\hat{\nu}i})R_1(S_1-S_0)$ |
| (iv) | $(1-e^{2r\pi\hat{\nu}i})(R_1-R_0)S_1$ |

where

$$R_0 = i\exp\left(\frac{re^{-\frac{\pi i}{4}}\hat{\xi}}{2}(-i\hat{\xi}^2-2\hat{\nu})^{\frac{1}{2}}-(r\hat{\nu}+\frac{1}{2})\log(e^{-\frac{\pi i}{4}}\hat{\xi}+(-i\hat{\xi}^2-2\hat{\nu})^{\frac{1}{2}})\right), \quad \text{(B.2)}$$

$$R_1 = \exp\left(-\frac{re^{-\frac{\pi i}{4}}\hat{\xi}}{2}(-i\hat{\xi}^2-2\hat{\nu})^{\frac{1}{2}}-(r\hat{\nu}+\frac{1}{2})\log(e^{-\frac{\pi i}{4}}\hat{\xi}-(-i\hat{\xi}^2-2\hat{\nu})^{\frac{1}{2}})\right), \quad \text{(B.3)}$$

$$S_0 = i\exp\left(\frac{re^{-\frac{\pi i}{4}}\hat{\eta}}{2}(-i\hat{\eta}^2+2\hat{\nu})^{\frac{1}{2}}+(r\hat{\nu}+\frac{1}{2})\log(e^{-\frac{\pi i}{4}}\hat{\eta}+(-i\hat{\eta}^2+2\hat{\nu})^{\frac{1}{2}})\right), \quad \text{(B.4)}$$

$$S_1 = \exp\left(-\frac{re^{-\frac{\pi i}{4}}\hat{\eta}}{2}(-i\hat{\eta}^2+2\hat{\nu})^{\frac{1}{2}}+(r\hat{\nu}+\frac{1}{2})\log(e^{-\frac{\pi i}{4}}\hat{\eta}-(-i\hat{\eta}^2+2\hat{\nu})^{\frac{1}{2}})\right). \quad \text{(B.5)}$$

In order to find these expansions explicitly in phase-amplitude form we must also expand the $1/\sin^2(\nu\pi)$ term as a series of exponentials (in a similar manner to (4.56)), but we omit the details of this.

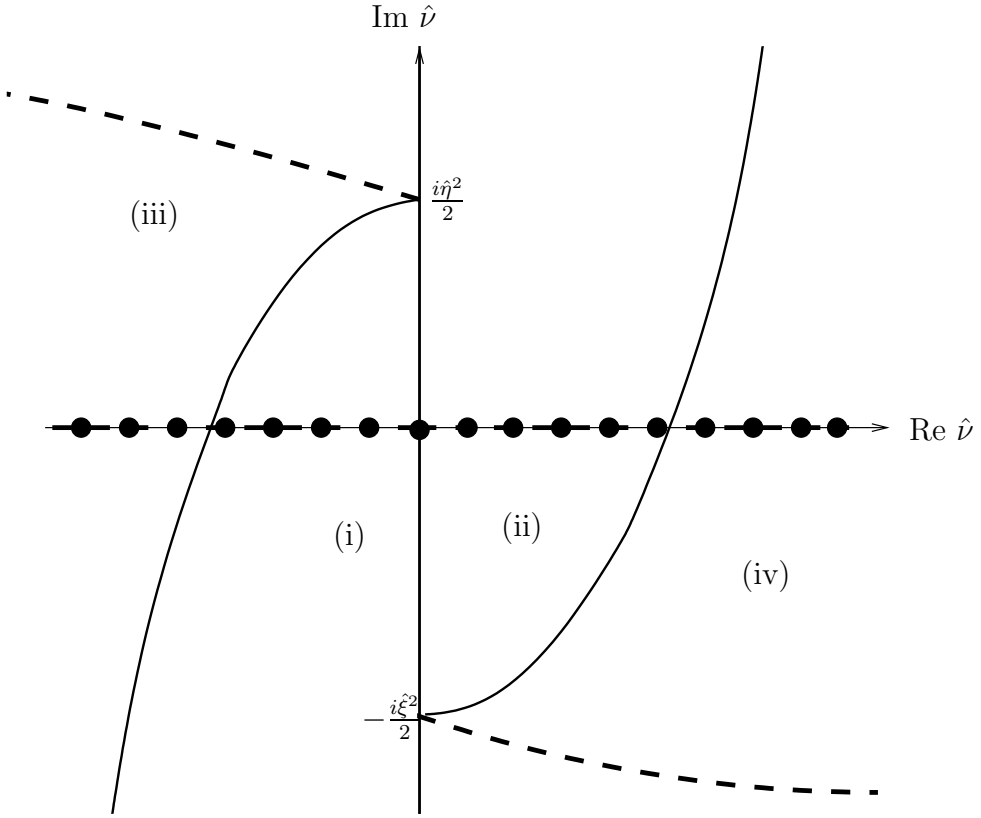


**Figure B.1:** Regions of differing asymptotic behaviour in the $\hat{\nu}$ plane for the integrands of $I_s$ and $I_s^1$.

For the integral $I_s^1$ (only considered for $\xi < 0$) the expansion is identical form to the previous one, but with $\xi$ replaced by $|\xi|$ and an additional factor $e^{\nu\pi i}$.

In order to find the expansion of the integrand of $I_s^2$ (again only considered for $\xi < 0$) we must first apply the reflection formula (A.8), which gives us that

$$D_{-1-\nu}(p\,|\xi\,|) = \overline{D_{-1-\bar{\nu}}(\bar{p}\,|\xi\,|)}. \tag{B.6}$$

Then we find that the integrand has approximation

$$-\frac{\Gamma(-r\hat{\nu})}{8\pi\sqrt{r}\cos\frac{\phi_0}{2}}\frac{\exp\left\{r\hat{\nu}\log(\tan\frac{\phi_0}{2}) - r\hat{\nu}\log 2 - r\hat{\nu} + \frac{r\hat{\nu}\pi i}{2}\right\}}{\sin(r\hat{\nu}\pi)(i\,|\hat{\xi}\,|^2 + 2\hat{\nu})^{\frac{1}{4}}(-i\hat{\eta}^2 + 2\hat{\nu})^{\frac{1}{4}}}K. \tag{B.7}$$

On expanding the gamma function using Stirling's approximation we have

$$-\frac{1}{4\sqrt{2\pi r}\cos\frac{\phi_0}{2}}\frac{\exp\left\{r\hat{\nu}\log(\tan\frac{\phi_0}{2}) - (r\hat{\nu}+\frac{1}{2})\log(-\hat{\nu}) - r\hat{\nu}\log 2 + \frac{r\hat{\nu}\pi i}{2}\right\}}{\sin(r\hat{\nu}\pi)(i\,|\hat{\xi}\,|^2 + 2\hat{\nu})^{\frac{1}{4}}(-i\hat{\eta}^2 + 2\hat{\nu})^{\frac{1}{4}}}K, \tag{B.8}$$

for $|\arg(-\nu)| < \pi$, and on using

$$\Gamma(-\nu) = -\frac{\pi}{\Gamma(\nu)\nu\sin(\nu\pi)} \sim \sqrt{\frac{\pi}{2}}\frac{\nu^{-\nu-\frac{1}{2}}e^{\nu}}{\sin(\nu\pi)}, \tag{B.9}$$

we have that the integrand has expansion

$$\frac{1}{8\sqrt{2\pi r}\cos\frac{\phi_0}{2}}\frac{\exp\left\{r\hat{\nu}\log(\tan\frac{\phi_0}{2}) - (r\hat{\nu}+\frac{1}{2})\log(\hat{\nu}) - r\hat{\nu}\log 2 + \frac{r\hat{\nu}\pi i}{2}\right\}}{\sin^2(r\hat{\nu}\pi)(i\,|\hat{\xi}\,|^2 + 2\hat{\nu})^{\frac{1}{4}}(-i\hat{\eta}^2 + 2\hat{\nu})^{\frac{1}{4}}}K \tag{B.10}$$

in $|\arg\nu| < \pi$. For the integrand of $I_s^2$ the regions in the $\hat{\nu}$ plane are different to before, because the Stokes lines of the $\xi$- dependent PCFs differ. The boundaries are now as in Figure B.2, and the behaviour of $K$ is given by

| Region | $K$ |
|---|---|
| (i) | $R_1S_1$ |
| (ii) | $R_1(S_1 - S_0)$ |
| (iii) | $(R_1 - R_0)S_1$ |
| (iv) | $(R_1 - R_0)(S_1 - S_0)$ |
| (v) | $R_1S_1(1 - e^{-2\nu\pi i})(1 - e^{2\nu\pi i})$ |

where

$$R_0 = i\exp\left(\frac{re^{\frac{\pi i}{4}}\,|\hat{\xi}|}{2}(i\,|\hat{\xi}\,|^2 + 2\hat{\nu})^{\frac{1}{2}} + (r\hat{\nu}+\frac{1}{2})\log(e^{\frac{\pi i}{4}}\,|\hat{\xi}| + (i\,|\hat{\xi}\,|^2 + 2\hat{\nu})^{\frac{1}{2}})\right), \tag{B.11}$$

$$R_1 = \exp\left(-\frac{re^{\frac{\pi i}{4}}\,|\hat{\xi}|}{2}(i\,|\hat{\xi}\,|^2 + 2\hat{\nu})^{\frac{1}{2}} + (r\hat{\nu}+\frac{1}{2})\log(e^{\frac{\pi i}{4}}\,|\hat{\xi}| - (i\,|\hat{\xi}\,|^2 + 2\hat{\nu})^{\frac{1}{2}})\right), \tag{B.12}$$

$$S_0 = i\exp\left(\frac{re^{-\frac{\pi i}{4}}\hat{\eta}}{2}(-i\hat{\eta}^2 + 2\hat{\nu})^{\frac{1}{2}} + (r\hat{\nu}+\frac{1}{2})\log(e^{-\frac{\pi i}{4}}\hat{\eta} + (-i\hat{\eta}^2 + 2\hat{\nu})^{\frac{1}{2}})\right), \tag{B.13}$$

$$S_1 = \exp\left(-\frac{re^{-\frac{\pi i}{4}}\hat{\eta}}{2}(-i\hat{\eta}^2 + 2\hat{\nu})^{\frac{1}{2}} + (r\hat{\nu}+\frac{1}{2})\log(e^{-\frac{\pi i}{4}}\hat{\eta} - (-i\hat{\eta}^2 + 2\hat{\nu})^{\frac{1}{2}})\right). \tag{B.14}$$

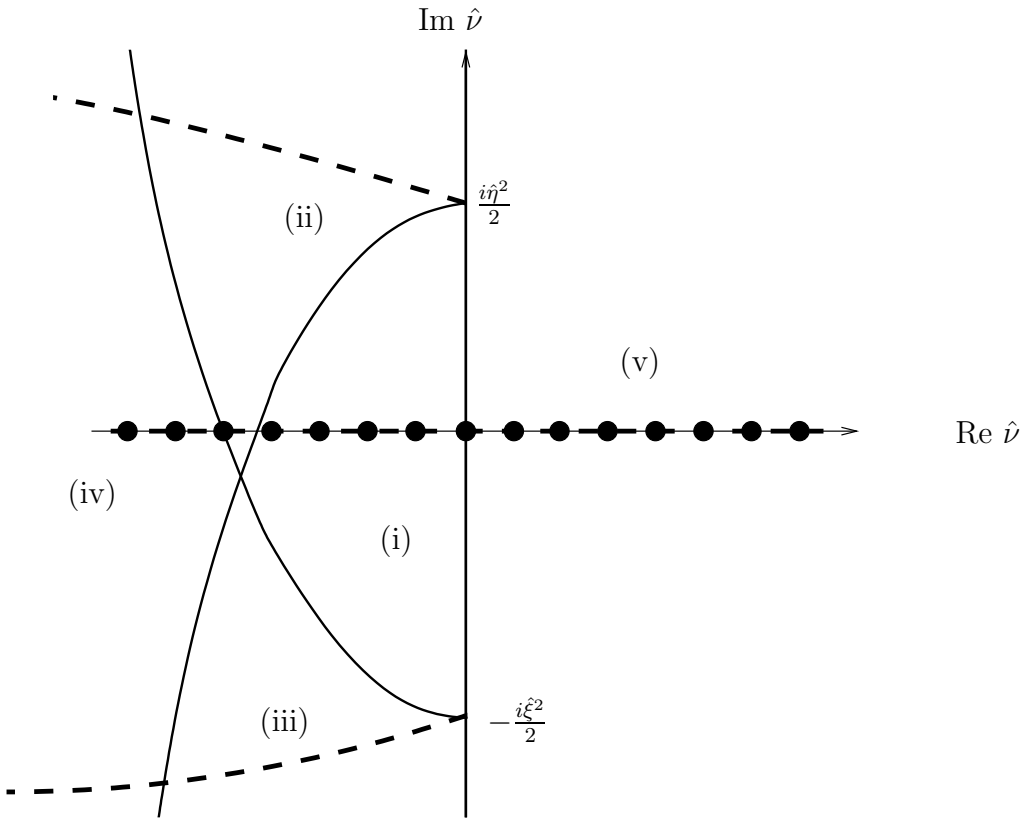


**Figure B.2:** Regions of differing asymptotic behaviour in the $\hat{\nu}$ plane for the integrand of $I_s^2$.

## B.2 Saddle points

We now wish to identify the points at which the derivative of the phase of the above expansions vanishes, which are known as the saddle-points of the approximations, as these play a sigificant role in the expansion of the integrals.

These expansions are fairly complicated, because of the Stokes lines of the PCFs and the branch cuts in their approximations. However, for the integrand of $I_s$ the phase is always of the form

$$\begin{aligned} u &= \pm_1 \frac{e^{-\frac{\pi i}{4}}\hat{\xi}}{2}(-i\hat{\xi}^2 - 2\hat{\nu})^{\frac{1}{2}} - \hat{\nu}\log(e^{-\frac{\pi i}{4}}\hat{\xi} \pm_1 (-i\hat{\xi}^2 - 2\hat{\nu})^{\frac{1}{2}}) \\ &\quad \pm_2 \frac{e^{-\frac{\pi i}{4}}\eta}{2}(-i\hat{\eta}^2 + 2\hat{\nu})^{\frac{1}{2}} + \hat{\nu}\log(e^{-\frac{\pi i}{4}}\hat{\eta} \pm_2 (-i\hat{\eta}^2 + 2\hat{\nu})^{\frac{1}{2}}) \\ &\quad + 2n\hat{\nu}\pi i + 2\mathrm{Sgn}(\mathrm{Im}\ \hat{\nu})\hat{\nu}\pi i + \nu\log\tan\frac{\phi_0}{2} \end{aligned} \tag{B.15}$$

where $\pm_1$ is $+$ when we take the $R_0$ contribution and $-$ when we take the $R_1$ contribution, and similarly for $\pm_2$ and $S_0$, $S_1$. Here n is one of $-1$, 0 or 1, depending upon the $e^{\pm 2\nu\pi i}$

pre-factor of the expansion. In any case we may differentiate this phase to give

$$\begin{aligned}\frac{du}{d\nu} &= -\log(e^{-\frac{\pi i}{4}}\hat{\xi} \pm_1 (-i\hat{\xi}^2 - 2\hat{\nu})^{\frac{1}{2}}) + \log(e^{-\frac{\pi i}{4}}\hat{\eta} \pm_2 (-i\hat{\eta}^2 + 2\hat{\nu})^{\frac{1}{2}}) \\ &\quad +2n\pi i + 2\mathrm{Sgn}(\mathrm{Im}\ \hat{\nu})\pi i + \log\tan\frac{\phi_0}{2} \end{aligned} \tag{B.16}$$

It is possible to find from this expression that Im $\frac{du}{d\nu}$ is positive in the upper half of the complex $\nu$ plane, and negative in the lower half plane, so the integrand decays exponentially away from the real axis, and there cannot be a saddle point.

For $I_s^1$ the phase is

$$\begin{aligned} u &= \pm_1 \frac{e^{-\frac{\pi i}{4}}\,|\hat{\xi}|}{2}(-i\hat{\xi}^2 - 2\hat{\nu})^{\frac{1}{2}} - \hat{\nu}\log(e^{-\frac{\pi i}{4}}\,|\hat{\xi}| \pm_1(-i\hat{\xi}^2 - 2\hat{\nu})^{\frac{1}{2}}) \\ &\quad \pm_2 \frac{e^{-\frac{\pi i}{4}}\hat{\eta}}{2}(-i\hat{\eta}^2 + 2\hat{\nu})^{\frac{1}{2}} + \hat{\nu}\log(e^{-\frac{\pi i}{4}}\hat{\eta} \pm_2 (-i\hat{\eta}^2 + 2\hat{\nu})^{\frac{1}{2}}) \\ &\quad +2n\hat{\nu}\pi i + 2\mathrm{Sgn}(\mathrm{Im}\ \hat{\nu})\hat{\nu}\pi i + \hat{\nu}\log\tan\frac{\phi_0}{2} + \hat{\nu}\pi i. \end{aligned} \tag{B.17}$$

This differentiates to give

$$\begin{aligned}\frac{du}{d\nu} &= -\log(e^{-\frac{\pi i}{4}}\,|\hat{\xi}| \pm_1(-i\hat{\xi}^2 - 2\hat{\nu})^{\frac{1}{2}}) + \log(e^{-\frac{\pi i}{4}}\hat{\eta} \pm_2 (-i\hat{\eta}^2 + 2\hat{\nu})^{\frac{1}{2}}) \\ &\quad +2n\pi i + 2\mathrm{Sgn}(\mathrm{Im}\ \hat{\nu})\pi i + \log\tan\frac{\phi_0}{2} + \pi i, \end{aligned} \tag{B.18}$$

and exponentiating this expression we have that any saddle point must satisfy a relationship of the form

$$\frac{e^{-\frac{\pi i}{4}}\hat{\eta} \pm_2 (-i\hat{\eta}^2 + 2\hat{\nu})^{\frac{1}{2}}}{e^{-\frac{\pi i}{4}}\,|\hat{\xi}| \pm_1(-i\hat{\xi}^2 - 2\hat{\nu})^{\frac{1}{2}}}\tan\frac{\phi_0}{2} = -1. \tag{B.19}$$

Using the fact that $\hat{\xi} = \sqrt{2}\cos\frac{\phi}{2}$, $\hat{\eta} = \sqrt{2}\sin\frac{\phi}{2}$ we find that

$$\left(|\cos\frac{\phi}{2}| \pm_1(\cos^2\frac{\phi}{2} - \hat{\nu}i)^{\frac{1}{2}}\right) = -\tan\frac{\phi_0}{2}\left(\sin\frac{\phi}{2} \pm_2 (\sin^2\frac{\phi}{2} + \hat{\nu}i)^{\frac{1}{2}}\right), \tag{B.20}$$

and manipulating this expression we can obtain the additional constraint

$$\left(\sin\frac{\phi}{2} \mp_2 (\sin^2\frac{\phi}{2} + \nu i)^{\frac{1}{2}}\right) = \tan\frac{\phi_0}{2}\left(\left|\cos\frac{\phi}{2}\right| \mp_1 (\cos^2\frac{\phi}{2} - \nu i)^{\frac{1}{2}}\right). \tag{B.21}$$

This pair of equations (B.20), (B.21) actually provide a sufficient condition for $\hat{\nu}$ to be a saddle point, and we may solve them as linear equations in $(\cos^2\frac{\phi}{2} - \nu i)^{\frac{1}{2}}$ and $(\sin^2\frac{\phi}{2} + \nu i)^{\frac{1}{2}}$ to give

$$(\cos^2\frac{\phi}{2} - \hat{\nu}i)^{\frac{1}{2}} = \pm_1\cos(\frac{\phi}{2} + \phi_0), \tag{B.22}$$

$$(\sin^2\frac{\phi}{2} + \hat{\nu}i)^{\frac{1}{2}} = \pm_2\sin(\frac{\phi}{2} + \phi_0). \tag{B.23}$$

Both these equations have the solution

$$\hat{\nu} = -i \sin(\phi + \phi_0) \sin(\phi_0). \tag{B.24}$$

We note that this saddle point must occur along the imaginary axis in the $\nu$-plane, in between the two branch points of the phase at $-\hat{\xi}^2/2$ and $\hat{\eta}^2/2$. From Figure B.1 we see that in this region only the $R_1$ and $S_1$ contributions to the expansion of the integrand are present. Therefore we must take the lower choice of signs in the above expressions. In addition to this, we also require that we can solve equations (B.22) and (B.23) for $\nu$. Since in these expressions the square root is the usual branch (cut along the negative real axis), we require that the real parts of the right-hand sides are both positive. It is then easy to see that such a saddle point for $I_s^1$ can only occur when $2\pi - \phi_0 < \phi < 3\pi - 2\phi_0$.

For the integrand of $I_s^2$ the phase is

$$\begin{aligned} u &= \hat{\nu} \log \tan \frac{\phi_0}{2} + \frac{\hat{\nu}\pi i}{2} + \mathrm{Sgn}(\mathrm{Im}\hat{\nu})\hat{\nu}\pi i - \hat{\nu}\log 2 + (-\hat{\nu})\log(-\hat{\nu}) \\ &\quad \pm_1 \frac{e^{\frac{\pi i}{4}}\,|\hat{\xi}|}{2}(i\,|\hat{\xi}|^2 + 2\hat{\nu})^{\frac{1}{2}} + \hat{\nu}\log(e^{\frac{\pi i}{4}}\,|\hat{\xi}| \pm_1 (i\,|\hat{\xi}|^2 + 2\hat{\nu})^{\frac{1}{2}}) \\ &\quad \pm_2 \frac{e^{-\frac{\pi i}{4}}\hat{\eta}}{2}(-i\hat{\eta}^2 + 2\hat{\nu})^{\frac{1}{2}} + \hat{\nu}\log(e^{-\frac{\pi i}{4}}\hat{\eta} \pm_2 (-i\hat{\eta}^2 + 2\hat{\nu})^{\frac{1}{2}}) + 2n\pi i\hat{\nu} \end{aligned} \tag{B.25}$$

which differentiates to give

$$\begin{aligned} \frac{du}{d\nu} &= \log \tan \frac{\phi_0}{2} + \frac{\pi i}{2} + \mathrm{Sgn}(\mathrm{Im}\hat{\nu})\pi i - \log 2 - \log(-\hat{\nu}) + 2n\pi i \\ &\quad + \log(e^{\frac{\pi i}{4}}\,|\hat{\xi}| \pm_1 (i\hat{\xi}^2 + 2\hat{\nu})^{\frac{1}{2}}) + \log(e^{-\frac{\pi i}{4}}\hat{\eta} \pm_2 (-i\hat{\eta}^2 + 2\hat{\nu})^{\frac{1}{2}}). \end{aligned} \tag{B.26}$$

Proceeding as before we find a necessary condition to be

$$\tan \frac{\phi_0}{2}(\sin \frac{\phi}{2} \pm_2 (\sin^2 \frac{\phi}{2}^2 + i\hat{\nu})^{\frac{1}{2}}) = \cos \frac{\phi}{2} \pm_1 (\cos^2 \frac{\phi}{2} - i\hat{\nu})^{\frac{1}{2}}) \tag{B.27}$$

(using the fact that $\xi < 0$ in the region for which we consider this integral). In the same manner as for the previous integral we find that $I_s^2$ has a saddle point, at $\nu = -i \sin\phi_0 \sin(\phi_0 + \phi)$, provided that $3\pi - 2\phi_0 < \phi < 2\pi$.

## B.3 Far-fields of the integrands (for large $|\nu|$)

To to ensure that our integrals converge upon the various contours of integration in the complex plane, it is necessary to find the behaviour of their integrands at infinity in the $\nu$ plane ($\nu \gg r$). Although the expansions of B.1 are still valid here, it proves simpler to approximate the PCFs contained in the integrands using expansions (A.12)

and (A.13). The $1/\sin(\nu\pi)$ term is written in terms of exponentials, and the gamma function expanded using Stirling's approximation. The leading order behaviour of the integrand of $I_s$ is found to be

$$\frac{\text{sign}(\text{Im }\nu)}{2\sqrt{2\pi}\cos\frac{\phi_0}{2}\sqrt{\nu}}\exp\left(\nu\log\tan\frac{\phi_0}{2}+\text{sign}(\text{Im }\nu)\left(\bar{p}\xi\sqrt{\nu}+\frac{\nu\pi}{2}\right)i-\bar{p}\eta\sqrt{\nu}\right), \tag{B.28}$$

for the integrand of $I_s^1$ we have

$$\frac{\text{sign}(\text{Im }\nu)}{2\sqrt{2\pi}\cos\frac{\phi_0}{2}\sqrt{\nu}}\exp\left(\nu\pi i+\nu\log\tan\frac{\phi_0}{2}+\text{sign}(\text{Im }\nu)\left(\bar{p}\,|\xi|\,\sqrt{\nu}+\frac{\nu\pi}{2}\right)i-\bar{p}\eta\sqrt{\nu}\right), \tag{B.29}$$

and the integrand of $I_s^2$ has expansion

$$\frac{1}{2\sqrt{2\pi}\cos\frac{\phi_0}{2}\sqrt{\nu}}\exp\left(\frac{\nu\pi i}{2}+\nu\log\tan\frac{\phi_0}{2}-\bar{p}\eta\sqrt{\nu}-p\,|\xi|\,\sqrt{\nu}\right). \tag{B.30}$$

Regions for which the integrand grows exponentially in size as we go to infinity are referred to as "hills", and those regions for which the integrand decays exponentially are called "valleys". These may be determined from the above expansions by considering the behaviour of the real part of exponent, and are shown in Figure B.3. Here the angle $\alpha$ is $\tan^{-1}\left(\frac{\pi}{2|\log\tan\frac{\phi_0}{2}|}\right)$ and $\gamma$ is $\tan^{-1}\left(\frac{3\pi}{2|\log\tan\frac{\phi_0}{2}|}\right)$. If $\frac{\pi}{2}<\phi_0<\pi$ then these figures are reflected in the imaginary axis.

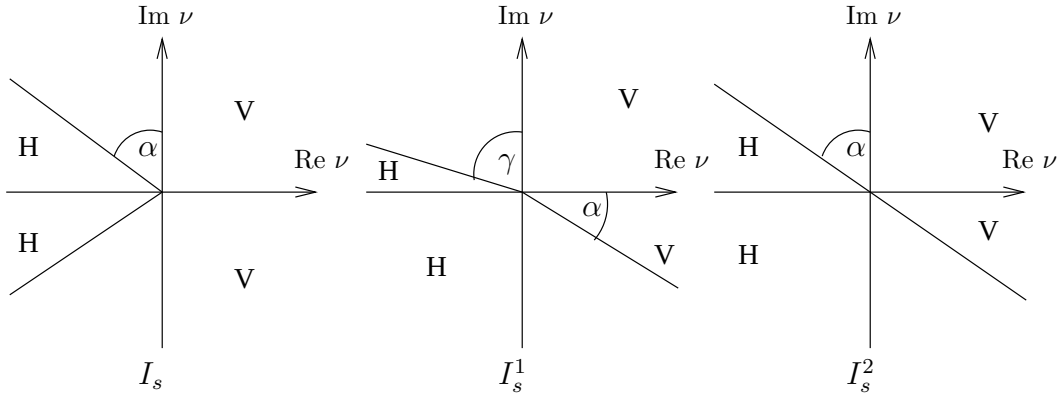


**Figure B.3:** Hills (H) and valleys (V) for the integrands of $I_s$, $I_s^1$ and $I_s^2$ in the complex $\nu$ plane. Here $\alpha=\tan^{-1}\left(\frac{\pi}{2|\log\tan\frac{\phi_0}{2}|}\right)$ and $\gamma=\tan^{-1}\left(\frac{3\pi}{2|\log\tan\frac{\phi_0}{2}|}\right)$.

# Appendix C

# Asymptotic Expansion of Ratio of $\beta$-dependent PCFs

The integrands of (4.60) and (4.61) differ from $I_s$ by a ratio of $\beta$-dependent PCFs. These terms may only be approximated in the limit of large $|\nu|$; when we utilise the results of section A.4.1 we find that they have leading order behaviour

$$\frac{D_{-1-\nu}(-\bar{p}\beta)}{D_{-1-\nu}(\bar{p}\beta)} \sim \exp(2\bar{p}\beta\sqrt{\nu}) \qquad \text{for } |\arg\nu|<\pi \tag{C.1}$$

$$\sim \frac{\sin(-\bar{p}\beta\sqrt{-\nu}+\frac{\nu\pi}{2})}{\sin(\bar{p}\beta\sqrt{-\nu}+\frac{\nu\pi}{2})} \quad \text{for } |\arg(-\nu)|<\pi \tag{C.2}$$

$$\frac{D'_{-1-\nu}(-\bar{p}\beta)}{D'_{-1-\nu}(\bar{p}\beta)} \sim \exp(2\bar{p}\beta\sqrt{\nu}) \qquad \text{for } |\arg\nu|<\pi \tag{C.3}$$

$$\sim \frac{\cos(-\bar{p}\beta\sqrt{-\nu}+\frac{\nu\pi}{2})}{\cos(\bar{p}\beta\sqrt{-\nu}+\frac{\nu\pi}{2})} \quad \text{for } |\arg(-\nu)|<\pi. \tag{C.4}$$

The restrictions on these regions of validity are due to the anti-Stokes lines of the PCFs, which are given by

$$|\text{Im }\nu| = \pm\frac{2\beta}{\pi}\,|\text{Re }\nu|^{\frac{1}{2}}\,. \tag{C.5}$$

and so the expansions are valid up to these lines (rather than to the positive or negative real axis). To avoid discontinuities in the behaviour of the ratio of functions across the negative real axis it proves useful to apply (A.11) to rewrite the PCFs contained in the numerators of the expressions, and this gives

$$\frac{D_{-1-\nu}(-\bar{p}\beta)}{D_{-1-\nu}(\bar{p}\beta)} = -e^{-\nu\pi i} + \frac{\sqrt{2\pi}}{\Gamma(1+\nu)}e^{-\frac{1}{2}\nu\pi i}\frac{D_\nu(p\beta)}{D_{-1-\nu}(\bar{p}\beta)}, \tag{C.6}$$

$$\frac{D'_{-1-\nu}(-\bar{p}\beta)}{D'_{-1-\nu}(\bar{p}\beta)} = e^{-\nu\pi i} - \frac{i\sqrt{2\pi}}{\Gamma(1+\nu)}e^{-\frac{1}{2}\nu\pi i}\frac{D'_\nu(p\beta)}{D'_{-1-\nu}(\bar{p}\beta)}, \tag{C.7}$$

and the large $|\nu|$ expansions become

$$\frac{D_{-1-\nu}(-\bar{p}\beta)}{D_{-1-\nu}(\bar{p}\beta)} \sim -e^{-\nu\pi i} - e^{-\frac{1}{2}\nu\pi i}\sin(\nu\pi)\frac{\exp(-p\beta\sqrt{-\nu})}{\sin(-\frac{\nu\pi}{2} - \bar{p}\beta\sqrt{-\nu})}, \tag{C.8}$$

$$\frac{D'_{-1-\nu}(-\bar{p}\beta)}{D'_{-1-\nu}(\bar{p}\beta)} \sim e^{-\nu\pi i} + ie^{-\frac{1}{2}\nu\pi i}\sin(\nu\pi)\frac{\exp(-p\beta\sqrt{-\nu})}{\cos(-\frac{\nu\pi}{2} - \bar{p}\beta\sqrt{-\nu})}, \tag{C.9}$$

valid in $|\arg(-\nu)| < \pi$

# Appendix D

# Perturbed Saddle Point Contributions

Laplace's method allows us to find asymptotic expansions (in the limit of large $k$) for integrals of the form

$$I(k) \quad \sim \quad \int_a^b f(x)e^{kg(x)}dx, \tag{D.1}$$

where $g(x)$ is a real-valued function. If $g(x)$ attains its maximum value at a single point $x_0$, then provided $f$ and $g$ are reasonably well behaved, the dominant contribution to the integral is supplied by a region near $x_0$. If $f(x)$ and $g(x)$ have suitable asymptotic expansions for $x$ near $x_0$ then it is possible to find an asymptotic expansion for $I(k)$; in the particular case when $x_0$ is at an interior point, $f$ and $g$ have power series about $x_0$ (which converge on a neighbourhood of $x_0$), and $g''(x_0) < 0$, we have that

$$I(k) = \left(\frac{2\pi}{k\,|\,g_2\,|}\right)^{\frac{1}{2}} e^{kg_0}\left(f_0 + k^{-1}\left\{\frac{f_1 g_3}{2\,|\,g_2\,|^2} + \frac{f_2}{2\,|\,g_2\,|} + \frac{f_0 g_4}{8\,|\,g_2\,|^2} + \frac{5f_0 g_3^2}{24\,|\,g_2\,|^3}\right\} + \mathcal{O}(k^{-2})\right), \tag{D.2}$$

where

$$f_n = f^{(n)}(x_0), \qquad g_n = g^{(n)}(x_0). \tag{D.3}$$

The higher order terms in this expansion are listed in [37, §5.3]. They may be found formally by substituting the power series into the integral, expanding the integrand when $x - x_0 = \mathcal{O}(k^{-\frac{1}{2}})$, and then replacing the upper and lower limits of integration by $\pm\infty$.

In Chapter 4 we will frequently want to find the large $k$ behaviour of integrals of the form

$$I(k) \quad \sim \quad \int_a^b f(x)e^{kg(x)+k^\alpha h(x)}dx \tag{D.4}$$

where $0 < \alpha < 1$. Integrals of this type are discussed in more detail (and with more rigour) in [100, §§9.2, 9.4]. We will only consider problems where $g$ has a quadratic maximum at $x_0$, and where all the functions involved have suitable power series which converge near $x_0$. On (formally) substituting these power series into the integral, making the change of variable $x = x_0 + k^{-\frac{1}{2}}\hat{x}$, and extending the limits of integration to infinity we have

$$I(k) \sim k^{-\frac{1}{2}} \int_{-\infty}^{\infty} (f_0 + k^{-\frac{1}{2}}\hat{x} f_1 + \ldots) e^{\left(kg_0 + \frac{1}{2}\hat{x}^2 g_2 + \frac{1}{6}k^{-\frac{1}{2}}\hat{x}^3 g_3 + \ldots\right) + \left(k^{\alpha} h_0 + k^{\alpha-\frac{1}{2}}\hat{x} h_1 + \frac{1}{2}k^{\alpha-1}\hat{x}^2 h_2 + \ldots\right)} d\hat{x}. \tag{D.5}$$

When $\alpha < \frac{1}{2}$ the additional terms in the phase just perturb the leading order result, and we find that

$$I(k) = \left(\frac{2\pi}{k\,|\,g_2\,|}\right)^{\frac{1}{2}} e^{kg_0 + k^{\alpha}h_0} \left\{ f_0 + k^{2\alpha-1}\frac{f_0 h_1^2}{2\,|\,g_2\,|} + k^{\alpha-1}\left(\frac{h_1 f_1}{|\,g_2\,|} + \frac{f_0 h_2}{2\,|\,g_2\,|}\right) + \mathcal{O}(k^{-1}, k^{3\alpha-\frac{3}{2}}) \right\}. \tag{D.6}$$

However when $\alpha = \frac{1}{2}$ we must retain additional terms in the phase of the exponent, and we find that

$$\begin{aligned} I(k) = &\left(\frac{2\pi}{k\,|\,g_2\,|}\right)^{\frac{1}{2}} e^{kg_0 + k^{\frac{1}{2}}h_0 + \frac{h_1^2}{2|g_2|^2}} \times \\ &\left\{ f_0 + k^{-\frac{1}{2}}\left(\frac{f_1 h_1}{|\,g_2\,|} + \frac{f_0 h_2}{2\,|\,g_2\,|} + \frac{f_0 g_3 h_1}{2\,|\,g_2\,|^2} + \frac{f_0 g_3 h_1^3}{6\,|\,g_2\,|^3} + \frac{f_0 h_1^2 h_2}{2\,|\,g_2\,|^2}\right) + \mathcal{O}(k^{-1}) \right\}. \end{aligned} \tag{D.7}$$

Alternatively the above expansions may be found formally by applying the standard saddle point formula with new phase $g^*(x) = g(x) + k^{\alpha-1}h(x)$. We may find an asymptotic expansion for the location of the saddle point in powers of $k^{\alpha-1}$, and then expand the standard saddle point formula in (fractional) powers of $k$.

# Bibliography


[1] J. Abad and J. Sesma. Computation of the regular confluent hypergeometric function. *Mathematica J.*, **5**(4):74–76, 1995.

[2] M.A. Abdel Moneum, Z. Shen, J.L. Volakis, and O. Graham. Hybrid PO-MoM analysis of large axi-symmetric radomes. *IEEE Transactions on Antennas and Propagation*, **49**(12):1657–1666, 2001.

[3] M. Abramowitz and I.A. Stegun, editors. *Handbook of Mathematical Functions*. Dover, 1965.

[4] A. Altintas, S. Ouardani, and V.B. Yurchenko. Complex source radiation in a cylindrical radome of metal-dielectric grating. *IEEE Transactions on Antennas and Propagation*, **47**(8):1293–1300, Aug 1999.

[5] I. Andronov and D. Bouche. The creeping and whispering gallery waves on the surface of a transparent body. *J. of Electromagnetic Waves and Applications*, **9**(4):503–520, 1995.

[6] I.V. Andronov, F. Molinet, and D. Bouche. *Asymptotic and hybrid methods in electromagnetics*. Number 51 in IEE electromagnetic waves series. Institution of Electrical Engineers, London, Aug 2005.

[7] X. Antoine. Fast approximate computation of a time-harmonic scattered field using the on-surface radiation condition method. *IMA Jornal of Applied Mathematics*, **66**:83–110, 2001.

[8] D. Arakaki, W. Yu, and R. Mittra. On the solution of a class of large body problems with partialcircular symmetry (multiple asymmetries) by using a hybrid-dimensional finite-difference time-domain (FDTD) method. *IEEE Transactions on Antennas and Propagation*, **49**(3):354–360, Mar 2001.

[9] E. Arvas and S. Ponnapalli. Scattering cross section of a small radome of arbitrary shape. *IEEE Transactions on Antennas and Propagation*, **37**(5):655–658, May 1989.

[10] V.M. Babich and V.S. Buldyrev. *Short Wavelength Diffraction Theory: Asymptotic Methods*. Springer-Verlag, London, 1990.

[11] C.A. Balanis. *Advanced engineering electromagnetics*. Wiley, 1989.

[12] M.V. Berry and C.J. Howls. Hyperasymptotics for integrals with saddles. *Proceedings of the Royal Society. London. Series A. Mathematical, Physical and Engineering Sciences*, **434**(1892):657–675, 1991.

[13] J.L. Blanchard and E.H. Newman. Numerical evaluation of parabolic cylinder functions. *IEEE Transactions on Antennas and Propagation*, **37**(4):519–522, 1989.

[14] M. Born and E. Wolf. *Priciples of Optics*. Cambridge University Press, 1999.

[15] J.M. Bosson. *Asymptotic approaches to oscillatory eigenvalue problems*. DPhil thesis, University of Oxford, 2003.

[16] D. Bouche. Etude des ondes rampants sur un corps convexe vérifiant une condition d'impédance par une méthode de développement asymptotique. *Annales des Télécommunications*, **47**(9–10):400–412, 1992. In French.

[17] J.J. Bowman, T.B.A. Senior, and P.L.E. Uslenghi, editors. *Electromagnetic and acoustic scattering by simple shapes*. Harper and Row, rev. printing edition, 1987.

[18] W.G.C. Boyd. The asymptotic analysis of canonical problems in high-frequency scattering theory I. Stratified media above a plane boundary. *Proceedings of the Cambridge Philosophical Society*, **74**(2):289–312, 1973.

[19] W.G.C. Boyd. The asymptotic analysis of canonical problems in high-frequency scattering theory II. The circular and parabolic cylinders. *Proceedings of the Cambridge Philosophical Society*, **74**(2):313–332, 1973.

[20] L. M. Brehkovskikh. *Waves in layered media*. Academic Press, New York, 2nd edition, 1980.

[21] J.A. Buck. *Fundamentals of optical fibres*. Wiley series on pure and applied optics. Wiley-Interscience, 1995.

[22] D.G. Burks, E.F. Graf, and M.D. Fahey. A high-frequency analysis of radome-induced radar pointing error. *IEEE Transactions on Antennas and Propagation*, **AP-30**(5):947–955, Sep 1982.

[23] W.D. Burnside and K.W. Burgener. High frequency scattering by a thin lossless dielectric slab. *IEEE Transactions on Antennas and Propagation*, **AP-31**(1):104–110, 1983.

[24] V. Buslaev. Scattered plane waves, spectral asymptotics and trace formulae in exterior problems. *Soviet Math. Dokl.*, **12**:591–595, 1971.

[25] D.C. Calvo. A wide-angle on-surface radiation condition applied to scattering by spheroids. *J. of the Acoustical Society of America*, **116**(3):1549–1558, Sep 2004.

[26] Jeng-Hwa Chang and Kuan-Kin Chan. Analysis of a two-dimensional radome of arbitrarily curved surface. *IEEE Transactions on Antennas and Propagation*, **38**(10):1565–1568, 1990.

[27] S.J. Chapman, J.M.H. Lawry, Ockendon J.R., and R.H. Tew. On the theory of complex rays. *SIAM Review*, **41**(3):417–509, 1999.

[28] Y.M. Chen. Diffraction by a smooth transparent object. *J. of Mathematical Physics*, **5**(6):820–832, 1964.

[29] T.M. Cherry. Expansions in terms of parabolic cylinder functions. *Proceedings of the Edinburgh Mathemaical Society*, **8**:50–65, 1949.

[30] J. Coats. *High Frequency Asymptotics of Antenna-Structure Interactions*. DPhil thesis, Oxford, 2002.

[31] David Colton and Rainer Kress. *Inverse acoustic and electromagnetic scattering theory*, **93** of *Applied Mathematical Sciences*. Springer-Verlag, Berlin, 1992.

[32] D.L. Colton and R. Kress. *Integral equation methods in scattering theory*. Wiley, 1983.

[33] C.A.A. de Carvalho and H.M. Nussenzveig. Time delay. *Physics Reports*, **364**:83–174, 2002.

[34] C.E. Dean and P.L. Marston. Critical angle light scattering from bubbles: an asymptotic series approximation. *Applied Optics*, **30**(33):4764–4775, 1991.

[35] B. Dietz, J.-P. Eckmann, C.-A. Pillet, U. Smilansky, and I. Usshishkin. Inside-outside duality for planar billards – A numerical study. *Physical Review E*, **51**(5):4222–4231, 1995. Part A.

[36] B. Dietz and U. Smilansky. A scattering approach to the quanitization of billiards — the inside–outside duality. *Chaos*, **3**(4):581–589, 1993.

[37] R.B. Dingle. *Asymptotic Expansions: Their Derivation and Interpretation*. Academic Press, London, 1973.

[38] E. Doron and U. Smilansky. Semiclassical quantization of chaotic billiards: a scattering approach. *Nonlinearity*, **5**:1055–1084, 1992.

[39] J.-P. Eckmann and C.-A. Pillet. Scattering phases and density of states for exterior domains. *Annales de l'Insitut Henri Poincare-Physique Theorique*, **62**(4):383–399, 1995.

[40] J.-P. Eckmann and C.-A. Pillet. Spectral duality for planar billiards. *Communications in Mathematical Physics*, **170**:283–313, 1995.

[41] J.-P. Eckmann and C.-A. Pillet. Zeta functions with Dirichlet and Neumann boundary conditions for exterior domains. *Helvetia Physica Acta*, **70**(1–2):44–65, 1997.

[42] P.D. Einziger and L.B. Felsen. Ray analysis of two dimensional radomes. *IEEE Transactions on Antennas and Propagation*, **AP-31**(6):870–884, 1983.

[43] P.D. Einziger and L.B. Felsen. Rigorous asymptotic analysis of transmission through a curved dielectric slab. *IEEE Transactions on Antennas and Propagation*, **AP-31**(6):863–870, 1983.

[44] J.C. Engineer, J.R. King, and R.H. Tew. Diffraction by slender bodies. *European Journal of Applied Mathematics*, **9**(2):129–158, 1998.

[45] N. Fiedler-Ferrari, N.M. Nussenzveig, and W.J. Wiscombe. Theory of near-critical-angle scattering from a curved interface. *Phyical Review A*, **43**(2):1005–1039, 1991.

[46] V.A. Fock. *Electromagnetic Diffraction and Propagation Problems*. Macmillian, New York, 1960.

[47] R. Frose and G. Uhlmann. Scattering and inverse scattering. Final Report of Conference, BIRS March 22 - 27, 2003.

[48] X.J. Gao and L.B. Felsen. Complex ray analysis of beam transmission through two-dimensioal radomes. *IEEE Transactions on Antennas and Propagation*, **AP-33**(9):983–975, 1985.

[49] A. Gil, J. Segura, and N.M. Temme. Integral representations for computing real parabolic cylinder functions. *Numerische Mathematik*, **98**:105–134, 2004.

[50] A. Glisson. An integral equation for electromagnetic scattering from homogeneous dielectric bodies. *IEEE Transactions on Antennas and Propagation*, **32**(2):173–175, Feb 1984.

[51] I. Gohberg and B.G. Krein. *Introduction to the theory of linear nonselfadjoint operators*. Translations of mathematical monographs, v. 18. American Mathematical Society, Providence, R.I., 1969.

[52] R.K. Gordon and R. Mittra. Finite element analysis of axisymmetric radomes. *IEEE Transactions on Antennas and Propagation*, **41**(7):975–981, Jul 1993.

[53] J.W. Helton and J.V. Ralston. The first variation of the scattering matrix. *J. Differential Equations*, **21**(2):378–394, 1976.

[54] E. Heyman. On the tunneling hypothesis for ray reflection and transmission at a concave dielectric boundary. *IEEE Transactions on Antennas and Propagation*, **AP-23**(9):978–986, 1984.

[55] E. Heyman and L.B. Felsen. Evanescent waves and complex rays for modal propagation in curved open waveguides. *SIAM J. on Applied Mathematics*, **43**(4):855–844, 1983.

[56] E. Heyman and L.B. Felsen. High frequency fields in the presence of a curved dielectric interface. *IEEE Transactions on Antennas and Propagation*, **AP-23**(9):969–978, 1984.

[57] E.J. Hinch. *Perturbation Methods*. Cambridge University Press, 1991.

[58] C.L. Holloway and E.F. Kuester. Impedance-type boundary conditions for a periodic interface between a dielectric and a highly conducting medium. *IEEE Transactions on Antennas and Propagation*, **48**(10):1660–1672, Oct 2000.

[59] D.J. Hoppe and Y. Rahmat-Samii. *Impedance Boundary Conditions in Electromagnetics*. Taylor and Francis, 1995.

[60] C.J. Howls. Hyperasymptotics for multidimensional integrals, exact remainder terms and the global connection problem. *Proceedings of the Royal Society. London. Series A. Mathematical, Physical and Engineering Sciences*, **453**(1966):2271–2294, 1997.

[61] T. Ishihara and L.B. Felsen. High-frequency propagation at long ranges near a concave boundary. *Radio Science*, **23**(6):997–1012, Nov–Dec 1988.

[62] T. Ishihara, L.B. Felsen, and A. Green. High-frequency field excited by a line source located on a perfectly conducting cylindrical surface. *IEEE Transactions on Antennas and Propagation*, **AP-26**(6):757–767, 1978.

[63] V.I. Ivanov. Diffraction of short plane waves on a parabolic cylinder. *USSR Comp. Math. and Math. Phys.*, **2**:255–271, 1963.

[64] V. Ja. Ivriĭ. The second term of the spectral asymptotics for a Laplace-Beltrami operator on manifolds with boundary. *Functional Anal. Appl.*, **14**(2):98–106, 1980.

[65] J. D. Jackson. *Classical Electrodynamics*. John Wiley and Sons, New York, 3rd edition, 1998.

[66] D.S. Jones. *The Theory of Electromagnetism*. Pergamon, 1964.

[67] D.S. Jones. Surface radiation conditions. *IMA J. of Applied Mathematics*, **41**:21–30, 1988.

[68] D.S. Jones. *Methods in electromagnetic wave propagation*. Clarendon Press, Oxford, 2nd edition, 1994.

[69] L. Kaminetzky and J.B. Keller. Diffraction coefficients for higher order edges and vertices. *SIAM Journal on Applied Mathematics*, **22**:109–134, 1972.

[70] L. Kaminetzky and J.B. Keller. Diffraction by edges and vertices of interfaces. *SIAM Journal on Applied Mathematics*, **28**:839–856, 1975.

[71] S.N. Karp and Jr Karal, F.C. Generalized impedance boundary conditions with applications to surface wave structures. In J. Brown, editor, *Electromagnetic Wave Theory*. Pergamon Press, Oxford, 1965.

[72] J.B. Keller. Reflection and transmission of electromagnetic wvaes by thin curved shells. *J. of Applied Physics*, **21**:896–901, September 1950.

[73] J.B. Keller. A geometrical theory of diffraction. *Proc. Symp. Appl. Math.*, **8**:27–52, 1958.

[74] J.B. Keller. The geometrical theory of diffraction. *J. of the Optical Society of America*, **52**:116–130, 1962.

[75] J.B. Keller and R.M. Lewis. Asymptotic methods for partial differential equations: the reduced wave equation and Maxwell's equations. In J.B. Keller, G. Papanicolau, and D. McLaughlin, editors, *Surveys in Applied Mathematics*. Plenum Publishing, 1995.

[76] J.B. Keller, R.M. Lewis, and B.D. Seckler. Asymptotic solution of some diffraction problems. *Communications on Pure and Applied Mathematics*, pages 207–265, 1956.

[77] L. Knockaert, F. Olyslager, and D. De Zutter. The diaphanous wedge. *IEEE Transactions on Antennas and Propagation*, **45**:1374–1381, Sep 1997.

[78] G.A. Kriegsmann, A. Taflove, and K.R. Umashankar. A new formulation of electromagnetic wave scattering using the on surface radiation condition method. *IEEE Transactions on Antennas and Propagation*, **35**:153–161, Feb 1987.

[79] P. Lax and R.S. Phillips. Decaying modes for the wave equation in the exterior of an obstacle. *Communications on Pure and Applied Mathematics*, 1969.

[80] P.D. Lax and R.S. Phillips. *Scattering theory*, **26** of *Pure and Applied Mathematics*. Academic Press Inc., second edition, 1989.

[81] B.R. Levy and J.B. Keller. Diffraction by a smooth object. *Communications on Pure and Applied Mathematics*, **12**:159–209, 1959.

[82] R.M. Lewis, N. Bleistein, and D. Ludwig. Uniform asymptotic theory of creeping waves. *Communications on Pure and Applied Mathematics*, **20**:296–328, 1967.

[83] Le-Wei Li, Mook-Seng Leong, Tat-Soon Yeo, and Yeow-Beng Gan. Electromagnetic radiation from a prolate spheroidal antenna enclosed in a confocal spheroidal radome. *IEEE Transactions on Antennas and Propagation*, **50**(11):1525–1533, Nov 2002.

[84] T.A. Lowdon. Integral representation of the Hankel function in terms of parabolic cylinder functions. *Quarterly Journal of Mechanics and Applied Mathematics*, **23**(2):315–327, 1970.

[85] Cai-Cheng Lu. A fast algorithm based on volume integral equation for analysis of arbitrarily shaped dielectric radomes. *IEEE Transactions on Antennas and Propagation*, **51**(3):606–612, Mar 2003.

[86] D. Ludwig. Diffraction by a circular cavity. *J. of Mathematical Physics*, **11**(5):1617–1630, May 1970.

[87] Y.L. Luke. Algorithms for rational approximations for a confluent hypergeometric function. *Utilitas Math.*, **11**:123–151, 1977.

[88] M.A. Lyalinov. Diffraction by a highly contrast transparent wedge. *J. Phys. A: Math. Gen.*, **32**:2183–2206, 1999.

[89] A. Majda and J. Ralston. An analogue of Weyl's theorem for unbounded domains. I. *Duke Math. J.*, **45**(1):183–196, 1978.

[90] A. Majda and J. Ralston. An analogue of Weyl's formula for unbounded domains. III. An epilogue. *Duke Math. J.*, **46**(4):725–731, 1979.

[91] E. Marx. Single integral equation for wave scattering. *J. of Mathematical Physics*, **23**(6):1057–1065, 1982.

[92] R.B. Melrose. Weyl asymptotics for the phase in obstacle scattering. *Comm. Partial Differential Equations*, **13**(11):1431–1439, 1988.

[93] R.B. Melrose. *Geometric Scattering Theory*. CUP, 1995.

[94] M.V. Merry and C.J. Howls. High orders of the Weyl expanions for quantum billiards: Resurgence of periodic orbis, and the Stokes phenomenon. *Proceedings of the Royal Society of London A*, **447**(1931):527–555, 1994.

[95] P. M. Morse and H. Feshbach. *Methods of theoretical physics*. McGraw-Hill Book Co., New York, 1953.

[96] E.H. Newman. Plane wave scattering by a material coated parabolic cylinder. *IEEE Transactions on Antennas and Propagation*, **38**(4):541–550, Apr 1990.

[97] H.M. Nussenzveig. High-frequency scattering by a transparent sphere: I. direct reflection and transmission. *J. of Mathematical Physics*, **10**(1):82–124, 1969.

[98] J.F. Nye. Spurious internal fields in scattering by a cylinder. *J. of Physics A: Mathematical and General*, **36**:4221–4237, 2003.

[99] J.R. Ockendon, S.D. Howison, A.A. Lacey, and A.B. Movchan. *Applied Partial Differential Equations*. Oxford University Press, 2003.

[100] F.W.J. Olver. *Asymptotics and special functions*. Academic Press, 1974.

[101] R. Orta, R. Tascone, and R. Zich. Performance degradation of dielectric radome covered antennas. *IEEE Transactions on Antennas and Propagation*, **AP-36**(12):1707–1713, Dec 1988.

[102] A.V. Osipov and A.N. Norris. The Malyuzhinets theory for scattering from wedge boundaries: A review. *Wave Motion*, **29**(4):313–340, 1999.

[103] R.H. Ott. Scattering by a parabolic cylinder – a uniform asymptotic expansion. *J. Math Phys.*, **26**(4):854–860, 1985.

[104] D.T. Paris. Computer-aided radome analysis. *IEEE Transactions on Antennas and Propagation*, **AP-18**:7–15, Jan. 1970.

[105] R.B. Paris. The asymptotic behaviour of pearcey's integral for complex variables. *Proceedings of the Royal Society of London A*, **432**(1886):391–426, 1991.

[106] P. Pelosi and P. Ya. Ufimtsev. The impedance-boundary condition. *IEEE Antennas and Propagation Magazine*, 1996.

[107] V. Petkov and G. Popov. Asymptotic behaviour of the scattering phase for nontrapping obstacles. *Ann. Inst. Fourier (Grenoble)*, **32**(3):vi, 111–149, 1982.

[108] H. Primakoff and J.B. Keller. Reflection and transmission of sound by thin curved shells. *J. of the Acoustical Society of America*, **19**(2):820–832, 1947.

[109] J. Ralston. Addendum to: "The first variation of the scattering matrix" (J. Differential Equations **21** (1976), no. 2, 378–394) by J. W. Helton and Ralston. *J. Differential Equations*, **28**(1):155–162, 1978.

[110] A.D. Rawlins. Diffraction by an acoustically penetrable or an electromagnetically dielectric half plane. *International J. Engineering Science*, **15**:569–578, 1977.

[111] A.D. Rawlins. Diffraction by, or diffusion into, a penetrable wedge. *Proceedings of the Royal Society of London A*, **455**(1987):2655–2686, 1999.

[112] S.R. Rengarajan and E.S. Gillespie. Asymptotic approximations in radome analysis. *IEEE Transactions on Antennas and Propagation*, **36**(3):405–414, Mar 1988.

[113] S.O. Rice. Diffraction of plane radio waves by a parabolic cylinder. *Bell Systems Technical Journal*, **33**:417–504, 1954.

[114] J.R. Richmond. Scattering by a dielectric cylinder of arbitary cross section shape. *IEEE Transactions on Antennas and Propagation*, **AP-13**(3):334–341, 1965.

[115] M.A. Ricoy and J.L. Volakis. Derivation of generalized transition/boundary conditions for planar multiple-layer structures. *Radio Science*, **25**(4):391–405, Jul-Aug 1990.

[116] J.R. Ringrose. *Compact Non-Self-Adjoint Operators*. Van Nostrand Reinhold, London, 1971.

[117] R.G. Rojas and Z. Al-hekail. Generalizes impedance/resistive boundary conditions for electromagnetic scattering problems. *Radio Science*, **24**(1):1–12, Jan–Feb 1989.

[118] B. Rulf. Relation between creeping waves and lateral waves on a curved interface. *J. of Mathematical Physics*, **8**(9):1785–1793, Sep 1967.

[119] B. Rulf. Uniform asymptotic theory of diffraction at an interface. *Communications on Pure and Applied Mathematics*, **21**:67–76, 1968.

[120] S.M. Rytov. Calcul du skin-effect par la méthode des perturbations. *J. Phys. USSR*, **3**:233–242, 1940.

[121] V. Saward. *Some Problems in Diffraction Theory*. DPhil thesis, Oxford, 1997.

[122] J. Segura and A. Gil. Parabolic cylinder functions of integer and half-integer orders for nonnegative arguments. *Computer Physics Communications*, **115**:69–86, 1998.

[123] T. B. A. Senior. Impedance boundary conditions for imperfectly conducting surfaces. *Appl. Sci. Res B*, **8**:418–436, 1960.

[124] T.B.A. Senior. Combined resistive and conductive sheets. *IEEE Transactions on Antennas and Propagation*, **AP-33**(5):577–579, May 1983.

[125] T.B.A. Senior. Generalized boundary and transition conditions and the question of uniqueness. *Radio Science*, **27**(6):929–934, Nov-Dec 1992.

[126] T.B.A. Senior and J.L. Volakis. Sheet simulation of a thin dielectric layer. *Radio Science*, **22**(7):1261–1272, 1987.

[127] T.B.A. Senior and J.L. Volakis. *Approximate boundary conditions in electromagnetics*. Number 41 in IEE E-M Waves Series. The Institution of Electrical Engineers, London, 1995.

[128] T.B.A. Senior and J.L. Volakis. Higher order impedance and absorbing boundary conditions. *IEEE Transactions on Antennas and Propagation*, **45**(1):107–114, Jan 1997.

[129] K. Siwiak, T.B. Dowling, and L.R. Lewis. Boresight errors induced by missile radomes. *IEEE Transactions on Antennas and Propagation*, **AP-27**(6):832–841, 1979.

[130] L.J. Slater. *Confluent hypergeometric functions*. Cambridge University Press, New York, 1960.

[131] B. D. Sleeman. Interior and exterior inverse problems for the Helmholtz equation. In G. F. Roach, editor, *Inverse problems and imaging*, number 245 in Pitman Research Notes in Mathematics Series, pages 166–199. Longman, 1991.

[132] U. Smilansky and I. Ussishkin. The smooth spectral counting function and the total phase shift for quantum billiards. *J. Physics A.: Math. Gen.*, **29**:2587–2597, 1996.

[133] V. I. Smirnov. *A course of higher mathematics. Vol. IV [Integral equations and partial differential equations]*. Translated by D.E. Brown; translation edited by I.N. Sneddon. Pergamon Press, Oxford, 1964.

[134] B. J. Smith. *A Complex Ray Approach to the Acoustics of Fluid-Loaded Structures*. PhD thesis, University of Nottingham, 1995.

[135] A.W. Snyder and J.D. Love. Reflection at a curved dielectric interface — electromagnetic tunnelling. *IEEE Transactions on Microwave Theory and Techniques*, **MTT-23**(1):134–141, 1975.

[136] A. Sommerfeld. Mathematische theorie der diffraction. *Mathematische Annalen*, **47**:317–374, 1896.

[137] J.A. Stratton. *Electromagnetic Theory*. Mc Graw-Hill, London, 1941.

[138] O.I. Sukharevsky, S.V. Kukobko, and A.Z. Sazonov. Volume integral equation analysis of a two dimensional radome with a sharp nose. *IEEE Transactions on Antennas and Propagation*, **53**(4):1500–1506, Apr 2005.

[139] N.M. Temme. Numerical and asymptotic aspects of parabolic cylinder functions. *J. of Computational and Applied Mathematics*, **121**:221–246, 2000.

[140] R.H. Tew, S.J. Chapman, J.R. King, J.R. Ockendon, B.J. Smith, and I. Zafarullah. Scalar wave diffraction by tangent rays. *Wave Motion*, **32**:363–380, 2000.

[141] R.H. Tew and J.R. Ockendon. Multiple scales expansions near critical rays. *SIAM J. on Applied Mathematics*, **52**(2):327–336, Apr 1992.

[142] G. Tricoles. Radiation patterns and boresight error of a microwave antena enclosed in an axially symmetric dielectric shell. *J. of the Optical Society of America. A.*, **54**:1094–1101, Sep 1963.

[143] K. Umashankar, A. Taflove, and S. Rao. Electromagnetic scattering by arbitrary shaped three-dimensional homogeneous lossy dielectric objects. *IEEE Transactions on Antennas and Propagation*, **34**(6):758–766, Jun 1986.

[144] F. Ursell. Exterior problems of acoustics. *Proccedings of the Cambridge Philosophical Society*, **74**:117–125, 1978.

[145] J. R. Wait. Scattering of a plane wave from a circular dielectric cylinder at oblique incidence. *Canadian Journal of Physics*, **33**:189–195, 1955.

[146] E.T. Whittaker and G.N. Watson. *Modern Analysis*. Cambridge university Press, 1920.

[147] R. Wong. *Asymptotic approximations of integrals*. Academic Press, 1989.

[148] D.C.F. Wu and R.C. Rudduck. Plane wave spectrum-surface integration technique for radome analysis. *IEEE Transactions on Antennas and Propagation*, **AP-22**(3):497–500, May 1974.

[149] R. Yamada. Excitation of a curved slab waveguide. *Japanese Journal of Applied Physics*, **18**(11):2105–2110, 1979.

[150] C. Yeh. Diffraction of waves by a dielectric parabolic cylinder. *J. of the Optical Society of America*, **57**(2):195–201, Feb 1967.

[151] M.S. Yeung. Single integral equation for electromagnetic scattering by three-dimensional homogeneous dielectric objects. *IEEE Transactions on Antennas and Propagation*, **47**(10):1615–1622, Oct 1999.

[152] E. Zauderer. Boundary layer and uniform asymptotic expansions for diffraction problems. *SIAM J. Applied Mathematics*, **19**(3):575–600, 1970.

[153] W.-J. Zhao, L.-W. Li, and Y.-B. Gan. Efficient analysis of antenna radiation in the presence of airborne dielectric radomes of arbitrary shape. *IEEE Transactions on Antennas and Propagation*, **53**(1):442–449, Jan 2005.